UNIVERSIDADE FEDERAL DE PERNAMBUCO
CENTRO DE TECNOLOGIA E GEOCIÊNCIAS
DEPARTAMENTO DE OCEANOGRAFIA
PROGRAMA DE PÓS-GRADUAÇÃO EM OCEANOGRAFIA

**LÉO COSTA AROUCHA**

# RESPOSTAS DOS FLUXOS DE $CO_2$ AOS VÓRTICES DA CORRENTE NORTE DO BRASIL

Recife
2021

**LÉO COSTA AROUCHA**

# RESPOSTAS DOS FLUXOS DE $CO_2$ AOS VÓRTICES DA CORRENTE NORTE DO BRASIL

Dissertação apresentada ao Programa de Pós-Graduação em Oceanografia da Universidade Federal de Pernambuco, como requisito parcial para a obtenção do título de Mestre em Oceanografia.

Área de concentração: Oceanografia Abiótica.

Orientadora: Profa. Dra. Dóris Regina Aires Veleda

Coorientadora: Profa. Dra. Nathalie Lefèvre

Recife

2021

Catalogação na fonte
Bibliotecário Gabriel Luz CRB-4/2222

A771r Aroucha, Léo Costa.
Respostas dos fluxos de $CO_2$ aos vórtices da corrente norte do Brasil / Léo Costa Aroucha.
142 f.; figs., abrev. e siglas, símb.

Orientadora: Profa. Dra. Dóris Regina Aires Veleda.
Coorientadora: Profa. Dra. Nathalie Lefèvre.
Dissertação (Mestrado) – Universidade Federal de Pernambuco. CTG. Programa de Pós-Graduação em Oceanografia, Recife, 2021.
Inclui referências e apêndice.

1. Oceanografia. 2. Vórtices da corrente norte do Brasil. 3. Fluxos de $CO_2$. 4. Variabilidade intra e interanual. I. Veleda, Dóris Regina Aires (Orientadora). II. Lefèvre, Nathalie (Coorientadora). III. Título.

UFPE

551.46 CDD (22. ed.) BCTG / 2022 – 133

**LÉO COSTA AROUCHA**

**RESPOSTAS DOS FLUXOS DE $CO_2$ AOS VÓRTICES DA CORRENTE NORTE DO BRASIL**

Dissertação apresentada ao Programa de Pós-Graduação em Oceanografia da Universidade Federal de Pernambuco, Centro de Tecnologia e Geociências, como requisito parcial para a obtenção do título de Mestre em Oceanografia. Área de concentração: Oceanografia Abiótica.

Aprovada em: 30/08/2021

**BANCA EXAMINADORA**

_____

Profa. Dra. Dóris Regina Aires Veleda (Orientadora)
Universidade Federal de Pernambuco

_____

Profa. Dra. Cláudia Klose Parise (Examinadora Externa)
Universidade Federal do Maranhão

_____

Prof. Dr. Luciano Ponzi Pezzi (Examinador Externo)
Instituto Nacional de Pesquisas Espaciais

_____

Profa. Dra. Monica Ferreira da Costa (Examinadora Interna)
Universidade Federal de Pernambuco

_____

Dr. Pedro Tyaquiçã da Silva Santos (Examinador Interno)
Universidade Federal de Pernambuco

## AGRADECIMENTOS

Primeiramente, gostaria de agradecer aos meus pais, Doda e Coca, que nunca mediram esforços para me fornecer toda a estrutura educacional e emocional que são inerentes a mim e que carregarei para o resto da minha trajetória. A eles, agradeço todo amor, apoio, paciência e incentivo que sempre me deram. Amo vocês. Essa Dissertação é nossa.

Agradeço também à minha amiga e orientadora, profa. Dóris Veleda, que sempre se fez presente durante a elaboração deste trabalho. Sua contribuição vai além de TCCs, Dissertações ou Teses, com palavras de incentivo, apoio e orientação no âmbito profissional e na vida. Dóris esteve presente em praticamente todo o meu caminho na produção científica e na minha vida nos últimos anos, e nunca mediu esforços para me oferecer uma ajuda, independente do que ela estivesse passando no momento. Dóris é um exemplo de força de vontade e determinação, e eu espero que essa troca possa perdurar por longos anos. Agradeço ainda à minha co-orientadora, Nathalie Lefèvre, pela paciência, apoio científico e conselhos que foram definitivamente úteis na concepção deste estudo. Agradeço também aos integrantes do LOFEC e CER - UFPE, pelo incentivo e apoio na realização deste trabalho, em especial à Francis Lopes e Pedro Tyaquiçã. Agradeço também ao CNPq pelo apoio financeiro na realização deste trabalho.

Gostaria também de ressaltar a importância da minha família, representada aqui também pelo meu irmão, cunhada, sobrinho, e por Mazé, que sempre me incentivaram com palavras de força, me mantendo no eixo sem deixar a peteca cair. Agradeço também a Pami, que foi de extrema importância tanto no incentivo quanto em me tranquilizar quanto a esta Dissertação, especialmente nos últimos meses. Queria também agradecer ao Sistema Único de Saúde do país, pela possibilidade da realização de uma campanha de vacinação em larga escala. O SUS salva vidas. Dedico esta Dissertação também a todos e todas que perderam parentes e amigos queridos na pandemia do COVID-19.

Por fim, queria dedicar essa Dissertação a duas pessoas em especial. Ao meu tio Sérgio, que nos deixou recentemente, que foi um grande educador, um dos pilares da família, e que sempre me incentivou a seguir a carreira acadêmico-científica, muito obrigado! Por fim, e especialmente, dedico este trabalho ao meu grandíssimo amigo Dayvid, nossa Britney, que partiu muito prematuramente e vai sempre iluminar nossos caminhos. *A saudade é imensa, amigo. Espero que todo este trabalho também te deixe orgulhoso. Amo você, eternamente. Um dia a gente se encontra*.

## RESUMO

A fim de investigar a variabilidade intra e interanual dos vórtices da Corrente do Norte do Brasil e entender o papel dos mesmos na biogeoquímica do Atlântico Tropical Norte Ocidental, especialmente em relação ao fluxo de $CO_2$, o algoritmo de detecção e rastreamento de momentum angular (AMEDA) foi usado para identificação de suas ocorrências, trajetórias e parâmetros dos mesmos, além dos impactos nos fluxos de $CO_2$. Com base em 24 anos (1993-2016) de dados de reanálise do ARMOR 3D, e 25 anos (1993-2017) de dados também de reanálise do modelo físico GLORYS e biogeoquímico BIORYS, identificamos uma taxa média de 5 vórtices liberados por ano. Os mesmos apresentam tempo de vida médio de 15,3 (± 5,4) semanas, raio médio baseado na velocidade (Rmax) de 139,8 (± 23,6) km e anomalia na altura média da superfície do mar (SSHa) de 9,4 (± 4,0) cm. A velocidade azimutal máxima observada média (Vmax) foi 0,27 (± 0,08) m / s, enquanto o valor médio do número de Rossby (Ro) foi 0,08 (± 0,04) e a energia cinética média (KE) foi de 255,3 (± 154,8) cm2 / s2. Além disso, a análise da fusão dos mesmos apontou que tal interação gerou um aumento significativo na energia (52%) e na velocidade (22%) do vórtice. Finalmente, observamos as anomalias verticais dos perfis de temperatura e salinidade, que indicaram um aprofundamento da termoclina e afundamento das águas costeiras e tropicais associado aos vórtices da Corrente Norte do Brasil. Ainda, a presença destas estruturas de mesoescala em 77% do tempo, variando similarmente com a salinidade da superfície do mar, mostrou a influência de tais vórtices na variância da salinidade na região. Este resultado também apontou para a salinidade como a principal responsável pelas anomalias positivas de fugacidade de $CO_2$, relacionadas aos núcleos dos vórtices. Além do mais, foi indicado que tal vórtice pode aumentar, em média, 38% do fluxo de $CO_2$ em seus núcleos em relação às águas externas. Acredita-se que anomalias positivas de salinidade e consequentemente de carbono inorgânico dissolvido nas regiões superficiais dos centros e das partes anteriores dos anéis foram responsáveis pelo aumento na covariância tanto da fugacidade quanto no fluxo de $CO_2$ diário, apesar que o aumento de temperatura da superfície do mar inerente aos vórtices anticiclônicos pode também ter contribuído para estes fluxos elevados.



Palavras-chave: vórtices da corrente norte do Brasil; fluxos de $CO_2$; variabilidade intra e interanual.

## ABSTRACT

In order to investigate intra- and inter-annual variability of North Brazil Current rings, and understand their role on the biogeochemistry of the Western Tropical North Atlantic, the angular momentum eddy detection and tracking algorithm (AMEDA) was used for identification of their occurrence, trajectories, and parameters, and also their impacts on $CO_2$ flux in the region. Based on 24 years (1993–2016) reanalysis data from ARMOR 3D and 25 years (1993 – 2017) from the physical GLORYS and biogeochemical BIORYS models, we identified an average rate of five NBC rings shed by year. The rings present an average lifetime of 15.3 (±5.4) weeks, average speedbased radius (Rmax) of 139.8 (±23.6) km, and mean sea surface height anomaly (SSHa) of 9.4 (±4.0) cm. The mean observed maximum azimuthal velocity (Vmax) was 0.27 (±0.08) m/s, while the averaged Rossby number (Ro) value was 0.08 (±0.04) and averaged kinetic energy (KE) was of 255.3 (±154.8) cm2 /s2. NBC rings have larger dimensions, rotate faster, live less, and transfer more energy in boreal winter months. In contrast, those shed during boreal summer and early fall last longer, have smaller diameters and carry less energy. Besides, the analysis of ring merging pointed that the interaction between North Brazil Current rings generated a significantly increase in ring energy (52%), and velocity (22%). Finally, we observed the vertical anomalies temperature and salinity profiles, which indicated a thermocline deepening and sinking of coastal and tropical waters due to North Brazil Current rings downwelling. In addition, the presence of North Brazil Current rings presence in 77% of the time, varying similarly as sea surface salinity, showed their rings influence on sea surface salinity variance at the region. This also pointed for salinity as the main responsible for positive $CO_2$ sea water fugacity anomalies related to ring cores. Furthermore, it was indicated that a NBC ring could increase, in average, 38% of the $CO_2$ flux at their cores in relation to surrounding waters. At the present study, it is believed that positive anomalies of salinity and consequently dissolved inorganic carbon at ring surface cores and trailing edges were responsible for this increase in the daily seawater $CO_2$ fugacity and $CO_2$ flux covariance, although the increased sea surface temperature inherent to anticyclonic rings might have contributed to the higher fluxes.



Keywords: north Brazil current rings; $CO_2$ fluxes; intra and inter-annual variability.

## LISTA DE FIGURAS

## LISTA DE ABREVIATURAS E SIGLAS

| | |
|---|---|
| aASM | Anomalia de Altura da Superfície do Mar |
| ACAS | Água Central do Atlântico Sul |
| AMEDA | Algoritmo de Detecção e Trajetória de Momento Angular de Vórtices |
| APAN | Águas Profundas do Atlântico Norte |
| ARMOR3D | Global Observed Ocean Physics Temperature Salinity Heights and Currents Reprocessing |
| ASM | Altura da Superfície do Mar |
| ATNO | Atlântico Tropical Norte Ocidental |
| CCNE | Contracorrente Norte Equatorial |
| cCSE | Ramo Central da Corrente Sul Equatorial |
| CMEMS | Copernicus Marine Environment Monitoring Service |
| CNB | Corrente Norte do Brasil |
| CNE | Corrente Norte Equatorial |
| CPBO | Corrente Profunda de Borda Oeste |
| CRMA | Célula de Revolvimento Meridional do Atlântico |
| CSE | Corrente Sul Equatorial |
| CTs | Ciclones Tropicais |
| DIC | Dissolved Inorganic Carbon |
| DJF | Dezembro-Janeiro-Fevereiro |
| EOFs | Funções Ortogonais Empíricas/Empirical Ortoghonal Functions |
| ENOS | El Niño Oscilação Sul |
| HN | Hemisfério Norte |
| HS | Hemisfério Sul |
| ITCZ | Intertropical Convergence Zone |
| JJA | Junho-Julho-Agosto |
| MAM | Março-Abril-Maio |
| NBC | North Brazil Current |
| NBCR | North Brazil Current Ring |
| nCSE | Ramo Sul da Corrente Sul Equatorial |
| NEMO | Nucleus for European Modelling of the Ocean |
| PC | Principal Component |

| | |
|---|---|
| SCBO | Sucorrente de Borda Oeste |
| SCE | Subcorrente Equatorial |
| SCNB | Subcorrente Norte do Brasil |
| SCNE | Subcorrente Norte Equatorial |
| SCSE | Subcorrente Sul Eqautorial |
| sCSE | Ramo Sul da Corrente Sul Equatorial |
| SON | Setembro-Outubro-Novembro |
| SSHa | Sea-Surface Height anomaly |
| SSS | Sea Surface Salinity |
| SST | Sea Surface Temperature |
| TA | Total Alkalinity |
| TSM | Temperatura da Superfície do Mar |
| VCNB | Vórtice da Corrente Norte do Brasil |
| WTNA | Western Tropical North-Atlantic |
| ZCIT | Zona de Convergência Intertropical |

## LISTA DE SÍMBOLOS

| | |
|---|---|
| C | Coeficiente de Fugacidade do gás |
| EC | Energia Cinética |
| $FCO_2$ | Fluxo de $CO_2$ entre oceano e atmosfera |
| $fCO_{2\ ATM}$ | Fugacidade de $CO_2$ na atmosfera |
| $fCO_{2\ SW}$ | Fugacidade de $CO_2$ no oceano |
| k | Velocidade de transferência do gás |
| KE | Kinetic Energy |
| MALN | Momento Angular Local Normalizado |
| OW | Parâmetro de Okubo-Weiss/Okubo-Weiss Parameter |
| $pH_2O$ | Pressão de vapor da água em 100% de umidade |
| Rd | Raio de deformação de Rossby do primeiro modo baroclínico |
| Rmax | Raio correspondente à máxima velocidade azimutal (Vmax) |
| Ro | Número de Rossby |
| S | Solubilidade do gás |
| Sc | Número de Schmidt |
| $U_{10}$ | Velocidade do vento à 10m da superfície |
| Vmax | Máxima velocidade azimutal |
| $xCO_2$ | Fração Molar de $CO_2$ atmosférico |

**SUMÁRIO**

# 1 INTRODUÇÃO

Esta dissertação está organizada em formato de artigos científicos, em diferentes discussões considerando as análises da variabilidade intra e interanual dos vórtices da Corrente Norte do Brasil (CNB) e seus possíveis impactos biogeoquímicos, especialmente em relação aos fluxos de $CO_2$. Os dados deste trabalho foram baseados nas reanálises de modelos físicos e biogeoquímicos. O autor desta dissertação foi bolsista de mestrado do Conselho Nacional de Desenvolvimento Científico e Tecnológico – CNPq (processo: 31021/2019-2). Este projeto foi apoiado pelo projeto TRIATLAS, que recebe financiamento do programa de inovação e pesquisa do Horizonte da União Europeia 2020 sob acordo de concessão número 817578, e pela Rede Brasileira de Mudanças Climáticas – Rede CLIMA (Concessão FINEP 01.13.0353-00).

No presente trabalho apresentamos um estudo inédito de análises da variabilidade intra e interanual dos vórtices da CNB e seus possíveis impactos biogeoquímicos, através da aplicação de um algoritmo de identificação de ocorrência e trajetória de vórtices em uma base dados de reanálise. Além disso, análises estatísticas de Funções Ortogonais Empíricas (EOFs) foram realizadas com o objetivo de avaliar o papel dos vórtices da CNB na biogeoquímica do ATNO, especialmente em relação a $FCO_2$. Esta última base de dados também foi aplicada ao AMEDA para identificação dos impactos destes vórtices em uma escala diária, utilizando dois vórtices no ano de 2009 como estudos de caso.

Este manuscrito se encontra estruturado em sete capítulos: o Capítulo 1 de carácter introdutório com informações gerais sobre o Atlântico Tropical, enfatizando sua biogeoquímica, especialmente os fluxos de $CO_2$, e de sua dinâmica geral, com ênfase nos vórtices da CNB. O Capítulo 2 descreve a área de estudo e as metodologias aplicadas ao longo do trabalho. Ambos os capítulos estão escritos na língua portuguesa. Os capítulos 3 e 4 apresentam os resultados na forma de dois artigos científicos, ambos escritos em inglês. O Capítulo 3 traz um artigo recentemente publicado com a análise da variabilidade intra e interanual dos vórtices da CNB, enquanto que o Capítulo 4 aborda o papel destes vórtices nos padrões dos parâmetros biogeoquímicos com enfoque no $FCO_2$. No Capítulo 5 são apresentadas as conclusões gerais de ambos os estudos, enquanto que no Capítulo 6 se resguardam as referências. No Capítulo 7 está inserido o Anexo referente ao artigo publicado.

## 1.1 ASPECTOS GERAIS

Esta seção tratará dos aspectos dinâmicos e bioquímicos do Atlântico Tropical, detalhando especialmente a dinâmica na região (seção 1.1.1), com enfoque na Corrente Norte do Brasil (CNB) (seção 1.1.2) e os vórtices relacionados à mesma (seção 1.1.3), além de aspectos da fugacidade de $CO_2$ neste oceano (seção 1.1.4).

### 1.1.1 Atlântico Tropical

O Atlântico Tropical apresenta circulação oceânica em superfície delimitada pelas bordas equatoriais dos giros subtropicais dos hemisférios norte e sul (LUMPKIN; GARZOLI, 2005). Os padrões de circulação presentes especificamente na região noroeste deste oceano (i.e. limitados, longitudinalmente entre 35-60ºW) possuem papel importante no transporte de massa, calor e sal entre o Hemisfério Norte (HN) e o Hemisfério Sul (HS) (SCHMITZ; RICHARDSON, 1991; SCHMITZ; MCCARTNEY, 1993). De fato, é esta a circulação, por exemplo, responsável pelo fechamento da Célula de Revolvimento Meridional do Atlântico (CRMA), causado pelo transporte em superfície de águas quentes do HS para o HN através da CNB, e pelo transporte profundo da Água Profunda do Atlântico Norte (APAN) em direção ao HS através da Subcorrente de Borda Oeste (SCBO). A SCBO é também conhecida como Corrente Profunda de Borda Oeste (CPBO) (JOHNS *et al.*, 2008; MEINEN *et al.*, 2012). Estima-se que a magnitude desta troca de massas d'água entre os hemisférios seja na ordem de 13 Sv (SCHMITZ; RICHARDSON, 1991). A região conta ainda com a presença de contracorrentes zonais e outras correntes de borda oeste, tornando a circulação ainda mais complicada nesta área (BOURLÈS *et al.*, 1999). A combinação de águas provenientes de ambos os hemisférios fornece um mecanismo de formação de massas d'água com características distintas, sendo isso indicativo do papel do Atlântico Tropical em misturar as águas com origens em diferentes hemisférios (BOURLÈS *et al.*, 1999).

Superficialmente a circulação no Atlântico Tropical é caracterizada por um fluxo da Corrente Sul Equatorial (CSE) em direção a oeste. O Atlântico Tropical Sul é caracterizado pela presença do ramo Sul da CSE (sCSE), a qual flui desde o Sul da costa da África (Figura 1) até a costa brasileira, onde a mesma se bifurca, dando origem à Subcorrente Norte do Brasil (SCNB) e Corrente do Brasil, com a primeira fluindo ao norte, atravessando a região equatorial, e a última fluindo à sul pela costa brasileira. Ao chegar a aproximadamente 5ºS, a SCNB se une ao ramo Central da CSE (cCSE) que vem de leste, formando assim a intensa CNB. A CNB

sofre retroflexão superficialmente em aproximadamente 7ºNLF e 48ºW, alimentando a CCNE. Esse giro equatorial é, portanto, constituído pela CNB e sua retroflexão, pela CCNE de fluxo de oeste, pela Corrente de Guiné (ARNAULT, 1987), e por parte da CSE que formam ou se juntam à CNB, fechando o giro (Figura 1) (LUMPKIN; GARZOLI, 2005). A circulação é ainda caracterizada por correntes profundas, apresentando estrutura vertical também bastante complexa. A bifurcação da Corrente Norte Equatorial (CNE) no HN é importante para alimentação tanto da CCNE quanto da Subcorrente Norte Equatorial (SCNE) (BOURLÈS*et al.*, 1999) (Figura 1). Além disso, a CNB e a sua componente subsuperficial, a Subcorrente Norte do Brasil (SCNB) alimentam correntes zonais que fluem para leste em latitudes e profundidades diferentes, como por exemplo, a Subcorrente Equatorial (SCE), centrada na termoclina, e a SCNE localizada abaixo da termoclina (SILVEIRA *et al.*, 1994; BOURLÈS *et al.*, 1999) (Figura 1). Como dito anteriormente, a CNE também contribui consideravelmente para a SCNE (Figura 1). Bourlès *et al.* (1999) obteve que o transporte médio do sistema CNB/SCNB é 22.1 ± 4.5 Sv, sendo 23.6 Sv no verão e 19.1 Sv no inverno. Ainda, o mesmo trabalho apontou que o sistema CCNE/SCNE possui transporte médio de 30.0 ± 7.3 Sv, sendo a diferença observada entre os dois diferentes sistemas devida à contribuição da CNE que, ao se retroflectar, alimenta o último. Outros estudos observaram que a SCBO, proveniente da região leste do Caribe também se junta à SCNE (JOHNS *et al.*, 1990; COLIN; BOURLÈS, 1994) (Figura 2).

Soma-se a toda complexidade da área a grande variação sazonal que as correntes do Atlântico Tropical apresentam. A CCNE e o ramo equatorial da CSE, por exemplo, apresentam máxima intensidade durante o inverno e primavera no HS (i.e. ~ junho-novembro) e enfraquecem no outono (RICHARDSON; WALSH, 1986; ARNAULT, 1987; RICHARDSON; REVERDIN, 1987). Da mesma forma, a CNB e a Corrente de Guiana também apresentam sazonalidade, com máximos também nos períodos de inverno e primavera no HS (RICHARDSON; WALSH, 1986; ARNAULT, 1987; JOHNS, *et al.*, 1998). Tais variações são ocasionadas pela sazonalidade em larga escala dos ventos alísios, influenciados primordialmente pela migração da ZCIT, com tais correntes atingindo o máximo quando a ZCIT está localizada na posição mais ao norte que possa alcançar (STRAMMA; SCHOTT, 1999).

O Atlântico Tropical é também caracterizado por ser uma região de grande ocorrência de furacões e ciclones tropicais. Por ser uma região tropical, apresentando alta Temperatura da Superfície do Mar (TSM), é de extrema importância o estabelecimento das características físicas da região, para previsão de possível intensificação ou não, além de como que a passagem de furacão pode afetar tal oceano. De fato, altas TSMs podem causar intensificação de Ciclones

Tropicais (CTs), além da passagem destas tempestades causarem um aprofundamento da camada de mistura, e diminuição da TSM, devido ao efeito de "*cold wake*" (CIONE; ULHLORN, 2003). Pasquero e Emanuel (2008) retrataram ainda o crescimento das anomalias de TSM na região a partir de 1950, indicando aumento de conteúdo de calor na superfície, fator crucial na intensificação de CTs. A máxima alteração de temperatura observada foi a 150m de profundidade, atingindo 0.65-0.7ºC de variação (PASQUERO; EMANUEL, 2008). Além disso, a dinâmica do Atlântico somado aos efeitos das suas piscinas quentes se mostrou também importante na taxa de precipitação e na intensificação de furacões na região (WANG *et al.*, 2006, HOUSON-GBO *et al.*, 2015). Outro fator primordial no Atlântico Tropical é a presença da pluma dos rios Orinoco e, principalmente, Amazonas. Acredita-se que tais plumas também sejam participantes nos eventos de intensificação de furacões por conta do efeito de camada de barreira (FFIELD, 2006). A descarga do Rio Amazonas, de fato, tem papel muito importante nesta bacia oceânica. Tal descarga do Amazonas já demonstrou ser influenciada pelos anos de ocorrência de El Niño Oscilação Sul (ENOS) (TYAQUIÇÃ *et al.*, 2017), além de ter capacidade de impactar a distribuição de nutrientes, microrganismos e fluxos de carbono (GOES *et al.*, 2014; ARAÚJO *et al.*, 2017). A seguir, há um maior detalhamento a respeito da CNB e, em seguida, o foco é direcionado aos vórtices desta corrente.

### 1.1.2 Corrente Norte do Brasil (CNB)

A CNB é uma intensa corrente de borda oeste de baixas latitudes no Atlântico Tropical, que flui na direção noroeste, transportando águas das camadas superiores dos oceanos que cruzam o equador (JOSEPH, 2013). Tem influência até aproximadamente 800m de profundidade, onde há a transição para a SCBO (JOHNS *et al.*, 1998), e seu surgimento tem origem na sCSE, que, ao atingir a região abaixo da ponta mais oriental do continente sul-americano, aproximadamente 10ºS, podendo variar de 8ºS em 100m até 20ºS em 500m de profundidade (VELEDA, 2008), posteriormente se bifurcando, dá origem à uma corrente fluindo à sul, a Corrente do Brasil, e uma fluindo à norte, a SCNB (Figura 1) (JOHNS *et al.*, 1998; LUMPKIN; GARZOLI, 2005; VELEDA *et al.*, 2012).

O ramo subsuperficial da CNB é mais conhecido como a SCNB, onde o sistema CNB/SCNB apresenta transporte médio anual de 22.1 ± 4.5 Sv, com o maior transporte concentrado no verão (BOURLÈS *et al.*, 1999). À medida que flui para norte, a CNB (antes uma corrente fraca e costeira) inicia um processo de intensificação, devido principalmente à contribuição da porção central da CSE em 4ºS (Figura 1) (LUMPKIN; GARZOLI, 2005). Tal

processo transfere o núcleo de máxima velocidade do sistema CNB/SCNB de 200m de profundidade para regiões superficiais, o que faz com que o sistema seja enfraquecido e haja total predominância da CNB em superfície (SCHOTT *et al.*, 1998). Contribui também para tal intensificação a confluência da porção norte da CSE entre 2-3ºN, que aceleram ainda mais a CNB (LUMPKIN; GARZOLI, 2005). Antes disso, ao cruzar a linha do equador, parte da CNB sofre retroflexão, originando e alimentando a SCE (LUMPKIN; GARZOLI, 2005).

Figura 1 – Padrão de circulação no Atlântico Tropical

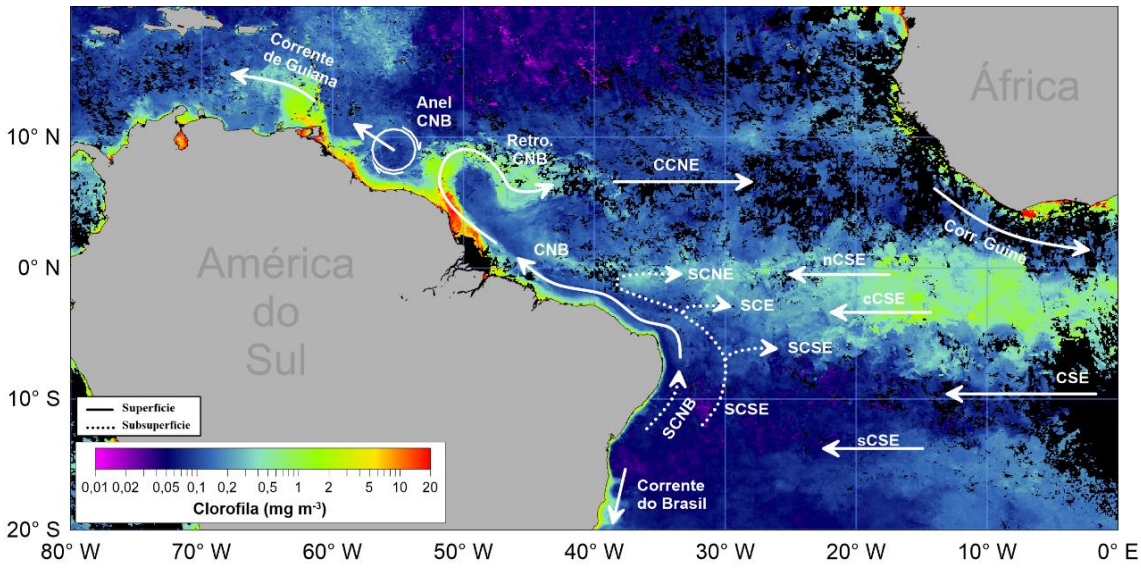


Fonte: O autor (2019)

Uma imagem de concentração de clorofila do MODIS/Aqua de 23 de setembro de 2003 foi utilizada para realçar os padrões de correntes. SCNB: Subcorrente Norte do Brasil; CNB: Corrente Norte do Brasil; SCNE: Subcorrente Norte Equatorial; SCE: Subcorrente Equatorial; SCSE: Subcorrente Sul Equatorial; CCNE: Contracorrente Norte Equatorial; nCSE: ramo norte da Corrente Sul Equatorial; cCSE: ramo central da Corrente Sul Equatorial; sCSE: ramo sul da Corrente Sul Equatorial.

A retroflexão intensifica a vorticidade do escoamento e pode, ocasionalmente, liberar grandes vórtices anticiclônicos de núcleo quente (DIDDEN; SCHOTT, 1993; JOHNS *et al.*, 2003). Tais vórtices são propagados para noroeste e são considerados a principal contribuição para a perenidade, ao longo da costa norte da América do Sul, da Corrente de Guiana, uma corrente que se estende abaixo da camada de Ekman influenciada pela CNB (LUMPKIN; GARZOLI, 2005). Lumpkin e Garzoli (2005) indicaram intensificação na corrente de Guiana associada à sazonalidade da retroflexão da CNB, onde a corrente se apresenta mais forte nos meses de ausência da retroflexão. A CNB tem papel fundamental em dois processos: o fechamento do giro equatorial gerado pelo regime de ventos, alimentando um sistema de Contracorrentes zonais (LUMPKIN; GARZOLI, 2005); e o favorecimento do transporte das

águas quentes superficiais do Atlântico do HS para o HN, sendo parte importante da CRMA (JOHNS *et al.*, 1998). Os vórtices relacionados à CNB são mais detalhados na próxima seção.

### 1.1.3 Vórtices da Corrente Norte do Brasil (VCNBs)

Vórtices oceânicos contribuem para distribuição de massas de água, sendo parte da circulação geral oceânica (OLSON, 1991). Desta forma, vórtices oceânicos, também chamados de anéis oceânicos, têm extrema importância no transporte e balanço global de energia, massa, calor, nutrientes, produtividade e ciclagem de elementos (OLSON, 1991; MCGILLICUDDY *et al.* 1998; BENITEZ-NELSON *et al.* 2007; VILLAS BÔAS *et al.*, 2015). Eles são geralmente associados às correntes de borda oeste, às instabilidades baroclínicas de correntes de larga escala, além de interações com topografia e forçantes atmosféricas (KAMENKOVICH *et al.*, 1986). Uma intensa corrente de borda oeste é a Corrente Norte do Brasil (CNB), a qual é considerada o padrão dominante da circulação em superfície no Atlântico Tropical Ocidental (Figura 1) (FRATANTONI; RICHARDSON, 2006).

A CNB flui predominantemente para noroeste ao longo da costa norte do Brasil e próximo de 6º N – 8º N e 45º - 50ºW, se separa da costa e retroflexiona para leste, alimentando a Contracorrente Norte Equatorial (CCNE) (Figura 1) (JOHNS *et al.*, 1990; JOHNS *et al.*, 2003; FONSECA *et al.*, 2004). Esta retroflexão intensifica a vorticidade do escoamento e pode, ocasionalmente, liberar grandes vórtices anticiclônicos de núcleo quente (DIDDEN; SCHOTT, 1993; JOHNS *et al.*, 2003), que são associados a subsidência de massas de água, anomalias positivas de Altura da Superfície do Mar (ASM) e aprofundamento da termoclina em seus núcleos (WILLIAMS; FOLLOWS, 2003; BAKUN, 2006).A retroflexão da CNB apresenta um ciclo sazonal associado com a migração da Zona de Convergência Intertropical (ZCIT) (FONSECA *et al.*, 2004). O deslocamento meridional da ZCIT faz com que os alísios de sudeste predominem de junho a novembro, desenvolvendo ao máximo a retroflexão nestes meses, enquanto que entre dezembro e maio a retroflexão é praticamente ausente (JOHNS *et al.*, 1998; GARZOLI *et al.*, 2004; LUMPKIN; GARZOLI, 2005). Além disso, estima-se que haja uma relação direta entre o volume transportado pela CNB e a latitude de penetração no HN que ela atinge. Quando este transporte é máximo, a máxima latitude de penetração também é alcançada e um vórtice quase sempre é liberado (GARZOLI *et al.*, 2003; GARZOLI *et al.*, 2004). Ou seja, quanto maior a latitude de penetração da retroflexão da CNB, maior é a chance de liberação de vórtice (GARZOLI *et al.*, 2003), indicando que os anos em que a CNB atingir mais vezes a sua máxima latitude seriam os anos com mais vórtices liberados. Os vórtices da CNB (aqui

denominados VCNBs) são liberados principalmente devido à pequena inclinação da costa da América do Sul entre 5ºN-8ºN (ZHARKOV; NOF, 2010).

O primeiro estudo que descreveu e identificou a presença dos vórtices dos VCNBs foi o realizado por Legeckis e Gordon (1982). Eles identificaram, através de dados de satélite de Temperatura da Superfície do Mar (TSM), a presença de anéis elípticos de núcleo quente que transladavam com velocidades variando entre 4-35km/dia (LEGECKIS; GORDON, 1982). Posteriormente, diversos trabalhos foram realizados com objetivos de analisar tais VCNBs (DIDDEN; SCHOTT, 1993; FRATANTONI *et al.* 1995; GONI; JOHNS, 2001; FRATANTONI; GLICKSON, 2002; JOHNS *et al.* 2003; FRATANTONI; RICHARDSON, 2006; JOCHUMSEN *et al.* 2010; CASTELÃO; JOHNS, 2011). Estes vórtices, tipicamente, apresentam um diâmetro médio de 400 km, máxima anomalia de ASM (aASM) de 5-30 cm (DIDDEN; SCHOTT, 1993; JOHNS *et al.* 2003; FRATANTONI; RICHARDSON, 2006), velocidades azimutais superficiais de 1 m/s e subsuperficiais de 15-20 cm/s, e podem se estender até profundidades maiores que 1000 m (JOHNS *et al.*, 1990; DIDDEN; SCHOTT, 1993; FRATANTONI *et al.*, 1995; FRATANTONI; GLICKSON, 2002; GONI; JOHNS, 2003, FRATANTONI; RICHARDSON, 2006). Os VCNBs se movem na direção noroeste, por 3 a 4 meses, em direção ao Mar do Caribe, com velocidade de translação de 7-20 km/dia, até atingir as Antilhas, onde começam a se dissipar (DIDDEN; SCHOTT, 1993; FRATANTONI *et al.*, 1995; FRATANTONI; GLICKSON, 2002; GONI; JOHNS, 2003; FRATANTONI; RICHARDSON, 2006; CASTELÃO; JOHNS, 2011). Estima-se que o número médio de vórtices por ano seja entre 3 e 7 (GONI; JOHNS, 2001; FRATANTONI; GLICKSON, 2002; GARZOLI *et al.*, 2003; GONI; JOHNS, 2003; JOHNS *et al.*, 2003; FRATANTONI; RICHARDSON, 2006; JOCHUMSEN *et al.*, 2010). Castelão e Johns (2011) apontaram para a presença de um "escudo dinâmico" nos VCNBs, gerado por uma vorticidade externa (positiva), inerente aos mesmos, de sentido oposto à interna (negativa), o que pode dificultar a fusão entre estes vórtices. Richardson *et al.* (2005) sugeriu que a interação entre os VCNBs com as ilhas Antilhas contribui na geração de outros vórtices anticiclônicos observados no arco de ilha a leste do Mar do Caribe. Ao atingir a região Caribenha, os vórtices causam alterações nos padrões de circulação local, além de gerarem variações nas salinidades superficiais e influenciarem na capacidade de recrutamento e crescimento de larvas planctônicas de peixes (COWEN; CASTRO, 1994; KELLY *et al.*, 2000; COWEN *et al.*, 2003). Por fim, os VCNBs são responsáveis pelo transporte de mais da metade do fluxo de calor da Célula de Revolvimento Meridional do Atlântico (CRMA) do HS para o HN (FRATANTONI *et al.* 2000; JOHNS *et al.*, 2003), sendo os mesmos também um dos principais mecanismos de transporte

de energia e massa do Atlântico Sul para o Atlântico Norte (FRATANTONI *et al.* 1995; FRATANTONI *et al.*, 2000; JOHNS *et al.*, 2003; CRUZ-GÓMEZ; SALCEDO-CASTRO, 2013).

### 1.1.4 $CO_2$ no Atlântico Tropical

O Atlântico Tropical, em geral, apresenta-se como uma região fonte de $CO_2$ para a atmosfera (LEFÈVRE *et al.*, 1998). Este fato está relacionado principalmente à ressurgência equatorial, processo que traz águas subsuperficiais ricas em $CO_2$ para a superfície, aumentando a saturação em superfície de carbono nesta região (LEFÈVRE *et al.*, 1998). Além disso, Andrié *et al.* (1986) perceberam no local um aumento na fugacidade de $CO_2$ ($fCO_2$), ou seja, a pressão parcial de $CO_2$, com um aumento de temperatura de leste a oeste nesta bacia oceânica. De fato, Takahashi *et al.* (1993) observou, considerando as demais variáveis constantes, uma taxa de aumento de $fCO_2$ no oceano de 4%/ºC. No entanto, percebem-se áreas de baixíssimas concentrações de carbono no Atlântico Tropical relacionadas à dispersão da pluma do Amazonas (KÖRTZINGER, 2003; COOLEY *et al.*, 2007; LEFÈVRE *et al.* 2010; LEFÈVRE *et al.* 2017). De fato, a pluma do Rio Amazonas tem grande influência na costa nordeste da América do Sul, no Mar do Caribe e no Oceano Atlântico Equatorial, especialmente em relação a fatores como: deposição e erosão costeira (FROIDEFOND *et al.*, 2002); aumento da biomassa fitoplanctônica e produtividade primária (SMITH; DEMASTER, 1996); distribuição de microorganismos (ARAÚJO *et al.*, 2017), aporte de nutrientes e, especialmente, sequestro de carbono (KÖRTZINGER, 2003; COOLEY *et al.*, 2007; LEFÈVRE *et al.* 2010; LEFÈVRE *et al.* 2017). O Amazonas é o rio que possui a maior descarga global e conta por 20% da entrada fluvial nos oceanos, além de ser responsável por quase metade de toda entrada de água doce no Atlântico Tropical Norte (CARTON, 1991). Tal descarga do Amazonas já demonstrou apresentar sazonalidade, com a maior descarga ocorrendo nos períodos de chuva, além de também ser influenciada pelos anos de ocorrência de ENOS (TYAQUIÇÃ *et al.*, 2017).

Diferentes fatores, como a salinidade, temperatura, pH e produtividade primária contribuem para que a pluma do Rio Amazonas seja caracterizada como uma região subsaturada de $CO_2$. Diversos trabalhos apontaram a salinidade como principal fator de controle da taxa fluxo de $CO_2$, onde quanto menor a salinidade, maior a captação de carbono pelos oceanos (KÖRTZINGER, 2003; LEFÈVRE *et al.* 2010; LEFÈVRE *et al.* 2017; LEFÈVRE *et al.* 2020). Este fato deve-se às menores salinidades em regiões oceânicas estarem associadas à diminuição da turbidez estuarina, aumento de nutrientes e consequente aumento de produção primária.

Ternon *et al.* (2000) estimaram que a produtividade primária na pluma do Rio Amazonas é responsável por 30% do consumo de $CO_2$ do Atlântico Tropical. Adicionalmente, a produtividade primária líquida na pluma do Rio Amazonas reduz em mais de cem vezes a concentração de $CO_2$na mesma (COOLEY *et al.*, 2007). Ainda, Lefèvre *et al.* (2020) indicaram que a diminuição de $fCO_2$ está associado com um pico moderado de clorofila na bóia 8ºN, 38ºW depois de 2 meses de transporte da água do rio. A Figura 1 ilustra altas concentrações de clorofila que podem ser observadas na foz do Amazonas. Além disso, Cooley *et al.* (2007) indicaram que as diversas condições sensíveis ao clima (como temperatura, ventos e precipitação), que controlam a dinâmica do rio, a solubilidade do $CO_2$, e a troca gasosa é que são responsáveis por tornar a pluma do Amazonas como sumidouro de carbono.

Há anos tentam-se estabelecer relações entre vórtices e balanço de carbono nos oceanos (MOURIÑO *et al.*, 2003). Mais recentemente, outros trabalhos foram desenvolvidos com o objetivo de avaliar os impactos da hidrodinâmica de vórtices em fluxos de $CO_2$ e a contribuição dos mesmos para o fluxo global dos oceanos (SONG *et al.*, 2016; ORSELLI *et al.*, 2019). De fato, demonstrou-se a importância dessas estruturas na modulação dos processos de oceano-atmosfera na trocas de gases. Vórtices de mesoescala apresentaram papel fundamental nestes processos na Passagem de Drake, no Oceano Austral, onde, no verão, vórtices anticiclônicos/ciclônicos eram capazes de captar mais/menos $CO_2$ que as águas adjacentes, respectivamente; enquanto que no inverno o oposto ocorria, os vórtices anticiclônicos/ ciclônicos liberavam mais/menos para a atmosfera, respectivamente (SONG *et al.*, 2016). Já Orselli *et al.* (2019) mostrou que vórtices anticiclônicos provenientes da corrente de Agulhas, que cruzam o Atlântico em direção à América do Sul, representam regiões pontuais de sumidouros de $CO_2$, podendo também contribuir para uma rápida acidificação da Água Central do Atlântico Sul (ACAS). Mouriño *et al.* (2003), por outro lado, identificaram que vórtices subtropicais no nordeste do Atlântico contribuíram menos de 1% para a produção líquida total da região, indicando pouca influência nos fluxos biogeoquímicos neste local. Mais recentemente, a TSM se mostrou como principal responsável na mudança de vórtices anticiclônicos de sumidouros para fontes $CO_2$ de para atmosfera na Confluência Brasil-Malvinas (PEZZI *et al.*, 2021). Desta forma, observa-se que os processos que afetam os fluxos de $CO_2$ no núcleo dos vórtices são bastante dinâmicos, estando os mesmos sujeitos às variações e particularidades de cada região.

Ffield (2005) observou que os VCNBs intensificados superficialmente não envolviam a pluma do Amazonas, e sim as águas tropicais da NBC, ficando a água menos salina apenas nos limites circundantes aos vórtices. Por outro lado, vórtices com maior intensidade em

profundidade conseguiram superficialmente capturar águas menos salinas (FFIELD, 2005). Desta forma, estima-se que o conhecimento da dinâmica do vórtice em questão e do ambiente que o contorna é também capital para os processos biogeoquímicos nos centros destes vórtices. Neste contexto, a análise da variabilidade espaço-temporal dos vórtices e suas características físicas são, de fato, cruciais para a melhor compreensão de aspectos de circulação global e dos processos físicos e biogeoquímicos responsáveis pela variabilidade do $CO_2$ no Atlântico Tropical Noroeste. Por fim, o estudo se mostra importante para o monitoramento espacial do balanço de $CO_2$ no Atlântico Tropical e, por consequência, na contribuição dos VCNBs nos fluxos de $CO_2$ em escala global.

No presente trabalho, o papel dos VCNBs nos fluxos de $CO_2$na região do Atlântico Tropical Noroeste foi analisado. Para tal, aplicou-se o algoritmo AMEDA às diferentes bases de dados de reanálise, afim de se realizar: um estudo de 24 anos da variação da dinâmica intra e interanual dos VCNBs e o papel da fusão nas características dos mesmos; um outro estudo com o objetivo de avaliar os impactos de alguns vórtices específicos nos fluxos de $CO_2$ entre oceano e atmosfera, apontando também para uma possível sazonalidade de tais impactos biogeoquímicos nessa região. No Capítulo 2 deste documento, detalha-se a metodologia aplicada neste trabalho.

## 1.2 OBJETIVOS

### 1.2.1 Geral

O objetivo principal deste trabalho é entender o papel dos Vórtices da Corrente Norte do Brasil na modulação dos fluxos de $CO_2$ do Atlântico Tropical Norte Ocidental.

### 1.2.2 Específicos

- Estudar a variabilidade espaço temporal e as características físicas dos VCNBs;
- Avaliar eventos específicos de formação e, principalmente, de fusão de VCNBs, concluindo com os possíveis impactos dessas interações vórtice-vórtice;
- Avaliar os impactos dos VCNBs nos fluxos totais de $CO_2$ entre oceano e atmosfera na região;

- Concluir estudos de caso para se obter mais detalhes a respeito da influência dos VCNBs nos fluxos de $CO_2$ em escalas sazonal e interanual.

# 2 METODOLOGIA

## 2.1 ÁREA DE ESTUDO

O presente trabalho teve como área de estudo uma região específica do Atlântico Tropical Ocidental, limitadas latitudinalmente entre 5º S - 15º N e longitudinalmente entre 45º W - 65º W (Figura 2). Tais limites foram selecionados com o objetivo de tornar a análise de geração e evolução dos VCNBs mais detalhada, haja vista que dentro destes limites ocorre a retroflexão da CNB (6º - 8º N e 45 - 48º W) e a consequente liberação dos vórtices. Além disso, é importante destacar que na área de estudo a presença das desembocaduras dos rios Amazonas (0,5º N; 50,5º W) e Orinoco (9,5º N; 61,5º W) (Figura 2) já demonstraram ser importantes para o a região de diversas formas (SMITH; DEMASTER, 1996; FROIDEFOND *et al.*, 2002; KÖRTZINGER, 2003; LEFÈVRE *et al.*, 2010), além de se relacionarem com os vórtices da CNB (FFIELD, 2005).Reitera-se aqui o papel de fonte de $CO_2$ que o Atlântico Tropical possui (LEFÈVRE *et al.*, 1998), enquanto que as regiões das plumas dos rios, especialmente a do Amazonas, estão relacionadas com sumidouro de carbono atmosférico (KÖRTZINGER *et al.*, 2003; COOLEY *et al.*, 2007).

Figura 2 – Área de Estudo delimitada e representação esquemática de um vórtice desprendido da retroflexão da CNB (círculo branco)

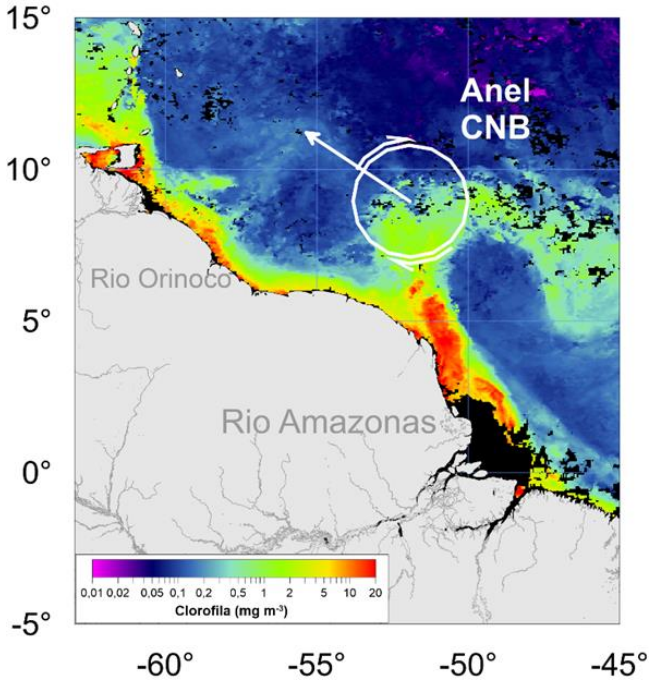


Fonte: cedido por Pedro Tyaquiçã (2019).

Uma imagem de concentração de clorofila do MODIS/Aqua de 23 de setembro de 2003 foi utilizada para realçar o padrão do VCNB além da foz dos rios Orinoco e Amazonas.

## 2.2 BASE DE DADOS

### 2.2.1 Dados de reanálise ARMOR 3D

Neste estudo foram utilizadas 24 anos (janeiro de 1993 - dezembro de 2016) de dados de reanálise semanais de altura absoluta da superfície do mar (m), e das componentes geostróficas zonais (u) e meridionais (v) a 50 m de profundidade das correntes (m/s), com resolução espacial de ¼º (0,25º).Estes dados, obtidos do *Global Observed Ocean Physics Temperature Salinity Heights and Currents Reprocessing* - ARMOR3D L4 (GUINEHUT *et al.*, 2012; MULET *et al.*, 2012), foram utilizados com o objetivo de detectar a ocorrência espaço-temporal dos VCNBs. Esta base de dados é desenvolvida através da combinação de dados de ASM, TSM, e salinidade, e dados *in situ* de perfis verticais de temperatura e salinidade, apresentando um campo 3D semanal de temperatura, salinidade e velocidade geostrófica (Verbrugge *et al.*, 2017). ARMOR 3D está disponível no CMEMS web portal (http://marine.copernicus.eu/services-portfolio/accessto-products/, ID do produto: MULTIOBS_GLO_PHY_REP_015_002) com a nova versão 4, atualizada em abril 2018. O produto usado no presente trabalho foi da versão 3 (ID do produto: GLOBAL_REP_PHYS_001_021). Além da análise da variabilidade espaço-temporal dos VCNBs, o ARMOR3D foi também útil para observação dos perfis verticais de temperatura e salinidade no centro dos VCNBs, e para avaliação dos impactos (especialmente na termoclina) que o movimento de subsidência de águas apresenta nestes locais. Ainda, a frequência semanal e resolução espacial de ¼º permitiu a caracterização dos vórtices da CNB, haja vista que são estruturas de mesoescala (de centenas de quilômetros), e a análise da variabilidade dos mesmos em longo prazo.

### 2.2.2 Modelo Mercator

O estudo sobre a contribuição dos VCNBs para a variabilidade espacial de variáveis biogeoquímicas, baseou-se na análise de anomalias de médias mensais dos dados diários do projeto Mercator Ocean (www.mercator-ocean.fr) através do modelo físico GLORYS12v1 (resolução espacial de 1/12º, e vertical de 50 níveis) e do modelo biogeoquímico BIORYS2V4 (resolução espacial de ¼º, e vertical de 75 níveis). A simulação do Mercator Ocean é baseada na plataforma de modelagem NEMO (Nucleus for European Modelling of the Ocean), possuindo uma cobertura global no período de 1993-2019.O componente biogeoquímico

PISCES (AUMONT *et al.*, 2015) é acoplado offline ao componente hidrodinâmico NEMO em uma frequência diária. Ambos os componentes são forçados por campos atmosféricos do ERA-Interim. O modelo biogeoquímico está disponível no catálogo do Copernicus Marine Service (product GLOBAL_REANALYSIS_BIO_001_029). Detalhes de tal simulação estão descritos no Quality Information Document (http://marine.copernicus.eu/documents/QUID/CMEMS-GLO-QUID-001-029.pdf). O modelo hidrodinâmico está disponível sob requerimento no balcão de atendimento do Mercator Ocean. Além disso, os dados diários dos modelos foram diretamente utilizados de forma a se realizar uma análise mais aprofundada da estrutura física e, especialmente, do impacto biogeoquímico destes vórtices nas águas em que os mesmos atuam.

## 2.3 ANÁLISES

### 2.3.1 Métodos de identificação de vórtices

Diversas metodologias foram utilizadas para identificação de vórtices e determinação de seus centros com eficácia. Inicialmente, foram utilizadas metodologias baseadas ou em características geométricas do campo de velocidade geostrófica ou em mapas de altimetria da superfície do mar. Um dos primeiros trabalhos que divulgou e aplicou uma destas metodologias foi o de McWilliams (1990), que utilizou a vorticidade relativa para identificação dos centros dos vórtices. Este método foi melhorado através da utilização de análise de ondeleta no campo de vorticidade (DOGLIOLI *et al.*, 2007). Muito se usou também o parâmetro de Okubo-Weiss (OW), que quantifica a importância relativa da rotação em relação à deformação, através de dados de corrente geostrófica (ISERN-FONTANET *et al.*, 2004; CHELTON *et al.*, 2007; CHAIGNEAU *et al.*, 2008). Assumindo que um vórtice coerente seria caracterizado por linhas de correntes fechadas ou espirais, outros trabalhos utilizaram apenas as características geométricas do campo de velocidade geostrófica na identificação de vórtices (SADARJOEN; POST, 2000; NENCIOLI *et al.* 2010). Mais recentemente, outras metodologias começaram a se destacar pelo seu caráter híbrido: considerando tanto os aspectos geométricos quanto os físicos dos vórtices (HALO *et al.* 2014; YI *et al.* 2014; MKHININI *et al.*, 2014). Estas, no entanto, utilizavam o OW para detecção de possíveis centros de vórtices, com exceção de Mkhnini *et al.* (2014). Este introduziu um novo parâmetro: o Momento Angular Local Normalizado (MALN), ou seja, o valor da integral do momento angular em uma área restrita. Este parâmetro será detalhado na seção 2.3.2. Atualmente, os algoritmos híbridos se tornaram

ainda mais eficazes com a inserção da identificação de eventos específicos de separação ou fusão de vórtices (LI *et al.,* 2014; LE VU *et al.*, 2018). Desta forma, os melhoramentos nas metodologias utilizadas para identificação de vórtices permitem a caracterização dos principais parâmetros dinâmicos destas estruturas, entre eles: velocidade azimutal máxima, raio de máxima velocidade azimutal, número de Rossby; além da identificação dos eventos de interação vórtice-vórtice, seja de fusão ou separação.

Através do *Angular Momentum Eddy Detection and Tracking Algorithm* (AMEDA) (LE VU *et al.*, 2018), um algoritmo híbrido, será realizada a identificação de ocorrência e da variabilidade espaço-temporal dos VCNBs neste estudo. Com o AMEDA, pode-se analisar os momentos de gênese, crescimento, intensificação, trajetória, fusão e separação dos vórtices, além dos parâmetros obtidos para cada vórtice formado. O AMEDA possui as seguintes propriedades, de acordo com Le Vu *et al.* (2018): algoritmo com parâmetros ajustáveis e robustos à diferentes resoluções espaço-temporais; facilidade de validação do algoritmo, haja vista que o cálculo de propriedades dos vórtices permite a comparação direta com dados in situ; identificação dos eventos de fusão e separação de vórtices, permitindo o acompanhamento com precisão da evolução dinâmica dos mesmos. Diversos trabalhos utilizaram recentemente este algoritmo. Iouannou *et al.* (2017) aplicou o mesmo para o estudo de Ierapetra eddies no Mar Mediterrâneo, enquanto que Garreau *et al.* (2018) usou a ferramenta para monitorar a trajetória de um vórtice anticiclônicos na bacia da Argélia. Por fim, o AMEDA foi utilizado também para estudo global dos vórtices (DE MAREZ *et al.*, 2020). O algoritmo será detalhado a seguir, na seção 2.3.2.

### 2.3.2 AMEDA

Destaca-se aqui os dois passos principais do AMEDA: a identificação dos centros dos vórtices e a determinação de sua trajetória. Para a identificação dos centros dos vórtices, o algoritmo se baseia em dois critérios: critério dinâmico e critério geométrico. Para o primeiro, AMEDA utiliza um método proposto por Mkhinini *et al.* (2014), que, ao invés de utilizar o OW, que é um parâmetro vastamente utilizado para identificação de centros de vórtices a partir de dados do campo de velocidade geostrófico (CHELTON *et al.*, 2007; CHAIGNEAU *et al.*, 2008), utiliza outro parâmetro dinâmico, o Momento Angular Local Normalizado (MALN), ou seja, o valor da integral do momento angular em uma área restrita. O MALN será 1 para os centros dos vórtices ciclônicos e -1 para os centros de vórtices anticiclônicos. Este parâmetro não depende da intensidade do vórtice e é utilizado para a distinção entre pontos hiperbólicos

(MALN alto) e pontos elípticos (MALN igual a zero) (LE VU *et al.*, 2018). Como o valor de MALN não é suficiente para garantir pontos de centros de vórtices realmente capazes de prender massas de água (LE VU *et al.*, 2018), o critério geométrico também é utilizado. Este último é baseado nas linhas dos campos de correntes e considera um ponto como o centro de um vórtice somente se os valores de MALN característicos de vórtices coincidirem com linhas de correntes fechadas ao seu redor. Ou seja, que as linhas de velocidade sejam invertidas quando cruzarem o centro do vórtice e que as direções dos vetores de velocidade mudem com um senso de rotação, onde vetores de velocidades vizinhos devem estar no mesmo quadrante ou em quadrantes adjacentes (NENCIOLI *et al.*, 2010). A determinação das trajetórias dos vórtices, por sua vez, é baseada na pesquisa a cada passo de tempo dos vórtices que estavam presentes no passo de tempo anterior. Para isso, AMEDA utiliza o método do Vizinho Local mais próximo, que consiste em associar, para cada centro de vórtice detectado em determinado passo, o outro mais próximo de mesmo sinal detectado no passo anterior em determinada área. Desta forma, o Algoritmo foi capaz tanto de identificar os centros dos vórtices, quanto em indicar suas prováveis trajetórias.

É importante destacar, no entanto, que análises criteriosas foram realizadas em cada passo de tempo (em cada semana) para a verificação de tais trajetórias e da duração dos vórtices. Além disso, ressalta-se que as configurações padrões dos parâmetros, utilizadas por Le Vu *et al.* (2018), foram praticamente mantidas, com exceção do *Rlim* (i.e. máximo tamanho do contorno característico do vórtice). Devido à problemas na identificação dos vórtices, os idealizadores do AMEDA (Briac Le Vu e Alexander Stegner) sugeriram uma alteração do *Rlim*, antes estabelecido como *Rlim=5Rd*, para *Rlim=10Rd*, sendo *Rd* o raio de deformação de Rossby do primeiro modo baroclínico na área de estudo. O *Rd* utilizado foi o analisado por Chelton *et al.* (1998) e é definido como a escala horizontal em que os efeitos rotacionais se tornam mais importantes do que efeitos de flutuação e gravidade. (NURSER; BACON, 2014). Nurser e Bacon (2014) também o definem como a escala horizontal do relaxamento geostrófico. O AMEDA também diferencia os momentos em que *Rmáx* (i.e. o raio correspondente à maior velocidade azimutal) (LE VU *et al.*, 2018) é maior que o raio do vórtice e o momento em que ambos os raios são praticamente semelhantes. Além disso, há também diferenciação entre vórtices ciclônicos e anticiclônicos.

A aASM para cada semana foi calculada da seguinte maneira:

$$aASM(x, y, t) = ASMs(x, y, t) - ASMm(x, y, s) \quad (1)$$

Onde: *ASMs* é a altura absoluta da superfície do mar para determinado ponto de determinada semana, *ASMm* é a média de *ASMs* obtida para cada ponto na semana específica de cada mês dos 24 anos observados, e *x*, *y*, *t*, *s* são a latitude, longitude, o passo de tempo e a semana específica do mês de cada centro de vórtice identificado, respectivamente. Ou seja, a *aASM* da 1ª semana de janeiro de 1993 será o *ASMs* desta semana menos o *ASMm* das primeiras semanas de janeiro de 1993-2014.

A partir do funcionamento do Algoritmo, com os vórtices identificados em cada tempo específico, passaram a ser computados os parâmetros para cada vórtice. Para cada VCNB foi escolhida uma semana específica para se ter tais parâmetros. Os parâmetros contados nesta semana representam cada vórtice específico, e, portanto, a semana a ser computada deve ser escolhida atentamente. O critério para a escolha da semana em que os parâmetros do vórtice seriam computados foi a principal assinatura em superfície dos vórtices, ou seja, a assinatura de *aASM*. Desta forma, os momentos de máxima *aASM* identificados nos centros dos vórtices (além de seus parâmetros) foram selecionados para representar os vórtices. Além disso, consideraram-se apenas os anéis liberados pela CNB que cruzaram a linha de 55ºW. Pequenas turbulências com durações menores que duas semanas e raios inferiores à 30 km na área de estudo, ocasionalmente, também eram consideradas vórtices pelo AMEDA. Acredita-se que tais dimensões turbulentas possam corresponder às ondas de Rossby, e, portanto, não foram consideradas como verdadeiros vórtices da CNB. De fato, ondas de Rossby provenientes do Leste também são incidentes na região, influenciando na dinâmica dos vórtices, mas na escala turbulenta. (Fratantoni and Richardson, 2006; Jochum and Malanotte-Rizzoli, 2003).

Através deste método foram computados os parâmetros representativos de cada vórtice. Foram analisados 3 parâmetros diretamente do AMEDA, sendo eles: *Vmáx*, *Rmáx*, *EC*. *Vmáx* indica a máxima velocidade azimutal (i.e. velocidade rotacional, ou seja, a velocidade do corpo em torno de seu próprio eixo), e é dado em metros por segundo (m/s). *Rmáx*, que já foi definido anteriormente, é também definido como o raio do círculo da mesma área com contorno fechado de aASM que apresentou máxima velocidade geostrófica média (MASON *et al.*, 2014). *Rmáx* é dado em quilômetros (km). *EC* é a energia cinética de cada vórtice, dada em metro ao quadrado por segundo ao quadrado ($m^2/s^2$).

Outro parâmetro foi obtido indiretamente do Algoritmo: o número adimensional de Rossby para os vórtices, *Ro*, que relaciona os efeitos de advecção e rotação em um vórtice (VANDENBROUCK *et al.*, 2000). Para os cálculos de *Ro*, utilizou-se também o *f*, o parâmetro de Coriolis para cada vórtice, também retirados do AMEDA, de forma que o número de Rossby foi calculado como a razão entre a força inercial e a força de Coriolis:

$$Ro = \frac{Vmáx}{fRmáx} \quad (2)$$

*Ro* representa força da rotação aplicada em relação aos termos não-lineares, comparando a importância da vorticidade relativa em relação à planetária, e possui valores na ordem de *Ro* ~$10^{-2}$, por exemplo, para um fluido geofísico, que apresenta larga dimensão espacial, e é fortemente influenciado por Coriolis (VANDENBROUCK *et al.*, 2000). *Ro* para vórtices anticiclônicos, é, por definição, negativo, em relação ao sentido de rotação (CASTELÃO; JOHNS, 2011). Observa-se que os vórtices anticiclônicos ao redor do globo possuem valores médios de *Ro* por volta de -0.1 (OLSON, 1991). No entanto, para este estudo, foi considerada apenas a magnitude tanto de *Vmáx* quanto de *Ro*, onde todos os valores indicativos de tais parâmetros estão representados em módulo. AMEDA já foi utilizado por trabalhos anteriores para a computação do número de Rossby (GARREAU *et al.*, 2018; DE MAREZ *et al.*, 2020). A*aASM* foi também computada para cada centro de vórtice encontrado. Desta forma, os parâmetros analisados inicialmente foram: *Vmáx*, *Rmáx*, *EC*, *Ro*, *aASM*. Os resultados observados para estas análises estão detalhados no Capítulo 3, enquanto que as análises para o Capítulo 4 são detalhadas nas próximas seções 2.3.3 e 2.3.4.

### 2.3.3 Funções Ortogonais Empíricas (EOFs) e Análise de Ondeleta

A partir dos dados diários do modelo Mercator, foram calculadas as anomalias mensais, que posteriormente, foram analisadas através das Funções Ortogonais Empíricas (EOFs). EOF é uma técnica estatística capaz de extrair características espaço-temporais inerentes à base de dados (WILKS, 1995). EOF se apresenta como uma ferramenta poderosa na decomposição de grandes bases de dados que variam no tempo e no espaço, e para a identificação dos modos dominantes. A técnica decompõe a matriz covariância em modos, representando a variabilidade no espaço e no tempo (WILKS, 1995). Os principais componentes estão associados com padrões espaciais para cada modo, representando a evolução com o tempo.

Como forma de representar os VCNBs na análise de EOF, o parâmetro de Okubo-Weiss foi calculado através de dados das correntes oceânicas como descrito por ISERN-FONTANET *et al.* (2004). Este parâmetro, como citado anteriormente, quantifica a importância da rotação em relação à deformação (ISERN-FONTANET *et al.*, 2004; CHELTON *et al.*, 2007; CHAIGNEAU *et al.*, 2008) e é definido como:

$$OW = s_n^2 + s_s^2 - \omega^2 \quad (3)$$

onde $s_n$, $s_s$ e ω são as componentes da velocidade, de cisalhamento da deformação, e a vorticidade relativa do fluxo, respectivamente, definidas como:

$$s_n = \frac{du}{dx} - \frac{dv}{dy} \quad (4)$$

$$s_s = \frac{dv}{dx} + \frac{du}{dy} \quad (5)$$

$$\omega = \frac{dv}{dx} - \frac{du}{dy} \quad (6)$$

onde um OW negativo indica que a vorticidade domina, e positivo a deformação domina.

Além disso, outra técnica aplicada no presente trabalho foi o método da Ondeleta/Ondeleta-Cruzada, que permite a detecção de sinais temporais na frequência e no domínio do tempo, detectando os sinais principais (VELEDA *et al.*, 2012). A análise de Ondeleta também identifica a periodicidade associada ao sinal, enquanto que a Ondeleta-Cruzada indica a periodicidade em que dois sinais apresentam covariância comum. Por fim, a análise de coerência de Ondeleta é um método para detecção de coerências significativas entre duas séries temporais no domínio de frequência do tempo (GRINSTED *et al*, 2004).

### 2.3.4 Estudo de Caso

A partir da visão geral apresentada pelas análises estatísticas, um estudo de caso foi realizado para o ano de 2009 (Figura 3) de forma a entender como os VCNBs podem afetar as variáveis envolvidas em tais estruturas, tanto em superfície quanto em profundidade, e, consequentemente, o fluxo de $CO_2$ entre oceano e atmosfera. Para tal, dados diários de correntes zonais e meridionais do GLORYS12v1 foram também aplicados ao AMEDA para a identificação dos VCNBs escolhidos como estudos de caso. As parametrizações utilizadas aqui foram as mesmas descritas anteriormente na seção 2.3.2. Posteriormente, a evolução em superfície e da estrutura vertical diária de cada vórtice ao transladar, e o consequente comportamento físico e biogeoquímico dos mesmos, foi avaliada. Dados do modelo físico do Mercator foram escolhidos para esta análise, em detrimento dos dados do ARMOR3D, devido aos primeiros apresentarem maior resolução espacial (1/12º x 1/4º, respectivamente) e temporal (diário e semanal, respectivamente), o que permitiria uma análise mais robusta, especialmente

em relação aos estudos de caso. Além disso, os dados do ARMOR3D se resumem às correntes geostróficas, e já foi demonstrado que ao assumir a presença de balanço geostrófico em um vórtice, há uma subestimação da velocidade azimutal do mesmo (DOUGLASS & RICHMAN, 2015). Desta forma, os dados de correntes do Mercator seriam mais indicados para esta análise mais minuciosa. Na próxima seção, detalham-se como os cálculos dos fluxos de $CO_2$ foram realizados no presente estudo.

### 2.3.5 Cálculo do fluxo de $CO_2$

Para análise das trocas de $CO_2$ entre oceano e atmosfera é necessário estimar a fugacidade (i.e. pressão parcial, indicado por $fCO_2$) do gás nos dois diferentes ambientes ($fCO_{2\,SW}$ e $fCO_{2\,ATM}$, respectivamente). Para o cálculo do primeiro, utilizaram-se dados superficiais diários e médias mensais de temperatura, salinidade, carbono inorgânico dissolvido (DIC), alcalinidade total (TA), silicato e fosfato, que foram aplicadas à ferramenta do CO2SYS (LEWIS; WALLACE, 1998; PIERROT *et al.*, 2006) no *matlab*, para se obter $fCO_{2\,SW}$. Para tal, utilizou-se a constante de dissociação de Merhbach *et al.* (1973), renovada por Dickson e Millero (1987).

O método de cálculo de $fCO_{2\,ATM}$ utilizado neste trabalho foi extensamente descrito por Ibánhez *et al.* (2017) e Lefèvre *et al.* (2017). Para o cálculo do $fCO_{2\,ATM}$ foram utilizados dados mensais e semanais de fração molar de $CO_2$ atmosférico ($xCO_2$) provenientes da rede NOAA GMD Carbon Cycle Cooperative Global Air Sampling Network (DLUGOKENCKY *et al.*, 2020), disponibilizados na NOAA/ESRL Global Monitoring Division (http://www.esrl.noaa.gov/gmd/dv/data), para a estação de Barbados (13.17ºN, 59.43ºW) (ID do produto: CO2_RPB_surface-flask_NOAA_ccgg). Através de dados de salinidade e TSM do modelo GLORYS12V1, $pH_2O$ (ou seja, pressão de vapor de água em 100% de umidade) foi medida. O coeficiente de fugacidade (C) foi calculado através de Weiss (1974). Desta forma, tendo P como a pressão atmosférica, o $fCO_{2\,ATM}$ foi calculado seguindo a equação:

$$fCO2_{ATM} = xCO_2\,(P - pH_2O)\,C \tag{7}$$

O fluxo de $CO_2$ (mmol $m^{-2}$ $d^{-1}$) entre oceano e atmosfera foi estimado baseando-se na ferramenta do *matlab* disponibilizada por Chapa (2020), que utiliza a seguinte equação:

$$F = kS(fCO2_{SW} - fCO2_{ATM}) \tag{8}$$

onde k (cm $h^{-1}$) é a velocidade de transferência de gás, e S ($molL^{-1}atm^{-1}$) a solubilidade deste gás (WEISS, 1974). Um fluxo positivo indica que o oceano é uma fonte de $CO_2$ para a atmosfera, enquanto que fluxos negativos indicam o oceano como sumidouro de $CO_2$, removendo carbono da atmosfera. Os fluxos e fugacidades de $CO_2$ foram calculados tanto em resoluções diárias quanto em mensais.

O k, por sua vez, é parametrizado em função da velocidade do vento (SWEENEY *et al.*, 2007) e o número adimensional de Schmidt, Sc (WANNINKHOF, 2014). Para tal, foram utlizados dados de reanálise diários e mensais da velocidade do vento a 10m ($U_{10}$) do ECMWF ERA5 (European Centre for Medium-Range Weather Forecasts), disponível em Copernicus Climate Change Service (C3S) (http://cds.climate.copernicus.eu/), aplicados a seguinte equação:

$$k = 0{,}27 \times U^2 \times 600/S_c \times 0{,}5 \quad (9)$$

# 3 ARTIGO 1 - INTRA- AND INTER-ANNUAL VARIABILITY OF NORTH BRAZIL CURRENT RINGS USING ANGULAR MOMENTUM EDDY DETECTION AND TRACKING ALGORITHM: OBSERVATIONS FROM 1993 TO 2016

**Citar como:** Aroucha, L.C.; Veleda, D.; Lopes, F. S.; Tyaquiçã, P.; Lefèvre, N.; Araujo, M. (2020). *Intra- and Inter-Annual Variability of North Brazil Current Rings using Angular Momentum Eddy Detection and Tracking Algorithm: Observations from 1993 to 2016,* **Journal of Geophysical Research: Oceans,** v.125, ed.12, https://doi.org/10.1029/2019JC015921

O primeiro artigo produto desta dissertação foi publicado pelo *Journal of Geophysical Research: Oceans*, volume 125, edição 12, https://doi.org/10.1029/2019JC015921. O mesmo trata de uma investigação da variação intra- e interanual da variabilidade dos vórtices da Corrente Norte do Brasil em 24 anos (1993-2016), através de um algoritmo híbrido de identificação de vórtices, estimando os impactos desta variabilidade em parâmetros dinâmicos de tais estruturas e em aspectos físicos da coluna d'água. A partir desse trabalho pode-se observar efeitos da dinâmica dos vórtices no perfil vertical de salinidade em seus centros, através do movimento de subsidência de águas, além de ser observada certa variação sazonal nas características (estimadas por parâmetros dinâmicos) de tais estruturas. Por fim, mostrou-se que eventos de fusão de vórtices na região podem significativamente aumentar a energia cinética dos mesmos. O presente trabalho tem como autores: Léo C. Aroucha[1,2,3], Dóris Veleda[1,2], Francis S. Lopes[1,2], Pedro Tyaquiçã[4], N. Lefèvre[4], e Moacyr Araujo[1,5]

[1]*Laboratory of Physical, Coastal and Estuarine Oceanography – LOFEC, Federal University of Pernambuco – UFPE, Recife, Brazil. leo_aroucha@hotmail.com*

[2]*Renewable Energy Center – CER, Federal University of Pernambuco – UFPE, Recife, Brazil,*

[3]*Department of Oceanography - UFPE, Cidade Universitária, Recife, Brazil,*

[4]*LOCEAN, IRD, Sorbonne Université Paris, Paris, France,*

[5]*Center for Risk Analysis and Environmental Modeling – CEERMA, Federal University of Pernambuco – UFPE, Recife, Brazil*

O artigo completo publicado está inserido no Anexo.

## 3.1 INTRODUCTION

The North Brazil Current (NBC) is an intense western boundary current, which is the dominant feature of the surface circulation in the Western Tropical North Atlantic (WTNA). It flows predominantly northwestward along Brazilian northern coast and, around 6°N–8°N and 45°W, the current separates from the coast and retroflects to the east, feeding the North Equatorial Countercurrent (NECC) (GARZOLI *et al.*, 2003; JOHNS *et al.*, 1990). This retroflection, which is related to the seasonal migration of the Intertropical Convergence Zone (ITCZ) (FONSECA *et al.*, 2004), can occasionally shed large anticyclonic rings, that are associated with positive anomalies of sea surface height (SSH) in their centers, traveling northwestward until colliding with the Lesser Antilles (DIDDEN & SCHOTT, 1993; FRATANTONI & RICHARDSON, 2006; JOCHUMSEN *et al.*, 2010; JOHNS *et al.*, 2003). The NBC retroflection is most developed between June and February and is nearly absent from March to May (JOHNS *et al.*, 1998). However, other mechanisms, rather than the meandering current, were proposed to explain NBC rings generation. Ma (1996) and Jochum and Malanotte-Rizzoli (2003) showed that equatorial Rossby waves that propagate westward and reflect at the Brazilian coast could generate these eddies. Moreover, they intensify when traveling northwestward due to the conservation of the potential vorticity (JOCHUM & MALANOTTE-RIZZOLI, 2003). The south American coastline inclination between 5°N and 8°N was shown to be important for ring generation (ZHARKOV & NOF, 2010). NBC rings are crucial in the interhemispheric transport of mass and heat in the Atlantic, being an essential part of the meridional overturning circulation (MOC) (FRATANTONI *et al.*, 2000; JOHNS *et al.*, 2003). Furthermore, they contribute to the dispersion of fresh nutrient-rich waters from the Amazon River toward the Caribbean (JOHNS *et al.*, 1990), also affecting local circulation, that influences planktonic fish larvae recruitment and growth (COWEN *et al.*, 2003). Given the importance of those rings, their study and record of their parameters are a key to the comprehension of physical and biogeochemical processes in the WTNA.

The first study that described the presence of the NBC rings was done by Legeckis and Gordon (1982). They used satellite sea surface temperature (SST) data to identify elliptical warm-core rings that move northwestward with velocities from 4 to 35 km/day (LEGECKIS & GORDON, 1982). In the following years, a number of studies contributed to the understanding of NBC rings dimensions and dynamics (DIDDEN & SCHOTT, 1993; FRATANTONI *et al.*, 1995; JOHNS *et al.*, 1990; PAULUHN & CHAO, 1999; RICHARDSON *et al.*, 1994), especially after the 1998–2001 NBC Ring Experiment (FRATANTONI & GLICKSON, 2002;

GARRAFFO *et al.*, 2003; GARZOLI *et al.*, 2003; GONI & JOHNS, 2001, 2003; JOHNS *et al.*, 2003). Those rings present typically a mean radius of 200 km, SSH anomaly of 30 cm, surface and subsurface azimuthal velocity of 1 m/s and 15–20 cm/s, respectively, and can reach over 1,000 m deep (DIDDEN & SCHOTT, 1993; FRATANTONI *et al.*, 1995; FRATANTONI & GLICKSON, 2002; FRATANTONI & RICHARDSON, 2006; GARRAFFO *et al.*, 2003; GONI & JOHNS, 2003; JOCHUMSEN *et al.*, 2010; JOHNS *et al.*, 2003; PAULUHN & CHAO, 1999). NBC rings travel with an average propagation speed of 8–15 km/day toward the Caribbean, for 3–4 months, until interacting with the Antilles, where they start to coalesce (DIDDEN & SCHOTT, 1993; FRATANTONI *et al.*, 1995; FRATANTONI & GLICKSON, 2002; FRATANTONI & RICHARDSON, 2006; GARZOLI *et al.*, 2003; JOHNS *et al.*, 1990; RICHARDSON *et al.*, 1994). It is estimated that on average 3–7 rings are detached from NBC per year (FRATANTONI *et al.*, 1995; FRATANTONI & GLICKSON, 2002; FRATANTONI & RICHARDSON, 2006; GARZOLI *et al.*, 2003; Jochumsen *et al.*, 2010; JOHNS *et al.*, 1990; MÉLICE & ARNAULT, 2017), yet some works indicated a rate of 8–9 rings/year (GARRAFFO *et al.*, 2003; JOHNS *et al.*, 2003). Although a lot is known about NBC rings dynamics, only few works performed a long-term study (JOCHUMSEN *et al.*, 2010; MÉLICE & ARNAULT, 2017; SHARMA *et al.*, 2009). Moreover, it is crucial to establish and understand the change of ring parameters and how they evolve through seasons and years to evaluate, for example, if there is a seasonal or year-to-year variation that could indicate periods of higher intensity, energy, or SSH anomaly.

Several methodologies were used to efficiently identify eddies and determine their centers and parameters. Initially, methodologies were based either on the geometric velocity fields of geostrophic currents or in altimetry maps of sea surface. Posteriorly, the methods started to be based on dynamical parameters. McWilliams (1990) was one of the firsts to use relative vorticity for eddy identification. This method was improved over the use of wavelet analysis on the vorticity field (DOGLIOLI *et al.*, 2007). Other parameter widely used was the Okubo-Weiss (OW), which quantifies the importance of rotation in relation to strain through geostrophic current data (CHAIGNEAU *et al.*, 2008). On the other hand, other works utilized only the geometry of the geostrophic velocity field for eddy identification, assuming these structures as coherent vortex if characterized by closed contour current lines (NENCIOLI *et al.*, 2010; SADARJOEN & POST, 2000). More recently, hybrid methodologies which consider both geometric and physical aspects (i.e., OW parameter) of eddies began to stand out (HALO *et al.*, 2014; YI *et al.* 2014). Mkhinini *et al.* (2014) introduced the local normalized angular momentum (LNAM), a new dynamical parameter for eddy detection, which represents the

normalized value of the angular momentum in a restricted area. This value will reach its extremum in the center of a solid core rotation (LNAM = +1 for cyclonic eddies and LNAM = −1 for anticyclonic). Currently, hybrid algorithms have become even more effective with the possibility of identification of eddy interaction through merging and splitting events (LE VU *et al.*, 2018; LI *et al.*, 2014). Therefore, the improvement on the methodologies used for eddy identification and tracking allows the characterization of the main dynamical parameters of these structures, such as: maximum azimuthal velocity (Vmax), speed-based radius (Rmax), and Rossby number (Ro), apart from the events of eddy interaction.

The angular momentum eddy detection and tracking algorithm (AMEDA) (LE VU *et al.*, 2018), will be used in this study for the identification of NBC rings occurrence, trajectories, and physical parameters. The main goal of this work is to apply the AMEDA, using SSH and geostrophic currents field data, in order to investigate the intra- and inter-annual variability of NBC rings occurrence and parameters. Also, an event of rings merging will be detailed in terms of parameters change, and identified trajectories will be commented. The significance of studying eddy merging and splitting events relies on the fact that these events are able to change eddy characteristics. Indeed, ring interaction can alter significantly eddy size, energy, and SSH signal, and the main cause of their occurrence are current-eddy-topography interactions and current variation (CUI *et al.*, 2019). Furthermore, the study goes through the previously results observed in published articles on NBC rings, for comparison with this AMEDA analysis. The study is organized as follows: in Section 2 the database and the study area are explored. The application of the data to AMEDA is described and the parameters measured are defined. In Section 3 we highlight the inter- and intra-annual variability of NBC rings, emphasizing how changes are observed in terms of their parameters. We also describe how vertical temperature and salinity profile change within eddies, and analyze the 4 observed merging events between two NBC rings with tracking identified by AMEDA. Finally, our results are compared with previous studies. Conclusion is presented in Section 4.

## 3.2 DATA AND METHODS

### 3.2.1 Database and Study Area

The data set used in this study consists of 24 years (January/1993–December/2016) of absolute SSH (i.e., geopotential height) and the components of the geostrophic current fields taken from “Global Observed Ocean Physics Temperature Salinity Heights and Currents

Reprocessing"—ARMOR 3D, with ¼° spatial resolution (e.g., GUINEHUT *et al.*, 2012; MULET *et al.*, 2012; BUONGIORNO NARDELLI *et al.*, 2016). This database results from the combination of sea level anomaly (SLA), SST, and sea surface salinity (SSS) data and in situ T, S vertical profiles measurements, presenting a global 3D weekly temperature, salinity, geostrophic velocities fields (VERBRUGGE *et al.*, 2017). ARMOR 3D is available at Copernicus Marine Environment Monitoring Service (CMEMS) web portal (http://marine.copernicus.eu/services-portfolio/accessto-products/, product id: MULTIOBS_GLO_ PHY_REP_015_002) with the newest Version 4, updated in April 2018. The product used here was the Version 3 (product id: GLOBAL_REP_PHYS_001_021). The domain of this work is restricted to the region 15°N–5°S, 63°W–45°W, which includes NBC retroflection area (ring generation), Amazon and Orinoco Rivers mouths, and the Lesser Antilles (ring demise). Indeed, NBC rings seems also to interact with Amazon and Orinoco waters (FFIELD, 2005; RUDZIN *et al.*, 2017). In addition, radiating Rossby waves from the east also reach this region, influencing ring dynamics (FRATANTONI & RICHARDSON, 2006; JOCHUM & MALANOTTE-RIZZOLI, 2003). We used data from 50 m deep, in order to reduce the surface signal of equatorial Rossby waves and also as an attempt to identify subsurface rings with a negligible surface signal. Finally, sea surface height anomaly (SSHa) were calculated based on the 24 years data. Taking the anomalies can filter the seasonal signal, that dominates the tropical Atlantic Ocean (ARNAULT & CHENEY, 1994), allowing a better analysis of intra-annual variability.

### 3.2.2 Detection Algorithm and Measured Parameters

The AMEDA (LE VU *et al.*, 2018) was used. It is a hybrid algorithm, based not only on dynamical parameters, but also on geometrical properties of the velocity field. In AMEDA, while the extremum LNAM (dynamical) indicates eddy centers, the closed streamlines (geometrical) indicates eddies boundaries, characterizing a structure as an eddy only if the grid point corresponds for both constraints (LE VU *et al.*, 2018). For eddy tracking, the algorithm uses the local nearest neighbor (LNN) method (LE VU *et al.*, 2018) and it also has the capacity to identify merging and splitting events. AMEDA has been used in a few works in the last years. Ioannou *et al.* (2017) applied this algorithm for the study of Ierapetra Eddies on the Mediterranean Sea, while Garreau *et al.* (2018) used the tool for tracking an anticyclonic eddy in the Algerian Basin.

The geostrophic velocities from ARMOR 3D were applied to AMEDA for ring identification, tracking, interaction with neighboring eddies, and for computation of their parameters. The first baroclinic Rossby radius of deformation (Rd) was calculated for each grid point, based on Chelton *et al.* (1998). This radius is defined as the length scale of geostrophic stretching, and at the equator Rd values are typically in scales of hundreds kilometers (CHELTON *et al.*, 1998; NURSER & BACON, 2014). Although a ¼° data set grid was used, the combination with the calculated Rd values is expected to be enough for normal functioning of AMEDA, since it is a robust algorithm for different space–time resolutions, and with tuneable parameters (LE VU *et al.*, 2018). Only the NBC rings that were clearly detached from the NBC retroflection and that crossed 55°W were taken into account in this analysis. Moreover, we maintained the default AMEDA configuration of excluding the eddies between the 5°N and 5°S equatorial band, since the NBC retroflection and rings trajectory are still further north. For each week of a ring occurrence, several parameters were measured. These parameters constantly varied from week to week and from ring to ring. Therefore, the week of maximum SSHa was chosen to be the representative for the rings. The parameters analyzed were: lifetime (weeks), Rmax (km), Vmax (m/s), Ro, KE (cm2 /s2), and SSHa (in cm). Ring lifetime corresponds to the number of weeks that the ring was identified by AMEDA. Rmax (in kilometers) indicates the radius of the closed streamlines corresponding to the module of the maximum azimuthal velocity (Vmax, in m/s). Ro is the dimensionless Rossby number defined as: Ro = Vmax/(f Rmax), where f is the Coriolis parameter at ring latitude. Ring kinetic energy (KE) is calculated from the geostrophic velocity field, is defined as KE = (uˆ2 + vˆ2)/2, and represents the mean KE for all the grid points within each ring. Finally, as previously cited, SSH anomalies were taken based on the 24 years data, providing the SSHa parameter.

## 3.3 RESULTS AND DISCUSSION

### 3.3.1 Observed Variability of NBC Rings Shedding Rates

It is important to initially highlight that this is the first study to apply an eddy detection algorithm for 24 years period in the NBC region. Although other works have also analyzed decadal time-series in NBC rings generation (JOCHUMSEN *et al.*, 2010; MÉLICE & ARNAULT, 2017), they did not used an eddy identification tool based on dynamical and geometrical constraints, identifying the NBC rings only by statistical analysis of sea level anomalies (MÉLICE & ARNAULT, 2017), or based on velocity fields of the modeled data

(JOCHUMSEN *et al.*, 2010). In the analyzed 24 years period, 121 NBC rings were observed to detach from the NBC retroflection and cross the 55°W longitude line. It provides an average shedding rate of five rings per year. The results for each year are presented in Figure 1a. Overall, previous studies estimate a rate from 2 to 9 rings per year, which varies according to the period covered and the method used by the study (e.g., DIDDEN & SCHOTT, 1993; GARZOLI *et al.*, 2003; JOCHUMSEN *et al.*, 2010; JOHNS *et al.*, 1990, 2003; MÉLICE & ARNAULT, 2017; SHARMA *et al.*, 2009). The comparison with other works, allow us to say that AMEDA results are reasonable. In fact, the ring shedding rate here obtained varied from a maximum of eight rings/year in 2005 to a minimum of three rings/year in 2006 (Figure 1a). However, the present study underestimated the average shedding rate when comparing with few others which pointed for a 7–9 rings/year average (JOHNS *et al.*, 2003; JOCHUMSEN *et al.*, 2010). This fact is thought to be mainly due to the presence of subsurface NBC rings, which present the maximum velocity signal at 200 m and no apparent surface signal (GARRAFFO *et al.*, 2003). Because the present work used only 50 m depth velocity fields data, possibly some subsurface NBC rings were not identified by AMEDA. Furthermore, Goni and Johns (2001), using altimeter data, identified 34 anticyclonic eddies from October 1992 to December 1998. In this study, which started to count from 1993, 29 NBC rings were identified from 1993 to 1998. In addition, 18 NBC rings were observed using ocean color imagery from September 1997 to September 2000 (FRATANTONI & GLICKSON, 2002), while we identified 16 NBC rings in the same period. Using in situ data from moorings and ship cruises, the NBC Rings Experiment (GARZOLI *et al.*, 2003; GONI & JOHNS, 2003; JOHNS *et al.*, 2003) found one ring in November/December 1998, two rings from February/March 1999, and one ring in June/2000. In the present work, we identified the presence of all of these rings in the periods cited. The generation dates and parameters of all the 121 identified rings in this study are summarized in Supporting Information (Table 3.S1). More recently, some works preceded in longer time series for NBC ring identification. Sharma *et al.* (2009) using drifting buoys, ADCP and satellite data identified 44 NBC rings in 8 years, with maximum shedding rates in 2005 and 2007, what is consistent with what was found in this study. Jochumsen *et al.* (2010) analyzed from the FLAME model all the NBC ring types generation in 15 years, indicating a shedding rate ranging from 4 to 8 rings/ year. In addition, the recent study from Mélice and Arnault (2017), using satellite altimeter and empirical mode decomposition, presented a mean rate of five rings generated by year, similar to the present study. Finally, although previous studies demonstrate some differences in the inter-annual ring generation rates, the similarities observed between them and the present work indicate AMEDA algorithm robustness and

efficiency for ring surveillance, since it identified the presence of NBC rings quite similarly to other studies using different methods. It is thought that when applying current velocity data from greater depths rather than only surface fields, the algorithm will also be able to recognize rings of larger subsurface signal.

Figure 1 – (a) Number of North Brazil Current (NBC) rings which crossed 55°W observed per year. (b) NBC rings seasonal climatology generated for 24 years period. Both (a) and (b) compare our results with Mélice and Arnault (2017) and Jochumsen *et al.* (2010)

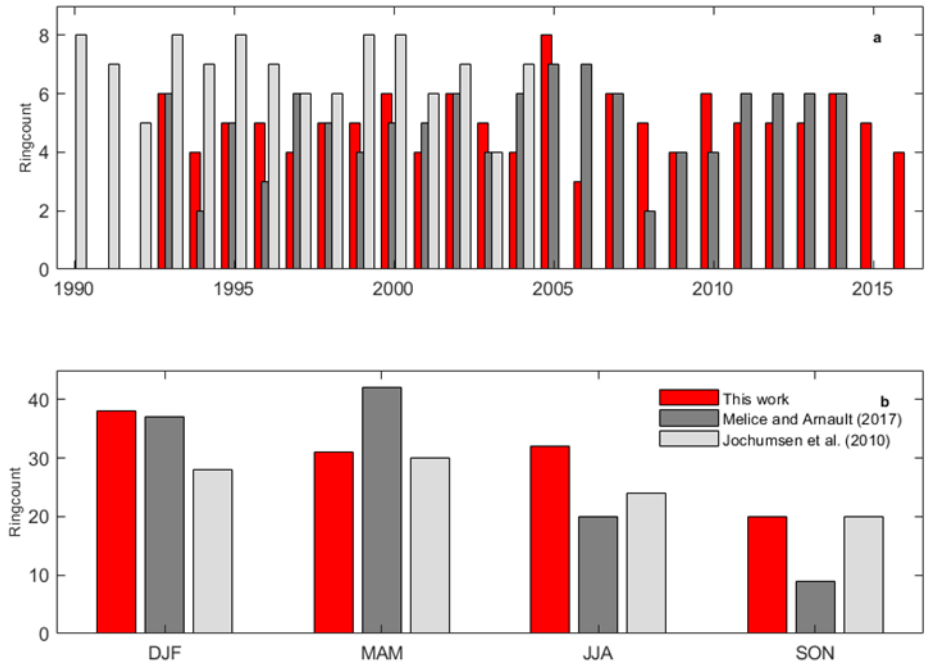


Source: the authors (2020).

Moreover, it is possible to notice a considerable year-to-year variability in NBC ring generation. This rate remained between 4 and 6 rings/year, (Figure 1a), in exception from 2005 to 2006, where the maximum and minimum ring frequency, respectively, was observed. Sharma *et al.* (2009) theorized a biannual pattern in NBC ring generation rates, where alternate years present a gap in ring formation during late spring and early summer. Therefore, it seems that the maximum number of NBC rings generated in 2005 was compensated by the lower generation rate in the following year. The year 2005 has maximum shedding rates and appears to be followed by a steady cycle of ring formation and migration (SHARMA *et al.*, 2009). It is still not clear which mechanisms drive this inter-annual variability on NBC ring generation. However, few works have pointed possible reasons for it, such as: penetration latitude (i.e., distance between the northernmost point of the retroflection and the arbitrary location of 0°S, 42°W) of NBC retroflection (GARZOLI *et al.*, 2003) and the influence of large-scale transport processes in Atlantic Basin (GONI & JOHNS, 2003). Garzoli *et al.* (2003) indicated that almost

every time NBC retroflection reaches its northernmost position, a ring is detached, although no clear seasonality is observed in NBC latitude of penetration. In addition, Goni and Johns (2003) speculated at least a weak relationship between ring generation and Northern Tropical Atlantic Index, based on possible links between ocean temperature variation and NBC rings shedding rate. Lastly, Sharma *et al.* (2009) indicated that ITCZ and forcing by trade winds are not the main factors influencing ring formation and migration. It is believed that several mechanisms might impact NBC rings generation, and further studies could highlight these relationships.

The results obtained for the ring generation as a function of the season are described in Figure 1b. We show that rings are formed in all months of the year, with a maximum ring generation in February, followed by March, June, and July. The minimum generation rate, in its turn, was observed in September-October-November trimester (SON) (Figure 1b). Those results agree with what was found in the literature, using different methods. Fratantoni *et al.* (1995) compared the modeled rings with observations from Richardson *et al.* (1994). They showed a maximum generation period from October to March, with the highest observation ring frequency in November and February, and the maximum modeled frequency in February, April, and May. Goni and Johns (2001) presented December and January as the months of greatest ring liberation. However, they have in 2003 pointed for different months as maximum (i.e., February and June) (GONI & JOHNS, 2003), which the latter agrees most with the current paper. Those previously cited works (FRANTANTONI *et al.*, 1995; GONI & JOHNS, 2001, 2003) presented minimum generation rate from July to October, which is in agreement with the smaller generation in August and September observed in the present study. October 2016 was the only month in the analyzed period, which was characterized by more than one ring shed (Table 3.S1).

The NBC ring maximum generation occurred from December to February (Figure 1b), while a minimum was observed from September to November. The December-January-February (DJF) trimester was responsible for 31.40% of NBC rings genesis in the 24 years, while 25.62% and 26.45% of rings were shed for March-April-May (MAM) and June-July-August (JJA) trimesters, respectively. It was verified a 47.37% reduction in ring generation rate between maxima (winter) and minima (fall) trimesters. Goni and Johns (2001) presented similar results using TOPEX altimetry data, with a maximum generation in boreal winter (DJF) and minimum in early boreal fall (SON), although from September to November the generation rate is quite the same as the previous months (MAM and JJA). On the other hand, Fratantoni and Glickson (2002) showed that the higher frequency of generation occurs from March to May, with equivalent frequency in the other trimesters. Also, Jochumsen *et al.* (2010) and Mélice and

Arnault (2017) presented similar results on the number of rings generated per trimester, with the highest frequencies at spring (MAM) and minimum at fall (SON). According to Fratantoni and Glickson (2002), no particular seasonality is detected in NBC ring generation and that the observed variations in the results of those studies are most likely to be due to different methodologies. Seasonality appears to be evident but inconsistent between successive years (SHARMA *et al.*, 2009). Therefore, from the present and previous studies, it is possible to clearly identify the trimester of the minimum generation rates, which evolves the months of September, October, and November, and that NBC rings appear to be more frequent in the first half of the year.

### 3.3.2 NBC Rings Parameters

Figure S1 indicates the frequency distribution of the parameters for each identified ring. Those parameters were obtained at the time step corresponding to the week of maximum SSHa. The parameters of all the 121 identified rings in this study are summarized in Table S1. The NBC rings presented an average lifetime of 15.3 (±5.4) weeks, with the higher frequency of lifetimes between 10 and 18 weeks (Figure S1a). The last identified rings in October 2016 (i.e., R120 and R121) were not considered as they were not entirely vanished by the end of 2016, so their lifetime could not be determined. The maximum ring duration was 31 weeks, and the minimum, 4 weeks. These results are in agreement with previous studies (GONI & JOHNS, 2001; RICHARDSON *et al.*, 1994). Indeed, Goni and Johns (2003) verified through satellite altimetry that NBC rings remain an average of 3.5 months in the region, with this time ranging from 2 to 5 months. Besides, Fratantoni and Richardson (2006), using floats and drifters, pointed for a lifetime ranging from 1 to 6 months, with an average of 3.3 months. The importance of ring lifetime relies on how long the vortex dynamics is able to trap the parcel of water within it. The length scale of the ring, Rmax ranged from a minimum of 87.3 km to a maximum of 204.8 km, with an average radius of 139.5 (±23.6) km. NBC rings were more frequent with Rmax ranging from 120 to 160 km (Figure S1b). In general, other works on NBC rings indicate a similar length scale, with diameters varying from 150 to 400 km (CASTELÃO & JOHNS, 2011; DIDDEN & SCHOTT, 1993; FRATANTONI *et al.*, 1995; FRATANTONI & GLICKSON, 2002; FRATANTONI & RICHARDSON, 2006; GONI & JOHNS, 2003; JOCHUMSEN *et al.*, 2010; RICHARDSON *et al.*, 1994). These length scales of hundreds of kilometers imply a considerable water mass transport along the northern Brazilian coast. It is estimated that an annual transport of 9.3 Sv by NBC rings, which represents an essential part

of the MOC return flow (JOHNS *et al.*, 2003). A mean SSHa of 9.4 (±4.0) cm was detected with a maximum value of 24.0 cm. The higher frequency observed was around 5–15 cm of SSHa (Figure S1f). Those results are consistent with those found in the literature. Didden and Schott (1993) found a 4 cm SSH variability associated with NBC rings, while Goni and Johns (2001) presented an average SSH residue of 8 cm. More recently, maximum surface elevation related to NBC rings was pointed to range around 20–30 cm (CASTELÃO & JOHNS, 2011; CRUZ-GÓMEZ & SALCEDO-CASTRO, 2013). Moreover, the lowest observed value for SSHa was 1.1 cm, which might indicate that this study could also identify NBC rings with small surface signal, such as subsurface rings. However, to trustworthily classify NBC rings it is necessary to have a vertical picture of its dynamics, including thermocline and maximum velocity depths. Then, since the present work is based only on SSHa values and a 1-level velocity database, NBC ring classification goes beyond the scope of this study.

Figure 2 – Monthly variation of the measured North Brazil Current rings parameter during the 24 years analysis: Ring lifetime (a), Rmax (b), Vmax (c), Rossby number (d), Kinetic Energy (e), SSH anomaly (f). The central red mark is the median, the edges of the box are the 25th and 75th percentiles, the whiskers extend to the most extreme datapoints, and individual red crosses are outliers

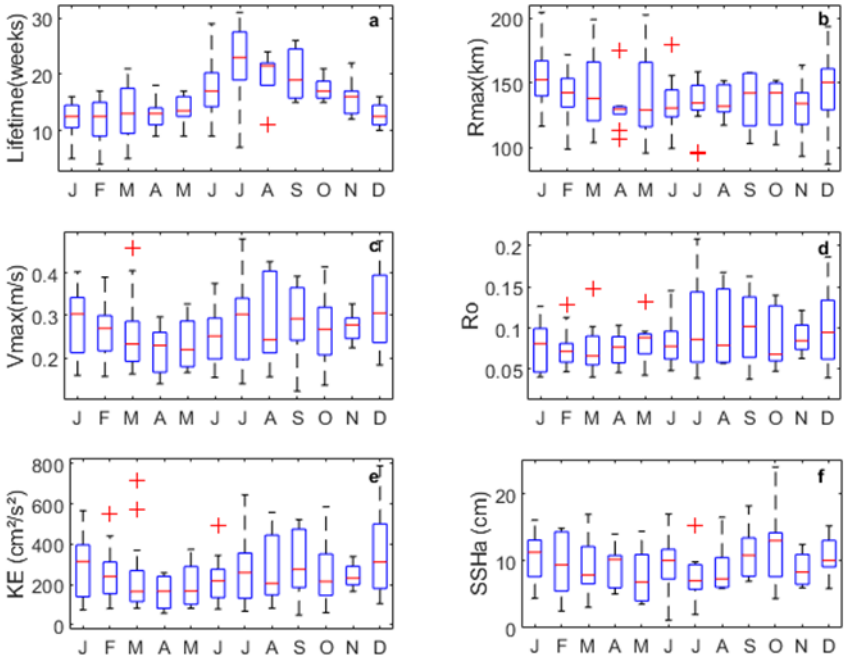


Source: the authors (2019).

The frequency of the maximum azimuthal velocity values (Vmax) computed from the NBC rings indicate a higher occurrence of rotational velocities from 20 to 30 cm/s (Figure 2c). The mean Vmax is 0.27 (±0.08) m/s, while the maximum and minimum are 0.48 m/s and 0.12 m/s, respectively. Previous works indicate that NBC rings swirl velocity vary from 12 to

84 cm/s (FRATANTONI *et al.*, 1995; FRATANTONI & RICHARDSON, 2006; RICHARDSON *et al.*, 1994). However, more recent studies established that Vmax could be even higher than 115 cm/s (CASTELÃO & JOHNS, 2011; CRUZ-GÓMEZ & SALCEDO-CASTRO, 2013). The reduced Vmax found in this study might be explained by several reasons. First, the week of maximum SSHa does not necessarily correspond to the time step of maximum Vmax. Then, it is possible that the values of Vmax are not the maximum rotational velocities that a ring reached during its lifetime. In addition to this, when using geostrophic velocities fields and assuming geostrophic balance within an eddy, its azimuthal velocity might be underestimated due to the negligence of inertial components of momentum balance (DOUGLASS & RICHMAN, 2015). Hence, Vmax values seemed to be underestimated in the present study. In addition to this, it is believed that the cyclogeostrophic force terms are important in disrupting eddy characterization from geostrophy in eddies with $Ro > 0.3$ (DOUGLASS & RICHMAN, 2015). It seems from the literature that NBC rings Ros are on the threshold of these values, in a way that only geostrophy might not characterize NBC rings perfectly. Moreover, Iouannou *et al.* (2019) indicated the need of ageostrophic corrections for mesoscale anticyclones which exceeds $Ro > 0.15$. Hence, aiming to quantify the amplitude of the ageostrophic velocity component, we performed velocity corrections for NBC rings with Ro equals or exceeding 0.15, based on the methodology of Ioannou *et al.* (2017). Results for velocity profiles corrections and percentual increase in Vmax for each of the eight analyzed rings are indicated in Figure S2 and Table S2, respectively. We verified a 30.0% average increase in cyclogeostrophic Vmax for those rings. Plus, the Pearson correlation index between Ro and Vmax increases for each ring ($p = 0.929$), showing the proportional increase in cyclogeostrophic Vmax in relation to a larger Ro, as expected and indicated by Ioannou *et al.* (2019). Although in this study only a few rings exceed $Ro > 0.15$, it is clear that ageostrophic corrections for rings with large Ro are indeed not negligible for reliable Vmax estimation.

Ro compares the importance of relative to planetary vorticity, and their values are variable around the globe. The high Ro values observed for the NBC rings region are due to the proximity of equator, an area of minimal Coriolis parameter. In this study, NBC rings presented an average Ro of 0.08 (±0.04) (Figure S1d), and maximum and minimum values of 0.21 and 0.04, respectively. Overall, it is expected that Ro values for anticyclones are negative. Yet, as we used the module of Vmax to measure Ro, only positive values were found. AMEDA has already been used for Ro computation (DE MAREZ *et al.*, 2020; GARREAU *et al.*, 2018). The definition of Ro in the present work is the vortex Ro, which is based on maximal azimuthal velocity, and was also used by Fratantoni *et al.* (1995) and Castelão and Johns (2011).

However, we highlight that various definitions of Ro exists and were applied for the NBC rings. Richardson et al (1994) and Cruz-Gómez and Salcedo-Castro (2013) defined Ro based on the core angular velocity (Ro (2) = Ω0/f, Ω0 = V (R)/R when R ≅ 0). For a Gaussian vortex, V(r) = Vmax/Rmax r e^ ((1 − r 2 /[Rmax2]/2), we get Ro (2) = 1.64*Ro. From the Ro definition, studies observed values between 0.13 and 0.26 (FRATANTONI *et al.*, 1995), and mean absolute Ro of 0.33 for the NBC region (CASTELÃO & JOHNS, 2011). From Ro (2) values shifted from 0.20 to 0.36 (RICHARDSON *et al.*, 1994; CRUZ-GÓMEZ & SALCEDO-CASTRO, 2013). Even though the 1.64 factor from Ro (2) to Ro, the values here obtained for Ro were still smaller than the ones cited in the literature using both definitions. As occurred for Vmax, the use of purely geostrophic fields generated this underestimation. Douglass and Richman (2015) using the core vorticity Ro definition (Ro (3) = ζ0/f, for a Gaussian vortex Ro (3) = 3.3*Ro) indicated that ageostrophic corrections in Vmax are needed for vortex Ro > 0.09. Here, we performed these corrections only for rings with Ro > 0.15, as previously cited (Figure S2 and Table S2), based on Ioannou *et al.* (2019). Table S2 also indicated the corrected cyclogeostrophic Ro for the eight analyzed rings.

Figure 3 – Year to year variability of the measured North Brazil Current rings parameters from 1994 to 2016. In exception, panel (a) only until 2015. Ring lifetime (a), Rmax (b), Vmax (c), Rossby number (d), Kinetic Energy (e), SSH anomaly (f). The central red mark is the median, the edges of the box are the 25th and 75th percentiles, the whiskers extend to the most extreme datapoints, and individual red crosses are outliers

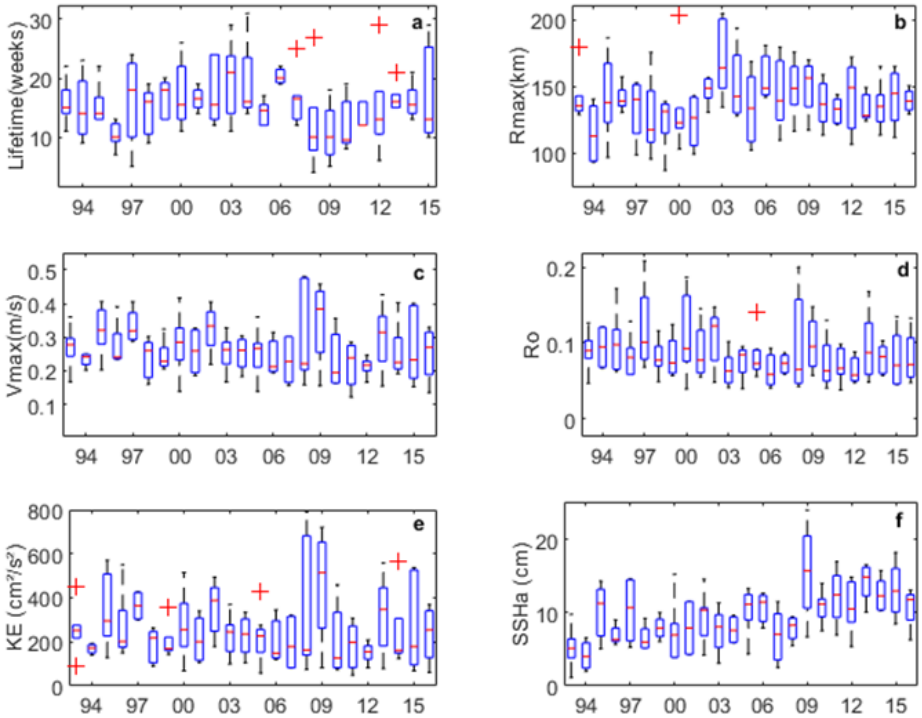


Source: the authors (2019).

Finally, the NBC rings KE in the present study varied from a minimum of 49.53 cm2 /s2 to a maximum of 789.93 cm2 /s2, with the highest frequency of rings with KE around 100–300 cm2 /s2 (Figure S2e). The average kinetic energy observed was 255.30 (±154.81) cm2 /s2. These results are in agreement with Didden and Schott (1993), who presented similar geostrophic NBC rings KE, changing from 100 to 300 cm2 /s2. The increased standard deviation represents significant changes in rings KE, indicating that rings shed by the NBC present diverse dynamical characteristics from ring to ring.

In order to investigate the seasonal variation of NBC rings characteristics, the variability of their parameters is plotted as a function of the month for the 24 years (Figure 2). All months were characterized, at least in one year, by a NBC ring formation. NBC rings last less in boreal winter and have an increased lifetime in boreal summer, especially from July to August (Figure 2a). Although boreal summer months presented higher variability from minimum to maximum values, the median lifetime for these months is still higher than the others. On the other hand, Rmax median values are increased in boreal winter (Figure 2b), even though a weak seasonal variability is observed. Sharma *et al.* (2009) also found low seasonal amplitude in NBC rings dimensions, with increased rings from October to March. Also, Ro and SSHa values did not present any clear seasonal variability (Figures 2d and 2f). In contrast, Vmax and KE show the highest median values in boreal winter months (Figures 2c and 2e). Vmax slightly increases in boreal summer, reaching a maximum in July. Similar behavior can be observed for KE. Didden and Schott (1993) associated KE changes in the NBC rings region with ring activity and the seasonal retroflection circulation, which, respectively, generated KE peaks in winter and a secondary summer maximum. More KE is available within NBC retroflection (SHARMA *et al.*, 2009). Therefore, Vmax and KE follow NBC retroflection seasonality. The maximum strength of NBC retroflection in boreal summer (RICHARDSON & WALSH, 1986) is verified in Figure 2c, while the maxima KE values are likely to be related to the beginning of NBC retroflection weakening in January (LUMPKIN & GARZOLI, 2005). The importance of studying such variability of parameters relies on the estimation of ring volume and energy within a ring, for example. Rings with larger dimensions are capable of wrapping a larger volume of water, while its lifetime indicates eddy capacity in maintaining that wrapped piece of water. At the same time, estimation on KE variation might indicate a seasonal energy transport within NBC rings. In general, NBC rings seem to have larger dimensions and rotate faster during boreal winter months, carrying more KE within them. This energy, however, is likely to dissipate more quickly, since, in boreal winter, NBC rings presented shorter lifetimes.

On the other hand, NBC rings shed during summer, and early boreal fall appears to last longer, to have smaller diameters, and carry less energy.

Figure 4 – Averaged climatological anomaly of North Brazil Current ring parameters for each year during the 24 years analyzed: Ring lifetime (a), Rmax (b), Vmax (c), Rossby number (d), Kinetic Energy (e), SSH anomaly (f)

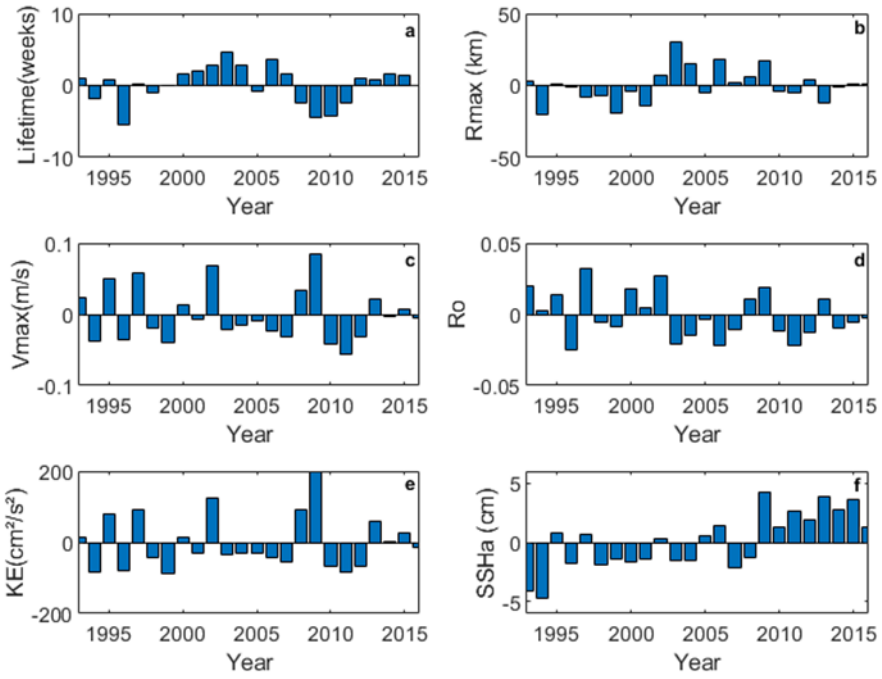


Source: the authors (2019).

The characteristics of the rings are plotted as a function of year to identify inter-annual variability (Figure 3). Ring lifetime is reduced in the last decade (Figure 3a). Very high values of lifetime are detected as outliers for some years (2007, 2008, 2012, and 2013). The highest ring dimension is in 2003, followed by 2006 and 2009 (Figure 3b). Sharma *et al.* (2009) pointed 2006 as the year with an average ring size larger than other years. The highest median rotational velocity was observed in 2009 (Figure 3c), following the year of maximum Vmax variation (i.e., 2008). Year 2009 was also the year of maximum KE and mainly SSHa (Figures 3e and 3f). We calculated an annual climatological anomaly for the 24 years and observed that 2009 presented the most significant anomaly of Vmax, KE, and SSHa (Figure 4). Foltz *et al.* (2012) identified an anomalous SST cooling in the Equatorial North Atlantic band (2°N–12°N) in 2009 and SST warming in the Equatorial South Atlantic (5°S–0°N) which produced a shift in wind direction, changed the ITCZ position and the rainfall rates over the region. Moreover, Tyaquiçã *et al.* (2017) indicated an increased Amazon River discharge in 2009. These events might have altered current dynamics in this region, contributing to change NBC ring parameters in this year. We verified from filtered monthly anomalies of salinity and

of zonal(u)-component of NBC in a longitudinal cut at 53°W, 3°N–7°N, from surface to 500 m deep, that 2009 year indeed presented an NBC intensity anomalous increase (Figure 5). This increase is indicated by a higher negative anomaly in the zonal component of NBC, and accompanied by salinity anomalies decease in the same year, showing a higher influence of Amazon plume in this year. Additionally, data for the 24 years of monthly Amazon discharge values recorded at the Óbidos Gauging Station, available from the Environmental Research Observatory– Geodynamical, hydrological, and biogeochemical control of erosion/alteration and material transport in the Amazon basin (ORE–HYBAM: http://www.ore-hybam. org), were used to estimate Amazon discharge inter-annual anomalies (Figure 5).

Figure 5 – Monthly anomalies of zonal(u)-component (a) and salinity (b) of North Brazil Current in a longitudinal cut at 53°W, 3°N–7°N, from the surface to 500 m deep ARMOR 3D product. (c) Indicates monthly anomalies of Amazon river discharge at the Óbidos Gauging available from the ORE–HYBAM

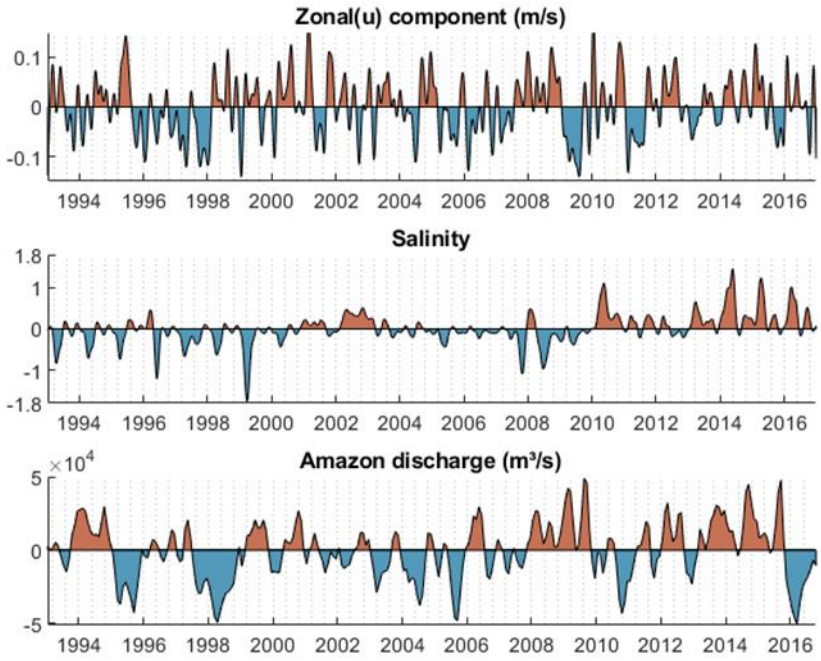


Source: the authors (2020).

From Amazon discharge is clear the positive anomaly during the entire 2009 year. An increased Amazon River runoff can contribute to NBC and its rings intensity by diminishing density through the influence of freshwater, generating an increase in current velocity. Moreover, Amazon River discharge could contribute to the increase in local vorticity, favoring rings intensity. Overall, it is believed that the combination of both increased NBC intensity and Amazon River runoff contributed for the 2009 intensity change in NBC rings dynamics. Another considerable pattern observed from 2009 is the positive trend in SSHa anomalies

(Figure 4f). This indicates that SSHa within NBC rings is increasing in the last years. This could be related to changes in ocean circulation during the last decades. NBC rings are very dynamic and variable, being subject to several oceanographic and atmospheric forcings that affect their characteristics. Therefore, a strong inter-annual variability of their parameters is expected. In addition, we attempted to correlate Atlantic climate indexes with NBC parameter anomalies. The highest observed correlation was 0.34 between SSHa and Atlantic multidecadal oscillation (AMO). Although it seems a weak correlation, the analyzed period covered only the positivephase of the AMO cycle, characterized by changes in a climate signal of 60–80 years. Further studies could analyze a long-term climatological ring data to compare with this climate index. NBC ring evolution in terms of eddy characteristics is highlighted in Section 3.3.

### 3.3.3 Rings Trajectory and Evolution: Merged Rings Case Studies

Regarding the trajectory of the 121 analyzed NBC rings, Figure 6 and Table S3 displays the location of rings formation, location of maximum SSHa, and location of final detection. In general, we can observe rings being generated in the NBC retroflection area, propagating northwestward along the coast until demise when reaching the Lesser Antilles (Figure 6). The location of rings SSHa max is spread along the area, indicating that SSHa max could be observed right after ring formation as well as close to ring demise. Generation area is limited from 53°W to east, while ring final detection settles mainly from 58°W to west, although few rings were last identified east of this longitude. NBCRs far eastern from 58°W identified in Figure 6 indicate rings that merged (e.g., R83 – see Table 3.S3). Rings centers demise were identified sitting northward or close to Barbados, and many were last verified before reaching Barbados. One ring translated differently, demising in the continental shelf near Orinoco River (Figure 6). Overall, rings decease occurred in regions influenced by the bottom bathymetry of Antilles. In fact, the influence of topography in finishing rings in the region has been well documented (FRATANTONI & RICHARDSON, 2006; JOCHUMSEN *et al.*, 2010). Additionally, their demise is strictly connected to the presence of the Lesser Antilles, which constitutes a barrier to ring translation (FRATANTONI & RICHARDSON, 2006). Interaction with the island leads to the destruction or the splitting of the incoming vortex into several smaller ones (FRATANTONI & RICHARDSON, 2006; TANABE & CENEDESE, 2008).

Studies showed that ring might also be identified west of the island chain, indicating few surviving rings after topography interaction (FRATANTONI & RICHARDSON, 2006; JOCHUMSEN *et al.*, 2010; MÉLICE & ARNAULT, 2017; TANABE & CENEDESE, 2008).

However, in our study the splitting of NBC rings encountering the Antilles was not detected by AMEDA, since the algorithm did not identify any NBCR west of the Antilles. This fact is mainly explained by the reduced study area, which imposes the tracking of rings with boundaries limited to 63°W.

Figure 6 – North Brazil Current rings position observed in the study area for three different moments during their lifetime: first week (blue); week of maximum sea surface height anomaly (yellow); last week (red). The background displays gridded bathymetry data from The General Bathymetric Charts of the Ocean (GEBCO), available at: https://www. gebco.net/

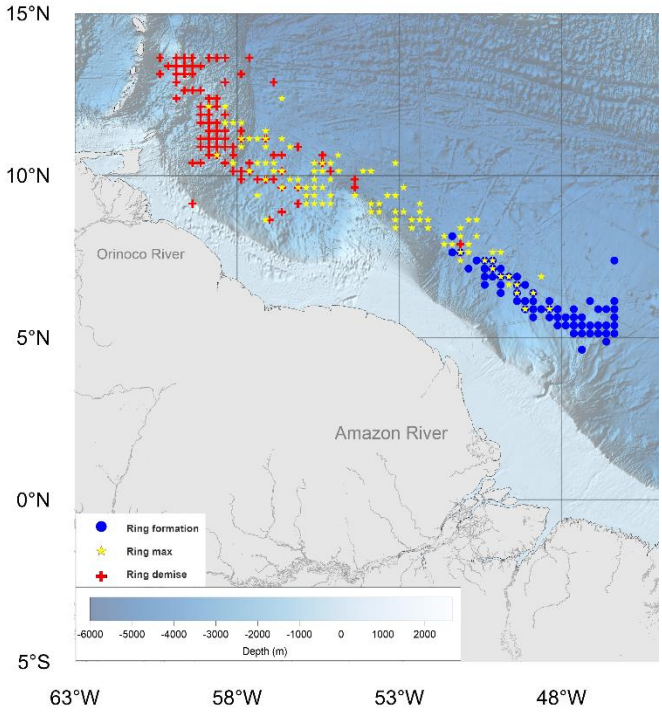


Source: the authors (2020).

Using rings center position (Table 3. S3) and exploring the potential of ARMOR 3D data set for vertical profiles, we evaluated the water masses carried by NBC rings and the vertical temperature and salinity anomaly profiles on a seasonal scale. The vertical T-S diagrams were built from ARMOR 3D data set until 1,000 m, and the identified water masses were depicted (Figure 7). We recorded three water masses carried by NBC rings: South Atlantic Central Water (SACW), those with temperatures $\leq 18$°C and salinities $\leq 36.0$; coastal water (CW), with temperatures $\geq 20$°C and salinities $\leq 35.4$ and tropical water (TW), with temperatures $\geq 20$°C and salinities $\geq 36.0$. Neumann-Leitão *et al.* (2018) using in situ data observed the same water masses distribution in this region. Figure 7 displays the T-S diagrams for NBC rings locations at three different life stages, and starting at the four different seasons. A clear seasonality is observed in the water masses within NBC rings. From the end of boreal

spring until JJA, CW from the Amazon River discharge is much more present in those eddies, while from September to February, the influence of TW is more pronounced is those vortex, and the CW is nearly absent (Figure 7). In fact, the seasonality of Amazon River runoff is known for decades, where the maximum monthly river discharge is in May and June (HELLWEGER & GORDON, 2002), demonstrating that the T-S diagram within an NBC eddy is related with their generation season. Additionally, NBC rings center presented similar T-S signatures during their translation, especially from their maxima week until their demise. It seems that rings in the starting week might not have enough intensity to trap water masses, reaching this stage of closed waters in vortex center during the following weeks. From the week of maxima SSHa, water masses are trapped until ring demise.

Figure 7 – T-S diagram for each ring generated in the four different seasons from ARMOR 3D data set: DJF (a), MAM (b), JJA (c), SON (d). DJF, December-January-February trimester; JJA, June-July-August trimester; MAM, March-April-May trimester; SON, September-October-November trimester.

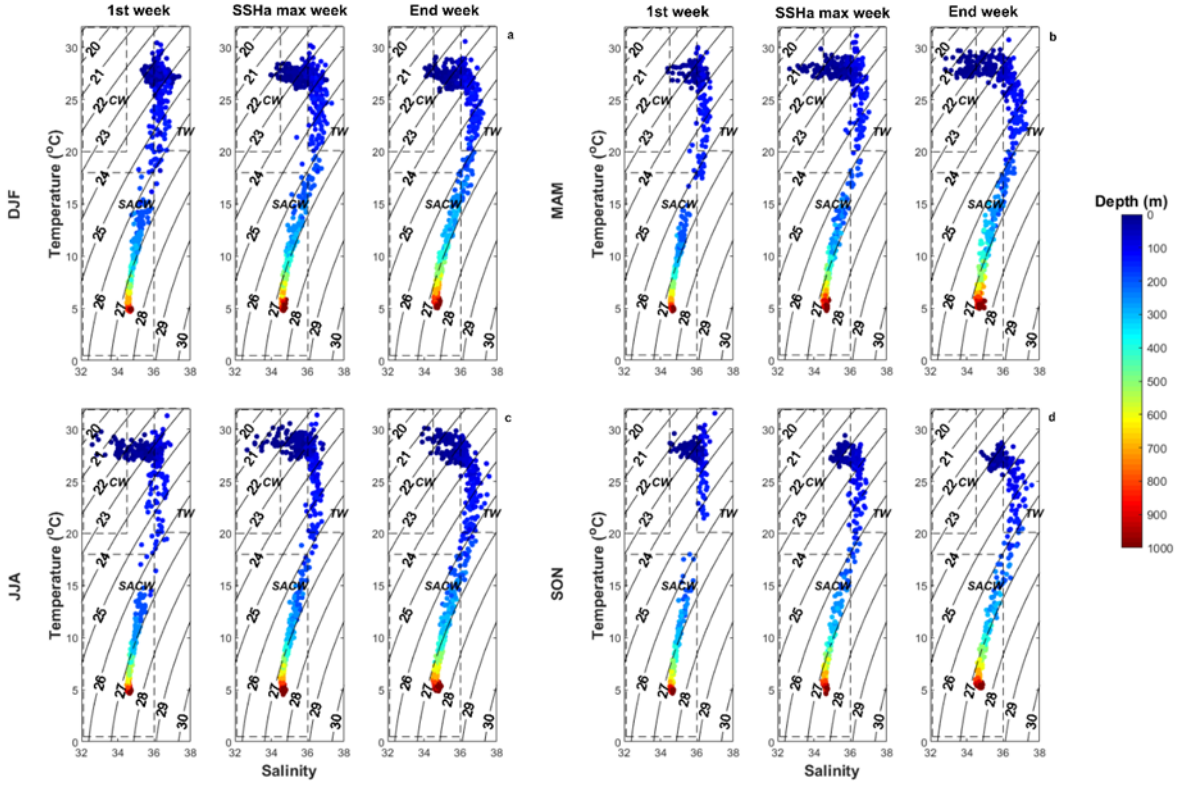


Source: the authors (2020).

Furthermore, we performed the temperature and salinity 3-month profiles anomalies for each ring center identified, removing the climatology (based on the 24-years data from ARMOR 3D) from ring vertical profiles for each position. Three-month anomaly profiles were calculated in the central points of initial, maximum and final rings positions. The greatest anomalies

observed in depth were located at ring SSHa maxima for both temperature and salinity (Figure 8). For initial and final positions, both the temperature and salinity anomalies profiles are not well defined, although rings initial position seems to relate to a stronger downward flux than final vortex locations (Figures S3a and S3b, respectively), since the latter is closer to Antilles bathymetry, what causes mixing. This behavior is an indication of an increased water downwelling in the eddy max position, while in initial and final positions the downward water flux at the ring center is weakened.

Figure 8 –Temperature (a) and salinity (b) profiles anomalies for each ring center identified for Max sea surface height anomaly position, removing the climatology from ring vertical profiles for each position

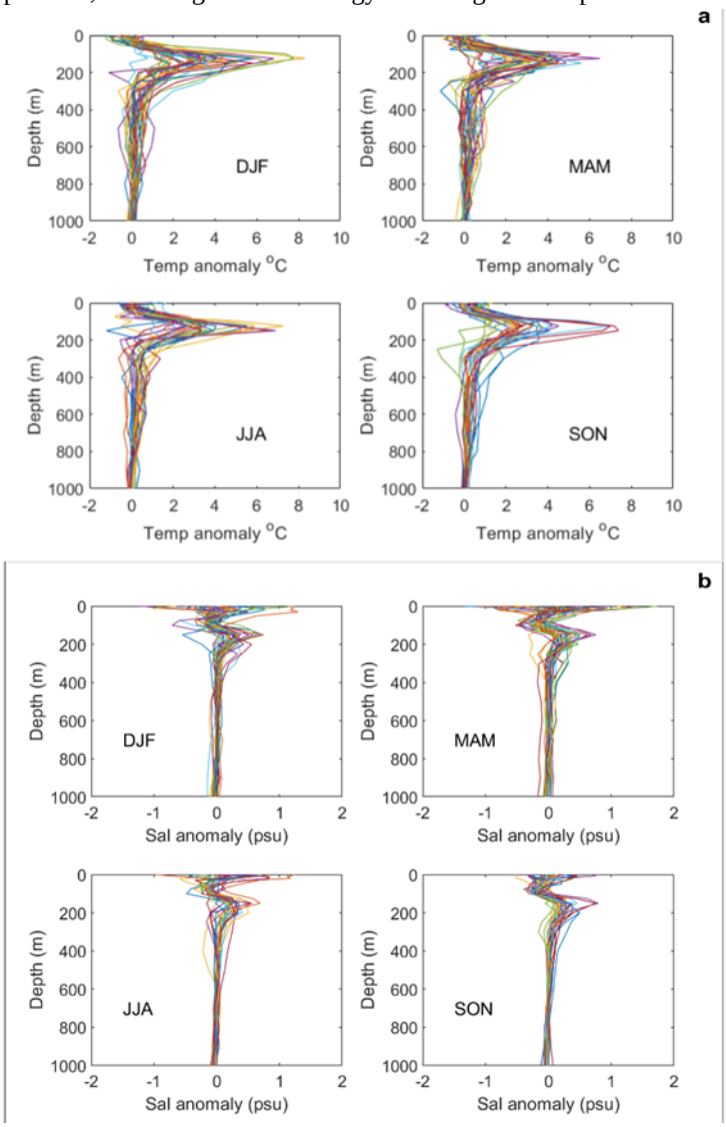


Source: the authors (2020).

Overall, regarding temperature profiles, maximum positive anomalies of 5°C are observed from 150 to 200 m deep, with no clear seasonality (Figure 8a). The downwelling

associated with anticyclonic eddies increased the thermocline depth until 200 m in this region. Polo *et al.* (2015) indicated maxima MLD of 80 m for the WTNA region, showing that NBC rings can generate deeper thermocline and consequently greater mixed layer depths. For salinities, in general, negative anomalies (∼-0.5) are observed at 100 m, settling above positive anomalies of 1.0 at 200 m (Figure 8b). These vertical salinity anomalies are also an indication of water sinking at NBC rings centers, that transport surface tropical saltier and coastal fresher waters to deeper layers. From this, the denser and saltier TWs settle under the less dense and fresher CW related to Amazon and Orinoco River plumes. Since Amazon discharge is more present in rings waters generated in JJA (Figure 7c), the most well-defined salinity anomalies profiles are referred to rings generated in this season, reaching SSHa max position at SON months, generating a more well-defined stratification insalinity anomalies profiles (Figure 8b). The increase in thermocline depth associated with sinking of riverine and TWs within NBC rings might spawn shifts on physical and biogeochemical features at WTNA, such as surface heat content, and CO2 saturation. Further studies on this could indicate those answers.

A striking innovation of AMEDA algorithm is the capacity to detect merging between two eddies, and this capacity was explored in the present study. We detected only four merging rings events in the 24-year study period for NBC eddies, indicating that NBC rings did not interact much within each other. However, Castelão and Johns (2011) pointed that the presence of an inner core surrounded by an outer core of opposite vorticity is able to "isolate" the NBC rings, allowing them to be very close to each other without merging (CASTELÃO & JOHNS, 2011). This structural configuration might explain why only 1 merging event was identified for each 6 years on average in the present study. In addition, few moments of NBC ring interaction with westward propagating anticyclonic eddies could be observed during the analyses. Plus, cyclonic eddies were also identified in certain weeks (Figure 9). Previous studies pointed for the formation of two different types of anticyclones in the region, the intermediate ones, and the NBC rings, that could coalesce within each other and generate deep-reaching rings (GARRAFFO *et al.*, 2003; JOCHUM & MALANOTTE-RIZZOLI, 2003). Cui *et al.* (2019) found that eddy merging is not likely to happen between eddies with similar intensities. Instead, the most common to happen is a strong eddy merging with a weaker one. Therefore, it is possible that NBC rings interact more often with weaker eddies (e.g., intermediate eddies, cleavaged eddies, eddies associated with NECC-NBC flow) present in the region than with other true NBC rings. Preceding works also identified cyclonic eddies in the region (DIDDEN & SCHOTT, 1993; FRATANTONI & RICHARDSON, 2006), which are

associated with the NBC/NECC system variability, as well as with the dynamics of the anticyclonic NBC rings.

Figure 9 –Large scale circulation features in Western Tropical North Atlantic over a sea surface height anomaly (SSHa) background from ARMOR 3D data set at week of 24th March 2009. R82 and R83 are two North Brazil Current (NBC) rings and two anticyclonic eddies identified by angular momentum eddy detection and tracking algorithm. Dashed (filled) lines represents outermost (Rmax) closed contour Rmax. Blue contours indicate anticyclonic eddies. Gray lines denotes large scale currents. SSHa smaller than 5 cm were removed for better visualization of rings. NECC, North Equatorial Countercurrent

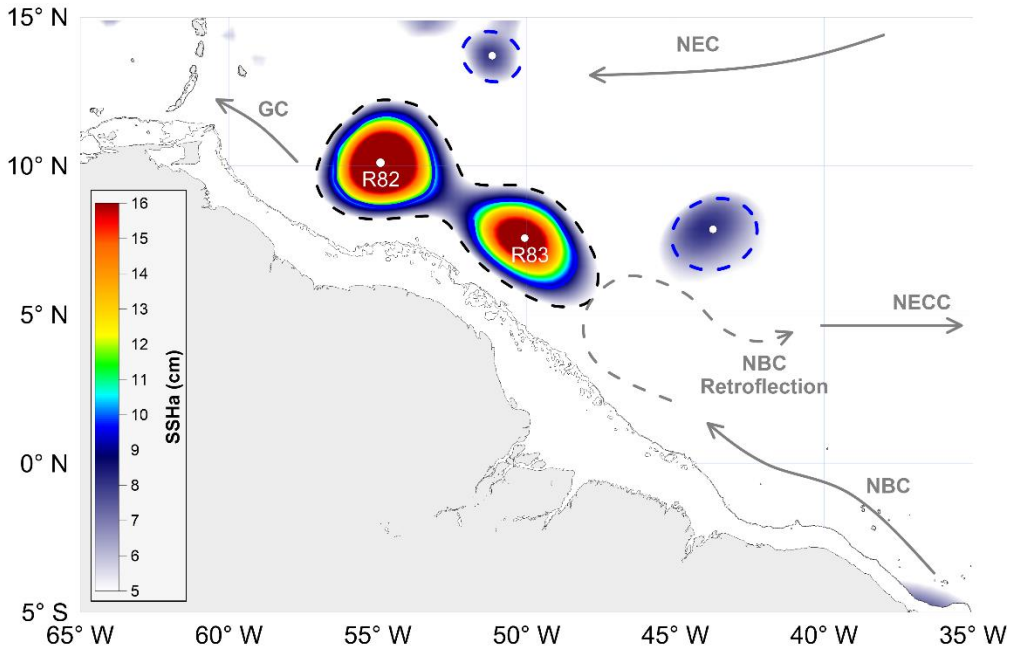


Source: the authors (2020).

In order to highlight the typical evolution of the dynamical parameters of NBC rings during their northwestward propagation along the coast, and to analyze if there are significant changes in rings parameterafter merging, we computed the parameters for every week of occurrence of the 8 isolated rings which turned to four merged rings events. Rings parameters evolution is depicted in Figure S4 and Table S4. Weeks with NaN values represent weeks that AMEDA could not identify eddy. Figure 10 shows the trajectories of rings in the four analyzed events. From the four events, three rings remained merged until their demise (Figures 10a, 10c, 10d), while one of them merged and then splitted into two rings after 2 weeks (Figure 10b). All observed merging rings were generated from 52°W to east, above 5°N, and traveled northwestward along the northern coast of Brazil (Figure 10). Plus, the four merging events took place from mid-February to start of April, where six isolated rings were generated in DJF, one in September and one in March. Dated only in the first half of the year, the time of merging events corresponds with the time of increased ring formation (Figure 1). Other works also

observed merging events only in this period (BARNIER *et al.*, 2001; FRATANTONI & RICHARDSON, 2006). It is believed that in the second half of the year the ring generation rate is not sufficient to promote a ring encounter when translating, before one of them demise in the Antilles. Still, regarding the location of merging events, all 4 events settled in the area indicated by the red rectangle in Figure 10. This area is located in a topographic depression between the start of Caribbean topography and the extended continental shelf from 53°W to 55°W (Figure 10). It is hypothesized that in this highlighted region NBC rings decelerate as reaching Antilles topography, allowing upcoming NBC rings to reach the previous eddy and merge. In fact, Barnier *et al.* (2001) indicated that a NBC eddy was slowed down as it encountered the Trinidad–Tobago topographic rise, which contributed for ring merging. The authors still indicated that such ring merging was also reported by Didden and Schott (1993). Further studies on the influence of this topography for the fusion of NBC rings are required. Lastly, Figure 10 also displays that rings trajectory right after merging are slightly deviated to west-southwest. De Marez *et al.* (2020) indicated that anticyclonic eddies are more likely to be orientated southwest-northeast due to the β-effect. It seems that NBC rings are also influenced by this effect.

Figure 10 –Merging rings trajectory. M1 from R20 (yellow) and R21 (blue) (a); M2 from R39 (yellow) and R40 (blue) (b); M3 from R78 (yellow) and R77 (blue) (c); M4 from R83 (yellow) and R82 (blue) (d). Red rectangle indicates area where all rings merged. Black lines represent rings trajectory. Circle size depicts Rmax. Circle height is four times lower that the real circle height based on Rmax. Circle shapes do not depict real ring shapes, are displayed only as ring representations

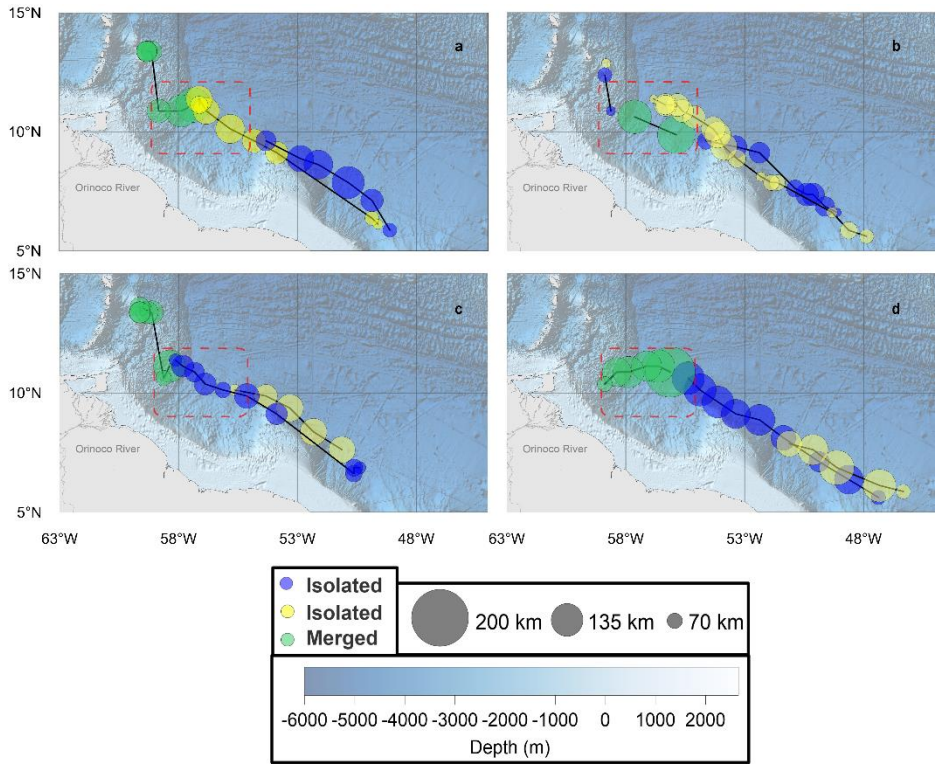


Source: the authors (2020).

In addition, the change on NBC ring vertical and translation structure is related not only to ring and current field dynamics but also to the influence of topography in the region, especially regarding ring demise (FRATANTONI & RICHARDSON, 2006; JOCHUMSEN *et al.*, 2010). Hence, since ring parameters evolve in time and could be strongly affected by bottom bathymetry, especially when the vortexes reach Caribbean coastal shelves, we attempted to evaluate the influence of topography in NBCRs parameters. To do that, we used the merged events M1 and M4 (Table 3.S4) as case studies for comparison of their parameters before and after reaching 58°W (i.e., where influence of bottom topography seems to increase), computing their characteristics only 1 week after they merged to remove merging effects, and performing t student tests. M3 merged after 58°W, where merging effects could superimpose topographic effects, so we did not consider this event as a case study. On the other hand, M2 splits when reaches 58°W, what could indicate bathymetry influence. For M1, we observed significant decrease in Rmax ($p = 0.002$), while total ratio and Vmax did not change ($p = 0.9432$ and $p = 0.7154$, respectively). In the case of M4, no shifts were observed at all (Rmax, $p = 0.1740$; total ratio, $p = 0.7800$; Vmax, $p = 0.1383$). By potential vorticity conservation, it was expected

that when reaching shallow waters eddies would flatten and increase their size, while diminish their velocities. However, only a significant reduction in Rmax was observed. This uncertainty might be due to effects of the bathymetry in the algorithm identification using this data set spatial resolution (1/4°), where further studies using an increased data resolution could better indicate current vectors around the island chain, improving ring identification, and allowing a finer evaluation of the effects of Lesser Antilles bathymetry in NBC ring parameters.

Table 1 –Test t-Student Between Isolated and Merged Rings.

| | **t-student** | **Mean solo** | **Mean merged** | **Significant difference (%)** |
|---|---|---|---|---|
| **Rmax** | 0.4091 | 113.6 *km* | 121.2*km* | Not |
| **Vmax** | **0.0291** | 0.23 *m/s* | 0.28 *m/s* | **+22.0** |
| **Ro** | **0.0194** | 0.11 | 0.08 | **-27.3** |
| **KE** | **0.0141** | 187.6 *cm2/s2* | 285.1 *cm2/s2* | **+52.0** |
| **SSHa** | 0.9775 | 6.4 *cm* | 6.4 *cm* | Not |

Source: the authors (2020).

Note. Significant differences were considered in a 95% confidence interval ($p < 0.05$) and are indicated in bold. Significant differneces (%) indicates the percentage of change between mean solo and mean merged rings parameters. Abbreviations: KE, kinetic energy; Ro, Rossby number; SSHa, sea surface height anomaly

Moreover, significant changes were observed for three parameters of NBC rings after rings merging. To address that, we performed t-student tests for the parameters computed for each of the eight isolated and the four merged NBC rings, which results are indicated in Table 3.1. We removed the weeks immediately before and right after ring merging from the test t, in order to remove effects of definition of the eddy radius during the merging event, since for a perfect merging between two symmetric eddies their radii should tend to zero just before a single eddy contour emerge (LE VU *et al.*, 2018). Significant changes were verified for Vmax, Ro and KE, while Rmax and SSHa did not present considerable difference between isolated and merged vortex (Table 3.1). Shift in Ro occurred due to increased Vmax and the maintenance of Rmax from isolated to merged eddies. A Vmax positive change of 22.0% resulted in merged rings with 52% more KE that the isolated, in average. This increase in ring KE might disrupt local circulation around Caribbean islands in a greater scale, impacting also fish larvae recruitment, and ocean-atmosphere energy exchanges. In addition, eddy merging events could function as a “large-scale energy pump” in the inverse energy cascades in two ways: from changes from small- to large-scale eddies and increasing residence time (KLEIN *et al.*, 2019; WANG *et al.* 2019). After merging, there is a significantly increase the total KE and

strengthen of the large geostrophic eddies by making them more coherent with a longer life time (KLEIN *et al.*, 2019). In this study, however, we did not identified shifts in Rmax after merging (rings maintained their length scale), and due to interaction with Antilles right after merging did not allow a longer residence time (i.e., they are not isolated eddies). Then, we cannot affirm that NBC rings play this role. Further studies on this might spark answers for this question. The increase ring KE was also observed by Cui *et al.* (2019). The authors reported that splitting or merging events can change eddy properties by a factor of 2 or more (CUI *et al.*, 2019). The observed changes in this study did not represent such a variation in eddy properties after merging. However, it showed that NBC ring merging has a considerable impact in its rotational speed, KE and intensity variation, and that those events should be taken into account when evaluating physical and biogeochemical impacts of NBC rings in the WTNA. On the other hand, Wang *et al.* (2019) stated that, overall, eddies KE decreased while total mechanical energy increased after merging, and that merging events require external energy input into rings. Therefore, we theorized that only in specific years this necessary energy input coincided with times of NBC rings close enough to merge with each other, making a NBC ring merging event such a rare event. More studies on the relation of ring merging years and climate indexes that could provide the required amount of energy for rings merging might elucidate this hypothesis. To evaluate how ring parameters are related with each other, we performed a correlation analysis between the computed parameters for the eight isolated the four merged rings, where Pearson correlation index are indicated in Table 3.S5. We observed that Vmax and KE are well correlated with all analyzed parameters, in exception of Ro, while SSHa did not present high correlation with Rmax. Therefore, the use of maximum KE as a proxy for rings maxima is more indicated than the SSHa used in this study, since it includes a correlation not only with ring speed and energy, but also with ring size.

## 3.4 CONCLUSIONS

We applied the AMEDA for the identification of NBC rings occurrence, trajectories, and physical parameters. This work uses a 24-year (1993–2016) reanalysis database of geopotential height and geostrophic velocity fields, standing as the first study to apply an eddy detection algorithm for NBC ring identification in a decadal period. The choice of AMEDA is based on its robustness and ease of use for eddy properties time series analysis, since it considers not only dynamical but also geometrical properties of the velocity field.

Here, we identified an average rate of five NBC rings shed by year, which presented an average lifetime of 15.3 (±5.4) weeks, Rmax from 87.3 to 204.8 km, with an average radius of 139.5 (±23.6) km, and were associated with mean SSHa within their centers of 9.4 (±4.0) cm. The mean observed Vmax was 0.27 (±0.08) m/s, while the averaged Ro value was 0.08 (±0.04) and averaged KE was 255.3 (±154.8) cm2 /s2. It is pointed that the azimuthal velocity and Ro values might be underestimated due to the use of purely geostrophic velocity fields. NBC rings occur more frequently in the first half of the year. In fact, a decrease in ring generation rate of 47.37% was detected between maxima (boreal winter) and minima (boreal fall) trimesters. Moreover, NBC rings have larger dimensions, rotate faster, and present shorter lifetimes in boreal winter months, also carrying more KE within them. On the other hand, NBC rings shed last longer, have smaller diameters, and carry less energy during summer and early boreal fall. 2009 was a year of anomalous conditions, since it presented maximum values of KE, Vmax, and SSHa associated with NBC rings. Another pattern identified in this work was the positive trend in SSHa anomalies from 2009 to 2016. This shows that SSHa within NBC rings is increasing in the last years, which could be further investigated.

Furthermore, we identified that downwelling within NBC rings center cause a thermocline deepening and anomalies in the salinity profile, indicating downward transport of tropical and CWs. Also, the analysis of T-S diagram allowed us to identify seasonality in relation to water masses in the interior of NBC rings. River water was observed within eddies center only in the ones formed from May to August, implying that NBC rings generated at those months might play different biogeochemical impacts in the WTNA region, such as shifts CO2 fugacity in the ocean and CO2 flux between ocean–atmosphere. The vertical change in temperature and salinity profiles can as well influence these physical and biogeochemical effects. More studies on this could provide this response. In addition, we observed in the year of 2009 a possible influence of Amazon River discharge on NBC ring dynamical parameters, such as Vmax and KE, through effects in water density, flow vorticity and velocity, what might also have contributed for a ring merging event in that year. Still, NBC rings merging events, although not very frequent, can significantly increase ring velocity and energy. However, the mechanism and energy supply that allow then to occur with NBC rings remains unclear. Moreover, these increase in ring KE can have an impact in the current dynamics around Caribbean, influencing, for example, phytoplankton distribution. Further works on this would provide this answer.

In this study, the use of reanalysis data associated with this AMEDA tool allowed the investigation of the intra- to inter-annual variability of NBC rings occurrence and dynamics.

Further, the algorithm demonstrated to be straightforward in the identification of interaction among rings, which facilitate the analysis of these events. Overall, quantifying ring parameters seasonal and inter-annual variability, and identifying interaction between eddies, is crucial for understanding ring dynamics and consequently its impacts on the physics and biogeochemistry of the ocean.

### 3.4.1 Data Availability Statement

ARMOR 3D data supplied by Copernicus Marine Environment Monitoring Service (CMEMS) at http:// marine.copernicus.eu/. The 24 years of monthly Amazon discharge values recorded at the Óbidos Gauging Station, are available from the Environmental Research Observatory– Geodynamical, hydrological, and biogeochemical control of erosion/alteration and material transport in the Amazon basin (ORE–HYBAM: http://www.ore-hybam.org).

### 3.4.2 Acknowledgments

This project was supported by the TRIATLAS project, which has received funding from the European Union's Horizon 2020 research and innovation program under grant agreement No 817578. The authors also acknowledge the support of the Brazilian Research Network on Global Climate Changes – Rede CLIMA (FINEP Grants 01.13.0353-00). The received funding did not lead to any conflict of interests regarding the publication of this manuscript. L. C. Aroucha thanks to Thomaz Arsouze, Briac Le Vu, and Alexandre Stegner for making AMEDA available and for the orientation of its use.

## 3.500 REFERENCES

ARNAULT, S., & CHENEY, R. E. Tropical Atlantic Sea level variability from Geosat (1985–1989). **Journal of Geophysical Research**, 99, 18207–18223. https://doi.org/10.1029/94JC01301, 1994.

BARNIER, B., REYNAUD, T., BECKMANN, A., BONING, C., MOLINES, J.-M., BARNARD, S., & JIA, Y. On the seasonal variability and eddies in the North Brazil Current: insight from model intercomparison experiments. **Progress in Oceanography**, 44, 195–230. https://doi.org/10.1016/S0079-6611(01)00005-2, 2001

BUONGIORNO NARDELLI, B., DROGHEI, R., & SANTOLERI, R. Multi-dimensional interpolation of SMOS sea surface salinity with surface temperature and in situ salinity data. **Remote Sensing of Environment**, 180, 392–402. https://doi.org/10.1016/j.rse.2015.12.052, 2016.

CASTELÃO, G. P., & JOHNS, W. E. Sea surface structure of North Brazil Current rings derived from shipboard and moored acoustic Doppler current profiler observations. **Journal of Geophysical Research**, 116(C1). https://doi.org/10.1029/2010JC006575, 2011.

CHAIGNEAU, A., GIZOLME, A., & GRADOS, C. Mesoscale eddies off Peru in altimeter records: Identification algorithms and eddy spatio-temporal patterns. **Progress in Oceanography,** 79, 106–119. https://doi.org/10.1016/j.pocean.2008.10.013, 2008.

CHELTON, D. B., DE SZOEKE, R. A., SCHLAX, M. G., EL NAGGAR, K., & SIWERTZ, N. Geographical variability of the first baroclinic Rossby radius of deformation. **Journal of Physical Oceanography,** 28, 433–459. https://doi.org/10.1175/1520-0485(1998)028%3C0433:GVOTFB%3E2.0.CO;2, 1998.

COWEN, R. K., SPONAUGLE, S., PARIS, C. B., LWIZA, K., FORTUNA, J., & DORSEY, S. Impact of North Brazil Current rings on local circulation and coral reef fish recruitment to Barbados, West Indies. In G. J. Goni & P. Malanotte-Rizzoli (Eds.), **Interhemispheric water exchange in the Atlantic Ocean**, Elsevier Oceanographic Series (Vol. 68, pp. 443–455), Amsterdam, Netherlands: Elsevier. https://doi.org/10.1016/S0422-9894(03)80157-5, 2003.

CRUZ-GÓMEZ, R., & SALCEDO-CASTRO, J. Analysis of horizontal and vertical ring structure based on analytical model and satellite data: Application to the North Brazil Current Rings. **Ocean Science Journal**, 48(2), 161–172. https://doi.org/10.1007/s12601-013-0013-2, 2013.

CUI, W., WANG, W., ZHANG, J., & YANG, J. Multi core structures and the splitting and merging of eddies in global oceans from satellite altimeter data. **Ocean Science**, 15, 413–430. https://doi.org/10.5194/os-15-413-2019, 2019.

DE MAREZ, C., CARTON, X., L'HÉGARET, P., MEUNIER, T., STEGNER, A., LE VU, B., & MORVAN, M. Oceanic vortex mergers are not isolated but influenced by the β-effect and surrounding eddies. **Scientific Reports**, 10(2897), https://doi.org/10.1038/s41598-020-59800-y, 2020.

DIDDEN, N., & SCHOTT, F. Eddies in the North Brazil Current retroflection region observed by Geosat altimetry. **Journal of Geophysical Research**, 98, 121–131. https://doi.org/10.1029/93JC01184, 1993.

DOGLIOLI, A. M., BLANKE, B., SPEICH, S., & LAPEYRE, G. Tracking coherent structures in a regional ocean model with wavelet analysis: Application to Cape Basin eddies. **Journal of Geophysical Research**, 112(C5). https://doi.org/10.1029/2006JC003952, 2007.

DOUGLASS, E. M., & RICHMAN, J. G. Analysis of ageostrophy in strong surface eddies in the Atlantic Ocean. **Journal of Geophysical Research: Oceans**, 120, 1490–1507. https://doi.org/10.1002/2014JC010350, 2015.

FFIELD, A. North Brazil Current rings viewed by TRMM Microwave Imager SST and the influence on Amazon River Plume**. Deep Sea Research Part I Oceanographic Research Papers,** 52, 137–160. https://doi.org/10.1016/j.dsr.2004.05.013, 2005.

FOLTZ, G. R., MCPHADEN, M. J., & LUMPKIN, R. A strong Atlantic Meridional Mode Event in 2009: The role of mixed layer dynamics. **Journal of Climate**, 25, 363–380. https://doi.org/10.1175/JCLI-D-11-00150.1, 2012.

FONSECA, C. A., GONI, G. J., JOHNS, W. E., & CAMPOS, E. J. D. Investigation of the North Brazil Current retroflection and north equatorial countercurrent variability. **Geophysical Research Letters**, 31. https://doi.org/10.1029/2004GL020054, 2004.

FRATANTONI, D. M., & GLICKSON, D. A. North Brazil Current ring generation and evolution observed with SeaWiFS. **Journal of Physical Oceanography**, 32, 1058–1074. https://doi.org/10.1175/1520-0485(2002)032%3C1058:NBCRGA%3E2.0.CO;2, 2002.

FRATANTONI, D. M., JOHNS, W. E., & TOWNSEND, T. L. Rings of the North Brazil Current: Their structure and behavior inferred from observations and a numerical simulation. **Journal of Geophysical Research,** 100, 10633–10654. https://doi.org/10.1029/95JC00925, 1995.

FRATANTONI, D. M., JOHNS, W. E., TOWNSEND, T. L., & HURLBURT, H. E. Low-latitude circulation and mass transport pathways in a model of the tropical Atlantic Ocean. **Journal of Physical Oceanography**, 30, 1944–1966. https://doi.org/10.1175/1520-0485(2000)030%3C1944LLCAMT%3E2.0.CO;2, 2000.

FRATANTONI, D. M., & RICHARDSON, P. L. The evolution and demise of North Brazil Current Rings. **Journal of Physical Oceanography**, 36, 1241–1264. https://doi.org/10.1016/S0422-9894(03)80154-X, 2006.

GARRAFFO, Z., JOHNS, W. E., CHASSIGNET, E., & GONI, G. North Brazil Current rings and transport of southern waters in a high-resolution numerical simulation of the North Atlantic. **In Interhemispheric water exchange in the Atlantic Ocean, Elsevier Oceanography Series** (Vol. 68, pp. 375–410), Amsterdam: Elsevier. https://doi.org/10.1016/S0422-9894(03)80155-1, 2003.

GARREAU, P., DUMAS, F., LOUAZEL, S., STEGNER, A., & LE VU, B. High-resolution observations and tracking of a dual-core anticyclonic eddy in the Algerian Basin. **Journal of Geophysical Research: Oceans**, 123(12), 9320–9339. https://doi.org/10.1029/2017JC013667, 2018.

GARZOLI, S. L., FFIELD, A., & YAO, Q. North Brazil Current rings and the variability in the latitude of retroflection. **In Interhemispheric water exchange in the Atlantic Ocean, Elsevier Oceanography Series** (Vol. 68, pp. 357–373), Amsterdam: Elsevier. https://doi.org/10.1016/S0422-9894(03)80154-X, 2003.

GONI, G. J., & JOHNS, W. E. A census of North Brazil Current rings observed from TOPEX/POSEIDON altimetry: 1992–1998. **Journal of Geophysical Research**, 28, 1–4. https://doi.org/10.1029/2000GL011717, 2001.

GONI, G. J., & JOHNS, W. E. Synoptic study of warm rings in the North Brazil Current retroflection region using satellite altimetry**. In Interhemispheric water exchange in the Atlantic Ocean**, Elsevier Oceanography Series (Vol. 68, pp. 335–356), Amsterdam: Elsevier. https://doi.org/10.1016/S0422-9894(03)80153-8, 2003.

GUINEHUT, S., DHOMPS, A.-L., LARNICOL, G., & LE TRAON, P.-Y. High resolution 3D temperature and salinity fields derived from in situ and satellite observations. **Ocean Science,** 8, 845–857. https://doi.org/10.5194/os-8-845-2012, 2012.

HALO, I., BACKEBERG, B., PENVEN, P., ANSORGE, I., REASON, C., & ULLGREN, J. Eddy properties in the Mozambique Channel: A comparison between observations and two numerical ocean circulation models. **Deep Sea Research Part II: Topical Studies in Oceanography**, 100, 38–53. https://doi.org/10.1016/j.dsr2.2013.10.015, 2014.

HELLWEGER, F. L., & GORDON, A. L. Tracing Amazon River water into the Caribbean Sea. **Journal of Marine Research,** 60, 537–549, 2002.

IOANNOU, A., STEGNER, A., LE VU, B., TAUPIER-LETAGE, I., & SPEICH, S. Dynamical evolution of intense Ierapetra Eddies on a 22-year long period. **Journal of Geophysical Research: Oceans**, 122(11), 9276–9298. https://doi.org/10.1002/2017JC013158, 2017.

IOANNOU, A., STEGNER, A., TUEL, A., LEVU, B., DUMAS, F., & SPEICH, S. Cyclostrophic corrections of AVISO/DUACS surface velocities and its application to mesoscale eddies in the Mediterranean Sea. **Journal of Geophysical Research: Oceans,** 124(12), 8913–8932. https://doi.org/10.1029/2019JC015031, 2019.

JOCHUM, M., & MALANOTTE-RIZZOLI, P. On the generation and importance of North Brazil Current rings. **Journal of Marine Research**, 61, 147–162. https://doi.org/10.1357/002224003322005050, 2003.

JOCHUMSEN, K., RHEIN, M., HÜTTL-KABUS, S., & BÖNING, C. W. On the propagation and decay of North Brazil Current rings. **Journal of Geophysical Research**, 115(C10). https://doi.org/10.1029/2009JC006042, 2010.

JOHNS, W. E., LEE, T. N., BEARDSLEY, R. C., CANDELA, J., LIMEBURNER, R., & CASTRO, B. Annual cycle and variability of the North Brazil Current. **Journal of Physical Oceanography,** 28, 103–128. https://doi.org/10.1175/1520-0485(1998)028%3C0103:ACAVOT%3E2.0.CO;2, 1998.

JOHNS, W. E., LEE, T. N., SCHOTT, F. A., ZANTOPP, R. J., & EVANS, R. H. The North Brazil Current retroflection: Seasonal structure and eddy variability. **Journal of Geophysical Research**, 95, 22103–22120. https://doi.org/10.1029/JC095iC12p22103, 1990.

JOHNS, W. E., ZANTOPP, R. J., & GONI, G. J. Cross-gyre transport by North Brazil Current rings. In G. J. Goni & P. Malanotte-Rizzoli (Eds.), **Interhemispheric water exchange in the Atlantic Ocean**, Elsevier Oceanographic Series (Vol. 68, pp. 411–441), Amsterdam: Elsevier. https://doi.org/10.1016/S0422-9894(03)80156-3, 2003.

KLEIN, P., LAPEYRE, G., SIEGELMAN, L., QIU, B., FU, L., TORRES, H., *ET AL*. Ocean-scale interactions from space. **Earth and Space Science**, 6, 795–817. https://doi.org/10.1029/2018ea000492, 2019.

LE VU, B., STEGNER, A., & ARSOUZE, T. Angular Momentum Eddy Detection and Tracking Algorithm (AMEDA) and its application to coastal eddy formation. **Journal of Atmospheric and Oceanic Technology**, 35, 739–762. https://doi.org/10.1175/JTECH-D-17-0010.1, 2018.

LEGECKIS, R., & GORDON, A. L. Satellite observations of the Brazil and Falkland currents – 1975 to 1976 and 1978**. Deep Sea Research Part A Oceanographic Research Papers**, 29, 375–401. https://doi.org/10.1016/0198-0149(82)90101-7, 1982.

LI, Q.-Y., SUN, L., LIU, S.-S., XIAN, T., & YAN, Y.-F. A new mononuclear eddy identification method with simple splitting strategies. **Remote Sensing Letters**, 5, 65–72. https://doi.org/10.1080/2150704X.2013.872814, 2014.

LUMPKIN, R., & GARZOLI, S. L. Near-surface circulation in the tropical Atlantic Ocean. **Deep Sea Research Part I: Oceanographic Research Papers**, 52, 495–518. https://doi.org/10.1016/j.dsr.2004.09.001, 2005.

MA, H. The dynamics of the North Brazil Current retroflection eddies. **Journal of Marine Research**, 54, 35–53. https://doi.org/10.1357/0022240963213493, 1996.

MCWILLIAMS, J. C. The vortices of two-dimensional turbulence. **Journal of Fluid Mechanics**, 219, 361–385. https://doi.org/10.1017/S0022112090002981, 1990.

MÉLICE, J.-L., & ARNAULT, S. Investigation of the intra-annual variability of the North Equatorial Countercurrent/North Brazil Current eddies and of the instability waves of the North tropical Atlantic Ocean using satellite altimetry and Empirical Mode Decomposition. **Journal of Atmospheric and Oceanic Technology**, 34, 2295–2310. https://doi.org/10.1175/JTECH-D-17-0032.1, 2017.

MKHININI, N., COIMBRA, A. L. S., STEGNER, A., ARSOUZE, T., TAUPIER-LETAGE, I., & BERANGER, K. Long-lived mesoscale eddies in the eastern Mediterranean Sea: Analysis of 20 years of AVISO geostrophic velocities. **Journal of Geophysical Research: Oceans**, 119, 8603–8626. https://doi.org/10.1002/2014JC010176, 2014.

MULET, S., RIOMIGNOT, M. -H. A., GUINEHUT, S., & MORROW, R. A new estimate of the global 3D geostrophic ocean circulation based on satellite data and in-situ measurements. **Deep Sea Research Part II: Tropical Studies in Oceanography**, 77–80, 70–81. https://doi.org/10.1016/j.dsr2.2012.04.012, 2012.

NENCIOLI, F., DONG, C., DICKEY, T., WASHBURN, L., & MCWILLIAMS, J. A vector geometry-based eddy detection algorithm and its application to a high-resolution numerical model product and high-frequency radar surface velocities in the Southern California Bight. **Journal of Atmospheric and Oceanic Technology**, 27(3), 564–579. https://doi.org/10.1175/2009JTECHO725.1, 2010.

NEUMANN-LEITÃO, S., MELO, P. A. M. C., SCHWAMBORN, R., DIAZ, X., FIGUEIREDO, L., SILVA, A., *ET AL.* Zooplankton from a reef system under the influence of the Amazon River Plume. **Frontiers in Microbiology**, 9, 355. https://doi.org/10.3389/fmicb.2018.00355, 2018.

NURSER, A. J. G., & BACON, S. The Rossby radius in the Arctic Ocean**. Ocean Science**, 10, 967–975. https://doi.org/10.5194/os-10-967-2014, 2014.

PAULUHN, A., & CHAO, Y. Tracking eddies in the subtropical North-Western Atlantic Ocean. **Physics and Chemistry of the Earth**, 24A, 415–421. https://doi.org/10.1016/S1464-1895(99)00052-6, 1999.

POLO, I., LAZAR, A., RODRIGUEZ-FONSECA, B., MIGNOT, J. Growth and decay of the equatorial Atlantic SST mode by means of closed heat budget in a coupled general

circulation model. **Frontiers of Earth Science**, 3, 37. https://doi.org/10.3389/feart.2015.00037, 2015.

RICHARDSON, P. L., HUFFORD, G. E., LIMEBURNER, R., & BROWN, W. S. North Brazil Current retroflection eddies. **Journal of Geophysical Research**, 99, 5081–5093. https://doi.org/10.1029/93JC03486, 1994.

RICHARDSON, P., & WALSH, D. Mapping climatological seasonal variations of surface currents in the tropical Atlantic using ship drifts. **Journal of Geophysical Research**, 91, 10537–10550. https://doi.org/10.1029/jc091ic09p10537, 1986.

RUDZIN, J. E., SHAY, L. K., JAIMES, B., & BREWSTER, J. K. Upper Ocean observations in eastern Caribbean Sea reveal barrier layer within a warm core eddy. **Journal of Geophysical Research: Oceans**, 122, 1057–1071. https://doi.org/10.1002/2016JC012339, 2017.

SADARJOEN, I. A., & POST, F. H. Detection, quantification, and tracking of vortices using streamline geometry. **Computers & Graphics**, 24, 333–341. https://doi.org/10.1016/S0097-8493(00)00029-7, 2000.

SHARMA, N., ANDERSON, S. P., BRICKLEY, P., NOBRE, C., & CADWALLADER, M. L. Quantifying the seasonal and inter-annual variability of the formation and migration pattern of North Brazil Current rings. **Conference paper presented at OCEANS 2009, MTS/IEEE Biloxi – Marine Technology for Our Future: Global and Local Challenge**, IEEE, pp. 1–7. https://doi.org/10.23919/OCEANS.2009.5422142, 2009.

TANABE, A., & CENEDESE, C. Laboratory experiments on mesoscale vortices colliding with an island chain. **Journal of Geophysical Research**, 113, C04022. https://doi.org/10.1029/2007JC004322, 2008.

TYAQUIÇÃ, P., VELEDA, D., LEFÈVRE, N., ARAUJO, M., NORIEGA, C., CANIAUX, G., *ET AL.* Amazon plume salinity response to ocean teleconnections. **Frontiers in Marine Science,** 4, 250. https://doi.org/10.3389/fmars.2017.00250, 2017.

VERBRUGGE, N., MULET, S., GUINEHUT, S., & BUONGIORNO-NARDELLI, B. ARMOR 3D: A 3D multi-observations T, S, U, V product of the ocean. **Geophysical Research Abstracts,** 19th EGU General Assembly, EGU2017, p. 17579, 2017.

WANG, Z.-F., SUN, L., QIU-YANG, L., & CHEMG, H. Two typical merging events of oceanic mesoscale anticyclonic eddies. **Ocean Science**, 15, 1545–1559. https://doi.org/10.5194/os-15-1545-2019, 2019.

YI, J., DU, Y., HE, Z., & ZHOU, C. Enhancing the accuracy of automatic eddy detection and the capability of recognizing the multi-core structures from maps of sea level anomaly. **Ocean Science**, 10, 39–47. https://doi.org/10.5194/os-10-39-2014, 2014.

ZHARKOV, V., & NOF, D. Why does the North Brazil Current regularly shed rings but the Brazil Current does not? **Journal of Physical Oceanography**, 40, 354–367. https://doi.org/10.1175/2009JPO4246.1, 2010.

## 3.6 SUPPORTING INFORMATION

Here we provide the values of the parameters for the weeks of maximum Sea Surface Height Anomaly (SSHa) for each of the 121 analyzed rings (Table 3.S1), and for the evolution of the isolated and merged rings parts of the four observed merges events (Table 3.S4). Also, we deliver each location for three different ring stages (Table 3.S3), the ageostrophic correction in current velocity field (Table 3.S2) and the observed correlations between ring parameters (Table 3.S5).

Regarding the figures, Figure S1 details the distribution of the values for analyzed parameters of each NBC ring. In addition, Figure S2 support the ageostrophic correction in current velocity field, and Figure S3 indicate the influence of ring dynamics in temperature and salinity profiles for the first and the final week of NBC rings. Finally, Figure S4 provides information on the evolution of ring parameters through time.

Figure S1 –Frequency distribution of values obtained for each measured NBC ring parameter.

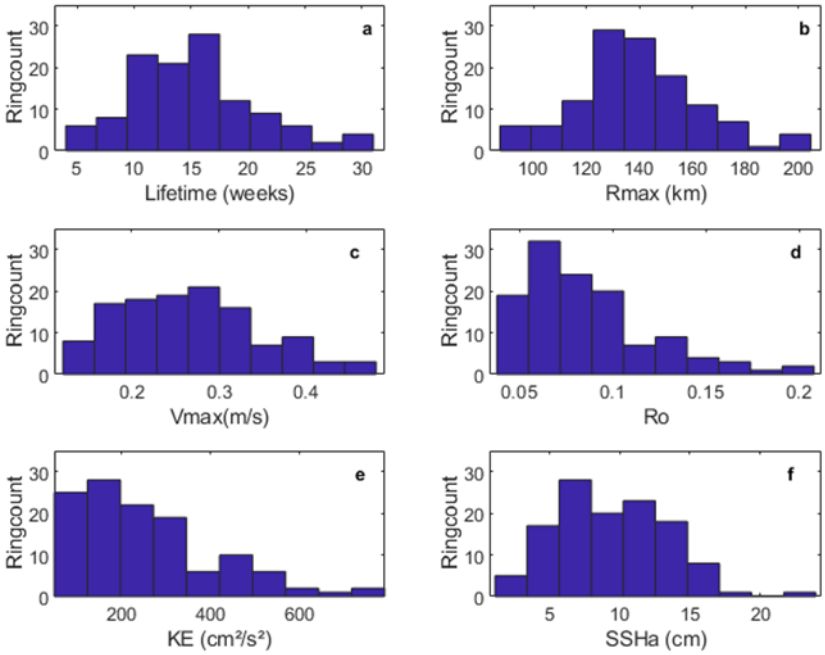


Source: the authors (2019).

Figure S2 –Velocity profiles of the eight observed rings in this study with Ro >= 0.15. The geostrophic profile is depicted with the black dotted line while cyclogeostrophic profile, calculated based on methodology of Iouannou *et al.* (2017), is shown in red

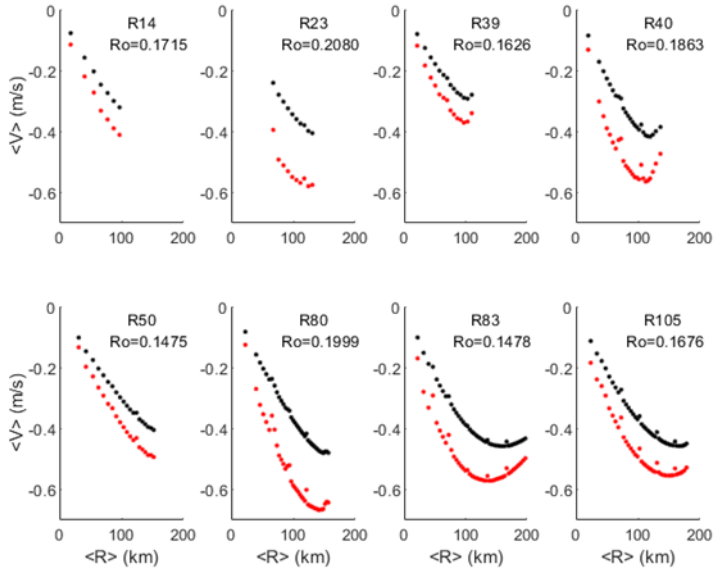


Source: the authors (2020).

Figure S3 –Temperature and salinity profiles anomalies for each ring center identified for position at the first week (a) and at the end week (b), removing the climatology from ring vertical profiles for each position

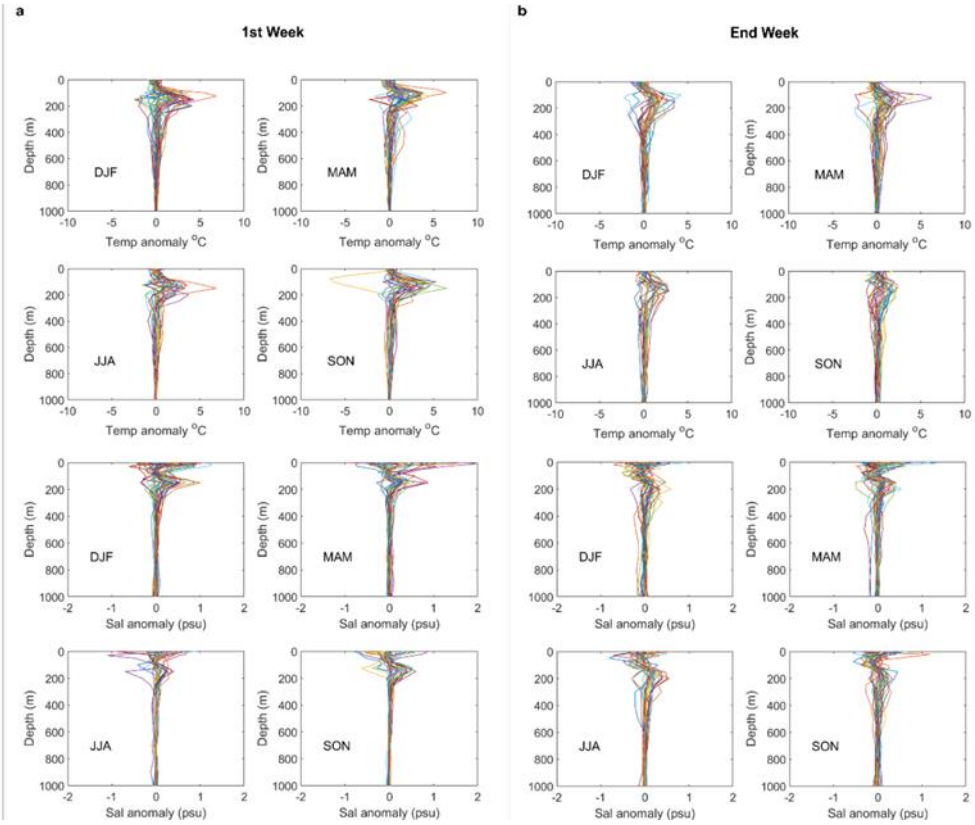


Source: the authors (2020).

Figure S4 –Merging rings parameter evolution. M1 (purple) from R20 (red) and R21 (blue) (A); M2 (purple) from R39 (red) and R40 (blue) (B); M3 (purple) from R78 (blue) and R77 (red) (C); M4 (purple) from R83 (blue) and R82 (red) (D)

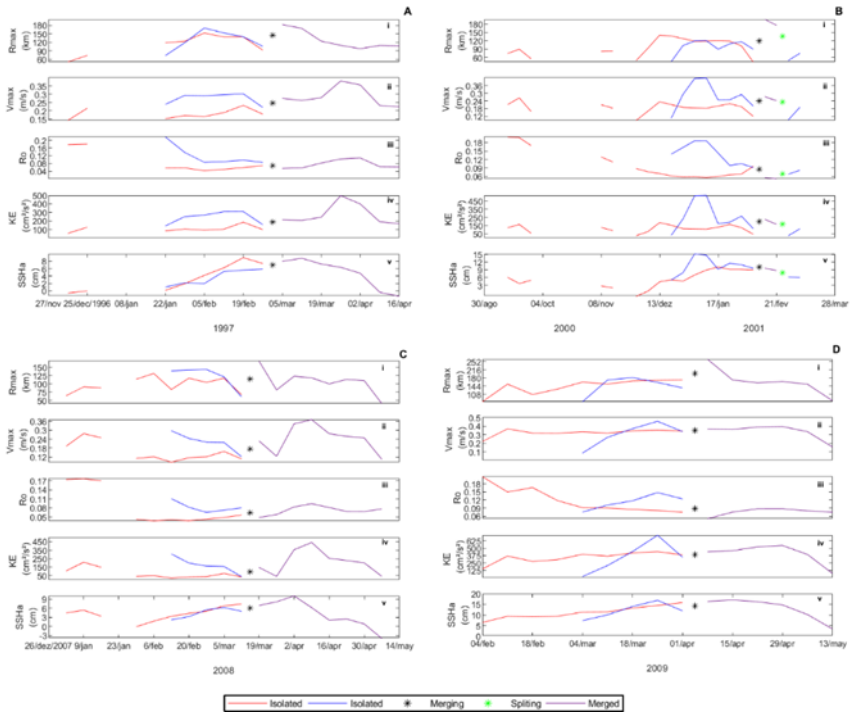


Source: the authors (2020).

Table S1 –Information and parameters values for the week of maximum SSHa obtained for each of the 121 rings analyzed in this study. Vmax and Ro values are for purely geostrophic velocities

| ID | Week of formation | Lifetime (weeks) | Rmax (km) | Vmax (m/s) | Ro | SSHa (cm) | KE (cm2/s2) | Merged with |
|---|---|---|---|---|---|---|---|---|
| ***R1*** | 20 Jan 1993 | 14 | 142.98 | 0.36 | 0.13 | 4.4 | 451.1 | No |
| ***R2*** | 24 Feb 1993 | 14 | 138.64 | 0.17 | 0.05 | 3.8 | 88.0 | No |
| ***R3*** | 7 Apr 1993 | 11 | 131.65 | 0.30 | 0.10 | 9.8 | 259.5 | Eddy |
| ***R4*** | 9 Jun 1993 | 18 | 180.11 | 0.29 | 0.09 | 1.1 | 275.9 | No |
| ***R5*** | 4 Aug 1993 | 22 | 132.82 | 0.27 | 0.09 | 5.9 | 244.7 | No |
| ***R6*** | 3 Nov 1993 | 16 | 128.96 | 0.24 | 0.08 | 6.4 | 217.0 | No |
| ***R7*** | 2 Feb 1994 | 9 | 140.58 | 0.25 | 0.07 | 5.1 | 192.4 | No |
| ***R8*** | 22 Jun 1994 | 12 | 130.65 | 0.20 | 0.07 | 2.8 | 139.7 | No |
| ***R9*** | 20 Jul 1994 | 23 | 95.32 | 0.24 | 0.12 | 2.0 | 161.1 | No |
| ***R10*** | 23 Nov 1994 | 16 | 93.39 | 0.25 | 0.12 | 6.5 | 182.4 | No |
| ***R11*** | 4 Jan 1995 | 15 | 186.36 | 0.31 | 0.06 | 11.2 | 295.4 | No |
| ***R12*** | 8 Mar 1995 | 13 | 138.12 | 0.41 | 0.10 | 14.3 | 570.3 | No |
| ***R13*** | 5 Apr 1995 | 13 | 131.80 | 0.20 | 0.07 | 5.0 | 128.6 | No |
| ***R14*** | 5 Jul 1995 | 22 | 96.89 | 0.32 | 0.17 | 7.4 | 259.8 | No |
| ***R15*** | 6 Dec 1995 | 14 | 161.02 | 0.37 | 0.10 | 12.8 | 487.3 | No |
| ***R16*** | 28 Feb 1996 | 10 | 157.22 | 0.39 | 0.13 | 5.6 | 549.4 | No |
| ***R17*** | 27 Mar 1996 | 13 | 137.13 | 0.24 | 0.06 | 6.3 | 150.1 | No |
| ***R18*** | 24 Jul 1996 | 7 | 130.71 | 0.24 | 0.08 | 6.2 | 202.0 | Eddy |
| ***R19*** | 6 Nov 1996 | 12 | 144.12 | 0.28 | 0.08 | 7.5 | 274.4 | No |
| ***R20*** | 18 Dec 1996 | 10 | 139.09 | 0.23 | 0.06 | 9.0 | 184.5 | Yes, R21 |
| ***R21*** | 22 Jan 1997 | 5 | 106.16 | 0.22 | 0.09 | 5.9 | 155.2 | Yes, R20 |
| ***R22*** | 26 Feb 1997 | 15 | 98.96 | 0.34 | 0.11 | 14.6 | 427.9 | Eddy |
| ***R23*** | 23 Jul 1997 | 24 | 130.88 | 0.41 | 0.21 | 7.0 | 421.6 | No |
| ***R24*** | 29 Oct 1997 | 21 | 150.15 | 0.29 | 0.07 | 14.3 | 299.3 | No |
| ***R25*** | 25 Feb 1998 | 11 | 117.60 | 0.28 | 0.08 | 7.3 | 263.8 | Eddy |
| ***R26*** | 22 Apr 1998 | 9 | 175.57 | 0.26 | 0.08 | 5.1 | 240.7 | No |

| | | | | | | | | |
|---|---|---|---|---|---|---|---|---|
| ***R27*** | 27 May 1998 | 17 | 95.80 | 0.19 | 0.09 | 9.2 | 110.5 | No |
| ***R28*** | 1 Jul 1998 | 19 | 137.35 | 0.16 | 0.05 | 5.1 | 89.5 | No |
| ***R29*** | 18 Nov 1998 | 16 | 112.63 | 0.30 | 0.12 | 6.0 | 218.2 | No |
| ***R30*** | 20 Jan 1999 | 13 | 138.66 | 0.32 | 0.10 | 8.8 | 357.9 | No |
| ***R31*** | 3 Mar 1999 | 20 | 136.36 | 0.23 | 0.06 | 7.8 | 165.9 | No |
| ***R32*** | 7 Jul 1999 | 19 | 124.44 | 0.21 | 0.06 | 6.9 | 143.2 | No |
| ***R33*** | 4 Aug 1999 | 18 | 131.34 | 0.22 | 0.07 | 6.0 | 169.4 | No |
| ***R34*** | 22 Dec 1999 | 13 | 87.25 | 0.25 | 0.12 | 10.0 | 176.4 | No |
| ***R35*** | 2 Feb 2000 | 13 | 118.73 | 0.28 | 0.08 | 8.5 | 278.6 | No |
| ***R36*** | 12 Apr 2000 | 18 | 126.02 | 0.23 | 0.09 | 6.0 | 179.1 | No |
| ***R37*** | 10 May 2000 | 13 | 202.76 | 0.33 | 0.10 | 3.8 | 375.1 | No |
| ***R38*** | 5 Jul 2000 | 22 | 133.95 | 0.14 | 0.04 | 3.8 | 68.4 | No |
| ***R39*** | 13 Sep 2000 | 26 | 120.29 | 0.20 | 0.06 | 10.1 | 130.7 | Yes, R40 |
| ***R40*** | 20 Dec 2000 | 11 | 119.82 | 0.42 | 0.19 | 15.2 | 515.5 | Yes, R39 |
| ***R41*** | 7 Feb 2001 | 16 | 143.12 | 0.20 | 0.06 | 4.2 | 125.6 | No |
| ***R42*** | 7 Mar 2001 | 17 | 112.21 | 0.19 | 0.07 | 4.3 | 106.3 | No |
| ***R43*** | 20 Jun 2001 | 19 | 99.45 | 0.32 | 0.15 | 11.4 | 276.9 | No |
| ***R44*** | 21 Nov 2001 | 14 | 141.01 | 0.33 | 0.09 | 11.5 | 339.2 | No |
| ***R45*** | 30 Jan 2002 | 12 | 141.56 | 0.36 | 0.11 | 14.6 | 435.9 | No |
| ***R46*** | 20 Feb 2002 | 17 | 145.50 | 0.22 | 0.05 | 10.3 | 179.0 | Eddy |
| ***R47*** | 10 Apr 2002 | 14 | 130.81 | 0.28 | 0.08 | 10.6 | 248.7 | No |
| ***R48*** | 15 May 2002 | 13 | 156.67 | 0.31 | 0.13 | 4.2 | 341.4 | No |
| ***R49*** | 26 Jun 2002 | 24 | 155.83 | 0.38 | 0.13 | 6.8 | 493.5 | No |
| ***R50*** | 7 Aug 2002 | 24 | 151.99 | 0.40 | 0.15 | 10.4 | 446.1 | No |
| ***R51*** | 22 Jan 2003 | 11 | 204.79 | 0.24 | 0.04 | 11.3 | 176.1 | Eddy |
| ***R52*** | 12 Feb 2003 | 15 | 153.55 | 0.26 | 0.07 | 8.0 | 244.7 | No |
| ***R53*** | 19 Mar 2003 | 21 | 199.26 | 0.33 | 0.10 | 3.0 | 369.5 | No |
| ***R54*** | 2 Jul 2003 | 29 | 134.64 | 0.17 | 0.05 | 5.9 | 99.9 | No |

| | | | | | | | | |
|---|---|---|---|---|---|---|---|---|
| ***R55*** | 12 Nov 2003 | 22 | 163.91 | 0.27 | 0.06 | 9.2 | 246.2 | No |
| ***R56*** | 21 Apr 2004 | 14 | 132.25 | 0.24 | 0.08 | 5.9 | 200.0 | No |
| ***R57*** | 2 Jun 2004 | 16 | 128.19 | 0.28 | 0.10 | 9.6 | 272.4 | No |
| ***R58*** | 14 Jul 2004 | 31 | 152.97 | 0.30 | 0.09 | 9.1 | 334.2 | No |
| ***R59*** | 29 Dec 2004 | 16 | 193.84 | 0.18 | 0.04 | 5.8 | 105.5 | No |
| ***R60*** | 23 Feb 2005 | 12 | 168.65 | 0.28 | 0.06 | 10.5 | 235.5 | No |
| ***R61*** | 23 Mar 2005 | 14 | 104.05 | 0.17 | 0.07 | 7.5 | 91.2 | No |
| ***R62*** | 27 Apr 2005 | 12 | 113.55 | 0.14 | 0.06 | 12.3 | 57.9 | Eddy |
| ***R63*** | 25 May 2005 | 16 | 125.15 | 0.27 | 0.09 | 12.6 | 238.1 | No |
| ***R64*** | 29 Jun 2005 | 12 | 142.41 | 0.25 | 0.07 | 11.4 | 218.8 | No |
| ***R65*** | 21 Sep 2005 | 15 | 157.45 | 0.28 | 0.07 | 10.8 | 275.9 | No |
| ***R66*** | 26 Oct 2005 | 17 | 102.38 | 0.27 | 0.14 | 4.3 | 213.4 | No |
| ***R67*** | 28 Dec 2005 | 15 | 157.26 | 0.36 | 0.09 | 13.2 | 427.0 | No |
| ***R68*** | 8 Mar 2006 | 19 | 180.76 | 0.19 | 0.04 | 11.4 | 119.4 | Eddy |
| ***R69*** | 21 Jun 2006 | 20 | 142.12 | 0.31 | 0.09 | 12.6 | 344.8 | Eddy |
| ***R70*** | 30 Aug 2006 | 22 | 148.79 | 0.21 | 0.06 | 7.9 | 149.0 | No |
| ***R71*** | 31 Jan 2007 | 12 | 169.40 | 0.30 | 0.08 | 11.4 | 321.9 | No |
| ***R72*** | 14 Feb 2007 | 17 | 124.92 | 0.16 | 0.06 | 2.5 | 81.6 | No |
| ***R73*** | 28 Mar 2007 | 13 | 179.35 | 0.27 | 0.09 | 6.6 | 236.6 | No |
| ***R74*** | 9 May 2007 | 16 | 109.80 | 0.17 | 0.07 | 3.5 | 82.9 | No |
| ***R75*** | 27 Jun 2007 | 17 | 130.60 | 0.18 | 0.06 | 7.4 | 122.7 | No |
| ***R76*** | 25 Jul 2007 | 25 | 148.20 | 0.30 | 0.08 | 9.8 | 316.6 | No |
| ***R77*** | 2 Jan 2008 | 10 | 66.92 | 0.11 | 0.06 | 7.4 | 35.1 | Yes, R78 |
| ***R78*** | 13 Feb 2008 | 4 | 120.73 | 0.22 | 0.07 | 6.3 | 157.9 | Yes, R77 |
| ***R79*** | 7 May 2008 | 9 | 175.59 | 0.22 | 0.04 | 8.3 | 161.9 | Eddy |
| ***R80*** | 9 Jul 2008 | 27 | 148.70 | 0.48 | 0.20 | 9.4 | 645.8 | No |

| | | | | | | | | |
|---|---|---|---|---|---|---|---|---|
| ***R81*** | 31 Dec 2008 | 11 | 161.35 | 0.48 | 0.14 | 9.2 | 789.9 | No |
| ***R82*** | 4 Feb 2009 | 9 | 171.78 | 0.34 | 0.07 | 15.9 | 388.7 | Yes, R83 |
| ***R83*** | 4 Mar 2009 | 5 | 160.59 | 0.46 | 0.15 | 16.9 | 719.8 | Yes, R82 |
| ***R84*** | 12 Aug 2009 | 11 | 117.44 | 0.16 | 0.06 | 6.7 | 83.0 | No |
| ***R85*** | 28 Oct 2009 | 18 | 152.10 | 0.41 | 0.11 | 24.0 | 586.5 | No |
| ***R86*** | 6 Jan 2010 | 9 | 152.40 | 0.16 | 0.04 | 11.6 | 74.2 | No |
| ***R87*** | 17 Feb 2010 | 10 | 131.54 | 0.21 | 0.06 | 10.7 | 143.7 | No |
| ***R88*** | 31 Mar 2010 | 8 | 123.66 | 0.16 | 0.05 | 7.5 | 83.0 | No |
| ***R89*** | 2 Jun 2010 | 9 | 113.75 | 0.18 | 0.06 | 14.0 | 109.8 | No |
| ***R90*** | 7 Jul 2010 | 16 | 158.85 | 0.31 | 0.10 | 9.4 | 334.2 | No |
| ***R91*** | 1 Sep 2010 | 19 | 142.37 | 0.36 | 0.13 | 11.8 | 459.7 | No |
| ***R92*** | 18 May 2011 | 12 | 133.36 | 0.17 | 0.07 | 14.4 | 94.8 | No |
| ***R93*** | 29 Jun 2011 | 16 | 123.07 | 0.27 | 0.10 | 17.0 | 260.2 | No |
| ***R94*** | 7 Sep 2011 | 16 | 121.64 | 0.12 | 0.04 | 6.9 | 49.5 | No |
| ***R95*** | 23 Nov 2011 | 12 | 139.45 | 0.29 | 0.09 | 12.4 | 307.0 | No |
| ***R96*** | 14 Dec 2011 | 12 | 143.99 | 0.24 | 0.07 | 10.1 | 197.9 | No |
| ***R97*** | 15 Feb 2012 | 6 | 172.01 | 0.22 | 0.05 | 14.8 | 155.2 | Eddy |
| ***R98*** | 7 Mar 2012 | 12 | 162.09 | 0.21 | 0.05 | 10.5 | 134.0 | No |
| ***R99*** | 4 Apr 2012 | 13 | 106.71 | 0.17 | 0.06 | 14.0 | 82.8 | No |
| ***R100*** | 16 May 2012 | 14 | 122.57 | 0.22 | 0.09 | 5.4 | 173.6 | No |
| ***R101*** | 20 Jun 2012 | 29 | 149.21 | 0.25 | 0.08 | 9.8 | 208.1 | No |
| ***R102*** | 9 Jan 2013 | 16 | 128.26 | 0.31 | 0.09 | 16.1 | 347.8 | No |
| ***R103*** | 13 Feb 2013 | 15 | 142.22 | 0.34 | 0.11 | 14.8 | 409.1 | No |
| ***R104*** | 26 Jun 2013 | 15 | 124.21 | 0.15 | 0.05 | 10.0 | 78.9 | No |
| ***R105*** | 14 Aug 2013 | 21 | 127.76 | 0.43 | 0.17 | 16.5 | 558.0 | No |
| ***R106*** | 23 Oct 2013 | 16 | 149.17 | 0.25 | 0.06 | 13.0 | 215.7 | No |
| ***R107*** | 8 Jan 2014 | 16 | 165.00 | 0.40 | 0.10 | 15.7 | 567.3 | No |
| ***R108*** | 5 Feb 2014 | 14 | 143.70 | 0.30 | 0.10 | 14.3 | 306.6 | No |
| ***R109*** | 16 Apr 2014 | 13 | 127.01 | 0.23 | 0.10 | 10.8 | 155.0 | No |
| ***R110*** | 4 Jun 2014 | 21 | 143.36 | 0.21 | 0.06 | 10.2 | 149.3 | No |

| | | | | | | | | |
|---|---|---|---|---|---|---|---|---|
| ***R111*** | 15 Oct 2014 | 15 | 113.80 | 0.19 | 0.06 | 13.7 | 124.6 | No |
| ***R112*** | 5 Nov 2014 | 18 | 123.75 | 0.22 | 0.07 | 10.3 | 166.0 | No |
| ***R113*** | 21 Jan 2015 | 13 | 164.99 | 0.19 | 0.05 | 8.4 | 104.5 | No |
| ***R114*** | 11 Mar 2015 | 10 | 112.17 | 0.23 | 0.07 | 12.9 | 179.5 | No |
| ***R115*** | 22 Apr 2015 | 11 | 128.80 | 0.15 | 0.05 | 10.6 | 68.3 | No |
| ***R116*** | 1 Jul 2015 | 29 | 144.89 | 0.40 | 0.13 | 15.3 | 536.8 | No |
| ***R117*** | 9 Sep 2015 | 24 | 158.16 | 0.39 | 0.10 | 18.2 | 522.7 | No |
| ***R118*** | 24 Feb 2016 | 6 | 135.59 | 0.30 | 0.08 | 13.0 | 312.6 | Eddy |
| ***R119*** | 30 Mar 2016 | 5 | 150.61 | 0.24 | 0.06 | 11.8 | 196.2 | No |
| ***R120*** | 5 Oct 2016 | 12, at least | 129.34 | 0.14 | 0.05 | 6.2 | 61.1 | No |
| ***R121*** | 19 Oct 2016 | 10, at least | 142.57 | 0.33 | 0.13 | 11.7 | 369.8 | No |

Source: the authors (2019).

Table S2 –Ageostrophic corrections in Vmax of rings with Ro => 0.15. Obs and Corr indicates modules of Vmax and Ro geostrophic (observed) and cyclogeostrophic (corrected), respectively.

| Ring ID | Ro_obs | Vmax_obs | Ro_corr | Vmax_corr | % Vmax increase |
|---|---|---|---|---|---|
| **R14** | 0.17 | 0.32 | 0.22 | 0.41 | 28.2 |
| **R23** | 0.21 | 0.41 | 0.30 | 0.58 | 42.9 |
| **R39** | 0.16 | 0.29 | 0.21 | 0.37 | 26.9 |
| **R40** | 0.19 | 0.42 | 0.25 | 0.56 | 35.4 |
| **R50** | 0.15 | 0.40 | 0.18 | 0.49 | 21.9 |
| **R80** | 0.20 | 0.48 | 0.28 | 0.67 | 39.0 |
| **R83** | 0.15 | 0.46 | 0.18 | 0.57 | 24.8 |
| **R105** | 0.17 | 0.46 | 0.20 | 0.55 | 21.2 |

Source: the authors (2020).

Table S3 –Location of 121 NBC rings identified by AMEDA in initial, maximum and final weeks.

| | Week of formation | | | Week of Max SSHa | | | End week | | |
|---|---|---|---|---|---|---|---|---|---|
| **ID** | Date | Lat (ºN) | Lon (ºW) | Date | Lat (ºN) | Lon (ºW) | Date | Lat (ºN) | Lon (ºW) |
| **R1** | 20 Jan 1993 | 5.875 | -48.125 | 10 Feb 1993 | 7.875 | -50.875 | 21 Apr 1993 | 11.125 | -59.125 |
| **R2** | 24 Feb 1993 | 5.125 | -46.625 | 21 Apr 1993 | 10.125 | -55.375 | 26 May 1993 | 13.625 | -59.375 |
| **R3** | 7 Apr 1993 | 5.375 | -47.125 | 28 Apr 1993 | 8.625 | -50.875 | 16 Jun 1993 | 11.125 | -57.875 |
| **R4** | 9 Jun 1993 | 4.875 | -46.625 | 7 Jul 1993 | 6.625 | -49.375 | 6 Oct 1993 | 10.375 | -58.375 |
| **R5** | 4 Apr 1993 | 5.375 | -47.375 | 24 Nov 1993 | 9.375 | -54.375 | 29 Dec 1993 | 9.875 | -57.875 |
| **R6** | 3 Nov 1993 | 5.125 | -47.375 | 8 Dec 1993 | 9.375 | -55.875 | 16 Feb 1994 | 12.375 | -58.625 |
| **R7** | 2 Feb 1994 | 6.375 | -49.875 | 2 Mar 1994 | 10.125 | -56.875 | 30 Mar 1994 | 11.875 | -58.875 |
| **R8** | 22 Jun 1994 | 6.125 | -48.875 | 24 Aug 1994 | 9.125 | -55.375 | 7 Sep 1994 | 9.875 | -56.875 |
| **R9** | 20 Jul 1994 | 5.375 | -47.125 | 5 Oct 1994 | 8.125 | -51.625 | 21 Dec 1994 | 11.375 | -58.875 |
| **R10** | 23 Nov 1994 | 5.625 | -48.125 | 28 Dec 1994 | 8.625 | -52.625 | 8 Mar 1995 | 11.875 | -58.375 |
| **R11** | 4 Jan 1995 | 5.875 | -49.125 | 22 Mar 1995 | 10.375 | -55.375 | 12 Apr 1995 | 11.625 | -58.875 |
| **R12** | 8 Mar 1995 | 7.125 | -50.125 | 10 May 1995 | 11.625 | -57.875 | 31 May 1995 | 13.625 | -59.625 |
| **R13** | 5 Apr 1995 | 5.875 | -46.625 | 10 May 1995 | 9.125 | -52.375 | 28 Jun 1995 | 8.625 | -56.875 |
| **R14** | 5 Jul 1995 | 6.875 | -50.375 | 30 Aug 1995 | 7.625 | -50.875 | 29 Nov 1995 | 11.875 | -58.875 |
| **R15** | 6 Dec 1995 | 6.875 | -49.875 | 17 Jan 1996 | 9.375 | -53.125 | 6 Mar 1996 | 13.625 | -59.375 |
| **R16** | 28 Feb 1996 | 6.625 | -49.125 | 13 Mar 1996 | 7.625 | -50.875 | 1 May 1996 | 10.625 | -58.125 |
| **R17** | 27 Mar 1996 | 5.625 | -46.375 | 5 Jun 1996 | 11.625 | -58.375 | 19 Jun 1996 | 13.125 | -60.375 |
| **R18** | 24 Jul 1996 | 7.375 | -50.375 | 14 Aug 1996 | 8.875 | -52.875 | 4 Sep 1996 | 9.125 | -56.125 |
| **R19** | 6 Nov 1996 | 5.125 | -47.125 | 25 Dec 1996 | 9.625 | -55.875 | 22 Jan 1997 | 10.125 | -58.125 |
| **R20** | 18 Dec 1996 | 6.125 | -49.625 | 19 Feb 1997 | 11.375 | -57.125 | 26 Feb 1997 | 11.125 | -57.125 |
| **R21** | 22 Jan 1997 | 5.875 | -49.125 | 26 Feb 1997 | 9.625 | -54.325 | 26 Feb 1997 | 9.625 | -54.325 |
| **R22** | 26 Feb 1997 | 6.875 | -49.625 | 28 May 1997 | 12.125 | -58.375 | 4 Jul 1997 | 12.625 | -59.125 |

| | | | | | | | | | |
|---|---|---|---|---|---|---|---|---|---|
| **R23** | 23 Jul 1997 | 5.625 | -47.625 | 30 Jul 1997 | 5.875 | -48.375 | 31 Dec 1997 | 13.375 | -59.125 |
| **R24** | 29 Oct 1997 | 5.625 | -48.125 | 4 Mar 1998 | 11.125 | -57.125 | 11 Mar 1998 | 13.375 | -59.625 |
| **R25** | 25 Feb 1998 | 6.625 | -49.875 | 22 Apr 1998 | 12.125 | -58.875 | 6 May 1998 | 13.625 | -60.375 |
| **R26** | 22 Apr 1998 | 5.375 | -46.875 | 13 May 1998 | 7.625 | -49.875 | 17 Jun 1998 | 10.375 | -55.375 |
| **R27** | 27 May 1998 | 5.375 | -47.625 | 15 Jul 1998 | 8.625 | -53.125 | 16 Sep 1998 | 13.625 | -59.375 |
| **R28** | 1 Jul 1998 | 5.375 | -47.375 | 28 Oct 1998 | 9.375 | -57.375 | 4 Nov 1998 | 13.625 | -57.625 |
| **R29** | 18 Nov 1998 | 5.875 | -48.625 | 20 Jan 1999 | 9.125 | -53.625 | 3 Mar 1999 | 10.875 | -58.625 |
| **R30** | 20 Jan 1999 | 5.375 | -47.625 | 24 Feb 1999 | 9.625 | -52.875 | 14 Apr 1999 | 13.375 | -59.375 |
| **R31** | 3 Mar 1999 | 6.875 | -49.375 | 19 May 1999 | 11.625 | -58.125 | 14 Jul 1999 | 12.875 | -58.375 |
| **R32** | 7 Jul 1999 | 6.625 | -50.375 | 3 Nov 1999 | 10.625 | -58.625 | 10 Nov 1999 | 10.375 | -59.125 |
| **R33** | 4 Aug 1999 | 5.125 | -46.625 | 24 Nov 1999 | 8.875 | -53.875 | 1 Dec 1999 | 10.875 | -58.875 |
| **R34** | 22 Dec 1999 | 5.875 | -49.125 | 9 Feb 2000 | 9.125 | -53.875 | 15 Mar 2000 | 11.875 | -58.875 |
| **R35** | 2 Feb 2000 | 5.875 | -48.375 | 19 Apr 2000 | 12.125 | -58.875 | 26 Apr 2000 | 12.625 | -59.375 |
| **R36** | 12 Apr 2000 | 5.875 | -48.375 | 3 May 2000 | 8.125 | -50.625 | 9 Aug 2000 | 13.625 | -58.875 |
| **R37** | 10 May 2000 | 5.375 | -46.625 | 31 May 2000 | 6.625 | -49.625 | 2 Aug 2000 | 10.125 | -56.625 |
| **R38** | 5 Jul 2000 | 5.375 | -48.125 | 1 Nov 2000 | 10.375 | -58.125 | 29 Nov 2000 | 11.375 | -58.875 |
| **R39** | 13 Sep 2000 | 5.625 | -47.875 | 17 Jan 2001 | 11.125 | -55.825 | 28 Feb 2001 | 12.875 | -58.825 |
| **R40** | 20 Dec 2000 | 6.625 | -49.125 | 3 Jan 2001 | 7.375 | -50.125 | 1 Mar 2001 | 12.375 | -58.875 |
| **R41** | 7 Feb 2001 | 5.875 | -48.875 | 11 Apr 2001 | 10.125 | -55.625 | 23 May 2001 | 13.625 | -59.625 |
| **R42** | 7 Mar 2001 | 5.125 | -47.125 | 6 Jun 2001 | 9.875 | -55.625 | 27 Jun 2001 | 11.625 | -58.625 |
| **R43** | 20 Jun 2001 | 5.625 | -47.875 | 29 Aug 2001 | 8.625 | -52.375 | 24 Oct 2001 | 8.875 | -56.625 |
| **R44** | 21 Nov 2001 | 6.375 | -49.375 | 6 Feb 2002 | 10.375 | -57.125 | 20 Feb 2002 | 11.125 | -58.875 |
| **R45** | 30 Jan 2002 | 7.125 | -50.125 | 20 Feb 2002 | 8.875 | -52.375 | 17 Apr 2002 | 11.875 | -59.125 |
| **R46** | 20 Feb 2002 | 5.375 | -46.625 | 8 May 2002 | 12.375 | -56.625 | 12 Jun 2002 | 13.625 | -58.375 |
| **R47** | 10 Apr 2002 | 5.375 | -47.625 | 19 Jun 2002 | 10.875 | -56.375 | 10 Jul 2002 | 12.625 | -59.625 |

| | | | | | | | | | |
|---|---|---|---|---|---|---|---|---|---|
| **R48** | 15 May 2002 | 5.625 | -47.625 | 22 May 2002 | 5.875 | -49.125 | 7 Aug 2002 | 11.375 | -58.625 |
| **R49** | 26 Jun 2002 | 5.375 | -47.875 | 17 Jul 2002 | 7.125 | -50.125 | 4 Dec 2002 | 10.625 | -58.875 |
| **R50** | 7 Aug 2002 | 5.125 | -47.625 | 6 Nov 2002 | 7.125 | -50.125 | 15 Jan 2003 | 9.625 | -56.125 |
| **R51** | 22 Jan 2003 | 7.125 | -50.375 | 19 Mar 2003 | 11.125 | -57.625 | 2 Apr 2003 | 11.875 | -59.125 |
| **R52** | 12 Feb 2003 | 5.375 | -46.375 | 9 Apr 2003 | 9.125 | -55.125 | 21 May 2003 | 13.125 | -59.625 |
| **R53** | 19 Mar 2003 | 6.125 | -46.375 | 28 May 2003 | 6.375 | -48.875 | 6 Aug 2003 | 9.625 | -56.625 |
| **R54** | 2 Jul 2003 | 5.375 | -47.625 | 31 Dec 2003 | 9.875 | -57.125 | 14 Jan 2004 | 10.875 | -58.625 |
| **R55** | 12 Nov 2003 | 5.125 | -47.625 | 10 Mar 2004 | 10.375 | -57.375 | 7 Apr 2004 | 10.625 | -58.625 |
| **R56** | 21 Apr 2004 | 5.625 | -46.375 | 9 Jun 2004 | 8.625 | -52.125 | 21 Jul 2004 | 11.375 | -58.375 |
| **R57** | 2 Jun 2004 | 5.125 | -46.875 | 18 Aug 2004 | 9.125 | -55.125 | 15 Sep 2004 | 10.625 | -58.125 |
| **R58** | 14 Jul 2004 | 5.375 | -47.375 | 8 Dec 2004 | 9.125 | -55.875 | 9 Feb 2005 | 13.625 | -59.375 |
| **R59** | 29 Dec 2004 | 6.125 | -49.375 | 16 Feb 2005 | 9.375 | -53.125 | 13 Apr 2005 | 13.375 | -59.875 |
| **R60** | 23 Feb 2005 | 6.375 | -48.875 | 20 Apr 2005 | 10.375 | -56.875 | 11 May 2005 | 12.125 | -58.625 |
| **R61** | 23 Mar 2005 | 5.375 | -46.875 | 1 Jun 2005 | 9.625 | -56.625 | 22 Jun 2005 | 10.875 | -58.875 |
| **R62** | 27 Apr 2005 | 5.875 | -48.625 | 18 May 2005 | 8.625 | -50.625 | 13 Jul 2005 | 13.375 | -59.375 |
| **R63** | 25 May 2005 | 5.625 | -47.375 | 10 Aug 2005 | 9.375 | -55.125 | 7 Sep 2005 | 11.125 | -58.875 |
| **R64** | 29 Jun 2005 | 5.125 | -46.875 | 17 Aug 2005 | 9.625 | -56.125 | 14 Sep 2005 | 12.125 | -58.875 |
| **R65** | 21 Sep 2005 | 5.125 | -47.125 | 23 Nov 2005 | 9.625 | -55.625 | 28 Dec 2005 | 13.625 | -60.375 |
| **R66** | 26 Oct 2005 | 5.625 | -48.375 | 14 Dec 2005 | 7.375 | -51.125 | 15 Feb 2006 | 10.625 | -56.875 |
| **R67** | 28 Dec 2005 | 7.375 | -50.125 | 15 Mar 2006 | 9.875 | -56.375 | 5 Apr 2006 | 11.375 | -58.625 |
| **R68** | 8 Mar 2006 | 5.125 | -46.375 | 7 Jun 2006 | 10.375 | -55.125 | 12 Jul 2006 | 13.125 | -59.375 |
| **R69** | 21 Jun 2006 | 5.375 | -47.625 | 23 Aug 2006 | 9.375 | -54.375 | 1 Nov 2006 | 13.625 | -59.625 |
| **R70** | 30 Aug 2006 | 6.625 | -49.375 | 20 Dec 2006 | 9.625 | -55.375 | 24 Jan 2007 | 12.875 | -59.875 |
| **R71** | 31 Jan 2007 | 6.875 | -50.125 | 14 Mar 2007 | 9.375 | -55.625 | 18 Apr 2007 | 13.625 | -59.625 |
| **R72** | 14 Feb 2007 | 5.875 | -46.375 | 4 Apr 2007 | 8.375 | -52.625 | 6 Jun 2007 | 13.375 | -60.125 |

| | | | | | | | | | |
|---|---|---|---|---|---|---|---|---|---|
| **R73** | 28 Mar 2007 | 6.125 | -47.125 | 18 Apr 2007 | 6.875 | -48.625 | 20 Jun 2007 | 9.875 | -56.875 |
| **R74** | 9 May 2007 | 7.375 | -46.375 | 20 Jun 2007 | 8.375 | -52.125 | 22 Aug 2007 | 11.625 | -58.875 |
| **R75** | 27 Jun 2007 | 5.625 | -48.125 | 5 Sep 2007 | 9.125 | -55.625 | 17 Oct 2007 | 10.375 | -59.375 |
| **R76** | 25 Jul 2007 | 5.375 | -47.125 | 19 Dec 2007 | 9.625 | -55.875 | 9 Jan 2008 | 10.375 | -58.375 |
| **R77** | 2 Jan 2008 | 6.875 | -50.375 | 12 Mar 2008 | 11.375 | -58.125 | 12 Mar 2008 | 11.375 | -58.125 |
| **R78** | 13 Feb 2008 | 7.625 | -51.125 | 5 Mar 2008 | 9.875 | -54.325 | 12 Mar 2008 | 10.125 | -55.625 |
| **R79** | 7 May 2008 | 6.125 | -49.125 | 4 Jun 2008 | 11.375 | -57.125 | 2 Jul 2008 | 13.625 | -58.625 |
| **R80** | 9 Jul 2008 | 5.375 | -47.125 | 10 Sep 2008 | 6.375 | -49.375 | 7 Jan 2009 | 10.125 | -55.125 |
| **R81** | 31 Dec 2008 | 5.875 | -48.875 | 21 Jan 2009 | 8.125 | -51.125 | 11 Mar 2009 | 10.125 | -57.875 |
| **R82** | 4 Feb 2009 | 5.625 | -47.375 | 1 Apr 2009 | 10.625 | -55.375 | 1 Apr 2009 | 10.625 | -55.375 |
| **R83** | 4 Mar 2009 | 5.875 | -46.375 | 25 Mar 2009 | 7.625 | -50.125 | 1 Apr 2009 | 7.875 | -51.125 |
| **R84** | 12 Aug 2009 | 7.625 | -51.375 | 23 Sep 2009 | 9.125 | -55.875 | 21 Oct 2009 | 9.875 | -57.375 |
| **R85** | 28 Oct 2009 | 6.875 | -49.375 | 6 Jan 2010 | 9.875 | -56.125 | 24 Feb 2010 | 13.625 | -59.375 |
| **R86** | 6 Jan 2010 | 6.875 | -49.875 | 17 Feb 2010 | 10.375 | -55.625 | 3 Mar 2010 | 11.375 | -57.875 |
| **R87** | 17 Feb 2010 | 6.875 | -49.625 | 17 Mar 2010 | 9.875 | -55.625 | 21 Apr 2010 | 11.875 | -58.875 |
| **R88** | 31 Mar 2010 | 5.875 | -47.625 | 21 Apr 2010 | 10.375 | -55.125 | 19 May 2010 | 11.625 | -58.875 |
| **R89** | 2 Jun 2010 | 5.625 | -48.375 | 14 Jul 2010 | 9.875 | -55.625 | 28 Jul 2010 | 10.125 | -57.625 |
| **R90** | 7 Jul 2010 | 7.125 | -50.875 | 21 Jul 2010 | 7.875 | -51.625 | 20 Oct 2010 | 12.375 | -59.875 |
| **R91** | 1 Sep 2010 | 5.875 | -48.125 | 20 Oct 2010 | 7.625 | -51.125 | 5 Jan 2011 | 13.125 | -59.375 |
| **R92** | 18 May 2011 | 6.125 | -49.375 | 1 Jun 2011 | 7.625 | -49.875 | 3 Aug 2011 | 9.875 | -57.125 |
| **R93** | 29 Jun 2011 | 6.625 | -49.375 | 31 Aug 2011 | 8.875 | -53.625 | 12 Oct 2011 | 10.875 | -58.875 |
| **R94** | 7 Sep 2011 | 5.625 | -48.125 | 14 Dec 2011 | 10.375 | -58.125 | 21 Dec 2011 | 11.125 | -58.625 |
| **R95** | 23 Nov 2011 | 8.125 | -51.375 | 14 Dec 2011 | 8.875 | -53.125 | 8 Feb 2012 | 13.625 | -59.875 |
| **R96** | 14 Dec 2011 | 5.375 | -47.875 | 15 Feb 2012 | 9.875 | -55.125 | 29 Feb 2012 | 10.625 | -56.625 |
| **R97** | 15 Feb 2012 | 7.125 | -50.375 | 29 Feb 2012 | 10.375 | -53.125 | 21 Mar 2012 | 10.875 | -58.125 |

| | | | | | | | | | |
|---|---|---|---|---|---|---|---|---|---|
| **R98** | 7 Mar 2012 | 6.125 | -46.375 | 18 Apr 2012 | 10.125 | -53.875 | 23 May 2012 | 11.125 | -58.625 |
| **R99** | 4 Apr 2012 | 5.375 | -47.125 | 6 Jun 2012 | 10.625 | -54.875 | 27 Jun 2012 | 10.875 | -58.375 |
| **R100** | 16 May 2012 | 5.125 | -47.625 | 20 Jun 2012 | 8.125 | -51.125 | 15 Aug 2012 | 13.125 | -57.875 |
| **R101** | 20 Jun 2012 | 5.375 | -47.125 | 31 Oct 2012 | 8.375 | -53.125 | 2 Jan 2013 | 10.875 | -59.125 |
| **R102** | 9 Jan 2013 | 6.875 | -49.875 | 10 Apr 2013 | 11.125 | -57.375 | 24 Apr 2013 | 13.625 | -59.375 |
| **R103** | 13 Feb 2013 | 5.875 | -48.125 | 3 Apr 2013 | 8.375 | -51.125 | 22 May 2013 | 12.875 | -56.875 |
| **R104** | 26 Jun 2013 | 7.375 | -50.625 | 11 Sep 2013 | 10.125 | -57.625 | 2 Oct 2013 | 11.125 | -58.625 |
| **R105** | 14 Aug 2013 | 7.125 | -49.875 | 2 Oct 2013 | 7.875 | -50.875 | 1 Jan 2014 | 11.625 | -58.875 |
| **R106** | 23 Oct 2013 | 5.125 | -46.875 | 29 Jan 2014 | 10.875 | -57.875 | 5 Feb 2014 | 11.375 | -58.375 |
| **R107** | 8 Jan 2014 | 6.875 | -49.875 | 5 Feb 2014 | 9.375 | -53.375 | 23 Apr 2014 | 10.625 | -58.125 |
| **R108** | 5 Feb 2014 | 5.875 | -48.125 | 12 Mar 2014 | 8.625 | -52.375 | 7 May 2014 | 13.625 | -59.875 |
| **R109** | 16 Apr 2014 | 5.375 | -47.375 | 21 May 2014 | 7.375 | -50.375 | 9 Jul 2014 | 13.125 | -59.375 |
| **R110** | 4 Jun 2014 | 5.625 | -48.875 | 27 Aug 2014 | 9.875 | -56.375 | 22 Oct 2014 | 11.625 | -59.125 |
| **R111** | 15 Oct 2014 | 5.125 | -47.375 | 31 Dec 2014 | 11.125 | -56.625 | 21 Jan 2015 | 11.375 | -58.625 |
| **R112** | 5 Nov 2014 | 5.875 | -48.875 | 11 Feb 2015 | 10.375 | -58.125 | 4 Mar 2015 | 11.875 | -59.125 |
| **R113** | 21 Jan 2015 | 7.125 | -50.125 | 18 Mar 2015 | 7.875 | -51.375 | 15 Apr 2015 | 13.125 | -59.875 |
| **R114** | 11 Mar 2015 | 7.375 | -50.625 | 6 May 2015 | 11.625 | -58.375 | 13 May 2015 | 12.125 | -59.125 |
| **R115** | 22 Apr 2015 | 7.625 | -51.375 | 17 Jun 2015 | 10.125 | -54.125 | 1 Jul 2015 | 10.875 | -56.125 |
| **R116** | 1 Jul 2015 | 5.375 | -47.375 | 26 Aug 2015 | 8.125 | -51.625 | 13 Jan 2016 | 9.125 | -59.375 |
| **R117** | 9 Sep 2015 | 5.125 | -47.125 | 13 Jan 2016 | 9.625 | -55.625 | 17 Feb 2016 | 10.625 | -58.625 |
| **R118** | 24 Feb 2016 | 6.125 | -48.375 | 16 Mar 2016 | 10.875 | -57.125 | 30 Mar 2016 | 11.125 | -58.375 |
| **R119** | 30 Mar 2016 | 5.875 | -46.875 | 20 Apr 2016 | 10.125 | -56.625 | 27 Apr 2016 | 10.375 | -57.625 |
| **R120** | 5 Oct 2016 | 4.625 | -47.375 | 7 Dec 2016 | 8.625 | -57.125 | NaN | NaN | NaN |
| **R121** | 19 Oct 2016 | 5.125 | -47.625 | 14 Dec 2016 | 6.875 | -49.875 | NaN | NaN | NaN |

Source: the authors (2020).

Table S4 – Observed values of the analyzed parameters for each week of eigth isolated rings (Rs) which merged into four merged (Ms) rings. NaN values are indicated in weeks that AMEDA did not identify the ring. Vmax and Ro values are for purely geostrophic velocities. Merged rings cells are highlighted in blue

| ID | Week | Rmax(km) | Vmax (m/s) | Ro | SSHa(cm) | KE (cm2/s2) | Lat (º) | Lon(º) |
|---|---|---|---|---|---|---|---|---|
| ***R20*** | 18 Dec 1996 | 51.50 | 0.14 | 0.18 | -0.6 | 53.6 | 6.125 | -49.625 |
| | 25 Dec 1996 | 74.12 | 0.22 | 0.18 | -0.1 | 124.9 | 6.375 | -49.875 |
| | 1 Jan 1997 | NaN | NaN | NaN | NaN | NaN | NaN | NaN |
| | 8 Jan 1997 | NaN | NaN | NaN | NaN | NaN | NaN | NaN |
| | 15 Jan 1997 | NaN | NaN | NaN | NaN | NaN | NaN | NaN |
| | 22 Jan 1997 | 118.49 | 0.15 | 0.06 | 0.1 | 81.8 | 9.125 | -53.875 |
| | 29 Jan 1997 | 123.79 | 0.17 | 0.06 | 1.9 | 104.2 | 9.625 | -54.825 |
| | 5 Feb 1997 | 152.43 | 0.17 | 0.04 | 4.2 | 91.5 | 10.125 | -55.825 |
| | 12 Feb 1997 | 138.84 | 0.19 | 0.05 | 6.2 | 102.0 | 10.875 | -56.825 |
| | 19 Feb 1997 | 139.09 | 0.23 | 0.06 | 9.0 | 184.5 | 11.375 | -57.125 |
| | 26 Feb 1997 | 92.66 | 0.18 | 0.07 | 7.4 | 97.7 | 11.125 | -57.125 |
| | | | | | | | | |
| ***R21*** | 22 Jan 1997 | 73.65 | 0.24 | 0.22 | 1.0 | 140.3 | 5.875 | -49.125 |
| | 29 Jan 1997 | 118.87 | 0.29 | 0.14 | 2.2 | 250.8 | 7.125 | -49.875 |
| | 5 Feb 1997 | 196.98 | 0.29 | 0.09 | 2.0 | 268.3 | 7.875 | -50.875 |
| | 12 Feb 1997 | 152.78 | 0.30 | 0.09 | 5.2 | 307.9 | 8.625 | -52.125 |
| | 19 Feb 1997 | 139.14 | 0.30 | 0.10 | 5.6 | 309.8 | 8.875 | -52.875 |
| | 26 Feb 1997 | 106.16 | 0.22 | 0.09 | 5.9 | 155.2 | 9.625 | -54.325 |
| | | | | | | | | |
| ***M1*** | 5 Mar 1997 | 182.24 | 0.28 | 0.05 | 8.0 | 212.8 | 11.125 | -57.375 |
| | 12 Mar 1997 | 168.87 | 0.26 | 0.06 | 8.8 | 205.5 | 10.875 | -57.875 |
| | 19 Mar 1997 | 124.09 | 0.28 | 0.08 | 7.3 | 242.7 | 10.875 | -58.825 |
| | 26 Mar 1997 | 109.48 | 0.38 | 0.10 | 6.4 | 497.1 | 13.375 | -59.125 |

| | | | | | | | | |
|---|---|---|---|---|---|---|---|---|
| | 2 Apr 1997 | 97.78 | 0.36 | 0.11 | 4.8 | 399.8 | 13.375 | -59.325 |
| | 9 Apr 1997 | 109.11 | 0.23 | 0.06 | -0.4 | 189.0 | 13.375 | -59.325 |
| | 16 Apr 1997 | 107.66 | 0.23 | 0.06 | -1.5 | 167.3 | 13.375 | -59.325 |
| | | | | | | | | |
| ***R39*** | 13 Sep 2000 | 74.38 | 0.21 | 0.20 | 6.1 | 123.6 | 5.625 | -47.875 |
| | 20 Sep 2000 | 89.96 | 0.26 | 0.20 | 3.7 | 163.9 | 5.875 | -48.625 |
| | 27 Sep 2000 | 55.93 | 0.16 | 0.17 | 5.0 | 57.4 | 6.625 | -49.325 |
| | 4 Oct 2000 | NaN | NaN | NaN | NaN | NaN | NaN | NaN |
| | 11 Oct 2000 | NaN | NaN | NaN | NaN | NaN | NaN | NaN |
| | 18 Oct 2000 | NaN | NaN | NaN | NaN | NaN | NaN | NaN |
| | 25 Oct 2000 | NaN | NaN | NaN | NaN | NaN | NaN | NaN |
| | 1 Nov 2000 | NaN | NaN | NaN | NaN | NaN | NaN | NaN |
| | 8 Nov 2000 | 82.11 | 0.21 | 0.13 | 2.8 | 127.2 | 7.875 | -51.625 |
| | 15 Nov 2000 | 83.02 | 0.18 | 0.11 | 2.0 | 88.9 | 7.875 | -51.875 |
| | 22 Nov 2000 | NaN | NaN | NaN | NaN | NaN | NaN | NaN |
| | 29 Nov 2000 | 48.98 | 0.09 | 0.09 | -1.3 | 26.6 | 8.125 | -52.325 |
| | 6 Dec 2000 | 93.55 | 0.16 | 0.08 | 0.7 | 76.1 | 8.875 | -53.325 |
| | 13 Dec 2000 | 140.66 | 0.23 | 0.07 | 4.4 | 186.3 | 9.375 | -53.875 |
| | 20 Dec 2000 | 137.84 | 0.21 | 0.06 | 5.2 | 154.6 | 9.875 | -54.125 |
| | 27 Dec 2000 | 128.40 | 0.19 | 0.06 | 4.6 | 112.6 | 10.125 | -54.325 |
| | 3 Jan 2001 | 118.85 | 0.19 | 0.06 | 7.0 | 109.7 | 10.625 | -55.125 |
| | 10 Jan 2001 | 119.31 | 0.18 | 0.06 | 8.9 | 106.8 | 10.875 | -55.625 |
| | 17 Jan 2001 | 120.29 | 0.20 | 0.06 | 10.1 | 130.7 | 11.125 | -55.825 |
| | 24 Jan 2001 | 119.21 | 0.22 | 0.07 | 9.2 | 164.6 | 11.125 | -56.325 |
| | 31 Jan 2001 | 102.09 | 0.20 | 0.07 | 9.2 | 125.0 | 11.125 | -56.325 |

| | | | | | | | | |
|---|---|---|---|---|---|---|---|---|
| | 7 Feb 2001 | 44.14 | 0.12 | 0.10 | 9.0 | 45.1 | 11.375 | -56.825 |
| | 14 Feb 2001 | NaN | NaN | NaN | NaN | NaN | NaN | NaN |
| | 21 Feb 2001 | NaN | NaN | NaN | NaN | NaN | NaN | NaN |
| | 28 Feb 2001 | 47.51 | 0.11 | 0.07 | 5.9 | 38.7 | 12.875 | -58.825 |
| | | | | | | | | |
| ***R40*** | 20 Dec 2000 | 45.39 | 0.11 | 0.14 | 5.1 | 31.6 | 6.625 | -49.125 |
| | 27 Dec 2000 | 103.29 | 0.29 | 0.16 | 7.9 | 231.5 | 6.875 | -49.625 |
| | 3 Jan 2001 | 119.82 | 0.42 | 0.19 | 15.2 | 515.5 | 7.375 | -50.125 |
| | 10 Jan 2001 | 120.89 | 0.42 | 0.19 | 14.7 | 519.9 | 7.375 | -50.375 |
| | 17 Jan 2001 | 90.19 | 0.25 | 0.14 | 9.2 | 174.1 | 7.625 | -50.875 |
| | 24 Jan 2001 | 109.57 | 0.25 | 0.10 | 11.6 | 191.1 | 9.125 | -52.375 |
| | 31 Jan 2001 | 117.19 | 0.29 | 0.10 | 11.0 | 266.7 | 9.375 | -53.375 |
| | 7 Feb 2001 | 90.26 | 0.20 | 0.09 | 9.6 | 113.4 | 9.625 | -54.625 |
| | 14 Feb 2001 | NaN | NaN | NaN | NaN | NaN | NaN | NaN |
| | 21 Feb 2001 | NaN | NaN | NaN | NaN | NaN | NaN | NaN |
| | 28 Feb 2001 | 48.97 | 0.09 | 0.07 | 6.2 | 25.6 | 10.875 | -58.625 |
| | 7 Mar 2001 | 75.33 | 0.19 | 0.08 | 6.0 | 110.9 | 12.375 | -58.875 |
| | | | | | | | | |
| ***M2*** | 14 Feb 2001 | 197.54 | 0.27 | 0.06 | 9.6 | 226.1 | 9.875 | -55.875 |
| | 21 Feb 2001 | 176.50 | 0.24 | 0.05 | 8.8 | 165.6 | 10.625 | -57.625 |
| | | | | | | | | |
| | | | | | | | | |
| ***R77*** | 2 Jan 2008 | 63.70 | 0.19 | 0.17 | 4.4 | 104.6 | 6.875 | -50.375 |
| | 9 Jan 2008 | 90.45 | 0.28 | 0.18 | 5.3 | 207.3 | 6.875 | -50.625 |
| | 16 Jan 2008 | 87.72 | 0.25 | 0.17 | 3.4 | 147.8 | 6.625 | -50.625 |
| | 23 Jan 2008 | NaN | NaN | NaN | NaN | NaN | NaN | NaN |
| | 30 Jan 2008 | 113.73 | 0.11 | 0.04 | -0.1 | 41.1 | 9.125 | -53.875 |

| | | | | | | | | |
|---|---|---|---|---|---|---|---|---|
| | 6 Feb 2008 | 130.97 | 0.12 | 0.04 | 1.7 | 48.4 | 9.875 | -55.125 |
| | 13 Feb 2008 | 82.52 | 0.09 | 0.04 | 3.3 | 22.2 | 10.125 | -56.125 |
| | 20 Feb 2008 | 116.63 | 0.12 | 0.04 | 4.3 | 34.5 | 10.375 | -56.875 |
| | 27 Feb 2008 | 104.09 | 0.12 | 0.04 | 5.0 | 37.9 | 10.875 | -57.325 |
| | 5 Mar 2008 | 116.67 | 0.16 | 0.05 | 6.8 | 75.2 | 11.125 | -57.825 |
| | 12 Mar 2008 | 66.92 | 0.11 | 0.06 | 7.4 | 35.1 | 11.375 | -58.125 |
| | | | | | | | | |
| ***R78*** | 13 Feb 2008 | 139.20 | 0.30 | 0.11 | 2.2 | 305.2 | 7.625 | -51.125 |
| | 20 Feb 2008 | 141.13 | 0.25 | 0.08 | 3.2 | 197.7 | 8.375 | -52.325 |
| | 27 Feb 2008 | 143.02 | 0.22 | 0.07 | 5.5 | 162.7 | 9.375 | -53.325 |
| | 5 Mar 2008 | 120.73 | 0.22 | 0.07 | 6.2 | 157.9 | 9.875 | -54.325 |
| | 12 Mar 2008 | 60.32 | 0.12 | 0.08 | 5.0 | 38.1 | 10.125 | -55.625 |
| | | | | | | | | |
| ***M3*** | 19 Mar 2008 | 168.30 | 0.23 | 0.05 | 6.9 | 145.9 | 11.125 | -58.375 |
| | 26 Mar 2008 | 81.08 | 0.13 | 0.06 | 8.1 | 40.8 | 10.625 | -58.625 |
| | 2 Apr 2008 | 122.49 | 0.34 | 0.08 | 10.1 | 354.3 | 13.375 | -59.125 |
| | 9 Apr 2008 | 117.67 | 0.37 | 0.09 | 6.2 | 440.0 | 13.375 | -59.325 |
| | 16 Apr 2008 | 99.53 | 0.28 | 0.08 | 2.1 | 252.6 | 13.625 | -59.625 |
| | 23 Apr 2008 | 113.16 | 0.26 | 0.07 | 2.4 | 228.3 | 13.375 | -59.625 |
| | 30 Apr 2008 | 109.23 | 0.25 | 0.07 | 0.8 | 199.7 | 13.375 | -59.625 |
| | 7 May 2008 | 39.95 | 0.11 | 0.08 | -4.0 | 41.2 | 13.625 | -59.325 |
| | | | | | | | | |
| ***R82*** | 4 Feb 2009 | 75.33 | 0.22 | 0.21 | 6.5 | 149.2 | 5.625 | -47.375 |
| | 11 Feb 2009 | 152.98 | 0.37 | 0.15 | 9.4 | 368.4 | 6.375 | -48.625 |
| | 18 Feb 2009 | 106.78 | 0.32 | 0.17 | 9.2 | 276.2 | 7.125 | -49.875 |
| | 25 Feb 2009 | 131.10 | 0.32 | 0.12 | 9.4 | 306.6 | 8.125 | -51.375 |

| | | | | | | | | |
|---|---|---|---|---|---|---|---|---|
| | 4 Mar 2009 | 162.04 | 0.33 | 0.09 | 11.4 | 397.4 | 8.875 | -52.375 |
| | 11 Mar 2009 | 153.40 | 0.32 | 0.09 | 11.5 | 365.6 | 9.125 | -53.375 |
| | 18 Mar 2009 | 167.03 | 0.35 | 0.09 | 13.3 | 420.3 | 9.625 | -54.125 |
| | 25 Mar 2009 | 169.85 | 0.35 | 0.08 | 14.5 | 441.4 | 10.125 | -54.875 |
| | 1 Apr 2009 | 171.78 | 0.34 | 0.07 | 15.9 | 388.7 | 10.625 | -55.375 |
| | | | | | | | | |
| ***R83*** | 4 Mar 2009 | 74.97 | 0.08 | 0.08 | 7.4 | 19.8 | 5.875 | -46.325 |
| | 11 Mar 2009 | 171.37 | 0.27 | 0.10 | 10.1 | 207.0 | 6.125 | -47.325 |
| | 18 Mar 2009 | 181.96 | 0.37 | 0.12 | 14.0 | 443.7 | 6.875 | -49.125 |
| | 25 Mar 2009 | 160.59 | 0.46 | 0.15 | 16.9 | 719.8 | 7.625 | -50.125 |
| | 1 Apr 2009 | 136.24 | 0.34 | 0.12 | 12.0 | 347.9 | 7.875 | -51.125 |
| | | | | | | | | |
| ***M4*** | 8 Apr 2009 | 263.33 | 0.37 | 0.05 | 16.4 | 440.3 | 10.875 | -56.125 |
| | 15 Apr 2009 | 171.45 | 0.36 | 0.08 | 17.1 | 457.8 | 11.125 | -56.625 |
| | 22 Apr 2009 | 158.86 | 0.39 | 0.09 | 16.3 | 523.3 | 11.125 | -57.125 |
| | 29 Apr 2009 | 164.58 | 0.40 | 0.09 | 14.7 | 546.6 | 10.875 | -57.875 |
| | 6 May 2009 | 152.43 | 0.34 | 0.08 | 10.2 | 394.0 | 10.875 | -58.375 |
| | 13 May 2009 | 79.22 | 0.16 | 0.07 | 3.4 | 71.9 | 10.375 | -58.875 |

Source: the authors (2020).

Table S5 – Pearson correlation index between ring parameters computed from the merging rings evolution. Correlations > 60 % are depicted in bold

| | **Rmax** | **Vmax** | **Ro** | **KE** | **SSHa** |
|---|---|---|---|---|---|
| **Rmax** | 1 | | | | |
| **Vmax** | **0.6303** | 1 | | | |
| **Ro** | 0.0976 | 0.3152 | 1 | | |
| **KE** | **0.6135** | **0.9643** | 0.2220 | 1 | |
| **SSHa** | 0.5397 | **0.6207** | 0.2746 | **0.6637** | 1 |

Source: the authors (2020).

# 4 ARTIGO 2 - $CO_2$ FLUX RESPONSE TO THE NORTH BRAZIL CURRENT RINGS

Este artigo representa o segundo produto desta dissertação e será submetido à revista *Frontiers in Marine Biogeochemistry* nos próximos meses. Este trata de uma investigação, baseada em análises estatísticas e dados físicos e biogeoquímicos de um modelo de reanálise oceânica, para analisar o papel dos Vórtices da Corrente Norte do Brasil na biogeoquímica, e especialmente nos fluxos de $CO_2$ entre oceano e atmosfera no Atlântico Norte Tropical Ocidental. Um algoritmo híbrido para identificação e rastreio destes vórtices é aplicado às anomalias das variáveis em uma escala diária. A partir desse trabalho pode-se observar que a variância destas estruturas corresponde aos consequentes aumentos de $fCO_{2\ SW}$ nos centros dos vórtices, com modos de covariância similares somando 29%. Observou-se que isto ocorre devido à concentração de DIC e sal nos núcleos dos anéis. Por fim, vórtices da CNB geraram em média anomalias positivas de $FCO_2$ de 0.38 mmol $m^{-2}$ $day^{-1}$ em relação às águas exteriores à estrutura entre 50ºW – 56ºW, atuando como núcleos de fonte de $CO_2$ para a atmosfera. O presente trabalho tem como autores: Léo C. Aroucha[1,2,3], Dóris Veleda[1,2,3], e N. Lefèvre[4].

[1]*Laboratory of Physical, Coastal and Estuarine Oceanography – LOFEC, Federal University of Pernambuco – UFPE, Recife, Brazil. leo_aroucha@hotmail.com*

[2]*Renewable Energy Center – CER, Federal University of Pernambuco – UFPE, Recife, Brazil,*

[3]*Department of Oceanography - UFPE, Cidade Universitária, Recife, Brazil,*

[4]*LOCEAN, IRD, Sorbonne Université Paris, Paris, France,*

[5]*Center for Risk Analysis and Environmental Modeling – CEERMA, Federal University of Pernambuco – UFPE, Recife, Brazil*

## 4.1 INTRODUCTION

North Brazil Current (NBC) rings are large anticyclonic warm-core rings, associated with positive anomalies of sea surface height (SSH) and downwelling in their centers. Aroucha *et al.* (2020) pointed that downwelling associated with NBC anticyclonic rings deepens thermocline and modifies the vertical salinity profile. These structures are shed from the NBC retroflection (6º-8ºN, 48º- 45ºW) in a 3-7 rings/year, and travel northwestward for 3 to 4 months, with a translation velocity from 7-20 km/day, until colliding with the Lesser Antilles (DIDDEN & SCHOTT, 1993; FRATANTONI & RICHARDSON, 2006; JOCHUMSEN *et*

*al.*, 2010; JOHNS *et al.*, 2003; AROUCHA *et al.*, 2020). They present typically a diameter from 300-400km, SSH anomalies reaching 30cm, surface azimuthal velocities of 1m/s, and extend deeper than 1000m (JOHNS *et al.*, 1990; DIDDEN; SCHOTT, 1993; FRATANTONI *et al.*, 1995; FRATANTONI; GLICKSON, 2002; GONI; JOHNS, 2003, FRATANTONI; RICHARDSON, 2006; AROUCHA *et al.*, 2020). Furthermore, they contribute to the dispersion of fresh nutrient-rich waters from the Amazon and Orinoco Rivers toward the Caribbean (JOHNS *et al.*, 1990) until the Gulf of Mexico (HUANG *et al.*, 2021), also affecting local circulation, that influences planktonic fish larvae recruitment and growth (COWEN *et al.*, 2003). In fact, Ffield (2005) observed that depth-intensified rings were able to capture riverine freshwater at the surface, while surface-intensified rings carry tropical Atlantic waters in their centers, with Amazon plume waters placed at the ring periphery.

The Amazon River discharge counts up to 20% of riverine input into the oceans, and nearly half of the fresh-water entry in the tropical North Atlantic (CARTON, 1991). The higher discharges are related to seasonal rainy periods in the South Atlantic continent and interannual variability under the influence of ENSO years (TYAQUIÇÃ *et al.*, 2017). Amazon River plume have been constantly linked to areas of very low carbon concentration in the Tropical Atlantic (KÖRTZINGER, 2003; COOLEY *et al.*, 2007; LEFÈVRE *et al.* 2010; LEFÈVRE *et al.* 2017). These previous works pointed to salinity as the main driver for $CO_2$ variations. On the one hand, the mixing of Amazon waters with oceanic waters decreases $fCO_2$ as a result of the carbon system properties. On the other hand, reduced estuarine turbidity and increased nutrient availability increase primary production, which causes $CO_2$ uptake. Ternon *et al.* (2000) estimated that primary productivity at the Amazon River plume is responsible for 30% of $CO_2$ consumption in the tropical Atlantic. Net primary productivity reduces over a hundred times the $CO_2$ concentration in this plume (COOLEY *et al.*, 2007), and chlorophyll high-peaks are connected to a decrease in ocean $CO_2$ fugacity($fCO_2$) (i.e., $CO_2$ partial pressures corrected for the behavior of a non-ideal gas) (LEFÈVRE *et al.*, 2020). Additionally, Cooley *et al.* (2007) indicated that ocean-atmosphere conditions, such as temperature, wind, and precipitation, control river dynamics, CO2 solubility, and gas exchange, affect the Amazon plume's extent sink of CO2. On the other hand, in general, the Tropical Atlantic is a region of $CO_2$ source to the atmosphere. (LEFÈVRE *et al.*, 1998). This fact is mainly related to the equatorial upwelling, which brings surface $CO_2$-rich waters from depth, increasing surface $CO_2$ saturation in this region (LEFÈVRE *et al.*, 1998).

It is believed that the presence of NBC rings trajectories over river plumes might change the ocean carbon export due to eddies dynamics. Some studies investigated relations between

carbon balance and ocean rings, and their importance in $CO_2$ exchange across the ocean-atmosphere interface (MOURIÑO *et al.*, 2003; SONG *et al.*, 2016; ORSELLI *et al.*, 2019). Mesoscale eddies were presented as a fundamental part of these processes at Drake Passage, where in the summer, anticyclonic (cyclonic) eddies were able to capture more (less) $CO_2$ than adjacent waters, while in winter, the opposite occurs (SONG *et al.*, 2016). Orselli *et al.* (2019), in its turn, showed that anticyclonic eddies from the Agulhas Leakage represents punctual regions of $CO_2$ sink in the Atlantic, also being able to contribute to South Atlantic Central Water acidification. On the contrary, Mouriño *et al.* (2003), identified that subtropical rings contributed to less than 1% of the total net production in the Northeastern Atlantic, suggesting a negligible influence of these rings.

Therefore, the processes affecting $CO_2$ fluxes in the ring cores vary from one region to another and depend on eddy dynamics. Given the complex environment of the WTNA (e.g., the presence of Amazon plume), the role of the NBC rings in changing the biogeochemical processes, and consequently, the air-sea $CO_2$ flux is still unclear. Thus, this study aims to comprehend how NBC rings dynamics might influence physical and especially biogeochemical processes in the WTNA, and if they can impact the air-sea $CO_2$ flux.

## 4.2 DATA AND METHODS

### 4.2.1. Study Area

The domain of this study is restricted to the WTNA region (5ºS-15ºN, 65ºW-45ºW), since it is the area of the NBC retroflection (6º-8ºN, 48º- 45ºW) leading to ring generation. In addition, we highlight the presence of both Amazon and Orinoco River plumes, which have demonstrated to be related to NBC rings (FFIELD, 2005) and to be important for the area as they affect physical and biogeochemical processes (SMITH; DEMASTER, 1996; FROIDEFOND *et al.*, 2002; KÖRTZINGER, 2003; LEFÈVRE *et al.*, 2010).

### 4.2.2. Mercator Model

In this study, we used: daily physical data from the GLORYS12v1 model, from 1993 to 2017, with a spatial and vertical resolution of 1/12º and 28 levels until 260m, respectively; and daily biogeochemical data from BIORYS2V4, with a spatial and vertical resolution of 1/4º and

35 levels until 300m, respectively. Both models are available from the Mercator Ocean project (www.mercator-ocean.fr). Mercator simulations are based on NEMO (Nucleus for European Modeling of the Ocean) modeling platform, with global coverage from 1993-2019. The biogeochemical component PISCES (AUMONT *et al.*, 2015) is coupled offline to the hydrodynamic component NEMO on a daily frequency. Both components are forced by atmospheric fields from ERA-Interim. BIORYS2V4 (product GLOBAL_REANALYSIS_BIO_001_029) is available at Copernicus Marine Service catalogs. Details for these simulations are described in Quality Information Document (http://marine.copernicus.eu/documents/QUID/CMEMS-GLO-QUID-001-029.pdf). The hydrodynamic model is available under requirement at the Mercator Ocean service desk. In addition, the biogeomichal parameters variability from the Mercator Model, which are fundamental part of this analysis, was evaluated in Lefèvre *et al.* (2020), when applying the Mercator model to analyse the Amazon River propagation in the WTNA.

### 4.2.3. Analysis

From the model's daily data, we initially performed anomalies of monthly means, and posteriorly, Empirical Orthogonal Functions (EOFs) were applied to understand the principal components of variability governing the analyzed variables. The EOF method is a statistical approach capable of extracting temporal and spatial varying inherent characteristics of large datasets (WILKS, 1995). The technique decomposes the covariance matrix into modes, representing the variability in time and space (WILKS, 1995). The principal components are associated with spatial patterns for each mode, describing the evolution over time.

In order to represent the NBC rings in the EOF analysis, the Okubo-Weiss (OW) parameter was calculated through ocean current data as described by Isern-Fontanet *et al.* (2004). This parameter quantifies the relative importance of rotation in relation to strain and deformation and is defined as$OW = s_n^2 + s_s^2 - \omega^2$, where $s_n$, $s_s$ and ω are the normal, and the shear components of strain, and the relative vorticity of the flow, respectively (ISERN-FONTANET *et al.*, 2004; CHELTON *et al.*, 2007; CHAIGNEAU *et al.*, 2008). A negative OW indicates that vorticity dominates, while deformation is stronger when positive OW values are observed.

Further, for the analysis of $CO_2$ exchange between ocean and atmosphere, it is necessary to estimate seawater $fCO_2$ ($fCO_{2\ SW}$) and atmospheric $fCO_2$ ($fCO_{2\ ATM}$). To calculate $fCO_{2\ SW}$, we applied daily and monthly means surface data of temperature, salinity, dissolved inorganic

carbon (DIC), total alkalinity (TA), silica, and phosphate to the CO2SYS Matlab tool (LEWIS; WALLACE, 1998; PIERROT *et al.*, 2006). Also, in this tool, we used the constant of dissociation from Merhbach *et al.* (1973), updated by Dickson & Millero (1987). The $fCO_{2\ ATM}$ calculation method used in this work was extensively described by Ibánhez *et al.* (2017) and Lefèvre *et al.* (2017). Monthly and event data of atmospheric CO2 molar fraction (xCO2) were obtained from NOAA GMD Carbon Cycle Cooperative Global Air Sampling Network (DLUGOKENCKY *et al.*, 2020), available at NOAA/ESRL Global Monitoring Division (http://www.esrl.noaa.gov/gmd/dv/data), for Barbados Station (13.17ºN, 59.43ºW) (product ID: CO2_RPB_surface-flask_NOAA_ccgg). Through salinity and SST from GLORYS12V1 model, $pH_2O$ (i.e., water vapor pressure at 100% humidity) was measured. The fugacity coefficient (C) was calculated from Weiss (1974).

The air-sea $CO_2$ flux (mmol $m^{-2}$ $d^{-1}$) is estimated using a bulk parameterization: $F = kS(fCO2_{sw} - fCO2_{atm})$, where k (cm $h^{-1}$) is the gas transfer velocity, and S ($molL^{-1}atm^{-1}$) is the gas solubility (WEISS, 1974). The k is parameterised as a function of wind speed (SWEENEY *et al.*, 2007) and Sc, the dimensionless Schmidt number (WANNINKHOF, 2014).

$$k = 0{,}27 \times U^2 \times 600/S_c \times 0{,}5$$

To estimate the gas transfer velocity (k), we used daily and monthly reanalysis data of 10m wind speed ($U_{10}$) from ECMWF ERA5 (European Centre for Medium-Range Weather Forecasts), available at Copernicus Climate Change Service (C3S) (http://cds.climate.copernicus.eu/). A positive flux indicates that the ocean is a $CO_2$ source to the atmosphere, while negative fluxes indicate the ocean as a $CO_2$ sink, removing carbon from the atmosphere. The $CO_2$ fluxes and fugacities were both calculated at daily and monthly resolution.

In addition, we present a study case analysis in 2009 in order to understand how the NBC rings might influence the variables within those structures, at the surface and depth, and consequently the ocean-atmosphere $CO_2$ flux. Through the application of daily GLORYS12v1 zonal and meridional components of ocean current to the Angular Momentum Eddy Detection and Tracking algorithm (AMEDA), described by Le Vu *et al.* (2018), the NBC rings were identified at the surface, and the evolution of their vertical structure was evaluated. AMEDA is an algorithm based not only on dynamical parameters, but also on geometrical properties of the velocity field, and having as well the capacity to track rings and identify merging and splitting events (LE VU *et al.*, 2018). AMEDA has been used in some works in the last years

(IOANNOU *et al.*, 2017; GARREAU *et al.*, 2018). In fact, Aroucha *et al.* (2020) also applied the AMEDA at the same region for the study of NBC rings intra and interannual variability.

## 4.3. RESULTS AND DISCUSSION

### 4.3.1 EOFs analysis

Several EOFs analysis of monthly SSH, OW, DIC, SSS and SST anomalies were performed to identify the dominant modes and principal components of variability governing these variables. The first mode explains 94.5% of total covariance for SSH (Figure S1, see Supporting Information). Positive signs from 50ºW to 55ºW followed by negative ones from 55ºW to 60ºW could be related to NBC retroflection and rings propagation. In fact, sea level anomalies have been applied to EOFs at the region in order to identify eddies trajectory (MÉLICE, J-L.; ARNAULT, S., 2017). Further, the PC1 evidence a positive trend in the SSH anomalies, which might be associated with global sea level rise, as was also previously noticed by Aroucha *et al.* (2020). Regarding OW, the first two EOFs modes together explains 77.7% of total covariance for the studied area (Figure 1 A, B). The first two modes separately retain similar values for covariance (40.3% in the first mode and 37.4% in the second mode), and this spatial pattern is likely associated with NBC rings translation dynamics. Indeed, two successive EOFs explaining equivalent amounts of variance are an indication of structures propagation (MÉLICE, J-L.; ARNAULT, S., 2017). At the same time, this spatial pattern is restricted to the east of 55ºW in both modes, in the area where NBC rings are mostly generated (Figure 1 A, B).

Individual EOFs were also applied to the variables used for the calculation of $fCO_{2\,SW}$: SST, SSS, DIC and TA. In the second EOF mode for DIC (Figure 2 B) and TA (not shown), a ‘ring-shaped’ spatial pattern is observed, similar to the one observed in Figure S1 for SSH. The EOFs for TA are not shown due to the similarities with DIC EOF, which is explained by a correlation coefficient between DIC and TA higher than 0.99 (LEFÈVRE *et al.*, 2020). The spatial pattern of positive covariance is restricted to the east of 55ºW, as observed for SSH (Figure 2 A) and OW (Figures 4.1 A, B), and is an indication of DIC and TA increase in the area of ring generation.

Figure 1 – First EOF (A) and PC1 evolution (C) of OW; Second EOF (B) and PC2 evolution (D) of OW

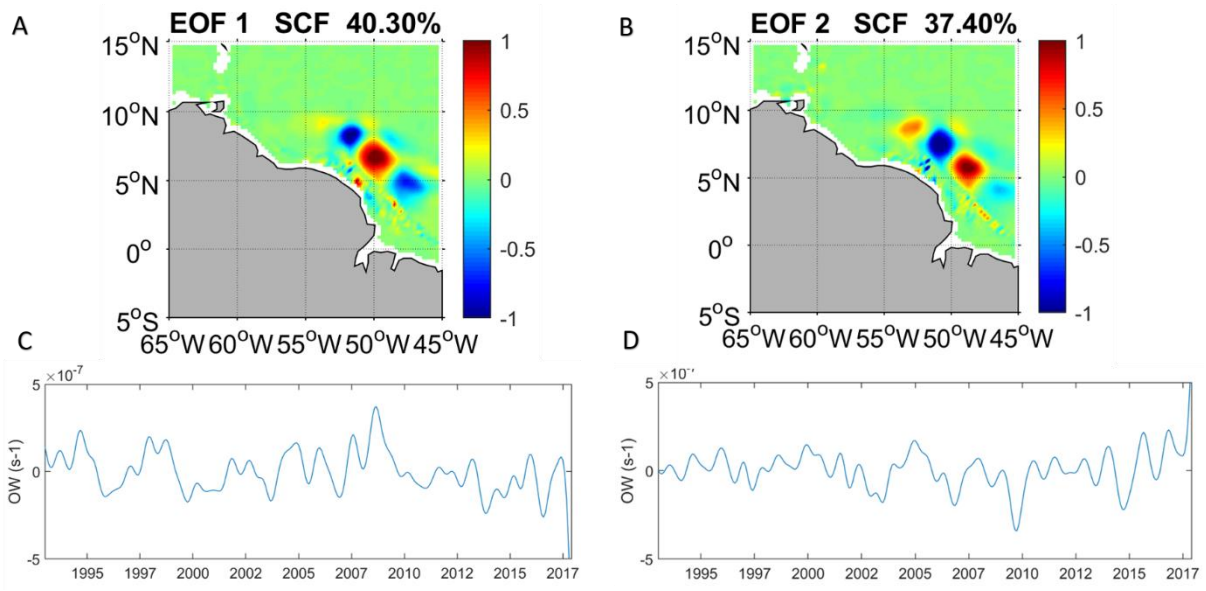


Source: the author (2020).

Figure 2 – First EOF (A) and PC1 evolution (C) of DIC; Second EOF (B) and PC2 evolution (D) of DIC;

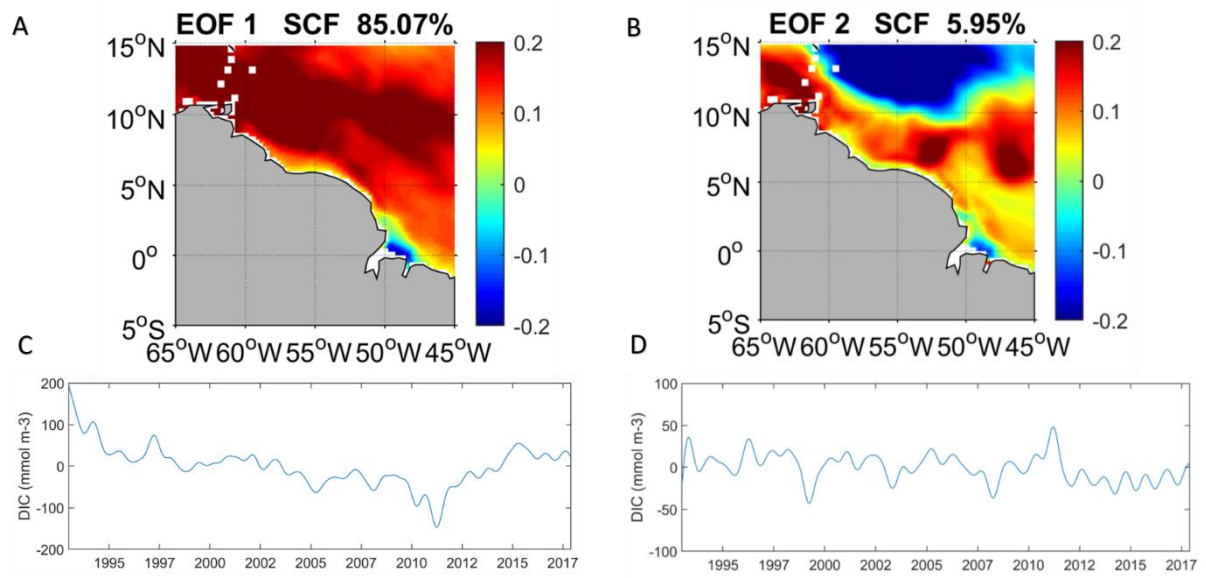


Source: the author (2020).

The first mode of EOF for DIC (Figure 2 A) indicates a spatial covariance related to the increased DIC concentration in the Tropical Atlantic region (LEFÈVRE *et al.* 1998), and the reduced DIC near the Amazon River mouth, associated with this freshwater discharge (KÖRTZINGER, 2003; COOLEY *et al.*, 2007; LEFÈVRE *et al.* 2010; LEFÈVRE *et al.* 2017). However, it does not mean that NBC rings do not influence on the dynamics of these variables, but that, in the monthly temporal scale, other mechanisms dominate the spatial covariance of these parameters in the region. The second mode of total covariance, although only representing

5.95% and 2.84% of the time for DIC (Figure 2 B) and TA (not shown) respectively, presented spatial patterns related to NBC dynamics. Further, the observed spatial structure reveals that the retroflection of the NBC and the consequent ring shedding transport high concentrations of DIC towards the eastern Atlantic and to the Carribean, respectively (Figure 2 B).

Figure 3 –Second coupled EOF (A) of DIC (left) and OW (B), and PC2 evolution (C)

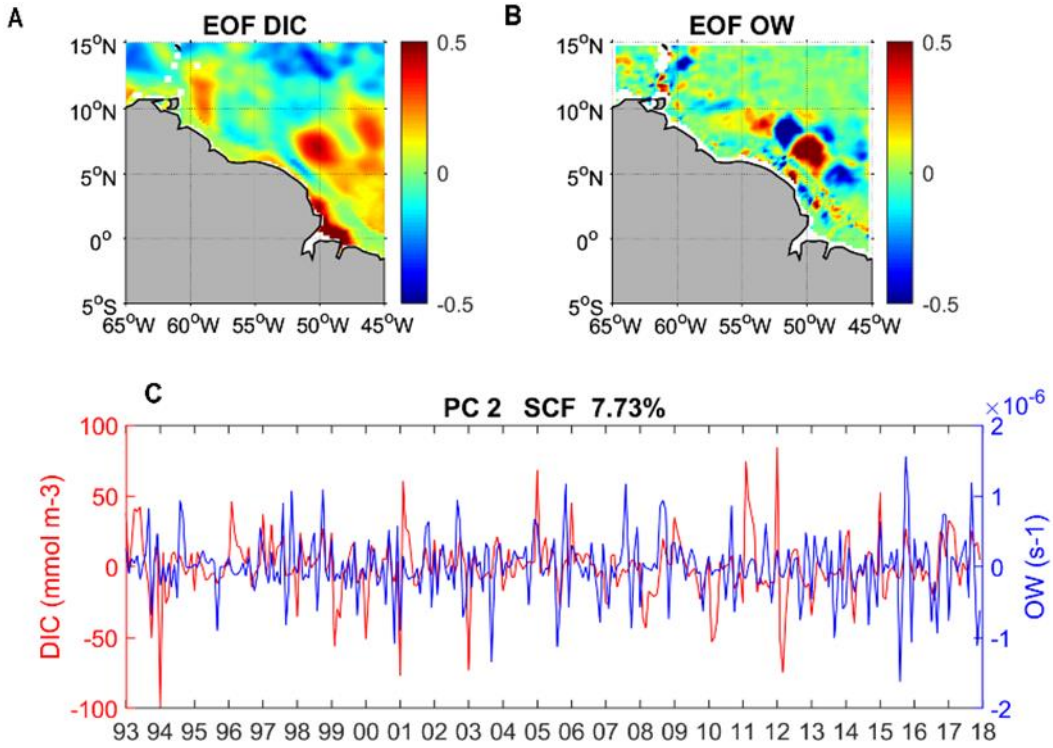


Source: the author (2021).

Furthermore, a coupled EOF between DIC and OW was performed in order to identify the corresponding modes of variance, showing the periods in which eddy dynamics, indicated by OW, and DIC concentration varies in the same way. The first mode (not shown) corresponded to 37.9% of total variance, but did not present any spatial pattern that might indicate NBC rings presence. The second EOF mode explains 7.73% of total covariance (Figure 3). The region of ring generation and trajectory showed by the OW EOF corresponds to an area of ring-shaped DIC concentration increase, with the higher values observed at the center of this structure (Figure 3 A). Also, DIC concentration is slightly reduced at ring frontal edge. An analogous but less intense pattern is also observed from 55ºW to 58ºW, with negative DIC values at the frontal edge of a 'ring-shaped' pattern characterized by positive values at the center of this structure (~56ºW). The presence of both patterns (i.e. more intense at 52ºW, and less

intense at 56ºW) following NBC rings trajectory area might be an indication of ring influence on DIC concentration during their translation (Figure 3 A).

Figure 4 –Second coupled EOF of $fCO_{2\,SW}$ (A) and OW (B), and PC2 evolution (C)

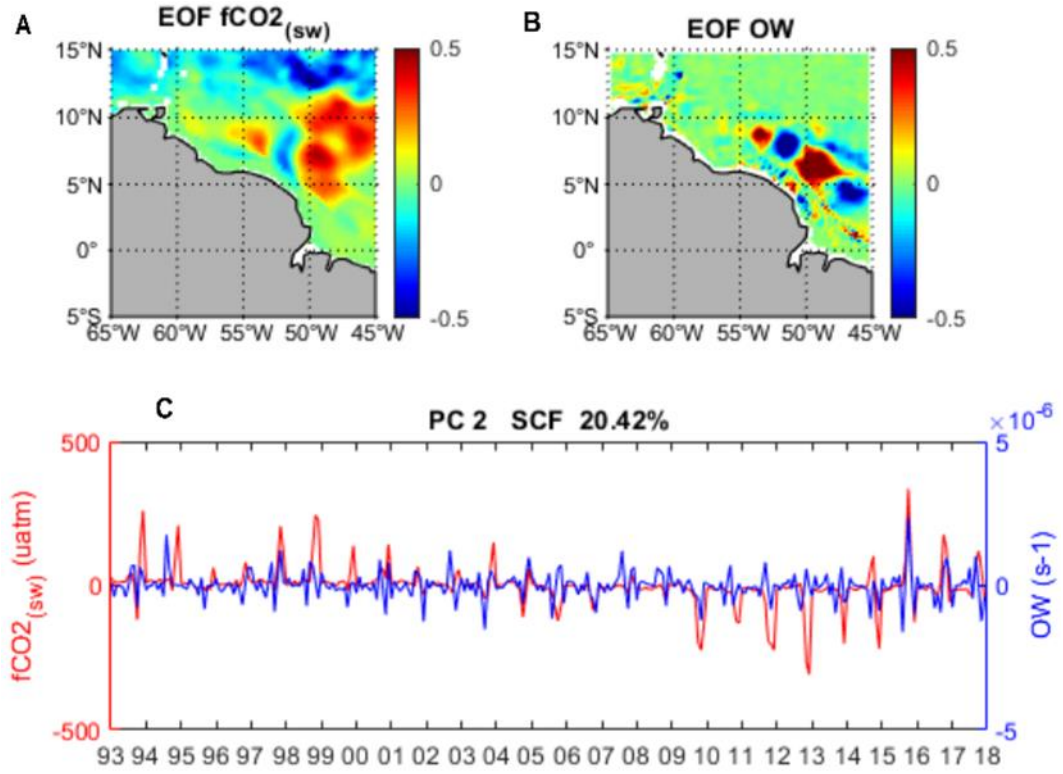


Source: the author (2021).

As previously cited, DIC concentration is not the only parameter used for $fCO_{2\,SW}$ values calculation. Therefore, it seems reasonable to also evaluate if $fCO_{2\,SW}$ present modes varying similarly as the patterns for OW. For the coupled $fCO_{2\,SW}$ - OW EOF, the second and the third modes of covariance explain together 29.1% of the total variance (Figures 4.4 and 4.5, respectively). Since, as cited for Figure 1, two successive EOFs explaining equivalent spatial patterns of variance indicates propagation of structures at the ocean, both modes showed in Figures 4.4 and 4.5 might be pointing to ring propagation at these different modes. Still, in Figure 4, where the second mode explains the most part of covariance (20.42%) is observed a similar but stronger spatial pattern in the area of NBC rings trajectory, when comparing to Figure 3, with a ring-shaped increase in $fCO_{2\,SW}$ saturation and higher concentration at the center of this structure, followed by a decrease at the frontal part of the ringlike pattern at 53ºW, and returning to increase this ring-shaped concentration in 54-55ºW (Figure 3). Similarly, for the third mode (Figure 5), this pattern of positive followed by negative anomalies is also in

agreement with the ring shedding pattern, although responsible for only 8.7% of the observed variability. Further, the first mode for $fCO_{2\,SW}$ vs OW coupled EOF (not shown) did not present any spatial pattern that could represent NBC rings incidence and corresponded to 45.76% of total variance. In addition, both the PCs associated to the second and the third mode of both former parameters (i.e., $fCO_{2\,SW}$ vs OW) displays a coupled time evolution (Figure 4 and Figure 5, under), which confirms an interannual dependence of the OW on the $fCO_{2\,SW}$ variance in the WTNA.

Figure 5 –Third coupled EOF of $fCO_{2\,SW}$ (A) and OW (B), and PC3 evolution (C)

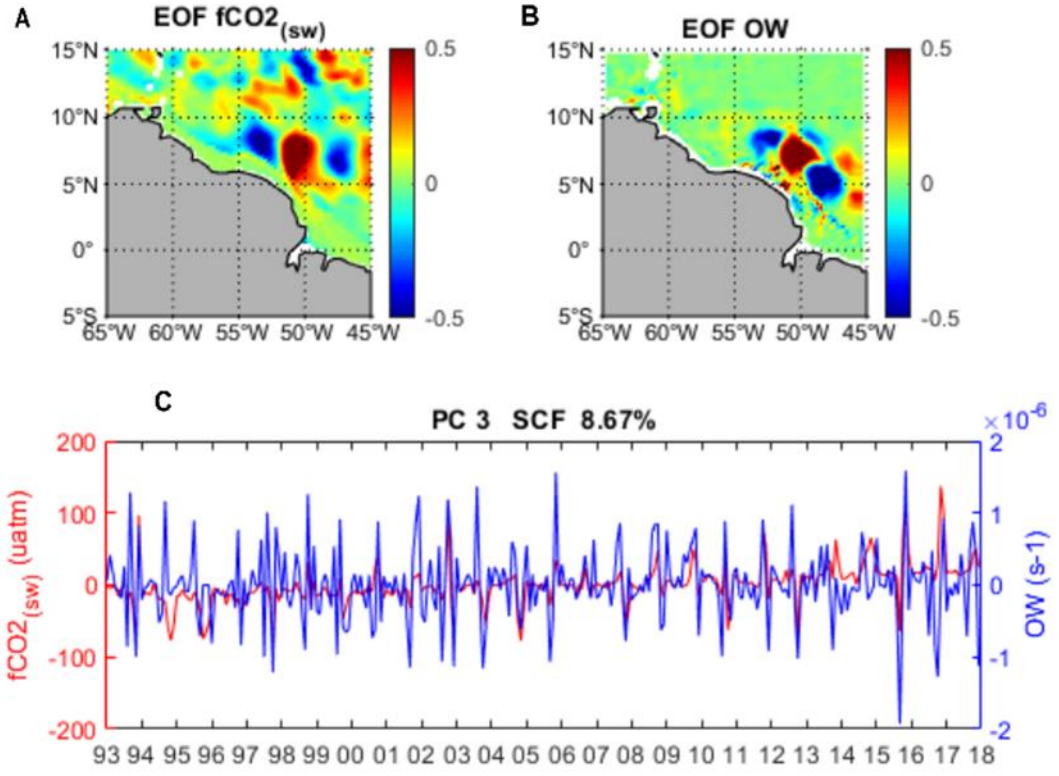


Source: the author (2021).

The coupled EOF $fCO_{2\,SW}$ vs OW (Figure 4) presented not only more modes of covariance related to NBC rings translation, but also increased percentage in these modes in relation to the DIC vs OW coupled EOF (Figure 3). This behaviour might be explained by the further influence of other variables in $fCO_{2\,SW}$ rather than DIC, such as Sea Surface Salinity (SSS) and Sea Surface Temperature (SST). In fact, CO2 budget in the tropics is likely to be affected by SSS and SST modifications (LEFEVRE et al 2020). Further, previous works pointed to SSS as the main driver for $CO_2$ variations at the WTNA (KÖRTZINGER, 2003; COOLEY *et al.*, 2007; LEFÈVRE *et al.* 2010; LEFÈVRE *et al.* 2017). At the same time, SST

within anticyclonic eddies has been pointed as the responsible for shifting $CO_2$ sinks to $CO_2$ sources (PEZZI *et al.*, 2021). Therefore, we performed coupled EOF between SSS vs OW and SST vs OW, in order to identify which of the both parameters present the highest similar covariance with OW, and consequently, with NBC rings.

Figure 6 –First mode of coupled EOF of SSS (A) and OW (B), and PC1 evolution (C)

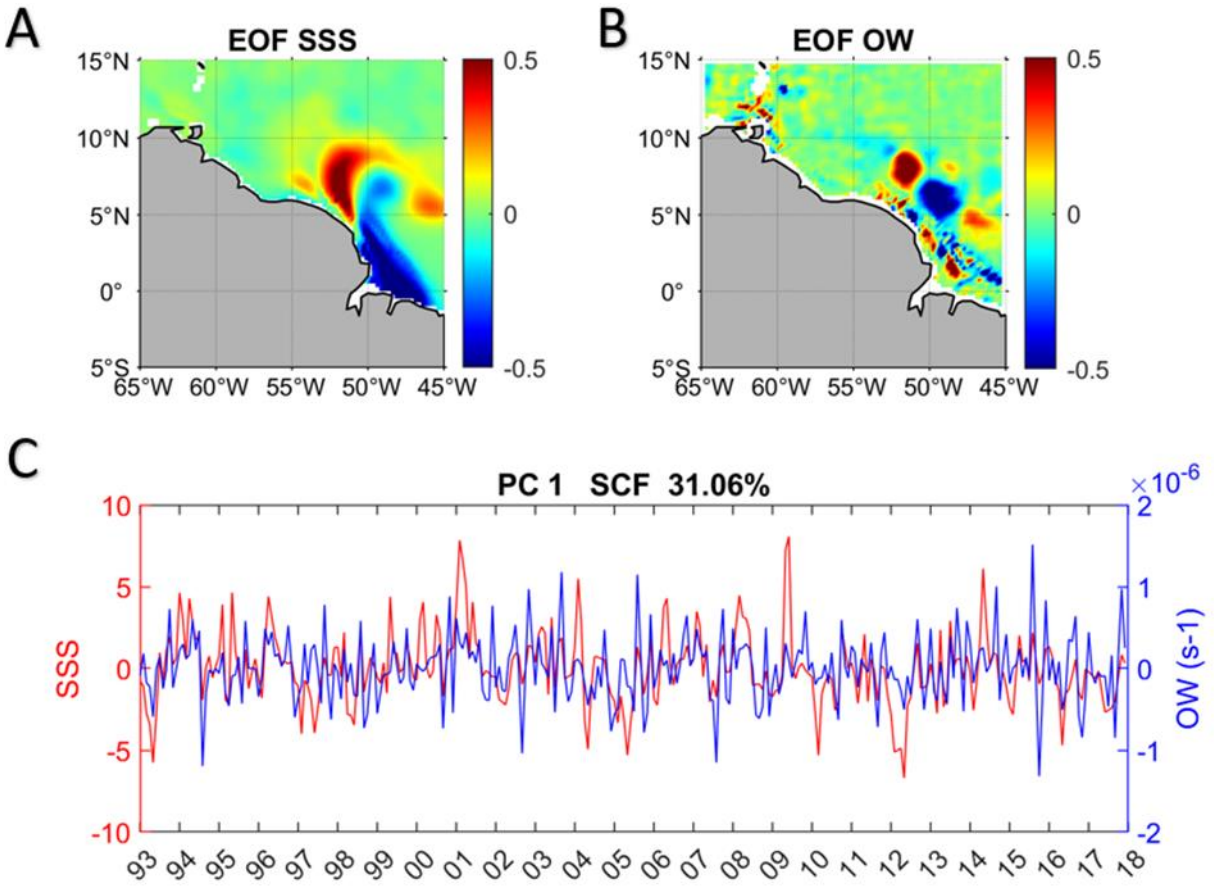


Source: the author (2021).

The successive EOFs, which explains equivalent amounts of variance and indicates structures propagation, were observed for the modes 1, 2 and 3 for the SSS vs OW coupled EOF, and represented together 77,3% of total covariance (Figures 4.6, 4.7, 4.8). These three modes together indicated the propagation of cores of SSS positive anomalies towards the west, in agreement with the OW and NBC rings translation. The presence of negative SSS anomalies is an indication of Amazon River Plume dispersion. In the first mode, the SSS positive anomaly core is being generated west of the Plume (31.1%) (Figure 6), while at the second mode the core is better delineated (26.1%) (Figure 7). In mode 3 this positive anomaly core is still present further west, although it is weakened (20.1%). These coupled EOFs gives a light to the

importance of NBC ring dynamics in trapping and transporting SSS positive anomalies cores. At the same time, positive anomalies cores of SST associated to mesoscale structures propagation were observed only for the second (8,5%) and third modes (6,8%) of variance of the SST vs OW coupled EOF (Figures 4.S2 and 4.S3, see Supporting Information). Together, these modes represented 15,3% of the total SST vs OW coupled covariance, much less of what was observed from SSS vs OW coupled EOFs (i.e., 77,3%), indicating that SSS covariance is likely to be more influenced to NBC dynamics than SST variance.

Overall, in this 25 years' analysis at monthly timescale, the NBC rings seem to be characterized by high $fCO_{2\,sw}$ concentrations in their centers and lower values at rings edges, as shown by the main modes of covariance for $fCO_{2\,sw}$ vs OW coupled EOF. It is believed that the mechanisms responsible for such influence are mainly the trapping, at eddies centers, of waters with positive anomalies of DIC concentration and SSS. Further, NBC rings dynamics are associated with SST increase in ring cores (i.e. anticyclonic rings). Therefore, since $fCO_{2\,sw}$ covariance is also amplified with SST intensification, SST might also contribute to the occurrence of $fCO_2$ positive anomalies at ring cores. Still, it seems that SSS plays here the most important role in strengthening $fCO_2$ covariance within NBC rings. This mechanism was further investigated through a NBC ring Study Case at daily time scale, and is untangled in the next session.

Figure 7 –Second mode of coupled EOF of SSS (A) and OW (B), and PC2 evolution (C)

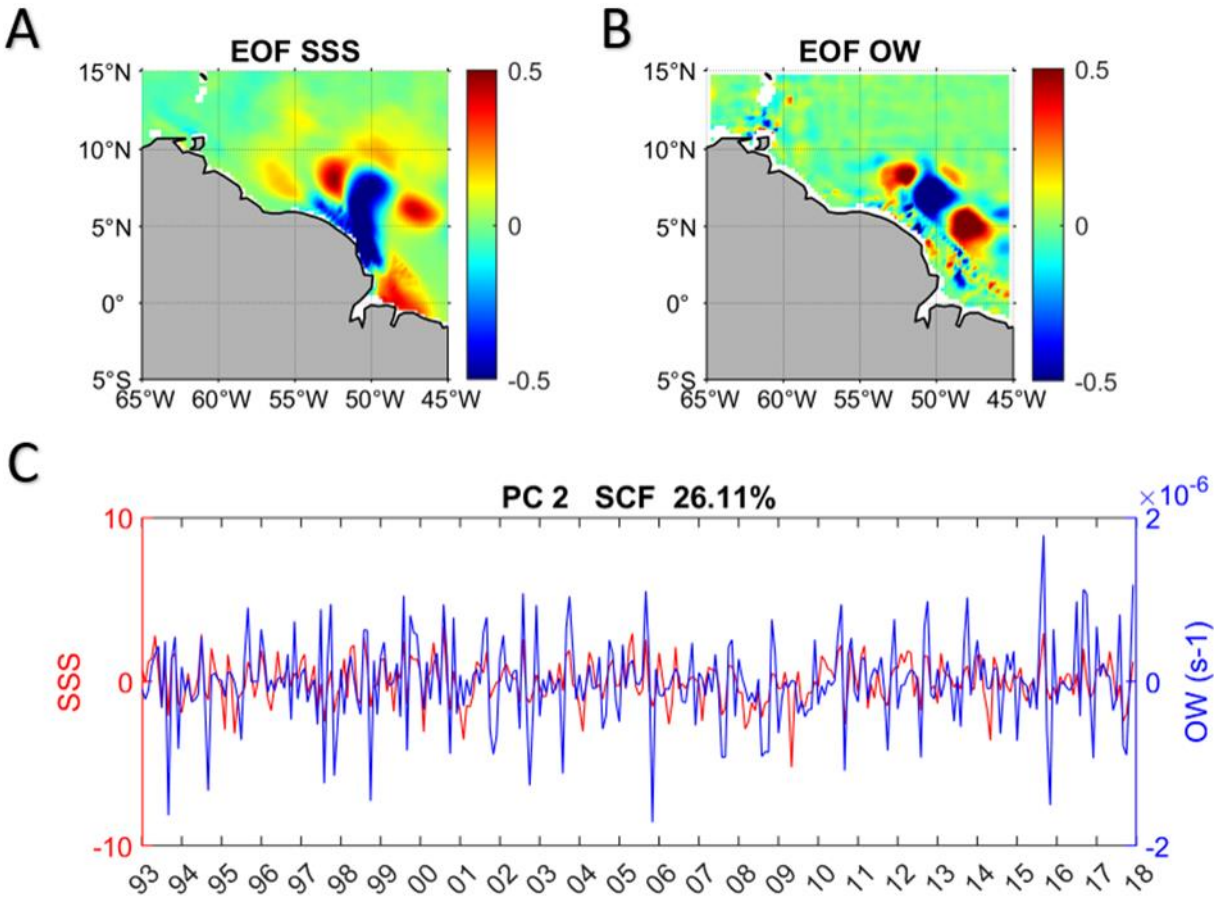


Source: the author (2021).

Figure 8 –Third mode of coupled EOF of SSS (A) and OW (B), and PC3 evolution (C)

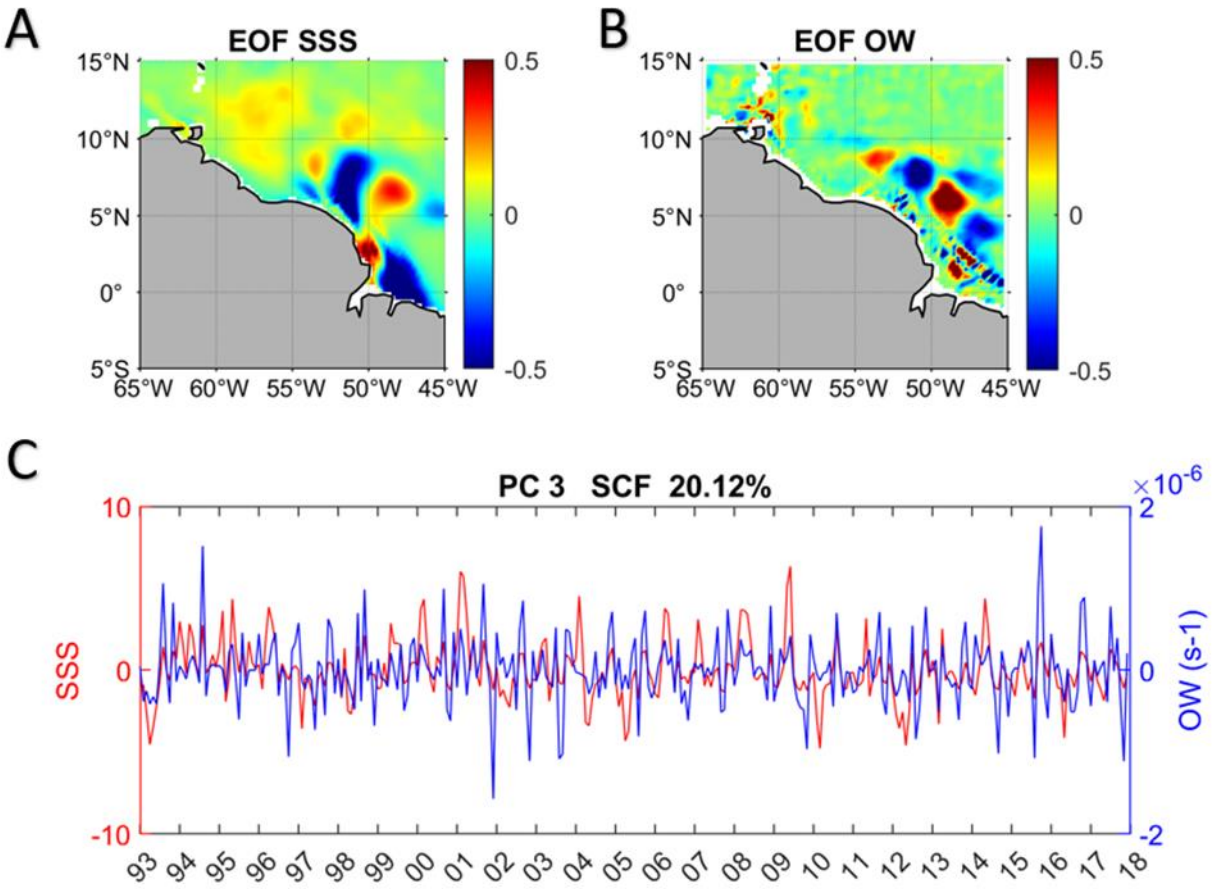


Source: the author (2021).

In order to confirm that the second and the third coupled EOFs of $fCO_{2\,SW}$ and OW are linked to NBC rings timescale variability, we performed a Wavelet Coherence (GRINSTED *et al.*, 2004) analysis between the PCs of the second and the third modes (Figure 9). The wavelet analysis identifies the periodicity associated to the signal (VELEDA *et al.*, 2012), while the Wavelet Coherence is a method for detecting significant coherence and phase between two time-series in the time-frequency domain (GRINSTED *et al*, 2004).

The PC2 Wavelet analysis highlighted the main coherences in periods of 4-6 months in specific years, with pronounced interannual variability, such as 2009 and 2016 years (Figure 9 A). At the same time, the PC3 Wavelet analysis indicated increased correlation in periods from 3 to 4 months, which were present in almost all analyzed years (Figure 9 B). These Wavelet Coherences pointed which period and years the coupling between OW and $fCO_{2SW}$ are significantly correlated and in phase. Hence, these local correlation periods for both EOF PCs illustrated in Figure 9 are an indication of NBC rings influence, since these structures average lifetime is 4 months (RICHARDSON *et al.*, 1994; GONI; JOHNS, 2001, 2003) being able to

last over 6 months in specific times (FRATANTONI; RICHARDSON, 2006; AROUCHA *et al.*, 2020). In most significant correlations (black line contours) there are predominant rightward arrows, indicating zero lag, which means the two signals are in phase. In specific few cases, arrows pointing slightly right-down in Figure 9 indicate that PCs of OW are leading the PCs of $fCO_{2\ SW}$ for both second and third modes. This is observed more strongly in PC3 at 4-month periodicity throughout almost all analysed years, and in rare years, in 6-8-month band periodicity periods (e.g. 2009).

Figure 9 –Wavelet Coherence for Principal Components (PCs) 2 (A) and 3 (B) of $fCO_{2\ SW}$ vs OW EOF.

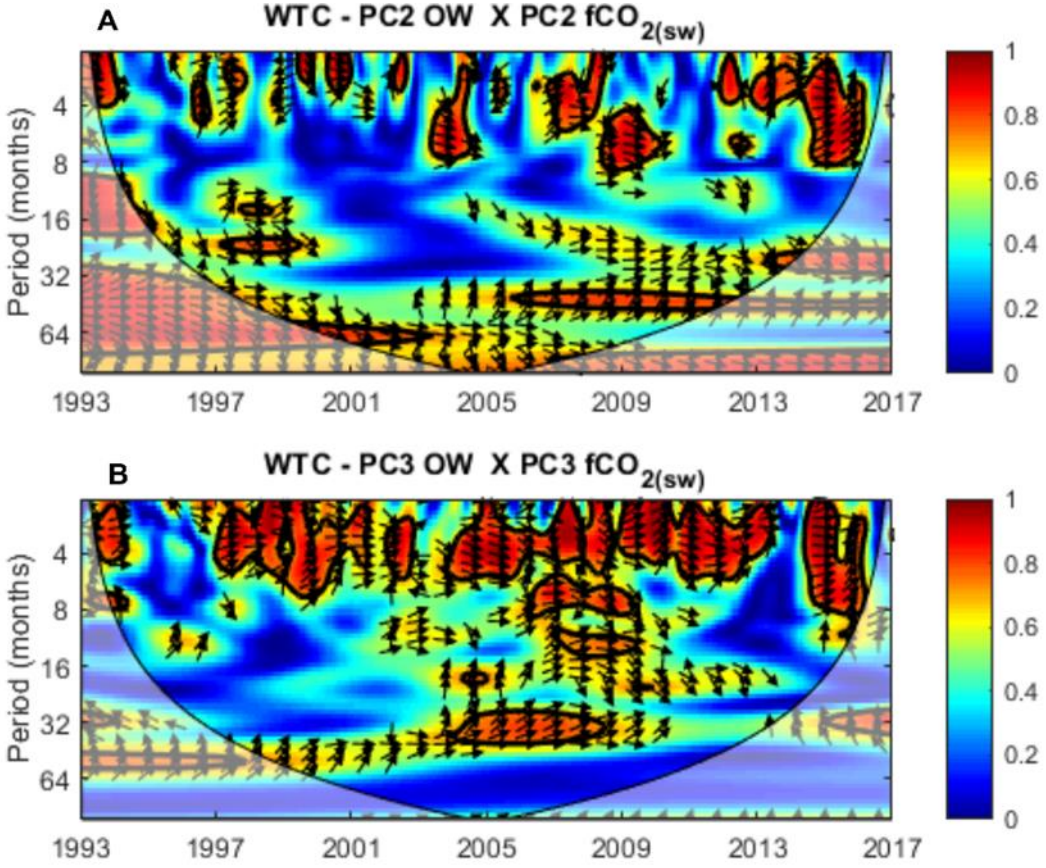


Source: the author (2021).

In fact, an anomalous SST warming in the Equatorial South Atlantic (5°S–0°N), which produced a shift in wind direction, changed the ITCZ position and the rainfall rates over the region were identified by Foltz *et al.* (2012) in 2009. In addition, in this year, NBC rings presented maximum azimuthal velocity, rings merging event in the first half of the year, and positives anomalies of Amazon discharge (TYAQUIÇÃ *et al.*, 2017; AROUCHA *et al.*, 2020). This temperature increase in this year combined with higher river discharge are likely to have contributed, respectively, to a decrease in flow density and to an enhance in vorticity at Amazon

River Plume region, which could have helped, at the same time, to intensify the shedded rings in this period (AROUCHA *et al.*, 2020). In addition to this, the 2009 presented a pronounced coherence also above 4-month periods between the OW and of $fCO_{2\ SW}$ in both PC2 and PC3 in Figure 9. Hence, it is believed that Amazon River waters effects on biogeochemistry of NBC rings trapped waters could be strongly noticed in 2009. Aiming to understand these effects, we selected study cases of NBC rings shedded in the 2009 year for a thorough analysis. We evaluated anomalies in DIC, salinity and chlorophyll concentrations at the surface and at the depth, in the WTNA during the passage of two NBC rings in this year, which is detailed in the next session.

### 4.3.2 Study Case in 2009

The two analysed NBC rings will be referred as R1 and R2. While R1 was generated in February 10$^{th}$ 2009, R2 was shed by NBC retroflection in march 2$^{nd}$ 2009. They translated for 69 and 49 days, respectively, until merging on april 19$^{th}$ 2009. These two rings and the merging event are in agreement with one of the four merging events of NBC rings depicted by Aroucha *et al.* (2020). Before merging, R1 (R2) presented average speed-based radius (Rmax) of 142.7 (132.3) km, with average maximum azimuthal velocity (Vmax) of 0.68 (0.52) m/s and mean kinetic energy (KE) of 1510.93 (933.16) cm²/s², leading to mean Rossby numbers (Ro) of 0.20 for both rings. The definition of Ro in the present study is the vortex Ro, which is based on Vmax and Rmax, and was applied by previous works at the region, reaching values that varied from 0.13 to 0.33 (FRATANTONI *et al.*, 1995; CASTELÃO; JOHNS, 2011; AROUCHA *et al.*, 2020). Also, as only the module of Vmax was applied to Ro calculation, positive values of Ro were observed, even though negative values are expected to occur for anticyclonic eddies. Regarding Rmax, length scales from NBC rings were between 200-400 km, while the mean Vmax vary from 0.12 to 0.84 m/s, and could exceed 1.15 m/s (AROUCHA *et al.*, 2020; CASTELÃO; JOHNS, 2011; FRATANTONI *et al.*, 1995; FRATANTONI; RICHARDSON, 2006; JOCHUMSEN *et al.*, 2010; RICHARDSON *et al.*, 1994). The KE results might indicate overestimation of KE when comparing to what has been observed (i.e. 100-300 cm²/s²) (DIDDEN; SCHOTT, 1993; AROUCHA *et al.*, 2020). However, these cited works used purely geostrophic velocities for KE computation, and underestimation of azimuthal velocity might occur when assuming geostrophic balance within an eddy, due to the negligence of inertial components of momentum balance (DOUGLASS; RICHMAN, 2015). Therefore, since the data used in the present work also considers the cyclogeostrophic terms,

the increased KE was expected. The parameters values for each individual ring before merging are showed in Table S4.1. After merging, the remaining NBC ring translated for further 25 days, demising in may 14$^{th}$ 2009 when encountering the Caribbean islands. The merged ring presented average Rmax of 120.2km, mean Vmax of 0.69m/s, with average KE of 1585.06 $cm^2/s^2$ and average Ro also of 0.20. The merging event also occurred at the merging NBC rings region pointed by Aroucha *et al.* (2020). A t-student test was performed to identify parameters changes from individual to merged rings. A significant increase in KE was detected only between R2 and the merged ring (i.e. p=0.0013), in agreement to what was reported by Aroucha *et al* (2020), that detected significant variation between isolated and merged rings in not only in KE, but also in Vmax and Ro parameters. The parameters values for the ring after merging are showed in Table S4.1.

R1 and R2 impacts on surface biogeochemistry are depicted in Figure 10 through the analysis of two snapshots from daily anomalies of salinity, DIC and chlorophyll. At the same time, the evolution of these three parameters within R1 and R2 are showed in Videos S4.1, S4.2 and S4.3, for salinity, DIC and chlorophyll, respectively. Both rings apparently evolve to an egg-like shape throughout the northwesternward translation as, described by CHEN *et al.* (2021), rather than a circle or ellipsoid geometry, even though R2 at march 25$^{th}$ 2009 is seemingly similar to an ellipsoid east of 52ºW. Regarding salinities, rings at their formation seem to initially trap positive anomalies and carry towards northwest (Figure 10 B, R2), when these anomalies are stirred and move away from rings centres in the direction of rings edges, as observed in Figures 4.10 A, B for R1. In general, positive (negative) surface salinity anomalies in this region are related to tropical (coastal) waters. The T-S diagram for R1 in march 25th 2009 at two different locations (Figure 11) indeed confirms that the negative surface anomalies indicate the presence of coastal waters (CW), with salinities <35.4 (i.e. Figure 11 A - 11ºN), while positive anomalies (i.e. Figure 11 B - 9ºN) are associated mainly with tropical waters (TW), with salinities >36.0, at the surface. At depth, TW and the South Atlantic Central Water (SACW) were also detected. In-situ data has already been used to detect the same waters masses distribution in the WTNA (NEUMANN-LEITÃO *et al.*, 2018).

Figure 10 – Anomalies for march 25th 2009: A) salinity; C) DIC; E) chlorophyll; and anomalies for april 4th 2009: B) salinity; D) DIC; F) chlorophyll. Anticyclonic rings maximum velocity contours are indicated by solid blue lines. Dashed (solid) grey lines indicate rings edges (trajectories), respectively. Black dots represent ring center

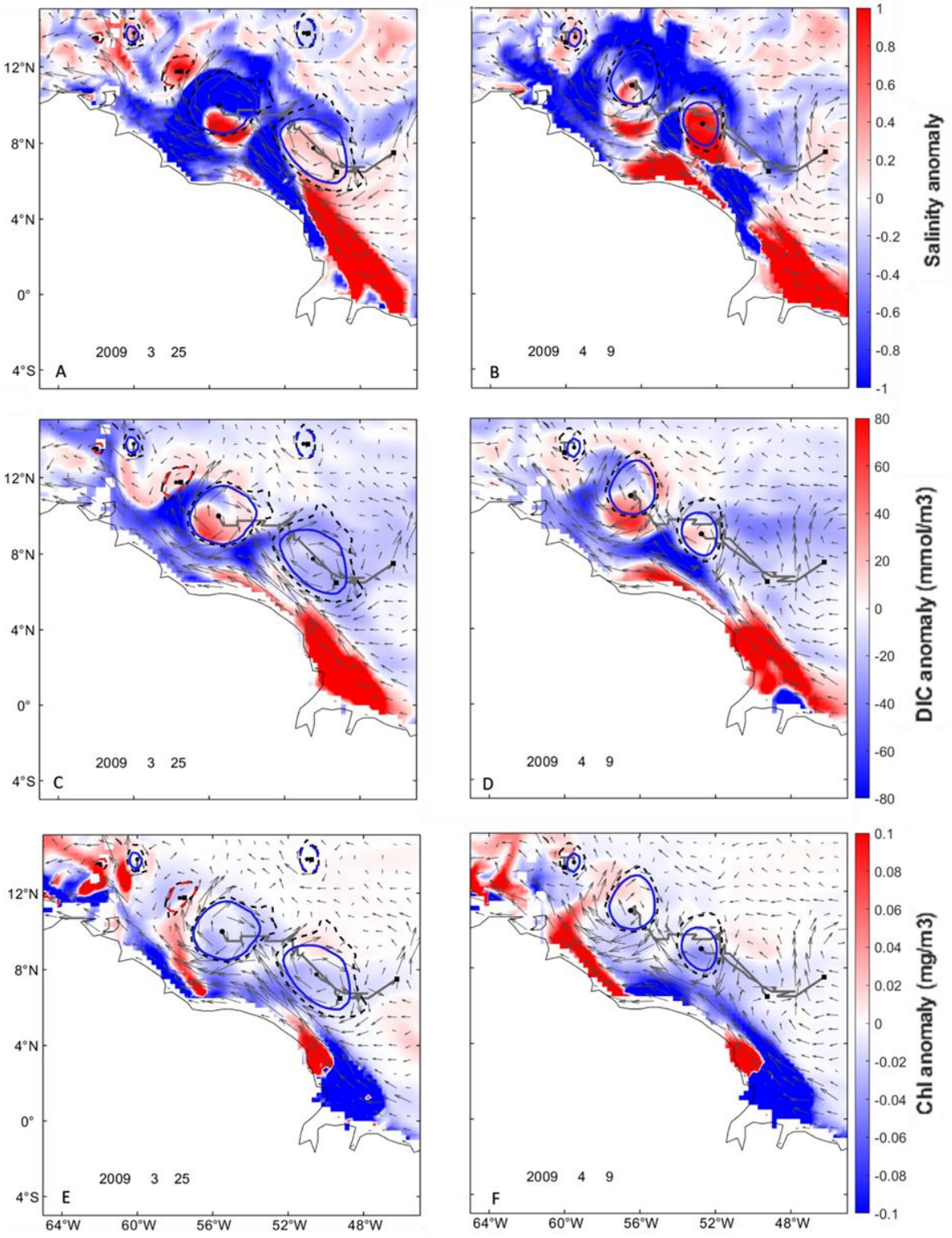


Source: the author (2021).

In relation to DIC, cores of intense positive anomalies, reaching 40 and 18 mmol $m^{-3}$ $day^{-1}$ at maximum core and ring centre, respectively, are generated in the centre of both R1 and R2, what indicates an accumulation of carbon at NBC ring cores. At the same time, DIC negative anomalies – minimum of -102 mmol $m^{-3}$ $day^{-1}$ – settle at these structures' edges, mainly at the frontal limits in an "comma-shape", being pushed towards the northwest (Figure 10 C, D). As previously cited, DIC variability in the Tropical Atlantic are mainly associated with salinities gradients due to the presence of Amazon River, where increased (decreased) DIC corresponds to increased (decreased) salinity (LEFÈVRE *et al.* 1998; KÖRTZINGER, 2003; COOLEY *et al.*, 2007; LEFÈVRE *et al.* 2010; LEFÈVRE *et al.* 2017). However, DIC anomalies appears to be intensively concentrated at vortex centres as rings translate through time, delineating ring cores more sharply than the salinity anomalies. It is believed that since salinities might also vary with precipitation/evaporation rates, the salinites shapes within the rings could be more prominently changed during ring lifetime.

On the other hand, the opposite is observed for chlorophyll concentration, which is decreased from maximum positive anomaly of 0.05 mg $m^{-3}$ at ring boundaries to negative anomalies at ring cores in the order of – 0.01 mg $m^{-3}$ (Figure 10 E, F). In fact, Huang *et al.* (2021) argued that a similar pattern is observed within NBC rings, with low-chlorophyll ring cores and high-chlorophyll ring edges, and showed that chlorophyll anomalies propagating from the WTNA, are able to cross the Lesser Antilles and enter the Gulf of Mexico. This is in agreement with high DIC in the cores (little/ no biological activity) and low DIC in the edge (carbon consumption increasing the chlorophyll concentration). Hence, it is believed that the surface edge of the ring is predominantly made of coastal or Amazon waters, as also depicted by Figure 11B, where CW is present at the edge of R1 until ~100m depth.

Positive chlorophyll anomalies, generated by the presence of high nutrient Amazon and Orinoco River plumes at the ocean, are carried at ring leading edges and pushed towards the Caribbean (Figure 10 E, F). This process is referred as eddy stirring, and ends up generating an asymmetric design in chlorophyll magnitudes between the leading and trailing ring boundaries, due to the interaction of the trailing edge to an ambient that has recently been influenced by the leading edge (MCGILLICUDDY, 2016). Negative chlorophyll anomalies at anticyclonic eddies cores might be a consequence of the outward radial displacement of phytoplankton biomass induced by radial momentum imbalance within those structures (ZHANG *et al.*, 2015). Increased chlorophyll concentrations in an area can generate carbon consumption, indicating a correspondent decrease in DIC concentration. The eddy stirring process that concentrates chlorophyll at vortex leading edges, and prevent this biological tracer to enter ring cores, might

explain, in addition to what has been discussed, the reduced DIC at R1 and R2 frontal boundaries and the increase in DIC anomalies at ring cores. Most part of the chlorophyll stirring in an anticyclonic eddy occurs through horizontal advection of water with high concentrations from adjacent areas (XU *et al.*, 2019). In addition, the frontal upwelling of nutrient-rich waters along the periphery of anticyclonic eddies due to shifts in isopycnals was observed in other studies (e.g. STRASS *et al.*, 2002; KAHRU *et al.*, 2007), and might also contribute in the present analysis of R1 and R2.

In order to evaluate rings characteristics at depth we performed latitudinal sections in R1 at two different longitudes and days: 55.5ºW at 25$^{th}$ march 2009; and 56.5ºW at 4$^{th}$ april 2009 for anomalies of DIC, chlorophyll, salinity and zonal current component. Anomalies of the zonal current component are depicted for both periods in Figure 12. Dashed lines indicate rings edges, while solid lines represent ring cores. These opposite anomalies indicate the clockwise rotation, inherent to anticyclonic rings in the Northern Hemisphere, and ring centre position between both opposite anomalies. R1 influence from the surface reached deeper than 250m (Figure 12), with maximum anomalies from 120m to 250m in march 25$^{th}$. At April 4$^{th}$, the maximum of intensity was restricted from 50m to 150m depth.

Figure 11 – Temperature-Salinity diagrams for R1 at march 25$^{th}$ 2009 in two different point: 55.5ºW, 11.0°N (A); 55.5ºW, 9.0°N (B). CW: Coastal Waters, SACW: South Atlantic Central Waters, TW: Tropical Waters

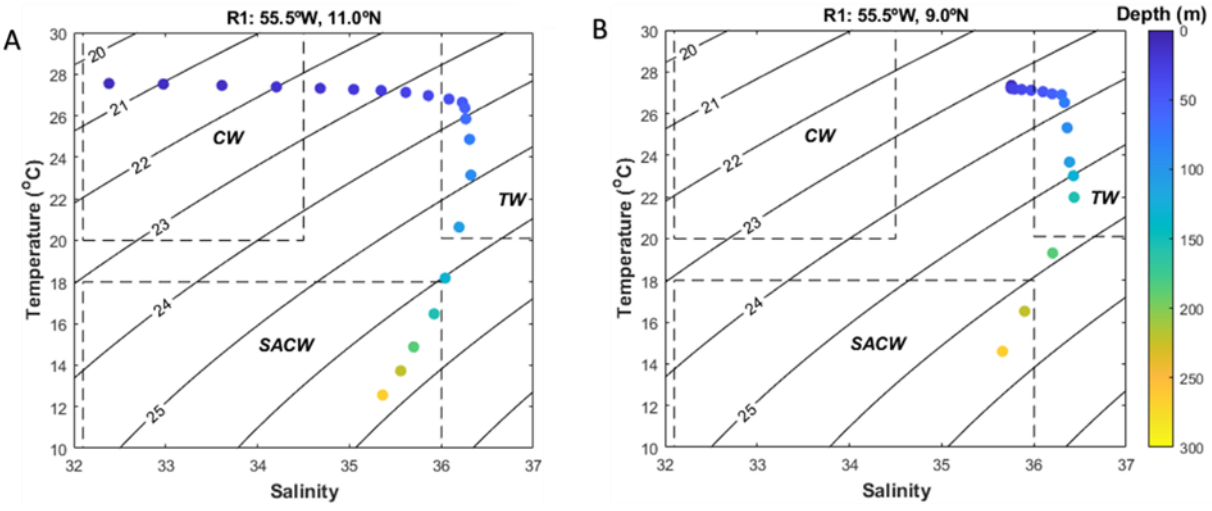


Source: the author (2021).

Regarding the biogeochemical structure at depth (Figure 13), there are noticed strong positive salinity and corresponding positive DIC anomalies at ring trailing edge, south of R1 centre at surface in march 25$^{th}$ (Figure 13 A, C.), enveloped by these parameters negative anomalies right after their cores and nearby their boundaries, until ~25-30m depth. This depth

corresponds to the maximum barrier layer depth and also mixed layer depths (i.e. 10m-50m) found by Balaguru *et al.* (2012). Negative salinity anomalies settle at the surface in the leading (higher latitude) edge of the ring, what can be observed both in 25th march and 09th april. At the same time, a salinity decrease from 100-200m at both moments is observed especially at rings leading edges, after ring core, reaching anomaly values higher than -1. Negative salinity anomalies ranging from -0.5 to -1 has been reported also from 100-200m depth within NBC rings cores (AROUCHA *et al.*, 2020). This decrease is better noticed at 25th march which is also the time when the salinity cores at surface are better delineated (Figure 13 A). At 9th April (Figure 13 B), these negative anomalies at depth are restricted from 100m-150m and the ring salinity signature at the surface in eddy trailing edge is almost inexistent. It is believed that R1 maxima zonal anomalies at march 25th, placed mainly from 150-250m, allowed negative salinity anomalies to reach depths further than 200m, and a better delineation of an anomalous positive core at surface. At the same time, at April 9th, due to the increased R1 intensity from closer to the surface until 150m depth, the salinity negative anomalies were shallower, and the positive anomalies were almost vanished from the surface in this day.

Figure 12 – Zonal (U) component anomaly for a) 25th march 2009 in latitudinal section at 55.5ºW; and b) 4th april 2009 in latitudinal section at 56.5ºW. Dashed lines indicate rings edges, while solid lines represent ring cores

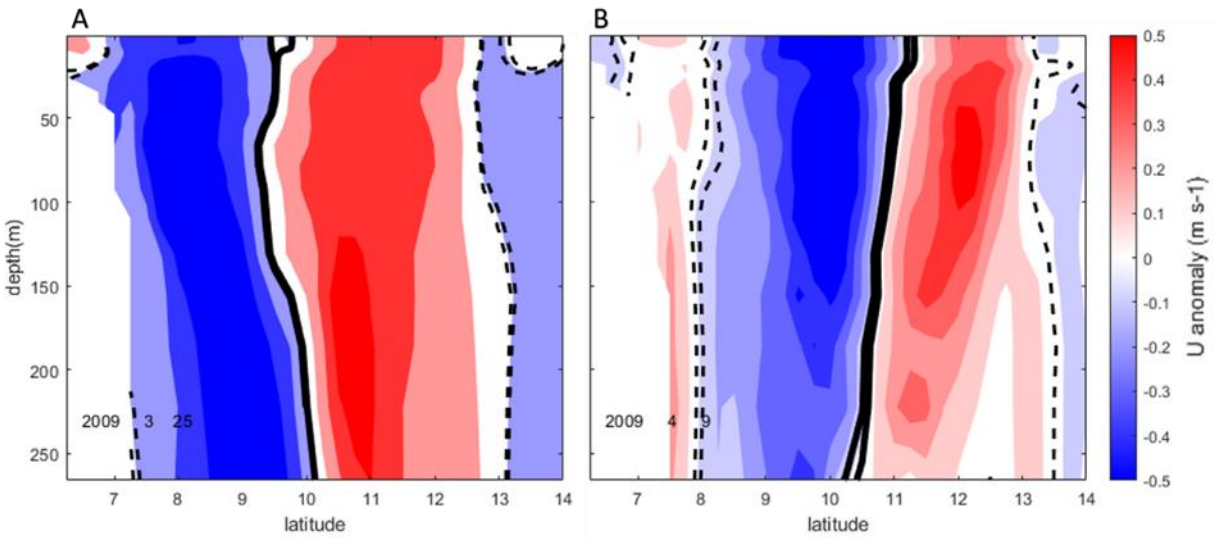


Source: the author (2021).

Further, DIC anomalies shifted from very strong positive anomalies until 30m to maximum observed negative anomalies at depths from 100-150m at the south of the R1 core, at ring subsurface trailing edge at both depicted days (Figure 13 C, D). It seems that R1

dynamics were able to trap at surface TW highly saline, retaining the positive salinity and DIC anomalies to the mixed layer depth. In its turn, it appeared that the CW low salinity and DIC water is being pushed down by this ring dynamics, settling between 50m-150m depth (Figure 13 A, C, D). Indeed, advection of highly saline and warm waters at the surface followed by coastal low temperature and salinity waters at further depth were found at the region within these anticyclonic rings (L'HEGARÈT *et al.,* 2021). A wide variety of submesoscale fronts, barrier layers and vertical movements of water are expected to be generated in the region due to the constant interaction from riverine Amazon waters, and NBC rings and retroflection. Further studies on NBC rings layering and mixture processes are being developed (L'HEGARÈT *et al.*, 2021) and will enhance the understanding of such dynamical region.

At the same time, positive anomalies of chlorophyll concentrations coincide with the fronts from high to low DIC concentration, especially from 80-110m, where the anomaly peaks were observed (Figure 13 E, F). We highlight that chlorophyll increase is mostly observed also at 100m, in R1 leading edges (12-13ºN), as well as the indicated chlorophyll increase at surface due to eddy stirring (Figure 10 E, F). At April 4$^{th}$, this increase is still in the above cited ring edge, although it situates closer to ring core (Figure 13 F). The high chlorohpyll anomaly at the ring trailing edge at subsurface and depth (50m-100m), close to the coast and in 25$^{th}$ of march, is mainly related to coastal water discharge.

Overall, it seems that NBC rings impact biogeochemical parameters in the WTNA both at the surface and at depth, although the mechanisms mostly at depth need further investigations and are beyond the scope of this work. What has been observed is the NBC rings capacity in concentrating DIC at their cores and trailing edges. Therefore, since an increase in DIC concentration might contribute to an increase in $fCO_{2\ SW}$ and consequently in $FCO_2$, the cores of NBC rings are likely to release more $CO_2$ than surrounding waters.

Figure 13 – Anomalies for R1 in march 25th 2009 in longitudinal section at 55.5ºW: A) salinity; C) DIC; E) chlorophyll; and anomalies for R1 in april 4th 2009 in longitudinal section at 56.5ºW.: B) salinity; D) DIC; F) chlorophyll. Dashed lines indicate rings edges, while solid lines represent ring cores

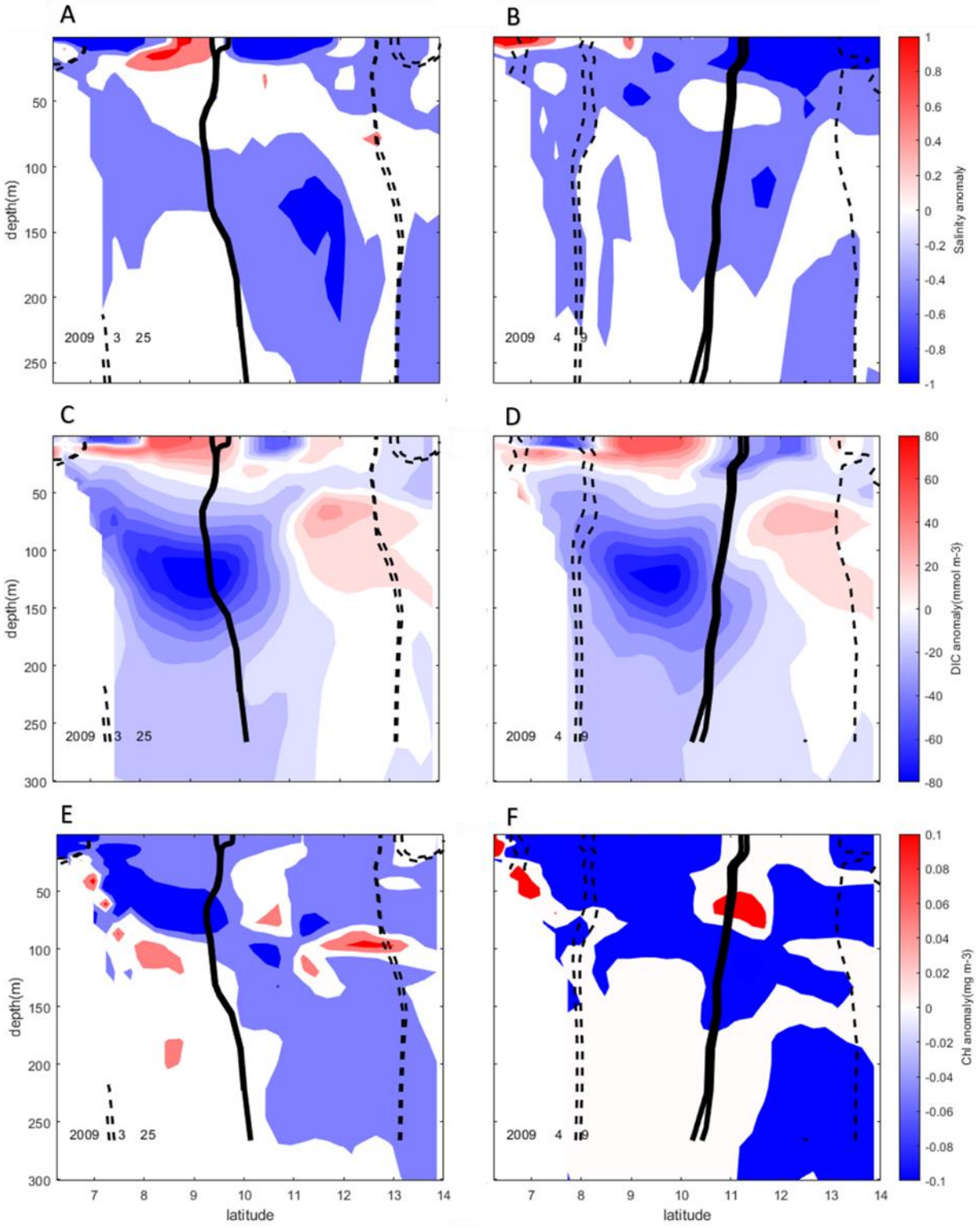


Source: the author (2021).

Snapshots of $FCO_2$ during the trajectory of R1 and R2 indicates a decrease in the $FCO_2$ source to the atmosphere within NBC rings while trey translate (Figure 14). The evolution of

$FCO_2$ anomaly within R1 and R2 cores location is showed in Video S4.4 and $FCO_2$ values for each tracked day is depicted in Table S4.1. When considering only ring positions to west of 50ºW (i.e. when rings are truly released from NBC rings): R1, R2 and the merged ring presented average positive anomalies of $CO_2$ fluxes from the ocean to the atmosphere of 0.06, 0.38, and 0.05 mmol $m^{-2}$ day, respectively. It is important to note that east this longitudinal section (50ºW) NBC rings are still being generated under strong influence of NBC, so considerations of ring cores position at these locations might be misleading. Maximum positive anomaly at R2 centered core was observed at 11$^{th}$ April (i.e. 0.94 mmol $m^{-2}$ day, depicted in Figure 14 C) and immediately before rings merging at 19$^{th}$ april (i.e. 1.32 mmol $m^{-2}$ $day^{-1}$, not shown, see Video S4.4). It seems that after 56ºW this positive flux is considerably reduced, indicated by both R1 and the merged ring reaching maximum of 0.19 mmol $m^{-2}$ $day^{-1}$ after this latitude. The strong positive $FCO_2$ at the beginning of rings trajectory tends to be reduced, with the partial pressures of $CO_2$ of both ocean and atmosphere naturally reaching an equilibrium. Indeed, this $fCO_{2\,SW}$ transported by NBC rings has been reported to be eroded over time (OLIVIER *et al.*, 2021). Also, biological carbon uptake during ring translation might contribute to flux reduction. In fact, Orselli *et al.* (2019) pointed that Agulhas rings were primarily driven by physical mechanisms, and as they translate, biological activity starts to control carbon uptake.

We highlight that: cores of positive anomalies of $CO_2$ fluxes, acting as a source of the gas to the atmosphere, with maximum of 1.32 mmol $m^{-2}$ $day^{-1}$, settled within the centre of R2 NBC ring. In addition, this mesoscale structure generated a mean increase of approximately 38% on $FCO_2$ in relation to the surrounding waters (i.e. anomalies around 0.0 mmol $m^{-2}$ $day^{-1}$), since positive anomalies of ring cores waters averaged approximately 0.38 mmol $m^{-2}$ $day^{-1}$. Absolute $FCO_2$ values were observed within anticyclonic eddies at the Brazil-Malvinas confluence, where their contribution as a source was estimated as 0.3 mmol $m^{-2}$ $day^{-1}$ (PEZZI *et al.*, 2021). This cited study pointed for SST increase in the core of anticyclone structures as the responsible for the shift from $CO_2$ sinks to $CO_2$ sources. In addition, temperature seemed to be important either in turning Agulhas eddies into $CO_2$ sinks of ~ -3.7 mmol $m^{-2}$ $day^{-1}$ (ORSELLI *et al.*, 2019). The CO2 budget in the tropics is likely, in fact, to be affected by surface salinity and temperature shifts (LEFEVRE et al 2020). At the present study, it is believed that positive anomalies of salinity and consequently DIC at ring cores were responsible for this increase in $FCO_2$, although the increased SST inherent to anticyclonic rings might have contributed to the higher fluxes.

Figure 14 – $FCO_2$ for march 25th 2009 (A), april 9th 2009 (B) april 11th 2009 (C) april 16th 2009 (D) at the WTNA. Anticyclonic rings maximum velocity contours are indicated by solid blue lines. Dashed (solid) grey lines indicate rings edges (trajectories), respectively. Black dots represent ring center

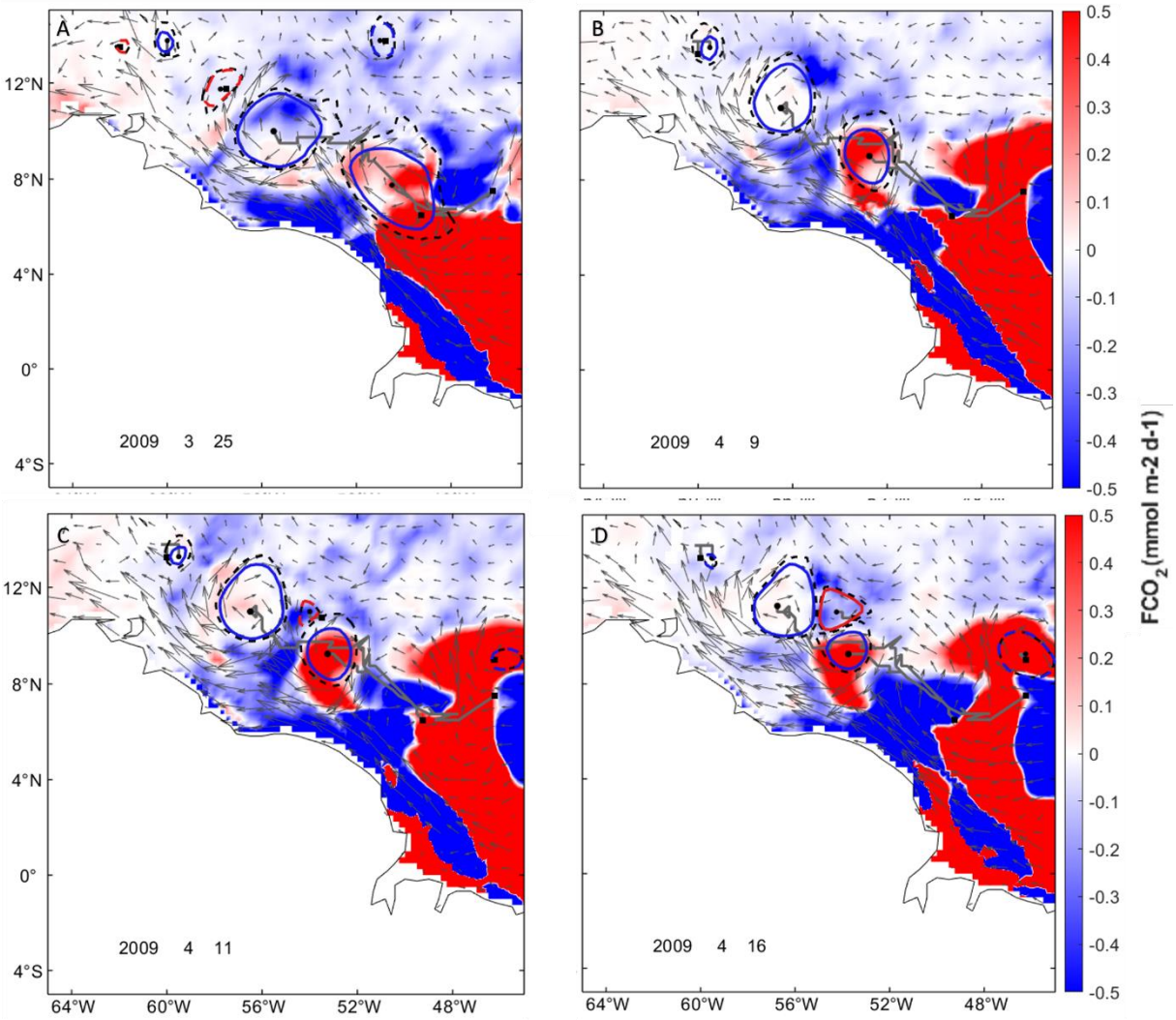


Source: the author (2021).

Overall, the presence of OW variance in 77% of the time and modes of the coupled EOF between OW and $fCO_{2\,SW}$ accounting for 29% of variance indicate that the influence of NBC rings in $fCO_{2\,SW}$ is considerable. In fact, NBC rings were associated in the present study with an 38% positive anomaly in $FCO_2$ in relation to the surrounding waters, demonstrating that these mesoscale features play an important role in increase the $CO_2$ outgassing in the WTNA. DIC and salinity positive anomalies centred at the ring cores and trailing edges are likely to play the role in increase carbon flux at these points. Further studies on vertical movements and small-scale disturbances in the region within those eddies might give light on what make these salinity anomalies remain trapped at the surface. We also hypothetise that NBC eddies effect on $FCO_2$, depending on the origin of the wrapped water, can diverge from the expected and

steer filaments that can act as a $CO_2$ sink, as initially also pointed by Olivier *et al.* (2021). In this study, however, the analysed rings were restricted to act as a $CO_2$ source, what is also observed to retain a considerable part of the variance.

## 4.4. CONCLUSION

We applied empirical orthogonal functions (EOFs) analysis for 25 years (1993–2017) reanalysis model to evaluate the role of NBC rings in biogeochemistry of WTNA, especially regarding $FCO_2$. This database was also applied to the AMEDA eddy tracking in order to identify NBC rings impacts in a daily timescale, taking two rings in the 2009 year as a case study.

In general, we could identify that NBC rings, embodied here by OW, presented variance in agreement with $fCO_{2\,SW}$ patchiness in 29% of the time when analysing the second and third EOF's modes. Also, the presence of OW covariance related to the translation of mesoscale features in 77% of the time, indicates that this influence occurs in a considerable period of time. In addition, OW and SSS varied similarly also in 77% of the time, showing NBC rings influence on SSS variance at the region. This also pointed for salinity as the main responsible for positive $fCO_{2\,SW}$ anomalies related to ring cores, since SSS covariance is likely to be more influenced to NBC dynamics than SST variance. Furthermore, it was indicated that a NBC ring could increase, in average, 38% of the $FCO_2$ at their cores in relation to surrounding waters. At the present study, it is believed that positive anomalies of salinity and consequently DIC at ring surface cores and trailing edges were responsible for this increase in $fCO_{2\,SW}$ covariance and in the daily $FCO_2$, although the increased SST inherent to anticyclonic rings might have contributed to the higher fluxes. Further studies on vertical movements and small-scale disturbances at the region within those eddies might give light on what make these salinity anomalies remain trapped at the surface.

Finally, it seems reasonable to affirm that NBC rings impact biogeochemical parameters at the WTNA both at the surface and at depth, although the mechanisms behind these impacts mostly at depth need further investigations. In fact, studies on NBC rings layering and mixture processes, and NBC rings biogeochemical impacts are being currently developed (L'HEGARÈT *et al.*, 2021; OLIVIER *et al.*, 2021). The contribution of this work, settles not only in observing NBC rings influence on carbon parameters variance in the WTNA, but also, on their contribution to the increase in $FCO_2$ to the atmosphere. An extensive study with more analysed rings would increase the sampling and could better reinforce this effect on $FCO_2$

anomalies. Furthermore, this work shows the capacity of these structures in concentrating DIC and highly saline waters at theirs cores and trailing edges; and it gives a light on what mechanism is responsible for maintaining the salinity anomaly at ring cores.

## 4.5. REFERENCES

ANDRIÈ, C., C. OUDOT, C. GENTHON, L. MEFIIVAT, CO2 fluxes in the tropical Atlantic during FOCAL cruises, **Journal of Geophysical Research**, 91, 11741-11755, 1986.

AROUCHA, L.C.; VELEDA, D.; LOPES, F. S.; TYAQUIÇÃ, P.; LEFÈVRE, N.; ARAUJO, M. Intra- and Inter-Annual Variability of North Brazil Current Rings using Angular Momentum Eddy Detection and Tracking Algorithm: Observations from 1993 to 2016, **Journal of Geophysical Research: Oceans**, v.125, ed.12, https://doi.org/10.1029/2019JC015921, 2020.

AUMONT, O., ETHÉ, C., TAGLIABUE, A., BOPP, L., GEHLEN, M. PISCES-v2: an ocean biogeochemical model for carbon and ecosystem studies. **Geoscientific Model Development** 8, 2465-2513. 2015.

CARTON J. A. Effect of seasonal surface freshwater flux on sea surface temperature in the Tropical Atlantic Ocean. **Journal of Geophysical Research**, v.96, p.12593–12598, 1991.

CASTELÃO, G. P.; JOHNS, W. E. Sea surface structure of North Brazil Current rings derived from shipboard and moored acoustic Doppler current profiler observations, **Journal of Geophysical Research,** 116, 2011.

CHAIGNEAU, A., A. GIZOLME, C. GRADOS. Mesoscale eddies off Peru in altimeter records: Identification algorithms and eddy spatio-temporal patterns. **Progress in Oceanography**, v.79, p.106–119, 2008.

CHELTON, D. B., M. G. SCHLAX, R. M. SAMELSON, R. A. DE SZOEKE. Global observations of large oceanic eddies. **Geophysical Research Letters**, v.34, 5p., 2007.

CHEN, G., YANG, J., HAN, G. Eddy morphology: Egg-like shape, overall spinning, and
oceanographic implications, **Remote Sensing of Environment**, 257, 112348, https://doi.org/10.1016/j.rse.2021.112348, 2021.

Cooley, S. R., V. J. Coles, A. Subramaniam, and P. L. Yager (2007), Seasonal variations in the Amazon plume-related
atmospheric carbon sink, Global Biogeochem. Cycles, 21, GB3014, doi:10.1029/2006GB002831
Cooley, S. R., V. J. Coles, A. Subramaniam, and P. L. Yager (2007), Seasonal variations in the Amazon plume-related
atmospheric carbon sink, Global Biogeochem. Cycles, 21, GB3014, doi:10.1029/2006GB002831
COOLEY, S. R.; COLES, V. J.; SUBRAMANIAM, A.; YAGER, P. L. Seasonal variations in the Amazon plume-related atmospheric carbon sink. **Global Biogeochemical Cycles**, 21, https://doi.org/10.1029/2006GB002831, 2007.

COWEN, R. K., S. SPONAUGLE, C. B. PARIS, K. LWIZA, J. FORTUNA, S. DORSEY. Impact of North Brazil Current rings on local circulation and coral reef fish recruitment to Barbados, West Indies. **Interhemispheric Water Exchange in the Atlantic**

**Ocean,** G. J. Goni and P. Malanotte-Rizzoli, Eds., Elsevier Oceanographic Series, v. 68, p.443–455, 2003.

DICKSON, A. G., MILLERO, F. J. A comparison of the equilibrium constants for the dissociation of carbonic acid in seawater media. **Deep Sea Research** 34, 1733–1743, doi: 10.1016/0198-0149(87)90021-5, 1987.

DIDDEN, N., SCHOTT, F. Eddies in the North Brazil Current Retroflection Region Observed by Geosat Altimetry. **Journal of Geophysical Research**, v.98, p.121-131, 1993.

DOUGLASS, E. M., RICHMAN, J. G. Analysis of ageostrophy in strong surface eddies in the Atlantic Ocean. **Journal of Geophysical Research: Oceans,** 120, 1490–1507. https://doi.org/10.1002/2014JC010350, 2015.

FFIELD, A. North Brazil Current Rings viewed by TRMM Microwave Imager SST and the influence on Amazon River Plume.**Deep Sea Research I**, v.52, p.137–160, 2005.

FOLTZ, G. R., MCPHADEN, M. J., LUMPKIN, R. A strong Atlantic Meridional Mode Event in 2009: The role of mixed layer dynamics. **Journal of Climate**, 25, 363–380. https://doi.org/10.1175/JCLI-D-11-00150.1. 2012.

FRATANTONI, D. M., W. E. JOHNS, T. L. TOWNSEND. Rings of the North Brazil Current: Their structure and behavior inferred from observations and a numerical simulation. **Journal of Geophysical Research**, v.100, p.10633-10654, 1995.

FRATANTONI, D. M., GLICKSON, D. A. North Brazil Current Ring generation and evolution observed with SeaWiFS. **Journal of Physical Oceanography**, v.32, p.1058–1074, 2002.

FRATANTONI, D. M., P. L. RICHARDSON. The evolution and demise of North Brazil Current rings. **Journal of Physical Oceanography**, v.36, p.1241–1264, 2006.

FROIDEFOND, J.M., GARDEL, L., GUIRAL, D.L., PARRA, M., TERNON, J.F. Spectral remote sensing reflectances of coastal waters in French Guiana under the Amazon influence. **Remote Sensing of Environment**, 80, 225–232, 2002.

GARREAU, P., DUMAS, F., LOUAZEL, S., STEGNER, A., LE VU, B. High-resolution observations and tracking of a dual-core anticyclonic eddy in the Algerian Basin. **Journal of Geophysical Research: Oceans**, 123(12), 9320–9339. https://doi.org/10.1029/2017JC013667, 2018.

GRINSTED, A., MOORE, J.; JEVREJEVA, S. Application of the cross wavelet transform and wavelet coherence to geophysical time series. **Nonlinear Processes Geophysics**, 11, 561–566, 2004.

GONI, G. J.; W. E. JOHNS. A Census of North Brazil Current Rings observed from TOPEX/Poseidon Altimetry: 1992-1998. **Journal of Geophysical Research**, v.28, p.1-4, 2001.

GONI, G. J., W. E. JOHNS. Synoptic study of warm rings in the North Brazil Current retroflection region using satellite altimetry. **Interhemispheric Water Exchange in the Atlantic Ocean** v.68, p.335-356, 2003.

HUANG, M., LIANG, X., ZHU, Y., LIU, Y., & WEISBERG, R. H. Eddies connect the tropical Atlantic Ocean and the Gulf of Mexico. **Geophysical Research Letters,** 48, e2020GL091277. https://doi.org/10.1029/2020GL091277, 2021.

IBÁNHEZ, J. S. P.; FLORES, M.; LEFÈVRE, N. Collapse of the tropical and subtropical North Atlantic CO2 sink in boreal spring of 2010. **Scientific Reports** 7, 41694; doi: 10.1038/srep41694, 2017.

IOANNOU, A., STEGNER, A., LE VU, B., TAUPIER-LETAGE, I., SPEICH, S. Dynamical Evolution of Intense Ierapetra Eddies on a 22 Year Long Period. **Journal of Geophysical Research: Oceans**, 2017.

ISERN-FONTANET, J.; FONT, J.; GARCÍA-LADONA, E.; EMELIANOV, M.; MILLOT, C.; TAUPIER-LETAGE, I. Spatial structure of anticyclonic eddies in the Algerian basin (Mediterranean Sea) analyzed using the Okubo–Weiss parameter. **Deep Sea Research Part II: Topical Studies in Oceanography**, Volume 51, Issues 25–26, p. 3009-3028, https://doi.org/10.1016/j.dsr2.2004.09.013, 2004.

JOCHUMSEN, K., RHEIN, M., HÜTTL-KABUS, S., BÖNING, C. W. On the propagation and decay of North Brazil Current rings. **Journal of Geophysical Research**, v.115, 2010.

JOHNS, W. E., T. N. LEE, F. A. SCHOTT, R. J. ZANTOPP, R. H. EVANS. The North Brazil Current retroflection: Seasonal structure and eddy variability. **Journal of Geophysical Research**, v.95, p.22103–22120, 1990.

JOHNS, W. E., R. J. ZANTOPP, G. J. GONI. Cross-gyre transport by North Brazil Current Rings. **Interhemispheric Water Exchange in the Atlantic Ocean,** v. 68, p.411–441, 2003.

LEFÈVRE, N., MOORE, G., AIKEN, J., WATSON, A., COOPER, D., LING, R. Variability of pCO2 in the tropical Atlantic in 1995. **Journal of Geophysical Research** 103, 5623–5634, 1998.

LEFÈVRE, N., DIVERRÈS, D., GALLOIS, F. Origin of CO2 undersaturation in the western tropical Atlantic. **Tellus B** 62, 595–607. 2010.

LEFÈVRE N, FLORES-MONTES M., GASPAR F. L., ROCHA C, JIANG S, DE ARAÚJO M. C., IBÁNHEZ, J. S. P. Net Heterotrophy in the Amazon Continental Shelf Changes Rapidly to a Sink of CO2 in the Outer Amazon Plume. **Frontiers in Marine Science** 4:278, 2017.

LEFÈVRE, N., TYAQUIÇÃ, P., VELEDA, D., PERRUCHE, C., JAN VAN GENNIP, S. Amazon River propagation evidenced by a CO2 decrease at 8°N, 38°W in September 2013.**Journal of Marine Systems,** https://doi.org/10.1016/j.jmarsys.2020.103419, 2020.

LE VU, B., STEGNER, A., ARSOUZE, T. Angular Momentum Eddy Detection and tracking Algorithm (AMEDA) and its application to coastal eddy formation. **Journal of Atmospheric Oceanic Technology,** v.35, p.739–762, 2018.

LEWIS, E., WALLACE, D. **Program Developed for CO2 System Calculations**. Oak Ridge National Laboratory Environmental Sciences Division, 1998.

L'HÉGARET, P., SPEICH, S., CHEN, Y, MANTA, G., OLIVIER, L., REVERDIN, G., POUPON, M., SCHÜTTE, F., KARSTENSEN, J., CARTON, X., LAXENAIRE, R., ZHANG, D., FOLTZ, G. EUREC4A-OA/ATOMIC experiment: Themohaline and dynamical descriptions of mesoscale and submesoscale structures of the Northwest Tropical Atlantic Ocean, **EGU General Assembly 21,** EGU21-10991, https://doi.org/10.5194/egusphere-egu21-10991, 2021.

KAHRU, M., MITCHELL, B. G., GILLE, S. T., HEWES, C. D., HOLM-HANSEN, O. Eddies enhance biological production in the Weddell-Scotia Confuence of the Southern Ocean. **Geophysical Research Letters,** 34, L14603, https://doi.org/10.1029/2007GL030430, 2007.

KÖRTZINGER, A. A significant sink of CO2 in the tropical Atlantic Ocean associated with the Amazon River plume. **Geophysical Research Letters** 30, 2287,2003.

KÖRTZINGER, A. The outer Amazon plume: an atmospheric CO2 sink, in: Liu, K.K., Atkinson, L., Quiñones, R., McManus, L.T. (Eds.), **Carbon and nutrient fluxes in continental margins: a global synthesis.** Springer, New York, pp. 450-453, 2010.

MCGILLICUDDY, D. J. Mechanisms of physical-biological-biogeochemical interaction at the oceanic mesoscale. **Annu Rev Mar Sci**, 8, 125–59, 2016.

MÉLICE, J.-L., ARNAULT, S. Investigation of the intra-annual variability of the North Equatorial Countercurrent/North Brazil Current eddies and of the instability waves of the North tropical Atlantic Ocean using satellite altimetry and Empirical Mode Decomposition. **Journal of Atmospheric and Oceanic Technology**, 34, 2295–2310. https://doi.org/10.1175/JTECH-D-17-0032.1. 2017.

MEHRBACH, C., CULBERSON, C. H., HAWLEY, J. E., PYTKOWICZ, R. M. Measurement of the apparent dissociation constants of carbonic acid in seawater at atmospheric pressure. **Limnol. Oceanogr.** 18, 897–907, doi: 10.4319/lo.1973.18.6.0897, 1973.

MOURIÑO, B., E. FERNÁNDEZ, H. ETIENNE, F. HERNÁNDEZ, S. GIRAUD. Significance of cyclonic SubTropical Oceanic Rings of Magnitude (STORM) eddies for the carbon budget of the euphotic layer in the subtropical northeast Atlantic, **Journal of Geophysical Research,** 108, 3383, doi:10.1029/2003JC001884, 2003.

NEUMANN-LEITÃO, S., MELO, P. A. M. C., SCHWAMBORN, R., DIAZ, X., FIGUEIREDO, L., SILVA, A., CAMPELO, R. P. S., JUNIOR, M. M., MELO, N. A. F. C., COSTA, A., ARAUJO, M., VELEDA, D. R. A., MOURA, R., THEMPSON, F. Zooplankton from a reef system under the influence of the Amazon River Plume. **Frontiers in Microbiology**, 9, 355. https://doi.org/10.3389/fmicb.2018.00355, 2018.

OLIVIER, L., BOUTIN, J., LEFÈVRE, N., REVERDIN, G., LANDSCHÜSZTER, P., SPEICH, S., KARSTENSEN, J. Impact of mesoscale eddies on salinity and CO2 ocean parameters in the western tropical Atlantic in February 2020, **EGU General Assembly 21,** 1253, https://doi.org/10.5194/egusphere-egu21-1253, 2021.

ORSELLI, I. B. M., KERR, R., AZEVEDO, J. L. L., GALDINO, F., ARAUJO, M., GARCIA, C. A. E. The sea-air CO2 net fluxes in the South Atlantic Ocean and the role played by Agulhas eddies. **Progress in Oceanography**, 170, p. 40-52, 2019.

PEZZI, L., P., SOUZA, R. B., SANTINI, M., MILLER, A. J., CARVALHO, J. T., PARISE, C. K., QUADRO, M. F., ROSA, E. B., JUSTINO, F., SUTIL, U. A., CABRERA, M., J., BABANIN, A., V., VOERMANS, J., NASCIMENTO, E. L., ALVES, R. C. M., MUNCHOW, G. B., RUBERT, J. Oceanic eddy-induced modifications to air–sea heat and CO2 fluxes in the Brazil-Malvinas Confluence. **Scientific Reports,** 11, 10648 https://doi.org/10.1038/s41598-021-89985-9, 2021.

PIERROT, D., LEWIS, E., WALLACE, D. W. R. **MS Excel Program Developed for CO2 System Calculations,** O.R.N.L. Oak Ridge, TN: Carbon Dioxide Information Analysis Center; U.S. Department of Energy, 2006.

RICHARDSON, P. L., HUFFORD, G. E., LIMEBURNER, R., BROWN, W. S. North Brazil Current retroflection eddies. **Journal of Geophysical Research**, 99, 5081–5093. https://doi.org/10.1029/93JC03486, 1994.

SMITH, W.O., DEMASTER, D.J. Phytoplankton biomass and productivity in the Amazon River plume: correlation with seasonal river discharge. **Continental Shelf Research**, 16, 291–319, 1996.

SONG, H., J. MARSHALL, D. R. MUNRO, S. DUTKIEWICZ, C. SWEENEY, D. J. MCGILLICUDDY, U. HAUSMANN. Mesoscale modulation of air-sea CO2 flux in Drake Passage, **Journal of Geophysical Research Oceans**, 121, 6635–6649, 2016.

STRASS, V. H., NAVEIRA-GARABATO, A. C., POLLARD, R. T., FISCHER, H., HENSE, I., READ, J. F., LEACH, H., SMETACEK, V. Mesoscale frontal dynamics: shaping the environment of primary production in the Antarctic CircumpolarCurrent. **Deep-Sea Research** Pt II 49, 3735–3769, 2002.

SWEENEY, C., GLOOR, E., JACOBSON, A.R., KEY, R.M., MCKINLEY, G., SARMIENTO, J.L., WANNINKHOF, R. Constraining global air-sea gas exchange for CO2 with recent bomb 14C measurements. **Global Biogeochemical Cycles** 21, doi: 10.1029/2006GB002784, 2007.

TAKAHASHI, T.; OLAFSSON, J.; GODDARD, J. G.; CHIPMAN, D. W.; SUTHERLAND, S. C. Seasonal variation of CO2 and nutrients in the high-latitudesurface oceans: A comparative study. **Global Biogeochemical Cycles**, v.7(4), p.843–878, doi:10.1029/93GB02263, 1993.

TERNON, J.F., OUDOT, C., DESSIER, A., DIVERRES, D. A seasonal tropical sink for atmospheric $CO_2$ in the Atlantic Ocean: the role of the Amazon River discharge. **Marine Chemistry**, 68, 183–201, 2000.

TYAQUIÇÃ, P.; VELEDA, D.; LEFÈVRE, N.; ARAUJO, M.; NORIEGA, C.; CANIAUX, G.; SERVAIN, J.; SILVA, T. Amazon Plume Salinity Response to Ocean Teleconnections. **Frontiers in Marine Science**, v. 4, p. 1, 2017.

VELEDA, D.; MONTAGNE, R.; ARAUJO, M. Cross-wavelet bias corrected by normalizing scales. **Journal of Atmospheric and Oceanic Technology**, v. 29, n. 9, p. 1401–1408. DOI: 10.1175/JTECH-D-11-00140.1. 2012.

WANNINKHOF, R. Relationship between wind speed and gas exchange over the ocean revisited, **Limnol. Oceanography - Meth**., 12, 351–362, https://doi.org/10.4319/lom.2014.12.351, 2014.

WEISS, R. F. Carbon dioxide in water and seawater: the solubility of a non-ideal gas, **Mar. Chem**., 2, 203–215, https://doi.org/10.1016/0304-4203(74)90015-2, 1974.

WILKS, D. S. **Statistical Methods in the Atmospheric Sciences.** Academic Press. p.467. 1995.

XU, G.; DONG, C.; LIU, Y., GAUBE, P., YANG, J. Chlorophyll Rings around Ocean Eddies in the North Pacific, **Scientific Reports**, 9, 2056, https://doi.org/10.1038/s41598-018-38457-8, 2019.

ZHANG, W., XUE, H., CHAI, F. NI, Q. Dynamical processes within an anticyclonic eddy revealed from Argo floats. **Geophysical Research Letters** 42, 2342–2350, https://doi.org/10.1002/2015GL063120, 2015.

## 4.6. SUPPORTING INFORMATION

Here we provide the first individual EOF mode and PC1 evolution for SSH (Figure S1), and the second and third modes of variance for the coupled EOFs between SST vs OW (Figures S2 e S3, respectively. Further, values of the parameters for each day of the two isolated rings (R1 and R2) which merged into one (M1) rings, and for this merged ring (Table S1). In addition, Videos 4.S1, 4.S2, 4.S3, and 4.S4 depict the evolution of anomalies of salinity, DIC, chlorophyll and $FCO_2$, respectively, through time during the days of the passage of R1, R2 an then the merged ring M1. Videos 4.S1, 4.S2, 4.S3, and 4.S4 are inserted in the PowerPoint in attachment (‘Videos_Dissertação_LeoAroucha.pptx’).

Figure S1 –First EOF (A) and PC1 evolution (B) of SSH

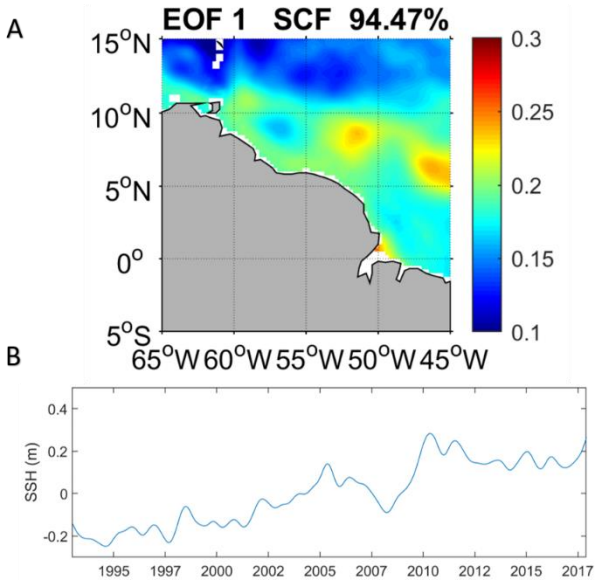


Source: the author (2020).

Figure S2 –Second coupled EOF of SST (A) and OW (B), and PC2 evolution (C)

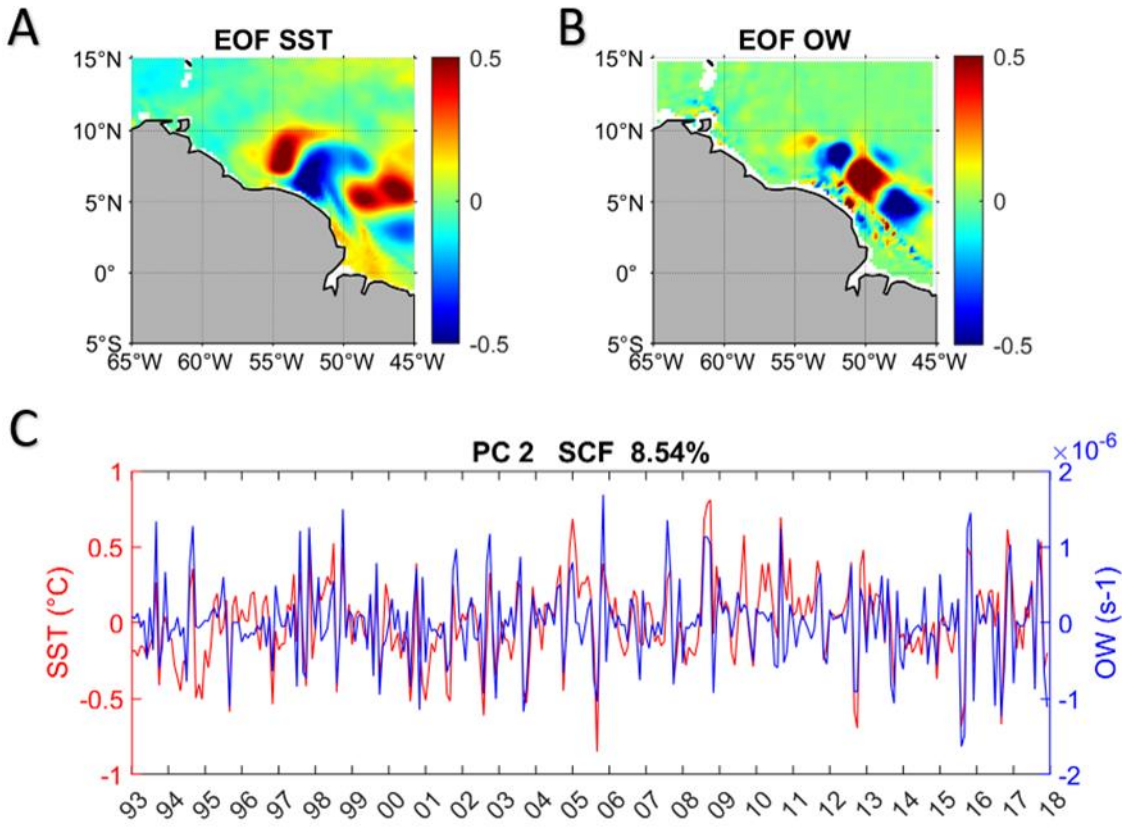


Source: the author (2021).

Figure S3 –Third coupled EOF of SST (A) and OW (B), and PC3 evolution (C)

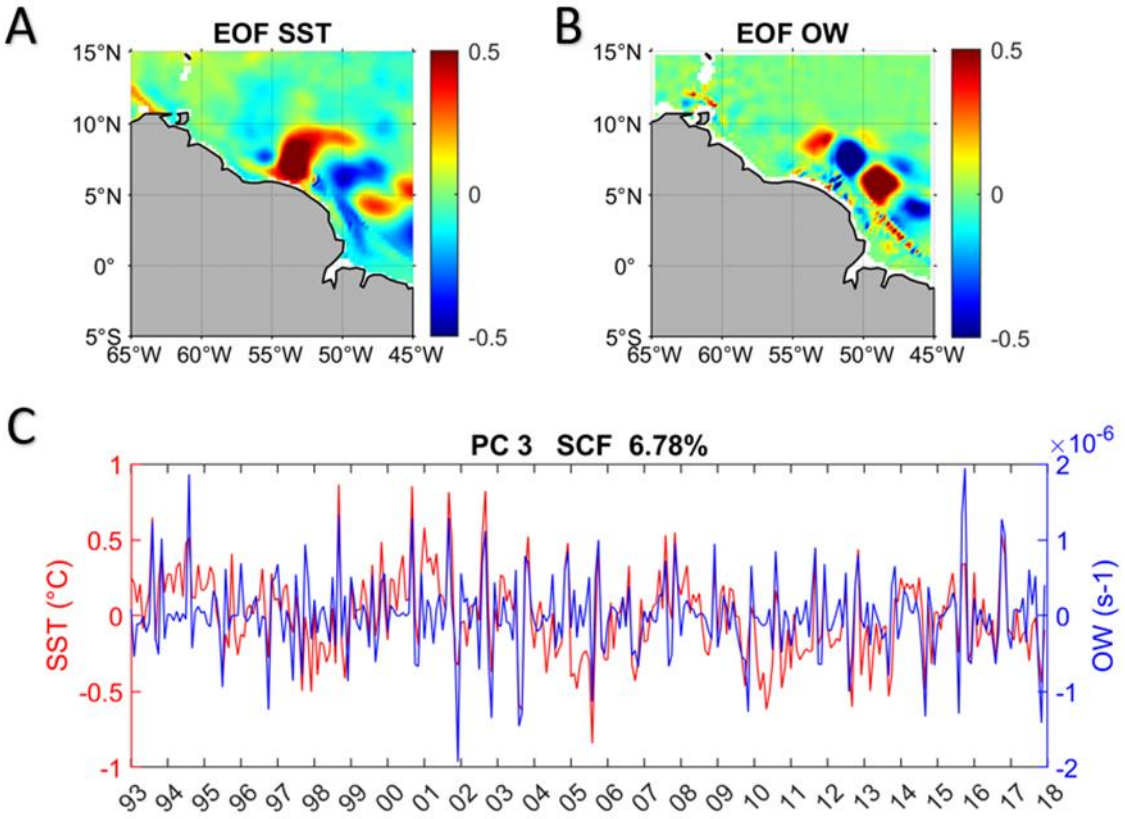


Source: the author (2021).

Table S1 – Observed values of the analyzed parameters for each day of two isolated rings (R1 and R2) which merged into one merged (M1) rings. NaN values are indicated in weeks that AMEDA did not identify the ring. Merged rings cells are highlighted in blue

| ID | DAY | Rmax(km) | Vmax (m/s) | Ro | KE (cm2/s2) | $FCO_2$ anomaly (mmol $m^{-2}$ $day^{-1}$) | Lat (º) | Lon(º) |
|---|---|---|---|---|---|---|---|---|
| ***R1*** | 10 Feb 2009 | 124.08 | 0.35 | 0.17 | 337.50 | 1.27 | 6.50 | -49.25 |
| | 11 Feb 2009 | 140.37 | 0.39 | 0.17 | 453.10 | 0.98 | 6.50 | -49.25 |
| | 12 Feb 2009 | 173.20 | 0.45 | 0.15 | 633.90 | 0.73 | 6.75 | -49.50 |
| | 13 Feb 2009 | 168.35 | 0.48 | 0.17 | 744.40 | 0.48 | 6.75 | -49.50 |
| | 14 Feb 2009 | 122.74 | 0.44 | 0.20 | 497.30 | 0.88 | 7.00 | -49.50 |
| | 15 Feb 2009 | 144.79 | 0.50 | 0.19 | 743.90 | 0.69 | 7.25 | -49.75 |
| | 16 Feb 2009 | 153.75 | 0.58 | 0.20 | 893.40 | 0.42 | 7.50 | -50.00 |
| | 17 Feb 2009 | 163.73 | 0.62 | 0.20 | 1204.10 | 0.47 | 7.50 | -50.00 |
| | 18 Feb 2009 | 165.49 | 0.66 | 0.20 | 1317.10 | 0.16 | 7.75 | -50.25 |
| | 19 Feb 2009 | 176.43 | 0.72 | 0.20 | 1617.90 | -0.01 | 8.00 | -50.50 |
| | 20 Feb 2009 | 148.27 | 0.66 | 0.21 | 1355.00 | 0.00 | 8.25 | -50.75 |
| | 21 Feb 2009 | 146.20 | 0.70 | 0.22 | 1526.40 | 0.00 | 8.50 | -51.00 |
| | 22 Feb 2009 | 144.43 | 0.75 | 0.23 | 1685.70 | 0.02 | 8.75 | -51.25 |
| | 23 Feb 2009 | 135.09 | 0.74 | 0.25 | 1688.40 | 0.00 | 8.75 | -51.25 |
| | 24 Feb 2009 | 150.42 | 0.83 | 0.25 | 2128.10 | 0.01 | 8.75 | -51.25 |
| | 25 Feb 2009 | 135.75 | 0.84 | 0.28 | 2049.80 | 0.00 | 8.75 | -51.50 |
| | 26 Feb 2009 | 140.76 | 0.84 | 0.26 | 2026.30 | 0.01 | 9.25 | -51.50 |
| | 27 Feb 2009 | 153.30 | 0.91 | 0.27 | 2293.30 | 0.00 | 8.75 | -51.75 |
| | 28 Feb 2009 | 142.53 | 0.85 | 0.25 | 1856.40 | 0.04 | 9.25 | -51.75 |
| | 01 Mar 2009 | 149.92 | 0.88 | 0.25 | 2151.30 | 0.06 | 9.50 | -51.75 |
| | 02 Mar 2009 | 148.89 | 0.86 | 0.24 | 2007.90 | 0.06 | 9.50 | -52.00 |

| | | | | | | | |
|---|---|---|---|---|---|---|---|
| 03 Mar 2009 | 151.42 | 0.84 | 0.22 | 1912.60 | 0.10 | 10.00 | -51.50 |
| 04 Mar 2009 | 151.89 | 0.82 | 0.22 | 1908.70 | 0.17 | 9.50 | -52.25 |
| 05 Mar 2009 | 148.22 | 0.83 | 0.23 | 1834.80 | 0.06 | 9.50 | -52.50 |
| 06 Mar 2009 | 159.39 | 0.81 | 0.21 | 2022.40 | 0.07 | 9.50 | -52.75 |
| 07 Mar 2009 | 168.97 | 0.85 | 0.21 | 2475.50 | 0.12 | 9.50 | -52.75 |
| 08 Mar 2009 | 128.98 | 0.79 | 0.26 | 2157.40 | 0.09 | 9.50 | -53.00 |
| 09 Mar 2009 | 129.38 | 0.75 | 0.24 | 1982.00 | 0.03 | 9.50 | -53.25 |
| 10 Mar 2009 | 134.53 | 0.82 | 0.25 | 2229.20 | 0.04 | 9.75 | -53.00 |
| 11 Mar 2009 | 127.85 | 0.83 | 0.26 | 2161.80 | 0.09 | 9.75 | -53.25 |
| 12 Mar 2009 | 133.81 | 0.82 | 0.25 | 2341.90 | 0.08 | 9.75 | -53.25 |
| 13 Mar 2009 | 128.32 | 0.72 | 0.23 | 1911.30 | 0.03 | 9.75 | -53.50 |
| 14 Mar 2009 | 134.38 | 0.75 | 0.23 | 1973.90 | 0.11 | 9.75 | -53.50 |
| 15 Mar 2009 | 129.90 | 0.77 | 0.24 | 2100.80 | 0.09 | 9.75 | -53.75 |
| 16 Mar 2009 | 114.01 | 0.77 | 0.27 | 1894.00 | 0.10 | 9.75 | -53.75 |
| 17 Mar 2009 | 120.40 | 0.76 | 0.26 | 1881.20 | 0.03 | 9.75 | -54.00 |
| 18 Mar 2009 | 121.70 | 0.76 | 0.25 | 1893.10 | 0.06 | 9.75 | -54.00 |
| 19 Mar 2009 | 114.40 | 0.75 | 0.27 | 1877.30 | 0.02 | 9.75 | -54.25 |
| 20 Mar 2009 | 115.29 | 0.67 | 0.24 | 1529.70 | -0.01 | 9.75 | -54.50 |
| 21 Mar 2009 | 118.90 | 0.63 | 0.22 | 1291.00 | 0.00 | 9.50 | -54.50 |
| 22 Mar 2009 | 136.36 | 0.68 | 0.21 | 1479.20 | 0.00 | 9.50 | -54.50 |
| 23 Mar 2009 | 158.96 | 0.69 | 0.18 | 1592.70 | 0.03 | 9.50 | -55.25 |
| 24 Mar 2009 | 154.99 | 0.64 | 0.17 | 1362.80 | 0.11 | 9.50 | -55.25 |
| 25 Mar 2009 | 174.32 | 0.60 | 0.14 | 1291.60 | -0.04 | 10.00 | -55.50 |
| 26 Mar 2009 | 186.47 | 0.63 | 0.13 | 1485.80 | -0.03 | 10.00 | -55.75 |
| 27 Mar 2009 | 171.70 | 0.65 | 0.15 | 1573.10 | -0.06 | 10.00 | -55.75 |

| | | | | | | | | |
|---|---|---|---|---|---|---|---|---|
| | 28 Mar 2009 | 152.45 | 0.61 | 0.15 | 1240.90 | 0.05 | 10.25 | -56.00 |
| | 29 Mar 2009 | 140.58 | 0.56 | 0.15 | 996.60 | 0.11 | 10.50 | -56.00 |
| | 30 Mar 2009 | 139.55 | 0.54 | 0.15 | 974.80 | 0.00 | 10.50 | -56.00 |
| | 31 Mar 2009 | 139.39 | 0.56 | 0.15 | 942.30 | 0.01 | 10.75 | -56.00 |
| | 01 Apr 2009 | 151.11 | 0.67 | 0.16 | 1506.00 | 0.00 | 10.75 | -56.00 |
| | 02 Apr 2009 | 138.55 | 0.66 | 0.17 | 1605.30 | 0.09 | 11.00 | -56.25 |
| | 03 Apr 2009 | 141.25 | 0.66 | 0.17 | 1547.00 | 0.13 | 11.00 | -56.25 |
| | 04 Apr 2009 | 126.22 | 0.69 | 0.20 | 1600.60 | 0.16 | 10.75 | -56.25 |
| | 05 Apr 2009 | 114.24 | 0.67 | 0.21 | 1501.50 | 0.00 | 11.00 | -56.50 |
| | 06 Apr 2009 | 117.55 | 0.69 | 0.21 | 1593.60 | 0.01 | 11.00 | -56.50 |
| | 07 Apr 2009 | 113.81 | 0.65 | 0.20 | 1428.60 | 0.04 | 11.25 | -56.25 |
| | 08 Apr 2009 | 120.11 | 0.67 | 0.20 | 1539.90 | 0.00 | 11.00 | -56.25 |
| | 09 Apr 2009 | 140.61 | 0.64 | 0.16 | 1270.40 | 0.01 | 11.00 | -56.50 |
| | 10 Apr 2009 | 139.75 | 0.64 | 0.16 | 1227.30 | 0.05 | 11.00 | -56.50 |
| | 11 Apr 2009 | 154.25 | 0.65 | 0.15 | 1334.30 | 0.05 | 11.00 | -56.50 |
| | 12 Apr 2009 | 154.71 | 0.61 | 0.14 | 1165.00 | 0.03 | 11.00 | -56.50 |
| | 13 Apr 2009 | 172.09 | 0.61 | 0.13 | 1361.40 | 0.13 | 11.00 | -56.75 |
| | 14 Apr 2009 | 156.70 | 0.49 | 0.11 | 944.98 | 0.03 | 11.00 | -56.75 |
| | 15 Apr 2009 | 133.61 | 0.45 | 0.12 | 586.95 | 0.03 | 11.25 | -56.75 |
| | 16 Apr 2009 | 148.05 | 0.52 | 0.12 | 1019.00 | 0.02 | 11.25 | -56.75 |
| | 17 Apr 2009 | 99.43 | 0.52 | 0.19 | 1049.10 | 0.02 | 11.00 | -57.00 |
| | 18 Apr 2009 | 165.27 | 0.48 | 0.11 | 932.80 | 0.07 | 11.00 | -57.00 |
| | 19 Apr 2009 | 100.31 | 0.50 | 0.18 | 875.41 | 0.15 | 11.00 | -56.75 |
| | | | | | | | | |
| ***R2*** | 02 Mar 2009 | 68.56 | 0.19 | 0.15 | 109.00 | -1.84 | 7.50 | -46.25 |

| | | | | | | | |
|---|---|---|---|---|---|---|---|
| 03 Mar 2009 | 89.70 | 0.26 | 0.16 | 184.80 | -1.58 | 7.50 | -46.25 |
| 04 Mar 2009 | 72.68 | 0.22 | 0.16 | 127.60 | -2.06 | 7.50 | -46.25 |
| 05 Mar 2009 | 98.73 | 0.27 | 0.14 | 192.60 | -1.79 | 7.50 | -46.25 |
| 06 Mar 2009 | 115.22 | 0.30 | 0.14 | 255.00 | -1.10 | 7.50 | -46.25 |
| 07 Mar 2009 | 100.28 | 0.25 | 0.13 | 180.70 | -0.92 | 7.50 | -46.25 |
| 08 Mar 2009 | 143.43 | 0.34 | 0.13 | 297.20 | -0.75 | 7.50 | -46.25 |
| 09 Mar 2009 | 165.65 | 0.38 | 0.14 | 386.60 | -0.07 | 6.50 | -47.75 |
| 10 Mar 2009 | 170.86 | 0.42 | 0.15 | 434.90 | -0.16 | 6.50 | -48.75 |
| 11 Mar 2009 | 155.72 | 0.41 | 0.15 | 397.40 | -0.35 | 6.75 | -48.00 |
| 12 Mar 2009 | NaN | NaN | NaN | NaN | NaN | NaN | NaN |
| 13 Mar 2009 | 138.68 | 0.37 | 0.16 | 385.90 | -0.49 | 6.75 | -47.75 |
| 14 Mar 2009 | 177.25 | 0.49 | 0.16 | 742.70 | -0.64 | 6.75 | -48.50 |
| 15 Mar 2009 | 150.26 | 0.44 | 0.17 | 582.10 | -0.62 | 6.75 | -48.75 |
| 16 Mar 2009 | 145.19 | 0.48 | 0.19 | 636.90 | -0.77 | 6.75 | -48.75 |
| 17 Mar 2009 | 150.93 | 0.47 | 0.18 | 684.30 | -0.33 | 7.00 | -49.00 |
| 18 Mar 2009 | 122.26 | 0.40 | 0.19 | 453.40 | -0.14 | 6.75 | -48.75 |
| 19 Mar 2009 | 148.40 | 0.45 | 0.18 | 586.30 | -0.21 | 6.75 | -49.00 |
| 20 Mar 2009 | 171.98 | 0.51 | 0.17 | 805.30 | -0.15 | 6.75 | -49.00 |
| 21 Mar 2009 | 166.43 | 0.50 | 0.17 | 667.80 | -0.22 | 7.00 | -49.50 |
| 22 Mar 2009 | 159.56 | 0.49 | 0.17 | 677.80 | 0.19 | 7.25 | -49.75 |
| 23 Mar 2009 | 165.28 | 0.54 | 0.18 | 824.00 | 0.37 | 7.25 | -49.75 |
| 24 Mar 2009 | 171.40 | 0.58 | 0.18 | 1038.10 | 0.24 | 7.50 | -50.25 |
| 25 Mar 2009 | 182.02 | 0.59 | 0.17 | 1132.50 | 0.46 | 7.75 | -50.50 |
| 26 Mar 2009 | 198.18 | 0.65 | 0.17 | 1386.50 | 0.41 | 7.75 | -50.50 |
| 27 Mar 2009 | 194.87 | 0.65 | 0.17 | 1387.30 | 0.25 | 7.75 | -50.50 |

| | | | | | | | | |
|---|---|---|---|---|---|---|---|---|
| | 28 Mar 2009 | 172.96 | 0.64 | 0.18 | 1281.60 | 0.23 | 8.25 | -51.25 |
| | 29 Mar 2009 | 156.29 | 0.61 | 0.19 | 1120.30 | 0.26 | 8.25 | -51.25 |
| | 30 Mar 2009 | 157.21 | 0.64 | 0.19 | 1357.90 | 0.03 | 8.50 | -51.50 |
| | 31 Mar 2009 | 155.46 | 0.62 | 0.18 | 1347.50 | 0.09 | 8.75 | -51.75 |
| | 01 Apr 2009 | 165.29 | 0.63 | 0.18 | 1402.30 | 0.06 | 8.50 | -51.50 |
| | 02 Apr 2009 | 139.81 | 0.66 | 0.22 | 1502.00 | 0.20 | 8.50 | -51.75 |
| | 03 Apr 2009 | 118.46 | 0.64 | 0.25 | 1398.60 | 0.13 | 8.50 | -52.00 |
| | 04 Apr 2009 | 119.61 | 0.71 | 0.27 | 1659.00 | 0.11 | 8.75 | -52.00 |
| | 05 Apr 2009 | 112.17 | 0.71 | 0.29 | 1564.80 | 0.11 | 8.75 | -52.25 |
| | 06 Apr 2009 | 117.62 | 0.69 | 0.27 | 1539.60 | 0.22 | 8.75 | -52.25 |
| | 07 Apr 2009 | 122.49 | 0.72 | 0.27 | 1702.20 | 0.30 | 8.75 | -52.50 |
| | 08 Apr 2009 | 116.18 | 0.68 | 0.26 | 1530.50 | 0.62 | 9.00 | -52.75 |
| | 09 Apr 2009 | 112.51 | 0.69 | 0.27 | 1593.70 | 0.45 | 9.00 | -52.75 |
| | 10 Apr 2009 | 107.83 | 0.64 | 0.26 | 1436.30 | 0.71 | 9.25 | -53.00 |
| | 11 Apr 2009 | 108.36 | 0.65 | 0.26 | 1390.20 | 0.94 | 9.25 | -53.25 |
| | 12 Apr 2009 | 117.47 | 0.68 | 0.25 | 1595.60 | 0.29 | 9.25 | -53.25 |
| | 13 Apr 2009 | 107.24 | 0.64 | 0.25 | 1346.30 | 0.33 | 9.25 | -53.50 |
| | 14 Apr 2009 | 91.77 | 0.51 | 0.24 | 922.02 | 0.67 | 9.25 | -53.75 |
| | 15 Apr 2009 | 96.78 | 0.49 | 0.22 | 833.51 | 0.37 | 9.25 | -53.75 |
| | 16 Apr 2009 | 87.33 | 0.55 | 0.27 | 934.20 | 0.66 | 9.25 | -53.75 |
| | 17 Apr 2009 | 88.82 | 0.59 | 0.28 | 1122.60 | 0.55 | 9.25 | -53.75 |
| | 18 Apr 2009 | 92.97 | 0.56 | 0.26 | 1024.80 | 0.28 | 9.00 | -54.00 |
| | 19 Apr 2009 | 64.63 | 0.44 | 0.30 | 629.51 | 1.32 | 9.00 | -54.50 |
| ***M1*** | 20 Apr 2009 | 98.54 | 0.52 | 0.19 | 991.89 | 0.06 | 11.00 | -57.00 |

| | | | | | | | |
|---|---|---|---|---|---|---|---|
| 21 Apr 2009 | 100.04 | 0.46 | 0.17 | 756.61 | 0.05 | 11.00 | -57.25 |
| 22 Apr 2009 | 100.14 | 0.47 | 0.17 | 773.21 | 0.03 | 11.00 | -57.25 |
| 23 Apr 2009 | 100.73 | 0.50 | 0.18 | 940.04 | 0.02 | 11.00 | -57.25 |
| 24 Apr 2009 | 125.15 | 0.51 | 0.15 | 1004.90 | 0.01 | 11.00 | -57.50 |
| 25 Apr 2009 | 123.39 | 0.51 | 0.15 | 1054.00 | 0.01 | 10.75 | -57.25 |
| 26 Apr 2009 | 113.71 | 0.53 | 0.17 | 984.60 | 0.07 | 10.75 | -57.50 |
| 27 Apr 2009 | 133.44 | 0.61 | 0.17 | 1311.10 | 0.03 | 10.75 | -57.50 |
| 28 Apr 2009 | 123.32 | 0.57 | 0.17 | 1013.90 | 0.02 | 10.75 | -57.75 |
| 29 Apr 2009 | 134.58 | 0.64 | 0.17 | 1370.50 | 0.04 | 10.75 | -57.75 |
| 30 Apr 2009 | 132.18 | 0.70 | 0.19 | 1809.50 | 0.01 | 11.25 | -58.25 |
| 01 May 2009 | 130.64 | 0.67 | 0.18 | 1703.20 | 0.19 | 11.00 | -58.25 |
| 02 May 2009 | 145.61 | 0.80 | 0.20 | 2243.30 | 0.01 | 11.00 | -58.25 |
| 03 May 2009 | 142.08 | 0.87 | 0.22 | 2572.10 | 0.01 | 11.25 | -58.50 |
| 04 May 2009 | 138.81 | 0.88 | 0.22 | 2477.60 | 0.01 | 11.50 | -58.75 |
| 05 May 2009 | 137.78 | 0.87 | 0.22 | 2425.90 | 0.08 | 11.50 | -58.50 |
| 06 May 2009 | 133.96 | 0.91 | 0.23 | 2695.60 | 0.16 | 11.50 | -58.75 |
| 07 May 2009 | 120.50 | 0.87 | 0.24 | 2189.10 | 0.11 | 12.00 | -58.75 |
| 08 May 2009 | 123.48 | 0.90 | 0.24 | 2204.40 | 0.04 | 11.75 | -58.75 |
| 09 May 2009 | 131.73 | 0.98 | 0.25 | 2422.20 | 0.03 | 11.75 | -58.75 |
| 10 May 2009 | 124.40 | 0.87 | 0.23 | 1965.90 | 0.04 | 12.25 | -59.00 |
| 11 May 2009 | 123.96 | 0.85 | 0.22 | 1877.40 | 0.08 | 12.50 | -59.00 |
| 12 May 2009 | 108.84 | 0.74 | 0.22 | 1474.60 | 0.12 | 12.25 | -59.00 |
| 13 May 2009 | 81.31 | 0.54 | 0.21 | 807.57 | 0.03 | 12.50 | -58.75 |
| 14 May 2009 | 77.57 | 0.44 | 0.18 | 557.34 | 0.04 | 12.25 | -58.75 |

Source: the author (2021).

Video 4.S1– Salinity anomalies for the evolution of R1, R2 and M1. The depicted evolution is from the first day of R1 detection (10th February 2009) to last day of M1 detection (14th May 2009).

Video 4.S2– DIC anomalies for the evolution of R1, R2 and M1. The depicted evolution is from the first day of R1 detection (10th February 2009) to last day of M1 detection (14th May 2009).

Video 4.S3– Chlorophyll anomalies for the evolution of R1, R2 and M1. The depicted evolution is from the first day of R1 detection (10th February 2009) to last day of M1 detection (14th May 2009).

Video 4.S4– $FCO_2$ anomalies for the evolution of R1, R2 and M1. The depicted evolution is from the first day of R1 detection (10th February 2009) to last day of M1 detection (14th May 2009).

Videos 4.S1, 4.S2, 4.S3, and 4.S4 are inserted in the PowerPoint in attachment ('Videos_Dissertação_LeoAroucha.pptx').

# 5. CONCLUSÕES

No presente trabalho dados de reanálise semanais de altura geopotencial e de campos de velocidade geostrófica de 24 anos (1993-2016) foram aplicados ao algoritmo AMEDA para identificação da ocorrência, trajetória e parâmetros físicos dos Vórtices da CNB, se posicionando como o primeiro estudo a aplicar um algoritmo de detecção de vórtices para identificação dos vórtices da CNB num período decenal. A escolha pelo AMEDA se baseia em sua robustez e facilidade para uso em análises de séries temporais de propriedades de vórtices, haja vista que o mesmo considera não apenas as propriedades dinâmicas, mas também as propriedades geométricas do campo de velocidade. Além disso, análises estatísticas de Funções Ortogonais Empíricas (EOFs) foram realizadas em 25 anos (1993 – 2017) de dados de reanálise de um outro modelo, com o objetivo de avaliar o papel dos vórtices da CNB na biogeoquímica do ATNO, especialmente em relação a $FCO_2$. Esta última base de dados também foi aplicada ao AMEDA para identificação dos impactos destes vórtices em uma escala diária, utilizando dois vórtices no ano de 2009 como estudos de caso.

Neste estudo foi identificada uma taxa média de 5 vórtices da CNB liberados por ano, que apresentaram um tempo de vida médio de 15.3 (±5.4) semanas, Rmax de 87.3 a 204.8 km, com raio médio de 139.5 (±23.6) km, e foram associados com anomalias de altura da superfície do mar médias de 9.4 (±4.0) cm. A Vmax média observada foi 0.27 (±0.08) m/s, enquanto que o valor de Ro médio foi 0.08 (±0.04) e a energia cinética média foi 255.3 (±154.8) cm2 /s2. É apontado que os valores de velocidade azimutal e de Ro podem estar subestimados devido ao uso de campos de velocidade puramente geostróficos. A ocorrência dos vórtices da NBC é mais frequente na primeira metade do ano. De fato, uma diminuição na taxa de geração dos mesmos de 47.37% foi detectada entre os trimestres de máxima (inverno boreal) e mínima (outono boreal) liberação. Além disso, vórtices da NBC apresentaram dimensões maiores, rotação mais rápida e apresentaram menor tempo de vida nos meses de inverno boreal, também carregando mais energia cinética neste período. Por outro lado, tais vórtices liberados durante o verão e no início do outono boreal tem diâmetros menores, duram mais e carregam menos energia. 2009 foi um ano de condições anômalas, haja vista que apresentou valores máximos de energia cinética, Vmax e anomalia de altura da superfície do mar associadas aos vórtices da CNB. Outro padrão identificado neste estudo foi a tendência positiva nas anomalias de altura da superfície do mar de 2009 a 2016. Isso mostra que estas alturas dentro destes vórtices estão aumentando nos últimos anos, o que pode ser futuramente investigado.

Ainda, foi identificado que subsidência de massas d'agua no centro dos vórtices da CNB geraram um aprofundamento da termoclina e anomalias no perfil vertical de salinidade, indicando transporte vertical para o fundo de águas tropicais e costeiras. A análise do diagrama T-S permitiu a identificação de sazonalidade em relação as massas d'água no interior dos mesmos vórtices. Água do rio foi observada no centro destas estruturas apenas nos formados entre Maio e Agosto, demonstrando que vórtices gerados neste período de meses podem ter impactos biogeoquímicos diferenciados na região do ATNO, como mudanças na fugacidade e fluxos de $CO_2$ entre oceano e atmosfera. A mudança vertical nos perfis de temperatura e salinidade também pode influenciar esses efeitos físicos e biogeoquímicos. Mais estudos sobre isso poderiam fornecer essa resposta. Além disso, foi observado no ano de 2009 uma possível influência da descarga do rio Amazonas nos parâmetros dinâmicos dos vórtices da CNB, como Vmax e KE, por meio de efeitos na densidade da água, vorticidade e velocidade do fluxo, o que também pode ter contribuído para um evento de fusão dos mesmos naquele ano. Ainda assim, eventos de fusão como estes, embora não muito frequentes, podem aumentar significativamente a velocidade e a energia dos vórtices. No entanto, o mecanismo e o fornecimento de energia que permitem que isso ocorra com anéis da CNB permanecem obscuros. Além disso, esses aumentos na energia cinética do vórtice fundido podem ter um impacto na dinâmica atual ao redor do Caribe, influenciando, por exemplo, a distribuição do fitoplâncton. Trabalhos adicionais sobre isso forneceriam esta resposta.

Além disso, foi identificado que os vórtices da CNB, representados aqui pelo OW, apresentaram variância de acordo com o padrão de $fCO_{2\,SW}$ em 29% do tempo, quando se analisa o segundo e terceiro modo dos EOF's. Ainda, a presença da covariância de OW relacionada com a translação de estruturas de mesoescala em 77% do tempo, indica que essa influência ocorre em um período significativo. OW e SSS variaram também similarmente em 77% do tempo, mostrando a influência de tais vórtices na variância da SSS na região. Este resultado também apontou para a salinidade como a principal responsável pelas anomalias positivas de $fCO_{2\,SW}$ relacionadas aos núcleos dos vórtices. Além do mais, foi indicado que um vórtice da CNB pôde aumentar, em média, 38% do $FCO_2$ em seus núcleos em relação às águas externas. No presente trabalho, acredita-se que anomalias positivas de salinidade e consequentemente de DIC nas regiões superficiais dos centros e das partes anteriores dos anéis foram responsáveis por esse aumento na covariância de $fCO_{2\,SW}$ e no $FCO_2$, diário, apesar que o aumento de TSM inerente aos vórtices anticiclônicos podem ter contribuído para estes fluxos elevados. Novos estudos sobre movimentos verticais e distúrbios de pequena escala na região

dentro desses redemoinhos podem esclarecer sobre o que faz com que essas anomalias de salinidade permaneçam presas na superfície.

Finalmente, parece razoável afirmar que os vórtices da NBC impactam nos parâmetros biogeoquímicos na região do ATNO, tanto na superfície quanto em profundidade, embora os mecanismos por trás desses impactos, especialmente em profundidade, precisam de maior investigação. De fato, estudos sobre processos de estratificação e mistura, e impactos biogeoquímicos destes vórtices estão sendo desenvolvidos atualmente (L'HEGARÈT *et al.*, 2021; OLIVIER *et al.*, 2021). A contribuição do presente trabalho está não só na observação da influência dos vórtices da CNB na variância dos parâmetros de carbono no ATNO, mas também em demonstrar a contribuição dos mesmo para aumentar o $FCO_2$ para a atmosfera. Um estudo extenso, com mais vórtices analisados, aumentaria a amostragem e poderiam reforçar este efeito nas anomalias dos fluxos de $CO_2$. Por fim, o estudo também mostra a capacidade dessas estruturas em concentrar em seus centros e limites anteriores águas com alta concentração de DIC e sal, e dá uma luz em qual mecanismo é responsável por manter tais anomalias.

Neste trabalho, o uso de dados de reanálise associados a ferramenta AMEDA permitiu a investigação da variabilidade intra e interanual da ocorrência e dinâmica dos vórtices da CNB. Além disso, o algoritmo demonstrou ser simples na identificação de interação entre os mesmos, o que facilita a análise desses eventos. No geral, quantificar a variabilidade sazonal e interanual dos parâmetros do vórtice e identificar a interação entre eles é crucial para a compreensão da dinâmica destas estruturas e, consequentemente, seus impactos na física e biogeoquímica do oceano. Da mesma forma, o presente estudo contribui na avaliação de impactos dos vórtices da CNB na biogeoquímica do ATNO, principalmente com a análise estatística, que residiu na observação da capacidade dos mesmos em concentrar DIC e águas altamente salinas em seus núcleos. Além disso, dá uma luz sobre qual mecanismo é responsável por manter a anomalia de salinidade nos núcleos dos anéis.

# REFERÊNCIAS

ANDRIÈ, C., C. OUDOT, C. GENTHON, L. MEFIIVAT, CO2 fluxes in the tropical Atlantic during FOCAL cruises, **Journal of Geophysical Research**, 91, 11741-11755, 1986.

ARAÚJO, M.; NORIEGA, C.; HOUNSOU-GBO, G. A.; VELEDA, D.; ARAUJO, J.; BRUTO, L.; FEITOSA, F.; FLORES-MONTES, M.; LEFÈVRE, N.; MELO, P.; OTSUKA, A.; TRAVASSOS, K.; SCHWAMBORN, R.; NEUMANN-LEITÃO, S. A Synoptic Assessment of the Amazon River-Ocean Continuum during Boreal Autumn: From Physics to Plankton Communities and Carbon Flux. **Frontiers in Microbiology**, v. 8, p. 1, 2017.

ARNAULT, S., CHENEY, R. E. Tropical Atlantic Sea level variability from Geosat (1985–1989). **Journal of Geophysical Research**, 99, 18207–18223. https://doi.org/10.1029/94JC01301, 1994.

AUMONT, O., ETHÉ, C., TAGLIABUE, A., BOPP, L., GEHLEN, M. PISCES-v2: an ocean biogeochemical model for carbon and ecosystem studies. **Geoscientific Model Development** 8, 2465-2513. 2015.

BAKUN, A. Fronts and eddies as key structures in the habitat of marine fish larvae: opportunity adaptive response and competitive advantage. **Scientia Marina,** v.70, p.105–122, 2006.

BARNIER, B., REYNAUD, T., BECKMANN, A., BONING, C., MOLINES, J.-M., BARNARD, S., JIA, Y. On the seasonal variability and eddies in the North Brazil Current: insight from model intercomparison experiments. **Progress in Oceanography**, 44, 195–230. https://doi.org/10.1016/S0079-6611(01)00005-2, 2001.

BENITEZ-NELSON, C. R., BIDIGARE, R. R., DICKEY, T. D., LANDRY, *et al.* Mesoscale eddies drive increased silica export in the subtropical Pacific Ocean. **Science**, v.316, p.1017–1021, 2007.

BUONGIORNO NARDELLI, B., DROGHEI, R., SANTOLERI, R. Multi-dimensional interpolation of SMOS sea surface salinity with surface temperature and in situ salinity data. **Remote Sensing of Environment,** 180, 392–402. https://doi.org/10.1016/j.rse.2015.12.052, 2016.

CASTELÃO, G. P.; JOHNS, W. E. Sea surface structure of North Brazil Current rings derived from shipboard and moored acoustic Doppler current profiler observations, **Journal of Geophysical Research,** 116, 2011.

CARTON J. A. Effect of seasonal surface freshwater flux on sea surface temperature in the Tropical Atlantic Ocean. **Journal of Geophysical Research**, v.96, p.12593–12598, 1991.

CHAIGNEAU, A., A. GIZOLME, C. GRADOS. Mesoscale eddies off Peru in altimeter records: Identification algorithms and eddy spatio-temporal patterns. **Progress in Oceanography**, v.79, p.106–119, 2008.

CHAPA, C. Air-sea CO2 flux (https://www.mathworks.com/matlabcentral/fileexchange/50190-air-sea-co2-flux), **MATLAB Central File Exchange**, 2020.

CHELTON, D. B., M. G. SCHLAX, R. M. SAMELSON, R. A. DE SZOEKE. Global observations of large oceanic eddies. **Geophysical Research Letters**, v.34, 5p., 2007.

CHEN, G., YANG, J., HAN, G. Eddy morphology: Egg-like shape, overall spinning, and oceanographic implications, **Remote Sensing of Environment**, 257, 112348, https://doi.org/10.1016/j.rse.2021.112348, 2021.

COOLEY, S. R.; COLES, V. J.; SUBRAMANIAM, A.; YAGER, P. L. Seasonal variations in the Amazon plume-related atmospheric carbon sink. **Global Biogeochemical Cycles**, 21, 2007. https://doi.org/10.1029/2006GB002831;

COWEN, R. K., L. R. CASTRO. Relation of coral reef fish larval distributions to island scale circulation around Barbados, West Indies**. Bulletin of Marine Science**, v.54, p.228–244, 1994.

COWEN, R. K., S. SPONAUGLE, C. B. PARIS, K. LWIZA, J. FORTUNA, S. DORSEY. Impact of North Brazil Current rings on local circulation and coral reef fish recruitment to Barbados, West Indies. **Interhemispheric Water Exchange in the Atlantic Ocean,** G. J. Goni and P. Malanotte-Rizzoli, Eds., Elsevier Oceanographic Series, v. 68, p.443–455, 2003.

CRUZ-GÓMEZ, R., SALCEDO-CASTRO, J. Analysis of Horizontal and Vertical Ring Structure based on Analytical Model and Satellite Data: Application to the North Brazil Current Rings. **Ocean Science Journal**, v.48(2), p.161-172, 2013.

CUI, W., WANG, W., ZHANG, J., YANG, J. Multi core structures and the splitting and merging of eddies in global oceans from satellite altimeter data. **Ocean Science**, 15, 413–430. https://doi.org/10.5194/os-15-413-2019, 2019.

DE MAREZ, C., CARTON, X., L'HÉGARET, P. *et al.* Oceanic vortex mergers are not isolated but influenced by the β-effect and surrounding eddies. **Scientific Reports**, 10, 2897,2020.

DICKSON, A. G., MILLERO, F. J. A comparison of the equilibrium constants for the dissociation of carbonic acid in seawater media. **Deep Sea Research** 34, 1733–1743, doi: 10.1016/0198-0149(87)90021-5, 1987.

DIDDEN, N., SCHOTT, F. Eddies in the North Brazil Current Retroflection Region Observed by Geosat Altimetry. **Journal of Geophysical Research**, v.98, p.121-131, 1993.

DOGLIOLI, A. M., BLANKE, B., SPEICH, S., LAPEYRE, G. Tracking coherent structures in a regional ocean model with wavelet analysis: Application to Cape Basin eddies. **Journal of Geophysical Research**, 112(C5). https://doi.org/10.1029/2006JC003952, 2007.

DOUGLASS, E. M., RICHMAN, J. G. Analysis of ageostrophy in strong surface eddies in the Atlantic Ocean. **Journal of Geophysical Research: Oceans,** 120, 1490–1507. https://doi.org/10.1002/2014JC010350, 2015.

FFIELD, A. North Brazil Current Rings viewed by TRMM Microwave Imager SST and the influence on Amazon River Plume. **Deep Sea Research I**, v.52, p.137–160, 2005.

FOLTZ, G. R., MCPHADEN, M. J., LUMPKIN, R. A strong Atlantic Meridional Mode Event in 2009: The role of mixed layer dynamics. **Journal of Climate**, 25, 363–380. https://doi.org/10.1175/JCLI-D-11-00150.1. 2012.

FONSECA, C. A., G. J. GONI, W. E. JOHNS, E. J. D. CAMPOS. Investigation of the North Brazil Current retroflection and North Equatorial Countercurrent variability. **Geophysical Research Letters**, 31, 2004, doi:10.1029/2004GL020054.

FRATANTONI, D. M., W. E. JOHNS, T. L. TOWNSEND. Rings of the North Brazil Current: Their structure and behavior inferred from observations and a numerical simulation. **Journal of Geophysical Research**, v.100, p.10633-10654, 1995.

FRATANTONI, D. M., W. E. JOHNS, T. L. TOWNSEND, H. E. HURLBURT. Low-latitude circulation and mass transport pathways in a model of the tropical Atlantic Ocean. **Journal of Physical Oceanography**, v.30, p.1944–1966, 2000.

FRATANTONI, D. M., GLICKSON, D. A. North Brazil Current Ring generation and evolution observed with SeaWiFS. **Journal of Physical Oceanography**, v.32, p.1058–1074, 2002.

FRATANTONI, D. M., P. L. RICHARDSON. The evolution and demise of North Brazil Current rings. **Journal of Physical Oceanography**, v.36, p.1241–1264, 2006.

FROIDEFOND, J.M., GARDEL, L., GUIRAL, D.L., PARRA, M., TERNON, J.F. Spectral remote sensing reflectances of coastal waters in French Guiana under the Amazon influence. **Remote Sensing of Environment**, 80, 225–232, 2002.

GARRAFFO, Z., JOHNS, W. E., CHASSIGNET, E., GONI, G. North Brazil Current rings and transport of southern waters in a high-resolution numerical simulation of the North Atlantic. In **Interhemispheric water exchange in the Atlantic Ocean**, Elsevier Oceanography Series (Vol. 68, pp. 375–410), Amsterdam: Elsevier. https://doi.org/10.1016/S0422-9894(03)80155-1, 2003.

GARREAU, P., DUMAS, F., LOUAZEL, S., STEGNER, A., LE VU, B. High-Resolution Observations and Tracking of a Dual-Core Anticyclonic Eddy in the Algerian Basin. **Journal of Geophysical Research: Oceans**, 123 (12), 9320 – 9339, 2018.

GARZOLI, S. L., FFIELD, A., YAO, Q. North Brazil Current Rings and the variability in the latitude of retroflection. **Interhemispheric Water Exchange in the Atlantic Ocean** v.68, p.357-373, 2003.

GARZOLI, S. L., A. FFIELD, W. E. JOHNS, Q. YAO. North Brazil Current retroflection and transports, **Journal of Geophysical Research**, v.109, 2004.

GONI, G. J.; W. E. JOHNS. A Census of North Brazil Current Rings observed from TOPEX/Poseidon Altimetry: 1992-1998. **Journal of Geophysical Research**, v.28, p.1-4, 2001.

GONI, G. J., W. E. JOHNS. Synoptic study of warm rings in the North Brazil Current retroflection region using satellite altimetry. **Interhemispheric Water Exchange in the Atlantic Ocean** v.68, p.335-356, 2003

GRINSTED, A., MOORE, J.; JEVREJEVA, S. Application of the cross wavelet transform and wavelet coherence to geophysical time series. **Nonlinear Processes Geophysics**, 11, 561–566, 2004.

GUINEHUT S., A.-L. DHOMPS, G. LARNICOL, P.-Y. LE TRAON. High resolution 3D temperature and salinity fields derived from in situ and satellite observations. **Ocean Sciences**, v.8, p.845–857, 2012.

HALO, I., BACKEBERG, B., PENVEN, P., ANSORGE, I., REASON, C., ULLGREN, J. Eddy properties in the Mozambique Channel: A comparison between observations and two numerical ocean circulation models**. Deep Sea Research Part II**: Topical Studies in Oceanography, 100, 38–53. https://doi.org/10.1016/j.dsr2.2013.10.015, 2014.

HELLWEGER, F. L., GORDON, A. L. Tracing Amazon River water into the Caribbean Sea. **Journal of Marine Research**, 60, 537–549, 2002.

HUANG, M., LIANG, X., ZHU, Y., LIU, Y., WEISBERG, R. H. Eddies connect the tropical Atlantic Ocean and the Gulf of Mexico. **Geophysical Research Letters,** 48, e2020GL091277. https://doi.org/10.1029/2020GL091277, 2021.

IBÁNHEZ, J. S. P.; FLORES, M.; LEFÈVRE, N. Collapse of the tropical and subtropical North Atlantic CO2 sink in boreal spring of 2010. **Scientific Reports** 7, 41694; doi: 10.1038/srep41694, 2017.

IOANNOU, A., STEGNER, A., LE VU, B., TAUPIER-LETAGE, I., SPEICH, S. Dynamical Evolution of Intense Ierapetra Eddies on a 22 Year Long Period. **Journal of Geophysical Research: Oceans**, 2017.

ISERN-FONTANET, J.; FONT, J.; GARCÍA-LADONA, E.; EMELIANOV, M.; MILLOT, C.; TAUPIER-LETAGE, I. Spatial structure of anticyclonic eddies in the Algerian basin (Mediterranean Sea) analyzed using the Okubo–Weiss parameter. **Deep Sea Research Part II: Topical Studies in Oceanography**, Volume 51, Issues 25–26, p. 3009-3028, https://doi.org/10.1016/j.dsr2.2004.09.013, 2004.

JOCHUM, M., MALANOTTE-RIZZOLI, P. On the generation and importance of North Brazil Current rings. **Journal of Marine Research**, 61, 147–162. https://doi.org/10.1357/002224003322005050, 2003.

JOCHUMSEN, K., RHEIN, M., HÜTTL-KABUS, S., BÖNING, C. W. On the propagation and decay of North Brazil Current rings. **Journal of Geophysical Research**, v.115, 2010.

JOHNS, W. E., T. N. LEE, F. A. SCHOTT, R. J. ZANTOPP, R. H. EVANS. The North Brazil Current retroflection: Seasonal structure and eddy variability. **Journal of Geophysical Research**, v.95, p.22103–22120, 1990.

JOHNS, W. E., R. C. BEARDSLEY, J. CANDELA, R. LIMEBURNER, B. CASTRO. Annual cycle and variability of the North Brazil Current**. Journal of Physical Oceanography**, v.28, p.103–128, 1998.

JOHNS, W. E., R. J. ZANTOPP, G. J. GONI. Cross-gyre transport by North Brazil Current Rings. **Interhemispheric Water Exchange in the Atlantic Ocean,** v. 68, p.411–441, 2003.

KELLY, P. S., K. M. M. LWIZA, R. K. COWEN, G. J. GONI. Low-salinity pools at Barbados, West Indies: Their origin, frequency, and variability. **Journal of Geophysical Research**, v.5, p.19669– 19708, 2000.

KLEIN, P., LAPEYRE, G., SIEGELMAN, L., QIU, B., FU, L., TORRES, H., *et al.* Ocean-scale interactions from space. **Earth and Space Science,** 6, 795–817. https://doi.org/10.1029/2018ea000492, 2019.

LEFÈVRE, N., MOORE, G., AIKEN, J., WATSON, A., COOPER, D., LING, R. Variability of pCO2 in the tropical Atlantic in 1995. **Journal of Geophysical Research** 103, 5623–5634, 1998.

LEFÈVRE, N., DIVERRÈS, D., GALLOIS, F. Origin of CO2 undersaturation in the western tropical Atlantic. **Tellus B** 62, 595–607. 2010;

LEFÈVRE N, FLORES-MONTES M., GASPAR F. L., ROCHA C, JIANG S, DE ARAÚJO M. C., IBÁNHEZ, J. S. P. Net Heterotrophy in the Amazon Continental Shelf Changes Rapidly to a Sink of CO2 in the Outer Amazon Plume. **Frontiers in Marine Science** 4:278, 2017.

LEFÈVRE, N., TYAQUIÇÃ, P., VELEDA, D., PERRUCHE, C., JAN VAN GENNIP, S. Amazon River propagation evidenced by a CO2 decrease at 8°N, 38°W in September 2013.**Journal of Marine Systems,** 2020, https://doi.org/10.1016/j.jmarsys.2020.103419

LEGECKIS, R.; GORDON, A. L. Satellite observations of the Brazil and Falkland currents--1975 to 1976 and 1978. **Deep-Sea Research**, v. 29, p.375-401, 1982.

LE VU, B., STEGNER, A., ARSOUZE, T. Angular Momentum Eddy Detection and tracking Algorithm (AMEDA) and its application to coastal eddy formation. **Journal of Atmospheric Oceanic Technology,** v.35, p.739–762, 2018.

LEWIS, E., WALLACE, D. **Program Developed for CO2 System Calculations**. Oak Ridge National Laboratory Environmental Sciences Division, 1998.

L'HÉGARET, P., SPEICH, S., CHEN, Y, MANTA, G., OLIVIER, L., REVERDIN, G., POUPON, M., SCHÜTTE, F., KARSTENSEN, J., CARTON, X., LAXENAIRE, R., ZHANG, D., FOLTZ, G. EUREC4A-OA/ATOMIC experiment: Themohaline and dynamical descriptions of mesoscale and submesoscale structures of the Northwest Tropical Atlantic

Ocean, **EGU General Assembly 21,** EGU21-10991, https://doi.org/10.5194/egusphere-egu21-10991, 2021.

LI, Q.-Y., SUN, L., LIU, S.-S., XIAN, T., YAN, Y.-F. A new mononuclear eddy identification method with simple splitting strategies. **Remote Sensing Letters**, 5, 65–72. https://doi.org/10.1080/2150704X.2013.872814, 2014.

LUMPKIN, R., S. L. GARZOLI. Near-surface circulation in the tropical Atlantic Ocean. **DeepSea Research II**, v.52, p.495–518, 2005.

KAHRU, M., MITCHELL, B. G., GILLE, S. T., HEWES, C. D., HOLM-HANSEN, O. Eddies enhance biological production in the Weddell-Scotia Confuence of the Southern Ocean. **Geophysical Research Letters,** 34, L14603, https://doi.org/10.1029/2007GL030430, 2007.

KAMENKOVICH, V.M., KOSHLYAKOV, M.N., MONIN, A. S. Synoptic Eddies in the Ocean. **Springer**, 444pp., 1986.

KÖRTZINGER, A. A significant sink of CO2 in the tropical Atlantic Ocean associated with the Amazon River plume. **Geophysical Research Letters** 30, 2287,2003.

MA, H. The dynamics of the North Brazil Current retroflection eddies. **Journal of Marine Research**, 54, 35–53. https://doi. org/10.1357/0022240963213493, 1996.

MCGILLICUDDY, D. J., ROBINSON, A. R., SIEGEL, D. A., JANNASCH, H. W., JOHNSON, T., DICKEY, T. D., MCNEIL, J., MICHAELS, A. F., KNAP, A. H. Influence of mesoscale eddies on new production in Sargasso Sea. **Nature**, v.394, p.263-266, 1998.

MCGILLICUDDY, D. J. Mechanisms of physical-biological-biogeochemical interaction at the oceanic mesoscale. **Annu Rev Mar Sci**, 8, 125–59, 2016.

MCWILLIAMS, J. C. The vortices of two-dimensional turbulence. **Journal of Fluid Mechanics**, 219, 361–385. https://doi.org/10.1017/ S0022112090002981, 1990.

MÉLICE, J.-L., ARNAULT, S. Investigation of the intra-annual variability of the North Equatorial Countercurrent/North Brazil Current eddies and of the instability waves of the North tropical Atlantic Ocean using satellite altimetry and Empirical Mode Decomposition. **Journal of Atmospheric and Oceanic Technology**, 34, 2295–2310. https://doi.org/10.1175/JTECH-D-17-0032.1. 2017.

MEHRBACH, C., CULBERSON, C. H., HAWLEY, J. E., PYTKOWICZ, R. M. Measurement of the apparent dissociation constants of carbonic acid in seawater at atmospheric pressure. **Limnol. Oceanogr.** 18, 897–907, doi: 10.4319/lo.1973.18.6.0897, 1973.

MKHININI, N., COIMBRA, A. L. S., STEGNER, A., ARSOUZE, T., TAUPIER-LETAGE, I., BERANGER, K. Long-lived mesoscale eddies in the eastern Mediterranean Sea: Analysis of 20 years of AVISO geostrophic velocities. **Journal of Geophysical Research: Oceans,** 119, 8603–8626, https://doi.org/10.1002/2014JC01017, 2014.

MOURIÑO, B., E. FERNÁNDEZ, H. ETIENNE, F. HERNÁNDEZ, S. GIRAUD. Significance of cyclonic SubTropical Oceanic Rings of Magnitude (STORM) eddies for the carbon budget of the euphotic layer in the subtropical northeast Atlantic, **Journal of Geophysical Research,** 108, 3383, doi:10.1029/2003JC001884, 2003.

MULET, S., M.-H. RIO, A. MIGNOT, S. GUINEHUT, R. MORROW. A new estimate of the global 3D geostrophic ocean circulation based on satellite data and in-situ measurements. **Deep Sea Research Part II:** Tropical Studies in Oceanography, 77–80(0), p.70–81, 2012.

NENCIOLI, F., DONG, C., DICKEY, T., WASHBURN, L., MCWILLIAMS, J. A vector geometry-based eddy detection algorithm and its application to a high-resolution numerical model product and high-frequency radar surface velocities in the Southern California Bight. **Journal of Atmospheric and Oceanic Technology,** 27(3), 564–579. https://doi.org/10.1175/2009JTECHO725.1, 2010.

NEUMANN-LEITÃO, S., MELO, P. A. M. C., SCHWAMBORN, R., DIAZ, X., FIGUEIREDO, L., SILVA, A., CAMPELO, R. P. S., JUNIOR, M. M., MELO, N. A. F. C., COSTA, A., ARAUJO, M., VELEDA, D. R. A., MOURA, R., THEMPSON, F. Zooplankton from a reef system under the influence of the Amazon River Plume. **Frontiers in Microbiology**, 9, 355. https://doi.org/10.3389/fmicb.2018.00355, 2018.

NURSER, A. J. G., BACON, S. The Rossby radius in the Arctic Ocean. **Ocean Science,** 10, 967–975. https://doi.org/10.5194/ os-10-967-2014, 2014.

OLIVIER, L., BOUTIN, J., LEFÈVRE, N., REVERDIN, G., LANDSCHÜSZTER, P., SPEICH, S., KARSTENSEN, J. Impact of mesoscale eddies on salinity and CO2 ocean parameters in the western tropical Atlantic in February 2020, **EGU General Assembly 21,** 1253, https://doi.org/10.5194/egusphere-egu21-1253, 2021.

OLSON, D.B. Rings in the ocean. **Annual Review of Earth Planetary Science,** v.19, p.283-311, 1990.

ORSELLI, I. B. M., KERR, R., AZEVEDO, J. L. L., GALDINO, F., ARAUJO, M., GARCIA, C. A. E. Thesea-airCO2netfluxesintheSouthAtlanticOceanandtheroleplayedby Agulhaseddies. **Progress in Oceanography**, 170, p. 40-52, 2019.

PAULUHN, A., CHAO, Y. Tracking eddies in the subtropical North-Western Atlantic Ocean. **Physics and Chemistry of the Earth**, 24A, 415–421. https://doi.org/10.1016/S1464-1895(99)00052-8, 1999.

PEZZI, L., P., SOUZA, R. B., SANTINI, M., MILLER, A. J., CARVALHO, J. T., PARISE, C. K., QUADRO, M. F., ROSA, E. B., JUSTINO, F., SUTIL, U. A., CABRERA, M., J., BABANIN, A., V., VOERMANS, J., NASCIMENTO, E. L., ALVES, R. C. M., MUNCHOW, G. B., RUBERT, J. Oceanic eddy-induced modifications to air–sea heat and CO2 fluxes in the Brazil-Malvinas Confluence. **Scientific Reports,** 11, 10648 https://doi.org/10.1038/s41598-021-89985-9, 2021.

PIERROT, D., LEWIS, E., WALLACE, D. W. R. **MS Excel Program Developed for CO2 System Calculations,** O.R.N.L. Oak Ridge, TN: Carbon Dioxide Information Analysis Center; U.S. Department of Energy, 2006.

POLO, I., LAZAR, A., RODRIGUEZ-FONSECA, B., MIGNOT, J. Growth and decay of the equatorial Atlantic SST mode by means of closed heat budget in a coupled general circulation model. **Frontiers of Earth Science**, 3, 37. https://doi.org/10.3389/feart.2015.00037, 2015.

RICHARDSON, P., WALSH, D. Mapping climatological seasonal variations of surface currents in the tropical Atlantic using ship drifts. **Journal of Geophysical Research**, 91, 10537–10550. https://doi.org/10.1029/jc091ic09p10537, 1986.

RICHARDSON, P. L., HUFFORD, G. E., LIMEBURNER, R., BROWN, W. S. North Brazil Current retroflection eddies. **Journal of Geophysical Research**, 99, 5081–5093. https://doi.org/10.1029/93JC03486, 1994.

RICHARDSON, P. L. Caribbean Current and eddies as observed by surface drifters. **Deep-Sea Research II**. 52, 429–463, 2005.

RUDZIN, J. E., SHAY, L. K., JAIMES, B., BREWSTER, J. K. Upper ocean observations in eastern Caribbean Sea reveal barrier layer within a warm core eddy. **Journal of Geophysical Research: Oceans,** 122, 1057–1071. https://doi.org/10.1002/2016JC012339, 2017.

SADARJOEN, I. A., POST, F. H. Detection, quantification, and tracking of vortices using streamline geometry. **Computers & Graphics**, 24, 333–341. https://doi.org/10.1016/S0097-8493(00)00029-7, 2000.

SHARMA, N., ANDERSON, S. P., BRICKLEY, P., NOBRE, C., CADWALLADER, M. L. Quantifying the seasonal and inter-annual variability of the formation and migration pattern of North Brazil Current rings. Conference paper presented at **OCEANS 2009, MTS/IEEE Biloxi – Marine Technology for Our Future: Global and Local Challenge,** IEEE, pp. 1–7. https://doi.org/10.23919/OCEANS.2009.5422142, 2009.

SMITH, W.O., DEMASTER, D.J. Phytoplankton biomass and productivity in the Amazon River plume: correlation with seasonal river discharge. **Continental Shelf Research**, 16, 291–319, 1996.

SONG, H., J. MARSHALL, D. R. MUNRO, S. DUTKIEWICZ, C. SWEENEY, D. J. MCGILLICUDDY, U. HAUSMANN. Mesoscale modulation of air-sea CO2 flux in Drake Passage, **Journal of Geophysical Research Oceans**, 121, 6635–6649, 2016.

STRASS, V. H., NAVEIRA-GARABATO, A. C., POLLARD, R. T., FISCHER, H., HENSE, I., READ, J. F., LEACH, H., SMETACEK, V. Mesoscale frontal dynamics: shaping the environment of primary production in the Antarctic Circumpolar Current. **Deep-Sea Research** Pt II 49, 3735–3769, 2002.

SWEENEY, C., GLOOR, E., JACOBSON, A.R., KEY, R.M., MCKINLEY, G., SARMIENTO, J.L., WANNINKHOF, R. Constraining global air-sea gas exchange for CO2 with recent bomb 14C measurements. **Global Biogeochemical Cycles** 21, doi: 10.1029/2006GB002784, 2007.

TAKAHASHI, T.; OLAFSSON, J.; GODDARD, J. G.; CHIPMAN, D. W.; SUTHERLAND, S. C. Seasonal variation of CO2 and nutrients in the high-latitude surface oceans: A

comparative study. **Global Biogeochemical Cycles**, v.7(4), p.843–878, doi:10.1029/93GB02263, 1993.

TANABE, A., CENEDESE, C. Laboratory experiments on mesoscale vortices colliding with an island chain. **Journal of Geophysical Research,** 113, C04022. https://doi.org/10.1029/2007JC004322, 2008.

TERNON, J.F., OUDOT, C., DESSIER, A., DIVERRES, D. A seasonal tropical sink for atmospheric $CO_2$ in the Atlantic Ocean: the role of the Amazon River discharge. **Marine Chemistry**, 68, 183–201, 2000.

TYAQUIÇÃ, P.; VELEDA, D.; LEFÈVRE, N.; ARAUJO, M.; NORIEGA, C.; CANIAUX, G.; SERVAIN, J.; SILVA, T. Amazon Plume Salinity Response to Ocean Teleconnections. **Frontiers in Marine Science**, v. 4, p. 1, 2017.

VELEDA, D.; MONTAGNE, R.; ARAUJO, M. Cross-wavelet bias corrected by normalizing scales. **Journal of Atmospheric and Oceanic Technology**, v. 29, n. 9, p. 1401–1408. DOI: 10.1175/JTECH-D-11-00140.1. 2012.

VERBRUGGE, N., MULET, S., GUINEHUT, S., BUONGIORNO-NARDELLI, B. ARMOR3D: A 3D multi-observations T, S, U, V product of the ocean, **Geophysical Research Abstracts**, 19, EGU2017-17579, EGU General Assembly, 2017.

VILLAS BÔAS, A. B., O. T. SATO, A. CHAIGNEAU, G. P. CASTELÃO. The signature of mesoscale eddies on the air-sea turbulent heat fluxes in the South Atlantic Ocean. **Geophysical Research Letters**, v.42, p.1856–1862, 2015.

WANG, Z.-F., SUN, L., QIU-YANG, L., CHEMG, H. Two typical merging events of oceanic mesoscale anticyclonic eddies. **Ocean Science**, 15, 1545–1559. https://doi.org/10.5194/os-15-1545-2019, 2019.

WANNINKHOF, R. Relationship between wind speed and gas exchange over the ocean revisited, **Limnol. Oceanography - Meth**., 12, 351–362, https://doi.org/10.4319/lom.2014.12.351, 2014.

WEISS, R. F. Carbon dioxide in water and seawater: the solubility of a non-ideal gas, **Mar. Chem**., 2, 203–215, https://doi.org/10.1016/0304-4203(74)90015-2, 1974.

WILLIAMS, R. G., FOLLOWS, M. J.: Physical transport of nutrients and the maintenance of biological production (Chapter 2), in: **Ocean Biogeochemistry**, Springer-Verlag, Berlin, edited by: Fasham, M. J. R., 19–51, 2003.

WILKS, D. S. **Statistical Methods in the Atmospheric Sciences.** Academic Press. p.467. 1995.

XU, G.; DONG, C.; LIU, Y., GAUBE, P., YANG, J. Chlorophyll Rings around Ocean Eddies in the North Pacific, **Scientific Reports**, 9, 2056, https://doi.org/10.1038/s41598-018-38457-8, 2019.

YI, J., DU, Y., HE, Z., ZHOU, C. Enhancing the accuracy of automatic eddy detection and the capability of recognizing the multi-core structures from maps of sea level anomaly. **Ocean Science**, 10, 39–47. https://doi.org/10.5194/os-10-39-2014, 2014.

ZHANG, W., XUE, H., CHAI, F. NI, Q. Dynamical processes within an anticyclonic eddy revealed from Argo floats. **Geophysical Research Letters** 42, 2342–2350, https://doi.org/10.1002/2015GL063120, 2015.

ZHARKOV, V., NOF, D. Why does the North Brazil Current regularly shed rings but the Brazil Current does not? **Journal of Physical Oceanography**, 40, 354–367. https://doi.org/10.1175/2009JPO4246.1, 2010.

# APÊNDICE A – ARTIGO PUBLICADO

Artigo gerado a partir do Capítulo 3 desta Dissertação. Foi publicado pelo *Journal of Geophysical Research: Oceans*, volume 125, edição 12, https://doi.org/10.1029/2019JC015921.

JGR Oceans

RESEARCH ARTICLE
10.1029/2019JC015921

**Key Points:**

- North Brazil Current (NBC) rings in boreal winter are larger, more energetic, faster rotating, and short living, in contrast with boreal summer and early fall
- Downwelling associated with NBC anticyclonic rings deepens thermocline and modify the vertical salinity profile
- NBC ring merging significantly increase NBC rings $V_{max}$ and kinetic energy

**Supporting Information:**

- Table S1
- Table S2
- Table S3
- Table S4
- Figure S1
- Figure S2
- Figure S3
- Figure S4

**Correspondence to:**
L. C. Aroucha,
leo.aroucha@ufpe.br

**Citation:**
Aroucha, L. C., Veleda, D., Lopes, F. S., Tyaquiçã, P., Lefèvre, N., & Araujo, M.. (2020). Intra- and inter-annual variability of North Brazil Current rings using angular momentum eddy detection and tracking algorithm: observations from 1993 to 2016. *Journal of Geophysical Research: Oceans*, *125*, e2019JC015921. https://doi.org/10.1029/2019JC015921

Received 26 NOV 2019
Accepted 24 OCT 2020



# Intra- and Inter-Annual Variability of North Brazil Current Rings Using Angular Momentum Eddy Detection and Tracking Algorithm: Observations From 1993 to 2016

**L. C. Aroucha[1,2,3], D. Veleda[1,2], F. S. Lopes[1,2], P. Tyaquiçã[4], N. Lefèvre[4], and M. Araujo[1,5]**

[1]Laboratory of Physical, Coastal and Estuarine Oceanography – LOFEC, Federal University of Pernambuco – UFPE, Recife, Brazil, [2]Renewable Energy Center – CER, Federal University of Pernambuco – UFPE, Recife, Brazil, [3]Now at Department of Oceanography - UFPE, Cidade Universitária, Recife, Brazil, [4]LOCEAN, IRD, Sorbonne Université Paris, Paris, France, [5]Center for Risk Analysis and Environmental Modeling – CEERMA, Federal University of Pernambuco – UFPE, Recife, Brazil

**Abstract** In order to investigate intra- and inter-annual variability of North Brazil Current (NBC) rings, angular momentum eddy detection and tracking algorithm (AMEDA) was used for identification of their occurrence, trajectories, and parameters. Based on 24 years (1993–2016) of geopotential height and geostrophic current fields reanalysis data from ARMOR 3D (¼°), we identified an average rate of five NBC rings shed by year. The rings present an average lifetime of 15.3 (±5.4) weeks, average speed-based radius ($R_{max}$) of 139.8 (±23.6) km, and mean sea surface height anomaly (SSHa) of 9.4 (±4.0) cm. The mean observed maximum azimuthal velocity ($V_{max}$) was 0.27 (±0.08) m/s, while the averaged Rossby number (Ro) value was 0.08 (±0.04) and averaged kinetic energy (KE) was of 255.3 (±154.8) $cm^2/s^2$. NBC rings have larger dimensions, rotate faster, live less, and transfer more energy in boreal winter months. In contrast, those shed during boreal summer and early fall last longer, have smaller diameters and carry less energy. Besides, the analysis of ring merging pointed that the interaction between NBC rings generated a significantly increase in ring energy (52%), and velocity (22%). Finally, we observed the vertical anomalies temperature and salinity profiles, which indicated a thermocline deepening and sinking of coastal and tropical waters due to NBC rings downwelling. This study emphasizes the robustness and efficiency of AMEDA for studying rings in the ocean and further theorizes possible impacts of NBC ring on ocean physical and biogeochemical features in the Western Tropical North Atlantic.

**Plain Language Summary** Oceanic rings are dynamical structures formed by strong current circulation, that are present in the sea like hurricanes are in the atmosphere. They can change seawater characteristics by changing the direction and velocity of ocean currents, and by carrying a parcel of water and its features (such as temperature, heat content, salinity, and nutrients) from one region to another in the ocean. Using 24 years of data, this study analyses the occurrence and characteristics of rings that originated from the North Brazil Current (NBC), in the Tropical Atlantic region. We examine how ring characteristics changed from year to year and from season to season. We use a computational algorithm that identifies and provides information about a ring based on the current direction and other physical parameters. We find that rings are larger, rotate faster, live less, and carry more energy in boreal winter months, while during boreal summer and early fall, they last longer, have smaller diameters, and carry less energy. Plus, the water flux downward associated with NBC eddies centers generates an increased in mixed layer and deepens the thermocline. Finally, we show that the when rings merge, they increase their energy and velocity.

## 1. Introduction

The North Brazil Current (NBC) is an intense western boundary current, which is the dominant feature of the surface circulation in the Western Tropical North Atlantic (WTNA). It flows predominantly northwestward along Brazilian northern coast and, around 6°N–8°N and 45°W, the current separates from the coast and retroflects to the east, feeding the North Equatorial Countercurrent (NECC; Garzoli et al., 2003; Johns

et al., 1990). This retroflection, which is related to the seasonal migration of the Intertropical Convergence Zone (ITCZ) (Fonseca et al., 2004), can occasionally shed large anticyclonic rings, that are associated with positive anomalies of sea surface height (SSH) in their centers, traveling northwestward until colliding with the Lesser Antilles (Didden & Schott, 1993; Fratantoni & Richardson, 2006; Jochumsen et al., 2010; Johns et al., 2003). The NBC retroflection is most developed between June and February and is nearly absent from March to May (Johns et al., 1998). However, other mechanisms, rather than the meandering current, were proposed to explain NBC rings generation. Ma (1996) and Jochum and Malanotte-Rizzoli (2003) showed that equatorial Rossby waves that propagate westward and reflect at the Brazilian coast could generate these eddies. Moreover, they intensify when traveling northwestward due to the conservation of the potential vorticity (Jochum & Malanotte-Rizzoli, 2003). The south American coastline inclination between 5°N and 8°N was shown to be important for ring generation (Zharkov & Nof, 2010). NBC rings are crucial in the interhemispheric transport of mass and heat in the Atlantic, being an essential part of the meridional overturning circulation (MOC) (Fratantoni et al., 2000; Johns et al., 2003). Furthermore, they contribute to the dispersion of fresh nutrient-rich waters from the Amazon River toward the Caribbean (Johns et al., 1990), also affecting local circulation, that influences planktonic fish larvae recruitment and growth (Cowen et al., 2003). Given the importance of those rings, their study and record of their parameters are a key to the comprehension of physical and biogeochemical processes in the WTNA.

The first study that described the presence of the NBC rings was done by Legeckis and Gordon (1982). They used satellite sea surface temperature (SST) data to identify elliptical warm-core rings that move northwestward with velocities from 4 to 35 km/day (Legeckis & Gordon, 1982). In the following years, a number of studies contributed to the understanding of NBC rings dimensions and dynamics (Didden & Schott, 1993; Fratantoni et al., 1995; Johns et al., 1990; Pauluhn & Chao, 1999; Richardson et al., 1994), especially after the 1998–2001 NBC Ring Experiment (Fratantoni & Glickson, 2002; Garraffo et al., 2003; Garzoli et al., 2003; Goni & Johns, 2001, 2003; Johns et al., 2003). Those rings present typically a mean radius of 200 km, SSH anomaly of 30 cm, surface and subsurface azimuthal velocity of 1 m/s and 15–20 cm/s, respectively, and can reach over 1,000 m deep (Didden & Schott, 1993; Fratantoni et al., 1995; Fratantoni & Glickson, 2002; Fratantoni & Richardson, 2006; Garraffo et al., 2003; Goni & Johns, 2003; Jochumsen et al., 2010; Johns et al., 2003; Pauluhn & Chao, 1999). NBC rings travel with an average propagation speed of 8–15 km/day toward the Caribbean, for 3–4 months, until interacting with the Antilles, where they start to coalesce (Didden & Schott, 1993; Fratantoni et al., 1995; Fratantoni & Glickson, 2002; Fratantoni & Richardson, 2006; Garzoli et al., 2003; Johns et al., 1990; Richardson et al., 1994). It is estimated that on average 3–7 rings are detached from NBC per year (Fratantoni et al., 1995; Fratantoni & Glickson, 2002; Fratantoni & Richardson, 2006; Garzoli et al., 2003; Jochumsen et al., 2010; Johns et al., 1990; Mélice & Arnault, 2017), yet some works indicated a rate of 8–9 rings/year (Garraffo et al., 2003; Johns et al., 2003). Although a lot is known about NBC rings dynamics, only few works performed a long-term study (Jochumsen et al., 2010; Mélice & Arnault, 2017; Sharma et al., 2009). Moreover, it is crucial to establish and understand the change of ring parameters and how they evolve through seasons and years to evaluate, for example, if there is a seasonal or year-to-year variation that could indicate periods of higher intensity, energy, or SSH anomaly.

Several methodologies were used to efficiently identify eddies and determine their centers and parameters. Initially, methodologies were based either on the geometric velocity fields of geostrophic currents or in altimetry maps of sea surface. Posteriorly, the methods started to be based on dynamical parameters. McWilliams (1990) was one of the firsts to use relative vorticity for eddy identification. This method was improved over the use of wavelet analysis on the vorticity field (Doglioli et al., 2007). Other parameter widely used was the Okubo-Weiss (OW), which quantifies the importance of rotation in relation to strain through geostrophic current data (Chaigneau et al., 2008). On the other hand, other works utilized only the geometry of the geostrophic velocity field for eddy identification, assuming these structures as coherent vortex if characterized by closed contour current lines (Nencioli et al., 2010; Sadarjoen & Post, 2000). More recently, hybrid methodologies which consider both geometric and physical aspects (i.e., OW parameter) of eddies began to stand out (Halo et al., 2014; Yi et al. 2014). Mkhinini et al. (2014) introduced the local normalized angular momentum (LNAM), a new dynamical parameter for eddy detection, which represents the normalized value of the angular momentum in a restricted area. This value will reach its extremum in the center of a solid core rotation (LNAM = +1 for cyclonic eddies and LNAM = −1 for anticyclonic). Currently, hybrid algorithms have become even more effective with the possibility of identification of eddy interaction

through merging and splitting events (Le Vu et al., 2018; Li et al., 2014). Therefore, the improvement on the methodologies used for eddy identification and tracking allows the characterization of the main dynamical parameters of these structures, such as: maximum azimuthal velocity ($V_{max}$), speed-based radius ($R_{max}$), and Rossby number (Ro), apart from the events of eddy interaction.

The angular momentum eddy detection and tracking algorithm (AMEDA) (Le Vu et al., 2018), will be used in this study for the identification of NBC rings occurrence, trajectories, and physical parameters. The main goal of this work is to apply the AMEDA, using SSH and geostrophic currents field data, in order to investigate the intra- and inter-annual variability of NBC rings occurrence and parameters. Also, an event of rings merging will be detailed in terms of parameters change, and identified trajectories will be commented. The significance of studying eddy merging and splitting events relies on the fact that these events are able to change eddy characteristics. Indeed, ring interaction can alter significantly eddy size, energy, and SSH signal, and the main cause of their occurrence are current-eddy-topography interactions and current variation (Cui et al., 2019). Furthermore, the study goes through the previously results observed in published articles on NBC rings, for comparison with this AMEDA analysis. The study is organized as follows: in Section 2 the database and the study area are explored. The application of the data to AMEDA is described and the parameters measured are defined. In Section 3 we highlight the inter- and intra-annual variability of NBC rings, emphasizing how changes are observed in terms of their parameters. We also describe how vertical temperature and salinity profile change within eddies, and analyze the 4 observed merging events between two NBC rings with tracking identified by AMEDA. Finally, our results are compared with previous studies. Conclusion is presented in Section 4.

## 2. Data and Methods

### 2.1. Database and Study Area

The data set used in this study consists of 24 years (January/1993–December/2016) of absolute SSH (i.e., geopotential height) and the components of the geostrophic current fields taken from "Global Observed Ocean Physics Temperature Salinity Heights and Currents Reprocessing"—ARMOR 3D, with ¼° spatial resolution (e.g., Guinehut et al., 2012; Mulet et al., 2012; Buongiorno Nardelli et al., 2016). This database results from the combination of sea level anomaly (SLA), SST, and sea surface salinity (SSS) data and in situ T, S vertical profiles measurements, presenting a global 3D weekly temperature, salinity, geostrophic velocities fields (Verbrugge et al., 2017). ARMOR 3D is available at Copernicus Marine Environment Monitoring Service (CMEMS) web portal (http://marine.copernicus.eu/services-portfolio/accessto-products/, product id: MULTIOBS_GLO_PHY_REP_015_002) with the newest Version 4, updated in April 2018. The product used here was the Version 3 (product id: GLOBAL_REP_PHYS_001_021). The domain of this work is restricted to the region 15°N–5°S, 63°W–45°W, which includes NBC retroflection area (ring generation), Amazon and Orinoco Rivers mouths, and the Lesser Antilles (ring demise). Indeed, NBC rings seems also to interact with Amazon and Orinoco waters (Ffield, 2005; Rudzin et al., 2017). In addition, radiating Rossby waves from the east also reach this region, influencing ring dynamics (Fratantoni & Richardson, 2006; Jochum & Malanotte-Rizzoli, 2003). We used data from 50 m deep, in order to reduce the surface signal of equatorial Rossby waves and also as an attempt to identify subsurface rings with a negligible surface signal. Finally, sea surface height anomaly (SSHa) were calculated based on the 24 years data. Taking the anomalies can filter the seasonal signal, that dominates the tropical Atlantic Ocean (Arnault & Cheney, 1994), allowing a better analysis of intra-annual variability.

### 2.2. Detection Algorithm and Measured Parameters

The AMEDA (Le Vu et al., 2018) was used. It is a hybrid algorithm, based not only on dynamical parameters, but also on geometrical properties of the velocity field. In AMEDA, while the extremum LNAM (dynamical) indicates eddy centers, the closed streamlines (geometrical) indicates eddies boundaries, characterizing a structure as an eddy only if the grid point corresponds for both constraints (Le Vu et al., 2018). For eddy tracking, the algorithm uses the local nearest neighbor (LNN) method (Le Vu et al., 2018) and it also has the capacity to identify merging and splitting events. AMEDA has been used in a few works in the last years. Ioannou et al. (2017) applied this algorithm for the study of Ierapetra Eddies on the Mediterranean Sea, while Garreau et al. (2018) used the tool for tracking an anticyclonic eddy in the Algerian Basin.

The geostrophic velocities from ARMOR 3D were applied to AMEDA for ring identification, tracking, interaction with neighboring eddies, and for computation of their parameters. The first baroclinic Rossby radius of deformation ($R_d$) was calculated for each grid point, based on Chelton et al. (1998). This radius is defined as the length scale of geostrophic stretching, and at the equator $R_d$ values are typically in scales of hundreds kilometers (Chelton et al., 1998; Nurser & Bacon, 2014). Although a ¼° data set grid was used, the combination with the calculated $R_d$ values is expected to be enough for normal functioning of AMEDA, since it is a robust algorithm for different space–time resolutions, and with tuneable parameters (Le Vu et al., 2018). Only the NBC rings that were clearly detached from the NBC retroflection and that crossed 55°W were taken into account in this analysis. Moreover, we maintained the default AMEDA configuration of excluding the eddies between the 5°N and 5°S equatorial band, since the NBC retroflection and rings trajectory are still further north. For each week of a ring occurrence, several parameters were measured. These parameters constantly varied from week to week and from ring to ring. Therefore, the week of maximum SSHa was chosen to be the representative for the rings. The parameters analyzed were: lifetime (weeks), $R_{max}$ (km), $V_{max}$ (m/s), Ro, KE ($cm^2/s^2$), and SSHa (in cm). Ring lifetime corresponds to the number of weeks that the ring was identified by AMEDA. $R_{max}$ (in kilometers) indicates the radius of the closed streamlines corresponding to the module of the maximum azimuthal velocity ($V_{max}$, in m/s). Ro is the dimensionless Rossby number defined as: $Ro = V_{max}/(f\,R_{max})$, where $f$ is the Coriolis parameter at ring latitude. Ring kinetic energy (KE) is calculated from the geostrophic velocity field, is defined as $KE = (u^2 + v^2)/2$, and represents the mean KE for all the grid points within each ring. Finally, as previously cited, SSH anomalies were taken based on the 24 years data, providing the SSHa parameter.

## 3. Results and Discussion

### 3.1. Observed Variability of NBC Rings Shedding Rates

It is important to initially highlight that this is the first study to apply an eddy detection algorithm for 24 years period in the NBC region. Although other works have also analyzed decadal time-series in NBC rings generation (Jochumsen et al, 2010; Mélice & Arnault, 2017), they did not used an eddy identification tool based on dynamical and geometrical constraints, identifying the NBC rings only by statistical analysis of sea level anomalies (Mélice & Arnault, 2017), or based on velocity fields of the modeled data (Jochumsen et al., 2010). In the analyzed 24 years period, 121 NBC rings were observed to detach from the NBC retroflection and cross the 55°W longitude line. It provides an average shedding rate of five rings per year. The results for each year are presented in Figure 1a. Overall, previous studies estimate a rate from 2 to 9 rings per year, which varies according to the period covered and the method used by the study (e.g., Didden & Schott, 1993; Garzoli et al., 2003; Jochumsen et al., 2010; Johns et al., 1990, 2003; Mélice & Arnault, 2017; Sharma et al., 2009). The comparison with other works, allow us to say that AMEDA results are reasonable. In fact, the ring shedding rate here obtained varied from a maximum of eight rings/year in 2005 to a minimum of three rings/year in 2006 (Figure 1a). However, the present study underestimated the average shedding rate when comparing with few others which pointed for a 7–9 rings/year average (Johns et al., 2003; Jochumsen et al., 2010). This fact is thought to be mainly due to the presence of subsurface NBC rings, which present the maximum velocity signal at 200 m and no apparent surface signal (Garraffo et al., 2003). Because the present work used only 50 m depth velocity fields data, possibly some subsurface NBC rings were not identified by AMEDA. Furthermore, Goni and Johns (2001), using altimeter data, identified 34 anticyclonic eddies from October 1992 to December 1998. In this study, which started to count from 1993, 29 NBC rings were identified from 1993 to 1998. In addition, 18 NBC rings were observed using ocean color imagery from September 1997 to September 2000 (Fratantoni & Glickson, 2002), while we identified 16 NBC rings in the same period. Using in situ data from moorings and ship cruises, the NBC Rings Experiment (Garzoli et al., 2003; Goni & Johns, 2003; Johns et al., 2003) found one ring in November/December 1998, two rings from February/March 1999, and one ring in June/2000. In the present work, we identified the presence of all of these rings in the periods cited. The generation dates and parameters of all the 121 identified rings in this study are summarized in Supporting Information (Table S1). More recently, some works preceded in longer time series for NBC ring identification. Sharma et al. (2009) using drifting buoys, ADCP and satellite data identified 44 NBC rings in 8 years, with maximum shedding rates in 2005 and 2007, what is consistent with what was found in this study. Jochumsen et al. (2010) analyzed from the FLAME

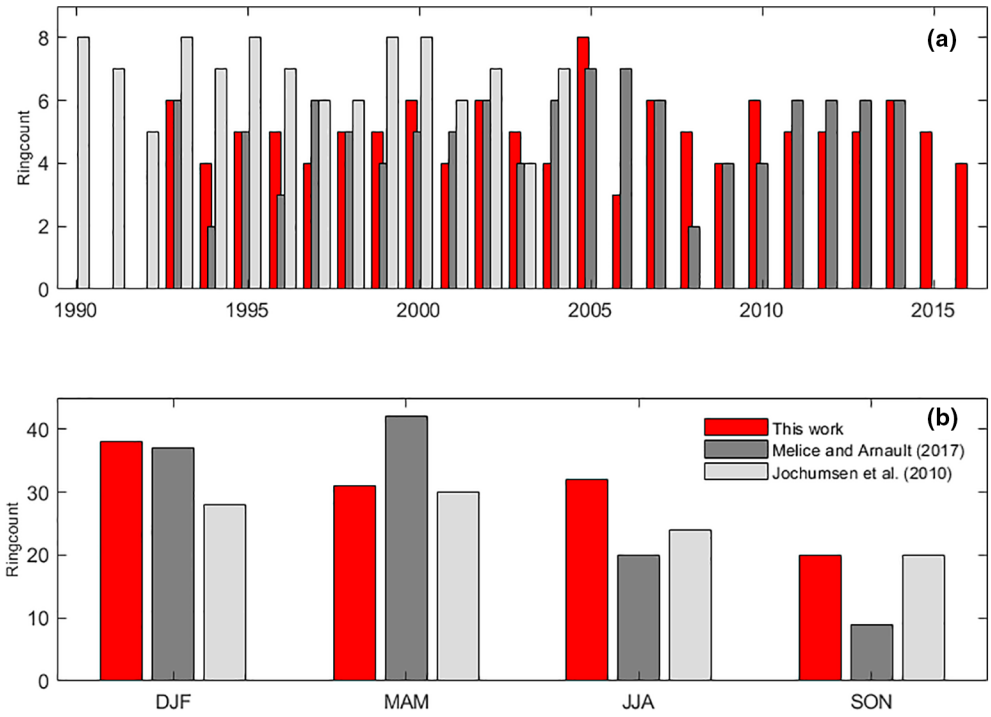


**Figure 1.** (a) Number of North Brazil Current (NBC) rings which crossed 55°W observed per year. (b) NBC rings seasonal climatology generated for 24 years period. Both (a) and (b) compare our results with Mélice and Arnault (2017) and Jochumsen et al. (2010).

model all the NBC ring types generation in 15 years, indicating a shedding rate ranging from 4 to 8 rings/year. In addition, the recent study from Mélice and Arnault (2017), using satellite altimeter and empirical mode decomposition, presented a mean rate of five rings generated by year, similar to the present study. Finally, although previous studies demonstrate some differences in the inter-annual ring generation rates, the similarities observed between them and the present work indicate AMEDA algorithm robustness and efficiency for ring surveillance, since it identified the presence of NBC rings quite similarly to other studies using different methods. It is thought that when applying current velocity data from greater depths rather than only surface fields, the algorithm will also be able to recognize rings of larger subsurface signal.

Moreover, it is possible to notice a considerable year-to-year variability in NBC ring generation. This rate remained between 4 and 6 rings/year, (Figure 1a), in exception from 2005 to 2006, where the maximum and minimum ring frequency, respectively, was observed. Sharma et al. (2009) theorized a biannual pattern in NBC ring generation rates, where alternate years present a gap in ring formation during late spring and early summer. Therefore, it seems that the maximum number of NBC rings generated in 2005 was compensated by the lower generation rate in the following year. The year 2005 has maximum shedding rates and appears to be followed by a steady cycle of ring formation and migration (Sharma et al., 2009). It is still not clear which mechanisms drive this inter-annual variability on NBC ring generation. However, few works have pointed possible reasons for it, such as: penetration latitude (i.e., distance between the northernmost point of the retroflection and the arbitrary location of 0°S, 42°W) of NBC retroflection (Garzoli et al., 2003) and the influence of large-scale transport processes in Atlantic Basin (Goni & Johns, 2003). Garzoli et al. (2003) indicated that almost every time NBC retroflection reaches its northernmost position, a ring is detached, although no clear seasonality is observed in NBC latitude of penetration. In addition, Goni and Johns (2003) speculated at least a weak relationship between ring generation and Northern Tropical Atlantic Index, based on possible links between ocean temperature variation and NBC rings shedding rate. Lastly, Sharma et al. (2009) indicated that ITCZ and forcing by trade winds are not the main factors influencing ring formation and migration. It is believed that several mechanisms might impact NBC rings generation, and further studies could highlight these relationships.

The results obtained for the ring generation as a function of the season are described in Figure 1b. We show that rings are formed in all months of the year, with a maximum ring generation in February, followed by March, June, and July. The minimum generation rate, in its turn, was observed in September-October-November trimester (SON) (Figure 1b). Those results agree with what was found in the literature, using different methods. Fratantoni et al. (1995) compared the modeled rings with observations from Richardson et al. (1994). They showed a maximum generation period from October to March, with the highest observation ring frequency in November and February, and the maximum modeled frequency in February, April, and May. Goni and Johns (2001) presented December and January as the months of greatest ring liberation. However, they have in 2003 pointed for different months as maximum (i.e., February and June) (Goni & Johns, 2003), which the latter agrees most with the current paper. Those previously cited works (Frantantoni et al., 1995; Goni & Johns, 2001, 2003) presented minimum generation rate from July to October, which is in agreement with the smaller generation in August and September observed in the present study. October 2016 was the only month in the analyzed period, which was characterized by more than one ring shed (Table S1).

The NBC ring maximum generation occurred from December to February (Figure 1b), while a minimum was observed from September to November. The December-January-February (DJF) trimester was responsible for 31.40% of NBC rings genesis in the 24 years, while 25.62% and 26.45% of rings were shed for March-April-May (MAM) and June-July-August (JJA) trimesters, respectively. It was verified a 47.37% reduction in ring generation rate between maxima (winter) and minima (fall) trimesters. Goni and Johns (2001) presented similar results using TOPEX altimetry data, with a maximum generation in boreal winter (DJF) and minimum in early boreal fall (SON), although from September to November the generation rate is quite the same as the previous months (MAM and JJA). On the other hand, Fratantoni and Glickson (2002) showed that the higher frequency of generation occurs from March to May, with equivalent frequency in the other trimesters. Also, Jochumsen et al. (2010) and Mélice and Arnault (2017) presented similar results on the number of rings generated per trimester, with the highest frequencies at spring (MAM) and minimum at fall (SON). According to Fratantoni and Glickson (2002), no particular seasonality is detected in NBC ring generation and that the observed variations in the results of those studies are most likely to be due to different methodologies. Seasonality appears to be evident but inconsistent between successive years (Sharma et al., 2009). Therefore, from the present and previous studies, it is possible to clearly identify the trimester of the minimum generation rates, which evolves the months of September, October, and November, and that NBC rings appear to be more frequent in the first half of the year.

### 3.2. NBC Rings Parameters

Figure S1 indicates the frequency distribution of the parameters for each identified ring. Those parameters were obtained at the time step corresponding to the week of maximum SSHa. The parameters of all the 121 identified rings in this study are summarized in Table S1. The NBC rings presented an average lifetime of 15.3 (±5.4) weeks, with the higher frequency of lifetimes between 10 and 18 weeks (Figure S1a). The last identified rings in October 2016 (i.e., R120 and R121) were not considered as they were not entirely vanished by the end of 2016, so their lifetime could not be determined. The maximum ring duration was 31 weeks, and the minimum, 4 weeks. These results are in agreement with previous studies (Goni & Johns, 2001; Richardson et al., 1994). Indeed, Goni and Johns (2003) verified through satellite altimetry that NBC rings remain an average of 3.5 months in the region, with this time ranging from 2 to 5 months. Besides, Fratantoni and Richardson (2006), using floats and drifters, pointed for a lifetime ranging from 1 to 6 months, with an average of 3.3 months. The importance of ring lifetime relies on how long the vortex dynamics is able to trap the parcel of water within it. The length scale of the ring, $R_{max}$ ranged from a minimum of 87.3 km to a maximum of 204.8 km, with an average radius of 139.5 (±23.6) km. NBC rings were more frequent with $R_{max}$ ranging from 120 to 160 km (Figure S1b). In general, other works on NBC rings indicate a similar length scale, with diameters varying from 150 to 400 km (Castelão & Johns, 2011; Didden & Schott, 1993; Fratantoni et al., 1995; Fratantoni & Glickson, 2002; Fratantoni & Richardson, 2006; Goni & Johns, 2003; Jochumsen et al., 2010; Richardson et al., 1994). These length scales of hundreds of kilometers imply a considerable water mass transport along the northern Brazilian coast. It is estimated that an annual transport of 9.3 Sv by NBC rings, which represents an essential part of the MOC return flow (Johns et al., 2003). A mean SSHa of 9.4 (±4.0) cm was detected with a maximum value of 24.0 cm. The higher frequency observed was

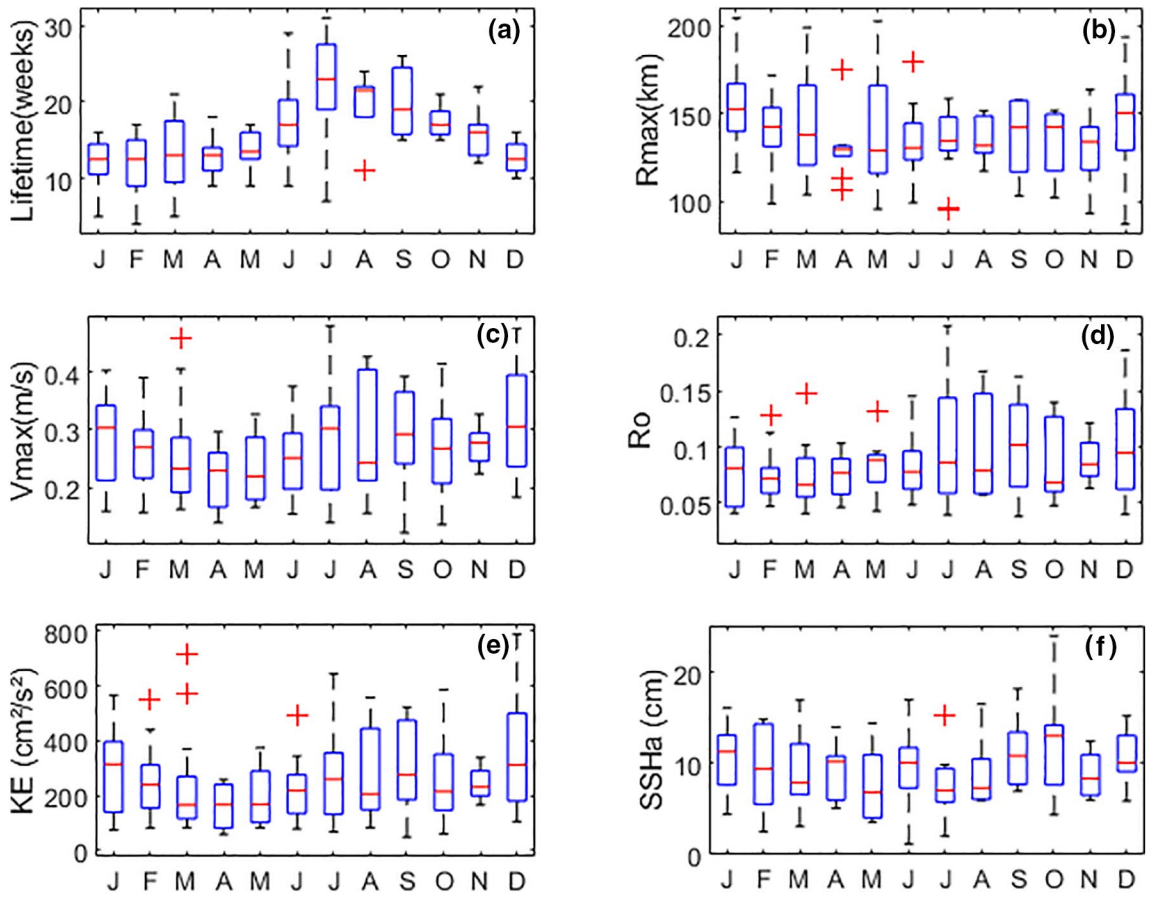


**Figure 2.** Monthly variation of the measured North Brazil Current rings parameter during the 24 years analysis: Ring lifetime (a), $R_{max}$ (b), $V_{max}$ (c), Rossby number (d), Kinetic Energy (e), SSH anomaly (f). The central red mark is the median, the edges of the box are the 25th and 75th percentiles, the whiskers extend to the most extreme datapoints, and individual red crosses are outliers.

around 5–15 cm of SSHa (Figure S1f). Those results are consistent with those found in the literature. Didden and Schott (1993) found a 4 cm SSH variability associated with NBC rings, while Goni and Johns (2001) presented an average SSH residue of 8 cm. More recently, maximum surface elevation related to NBC rings was pointed to range around 20–30 cm (Castelão & Johns, 2011; Cruz-Gómez & Salcedo-Castro, 2013). Moreover, the lowest observed value for SSHa was 1.1 cm, which might indicate that this study could also identify NBC rings with small surface signal, such as subsurface rings. However, to trustworthily classify NBC rings it is necessary to have a vertical picture of its dynamics, including thermocline and maximum velocity depths. Then, since the present work is based only on SSHa values and a 1-level velocity database, NBC ring classification goes beyond the scope of this study.

The frequency of the maximum azimuthal velocity values ($V_{max}$) computed from the NBC rings indicate a higher occurrence of rotational velocities from 20 to 30 cm/s (Figure 2c). The mean $V_{max}$ is 0.27 (±0.08) m/s, while the maximum and minimum are 0.48 m/s and 0.12 m/s, respectively. Previous works indicate that NBC rings swirl velocity vary from 12 to 84 cm/s (Fratantoni et al., 1995; Fratantoni & Richardson, 2006; Richardson et al., 1994). However, more recent studies established that $V_{max}$ could be even higher than 115 cm/s (Castelão & Johns, 2011; Cruz-Gómez & Salcedo-Castro, 2013). The reduced $V_{max}$ found in this study might be explained by several reasons. First, the week of maximum SSHa does not necessarily correspond to the time step of maximum $V_{max}$ . Then, it is possible that the values of $V_{max}$ are not the maximum rotational velocities that a ring reached during its lifetime. In addition to this, when using geostrophic velocities fields and assuming geostrophic balance within an eddy, its azimuthal velocity might be underestimated due to the negligence of inertial components of momentum balance (Douglass & Richman, 2015). Hence, $V_{max}$ values seemed to be underestimated in the present study. In addition to this, it is believed that

the cyclogeostrophic force terms are important in disrupting eddy characterization from geostrophy in eddies with Ro > 0.3 (Douglass & Richman, 2015). It seems from the literature that NBC rings Ros are on the threshold of these values, in a way that only geostrophy might not characterize NBC rings perfectly. Moreover, Iouannou et al. (2019) indicated the need of ageostrophic corrections for mesoscale anticyclones which exceeds Ro > 0.15. Hence, aiming to quantify the amplitude of the ageostrophic velocity component, we performed velocity corrections for NBC rings with Ro equals or exceeding 0.15, based on the methodology of Ioannou et al. (2017). Results for velocity profiles corrections and percentual increase in $V_{max}$ for each of the eight analyzed rings are indicated in Figure S2 and Table S2, respectively. We verified a 30.0% average increase in cyclogeostrophic $V_{max}$ for those rings. Plus, the Pearson correlation index between Ro and $V_{max}$ increases for each ring ($p = 0.929$), showing the proportional increase in cyclogeostrophic $V_{max}$ in relation to a larger Ro, as expected and indicated by Ioannou et al. (2019). Although in this study only a few rings exceed Ro > 0.15, it is clear that ageostrophic corrections for rings with large Ro are indeed not negligible for reliable $V_{max}$ estimation.

Ro compares the importance of relative to planetary vorticity, and their values are variable around the globe. The high Ro values observed for the NBC rings region are due to the proximity of equator, an area of minimal Coriolis parameter. In this study, NBC rings presented an average Ro of 0.08 (±0.04) (Figure S1d), and maximum and minimum values of 0.21 and 0.04, respectively. Overall, it is expected that Ro values for anticyclones are negative. Yet, as we used the module of $V_{max}$ to measure Ro, only positive values were found. AMEDA has already been used for Ro computation (de Marez et al., 2020; Garreau et al., 2018). The definition of Ro in the present work is the vortex Ro, which is based on maximal azimuthal velocity, and was also used by Fratantoni et al. (1995) and Castelão and Johns (2011). However, we highlight that various definitions of Ro exists and were applied for the NBC rings. Richardson et al (1994) and Cruz-Gómez and Salcedo-Castro (2013) defined Ro based on the core angular velocity (Ro(2) = $\Omega_0$/f, $\Omega_0 = V(R)/R$ when $R \quad 0$). For a Gaussian vortex, $V(r) = V_{max}/R_{max}\ r\ e\text{^}((1 - r^2/[R_{max2}]/2)$, we get Ro(2) = 1.64*Ro. From the Ro definition, studies observed values between 0.13 and 0.26 (Fratantoni et al., 1995), and mean absolute Ro of 0.33 for the NBC region (Castelão & Johns, 2011). From Ro(2) values shifted from 0.20 to 0.36 (Richardson et al., 1994; Cruz-Gómez & Salcedo-Castro, 2013). Even though the 1.64 factor from Ro(2) to Ro, the values here obtained for Ro were still smaller than the ones cited in the literature using both definitions. As occurred for $V_{max}$, the use of purely geostrophic fields generated this underestimation. Douglass and Richman (2015) using the core vorticity Ro definition (Ro(3) = ζ0/f, for a Gaussian vortex Ro(3) = 3.3*Ro) indicated that ageostrophic corrections in $V_{max}$ are needed for vortex Ro > 0.09. Here, we performed these corrections only for rings with Ro > 0.15, as previously cited (Figure S2 and Table S2), based on Ioannou et al. (2019). Table S2 also indicated the corrected cyclogeostrophic Ro for the eight analyzed rings.

Finally, the NBC rings KE in the present study varied from a minimum of 49.53 $cm^2/s^2$ to a maximum of 789.93 $cm^2/s^2$, with the highest frequency of rings with KE around 100–300 $cm^2/s^2$ (Figure S2e). The average kinetic energy observed was 255.30 (±154.81) $cm^2/s^2$. These results are in agreement with Didden and Schott (1993), who presented similar geostrophic NBC rings KE, changing from 100 to 300 $cm^2/s^2$. The increased standard deviation represents significant changes in rings KE, indicating that rings shed by the NBC present diverse dynamical characteristics from ring to ring.

In order to investigate the seasonal variation of NBC rings characteristics, the variability of their parameters is plotted as a function of the month for the 24 years (Figure 2). All months were characterized, at least in one year, by a NBC ring formation. NBC rings last less in boreal winter and have an increased lifetime in boreal summer, especially from July to August (Figure 2a). Although boreal summer months presented higher variability from minimum to maximum values, the median lifetime for these months is still higher than the others. On the other hand, $R_{max}$ median values are increased in boreal winter (Figure 2b), even though a weak seasonal variability is observed. Sharma et al. (2009) also found low seasonal amplitude in NBC rings dimensions, with increased rings from October to March. Also, Ro and SSHa values did not present any clear seasonal variability (Figures 2d and 2f). In contrast, $V_{max}$ and KE show the highest median values in boreal winter months (Figures 2c and 2e). $V_{max}$ slightly increases in boreal summer, reaching a maximum in July. Similar behavior can be observed for KE. Didden and Schott (1993) associated KE changes in the NBC rings region with ring activity and the seasonal retroflection circulation, which, respectively, generated KE peaks in winter and a secondary summer maximum. More KE is available within NBC retroflection

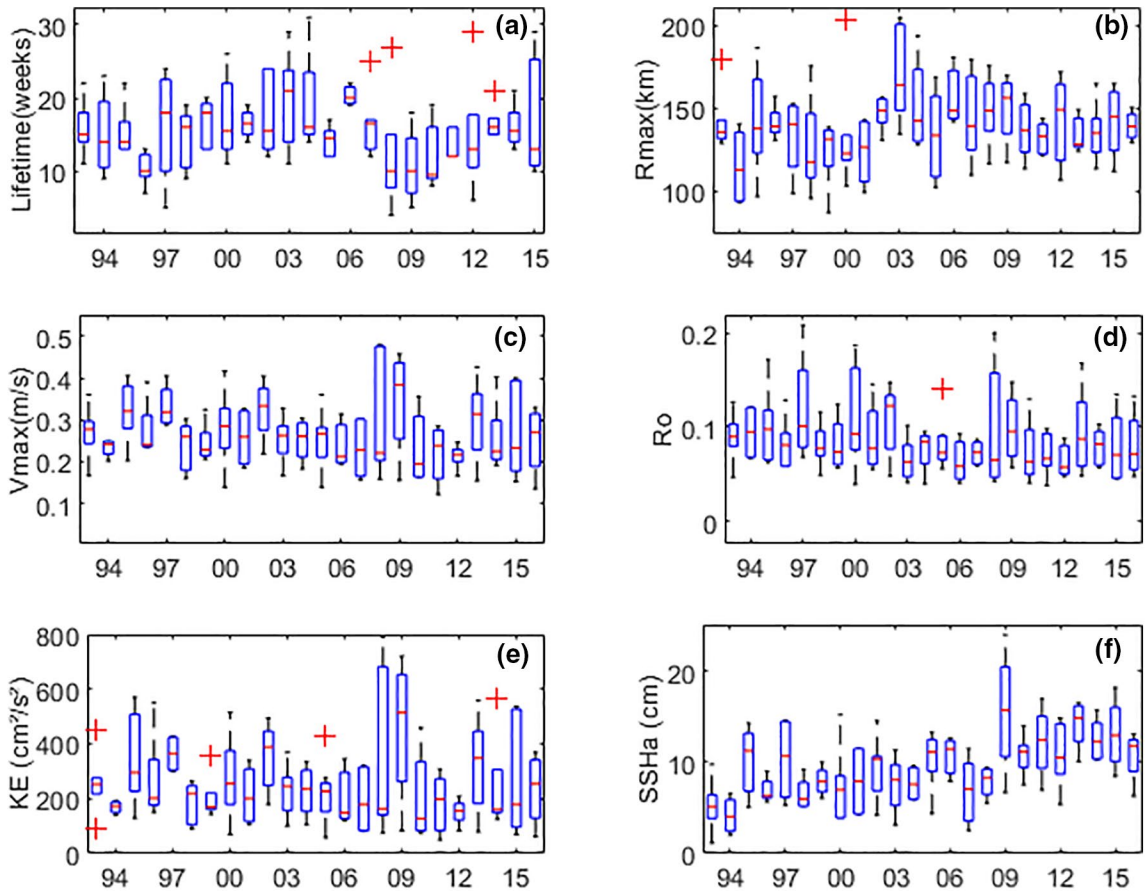


**Figure 3.** Year to year variability of the measured North Brazil Current rings parameters from 1994 to 2016. In exception, panel (a) only until 2015. Ring lifetime (a), $R_{max}$ (b), $V_{max}$ (c), Rossby number (d), Kinetic Energy (e), SSH anomaly (f). The central red mark is the median, the edges of the box are the 25th and 75th percentiles, the whiskers extend to the most extreme datapoints, and individual red crosses are outliers.

(Sharma et al., 2009). Therefore, $V_{max}$ and KE follow NBC retroflection seasonality. The maximum strength of NBC retroflection in boreal summer (Richardson & Walsh, 1986) is verified in Figure 2c, while the maxima KE values are likely to be related to the beginning of NBC retroflection weakening in January (Lumpkin & Garzoli, 2005). The importance of studying such variability of parameters relies on the estimation of ring volume and energy within a ring, for example. Rings with larger dimensions are capable of wrapping a larger volume of water, while its lifetime indicates eddy capacity in maintaining that wrapped piece of water. At the same time, estimation on KE variation might indicate a seasonal energy transport within NBC rings. In general, NBC rings seem to have larger dimensions and rotate faster during boreal winter months, carrying more KE within them. This energy, however, is likely to dissipate more quickly, since, in boreal winter, NBC rings presented shorter lifetimes. On the other hand, NBC rings shed during summer, and early boreal fall appears to last longer, to have smaller diameters, and carry less energy.

The characteristics of the rings are plotted as a function of year to identify inter-annual variability (Figure 3). Ring lifetime is reduced in the last decade (Figure 3a). Very high values of lifetime are detected as outliers for some years (2007, 2008, 2012, and 2013). The highest ring dimension is in 2003, followed by 2006 and 2009 (Figure 3b). Sharma et al. (2009) pointed 2006 as the year with an average ring size larger than other years. The highest median rotational velocity was observed in 2009 (Figure 3c), following the year of maximum $V_{max}$ variation (i.e., 2008). Year 2009 was also the year of maximum KE and mainly SSHa (Figures 3e and 3f). We calculated an annual climatological anomaly for the 24 years and observed that 2009 presented the most significant anomaly of $V_{max}$, KE, and SSHa (Figure 4). Foltz et al. (2012) identified an anomalous SST cooling in the Equatorial North Atlantic band (2°N–12°N) in 2009 and SST warming in the Equatorial South Atlantic (5°S–0°N) which produced a shift in wind direction, changed the ITCZ posi-

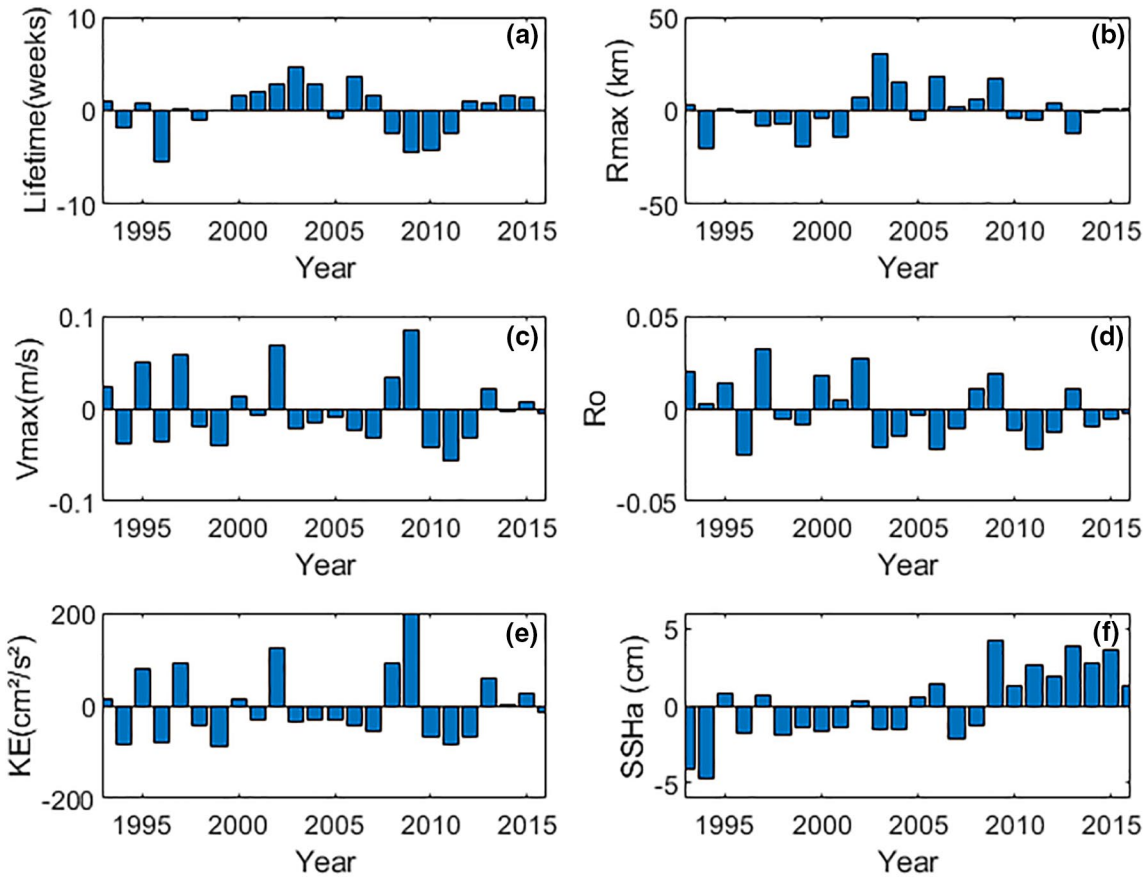


**Figure 4.** Averaged climatological anomaly of North Brazil Current ring parameters for each year during the 24 years analyzed: Ring lifetime (a), $R_{max}$ (b), $V_{max}$ (c), Rossby number (d), Kinetic Energy (e), SSH anomaly (f).

tion and the rainfall rates over the region. Moreover, Tyaquiçã et al. (2017) indicated an increased Amazon River discharge in 2009. These events might have altered current dynamics in this region, contributing to change NBC ring parameters in this year. We verified from filtered monthly anomalies of salinity and of zonal(u)-component of NBC in a longitudinal cut at 53°W, 3°N–7°N, from surface to 500 m deep, that 2009 year indeed presented an NBC intensity anomalous increase (Figure 5). This increase is indicated by a higher negative anomaly in the zonal component of NBC, and accompanied by salinity anomalies decease in the same year, showing a higher influence of Amazon plume in this year. Additionally, data for the 24 years of monthly Amazon discharge values recorded at the Óbidos Gauging Station, available from the Environmental Research Observatory– Geodynamical, hydrological, and biogeochemical control of erosion/alteration and material transport in the Amazon basin (ORE–HYBAM: http://www.ore-hybam.org), were used to estimate Amazon discharge inter-annual anomalies (Figure 5). From Amazon discharge is clear the positive anomaly during the entire 2009 year. An increased Amazon river runoff can contribute to NBC and its rings intensity by diminishing density through the influence of freshwater, generating an increase in current velocity. Moreover, Amazon river discharge could contribute to the increase in local vorticity, favoring rings intensity. Overall, it is believed that the combination of both increased NBC intensity and Amazon river runoff contributed for the 2009 intensity change in NBC rings dynamics. Another considerable pattern observed from 2009 is the positive trend in SSHa anomalies (Figure 4f). This indicates that SSHa within NBC rings is increasing in the last years. This could be related to changes in ocean circulation during the last decades. NBC rings are very dynamic and variable, being subject to several oceanographic and atmospheric forcings that affect their characteristics. Therefore, a strong inter-annual variability of their parameters is expected. In addition, we attempted to correlate Atlantic climate indexes with NBC parameter anomalies. The highest observed correlation was 0.34 between SSHa and Atlantic multidecadal oscillation (AMO). Although it seems a weak correlation, the analyzed period covered only the positive

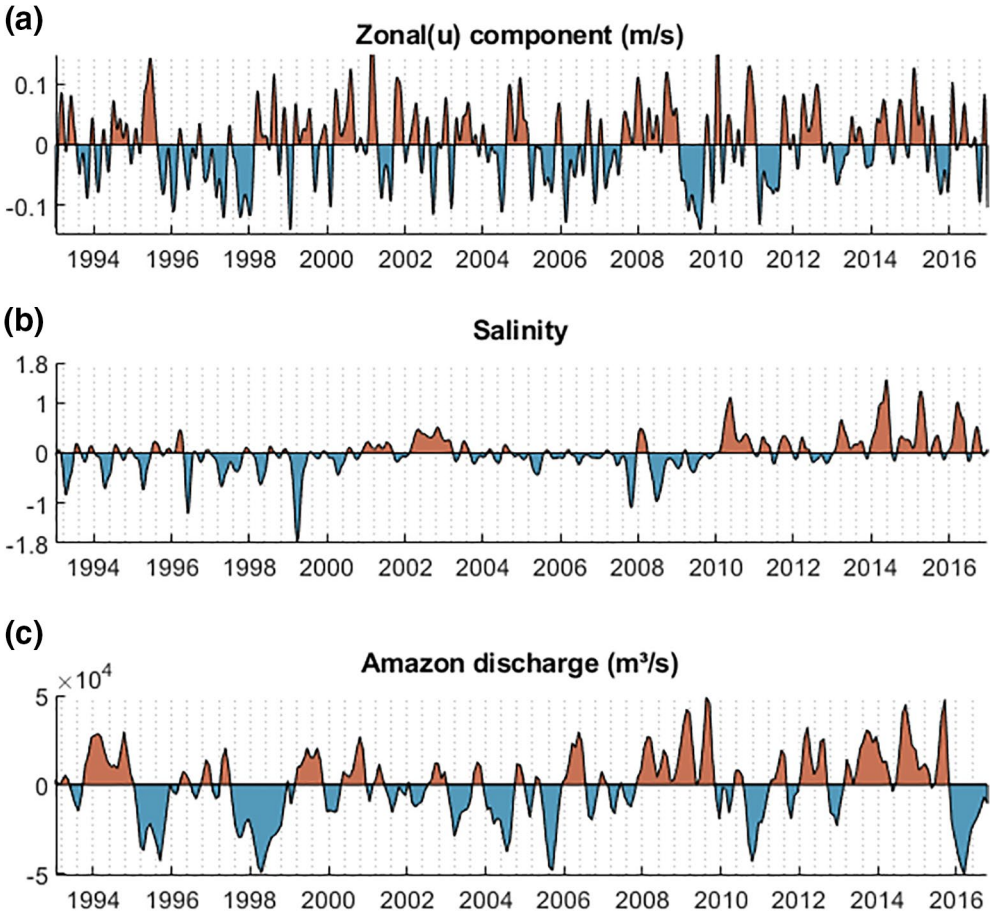


**Figure 5.** Monthly anomalies of zonal(u)-component (a) and salinity (b) of North Brazil Current in a longitudinal cut at 53°W, 3°N–7°N, from the surface to 500 m deep ARMOR 3D product. (c) Indicates monthly anomalies of Amazon river discharge at the Óbidos Gauging available from the ORE–HYBAM.

phase of the AMO cycle, characterized by changes in a climate signal of 60–80 years. Further studies could analyze a long-term climatological ring data to compare with this climate index. NBC ring evolution in terms of eddy characteristics is highlighted in Section 3.3.

### 3.3. Rings Trajectory and Evolution: Merged Rings Case Studies

Regarding the trajectory of the 121 analyzed NBC rings, Figure 6 and Table S3 displays the location of rings formation, location of maximum SSHa, and location of final detection. In general, we can observe rings being generated in the NBC retroflection area, propagating northwestward along the coast until demise when reaching the Lesser Antilles (Figure 6). The location of rings SSHa max is spread along the area, indicating that SSHa max could be observed right after ring formation as well as close to ring demise. Generation area is limited from 53°W to east, while ring final detection settles mainly from 58°W to west, although few rings were last identified east of this longitude. NBCRs far eastern from 58°W identified in Figure 6 indicate rings that merged (e.g., R83 – see Table S3). Rings centers demise were identified sitting northward or close to Barbados, and many were last verified before reaching Barbados. One ring translated differently, demising in the continental shelf near Orinoco River (Figure 6). Overall, rings decease occurred in regions influenced by the bottom bathymetry of Antilles. In fact, the influence of topography in finishing rings in the region has been well documented (Fratantoni & Richardson, 2006; Jochumsen et al., 2010). Additionally, their demise is strictly connected to the presence of the Lesser Antilles, which constitutes a barrier to ring translation (Fratantoni & Richardson, 2006). Interaction with the island leads to the destruction or the splitting of the incoming vortex into several smaller ones (Fratantoni & Richardson, 2006; Tanabe & Cenedese, 2008).

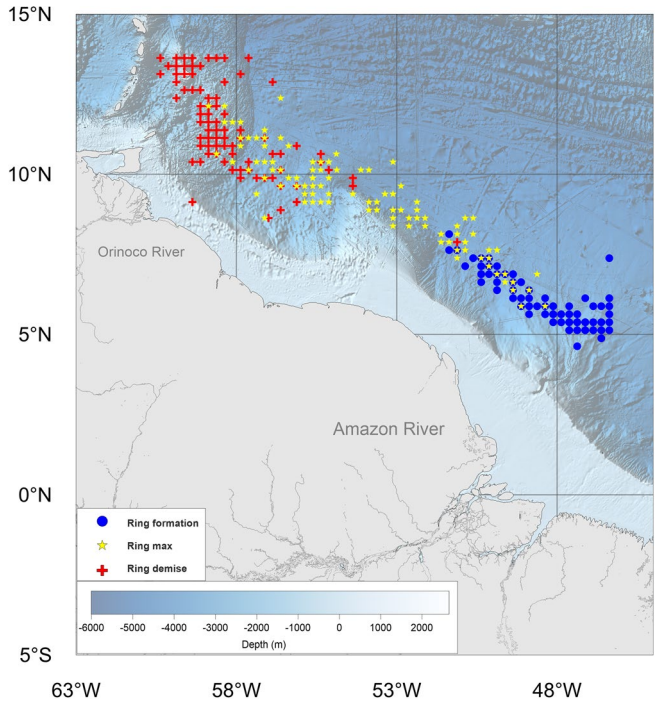


**Figure 6.** North Brazil Current rings position observed in the study area for three different moments during their lifetime: first week (blue); week of maximum sea surface height anomaly (yellow); last week (red). The background displays gridded bathymetry data from The General Bathymetric Charts of the Ocean (GEBCO), available at: https://www.gebco.net/.

Studies showed that ring might also be identified west of the island chain, indicating few surviving rings after topography interaction (Fratantoni & Richardson, 2006; Jochumsen et al., 2010; Mélice & Arnault, 2017; Tanabe & Cenedese, 2008). However, in our study the splitting of NBC rings encountering the Antilles was not detected by AMEDA, since the algorithm did not identify any NBCR west of the Antilles. This fact is mainly explained by the reduced study area, which imposes the tracking of rings with boundaries limited to 63°W.

Using rings center position (Table S3) and exploring the potential of ARMOR 3D data set for vertical profiles, we evaluated the water masses carried by NBC rings and the vertical temperature and salinity anomaly profiles on a seasonal scale. The vertical T-S diagrams were built from ARMOR 3D data set until 1,000 m, and the identified water masses were depicted (Figure 7). We recorded three water masses carried by NBC rings: South Atlantic Central Water (SACW), those with temperatures $\leq$ 18°C and salinities $\leq$ 36.0; coastal water (CW), with temperatures $\geq$ 20°C and salinities $\leq$ 35.4 and tropical water (TW), with temperatures $\geq$ 20°C and salinities $\geq$ 36.0. Neumann-Leitão et al. (2018) using in situ data observed the same water masses distribution in this region. Figure 7 displays the T-S diagrams for NBC rings locations at three different life stages, and starting at the four different seasons. A clear seasonality is observed in the water masses within NBC rings. From the end of boreal spring until JJA, CW from the Amazon river discharge is much more present in those eddies, while from September to February, the influence of TW is more pronounced is those vortex, and the CW is nearly absent (Figure 7). In fact, the seasonality of Amazon river runoff is known for decades, where the maximum monthly river discharge is in May and June (Hellweger & Gordon, 2002), demonstrating that the T-S diagram within an NBC eddy is related with their generation season. Additionally, NBC rings center presented similar T-S signatures during their translation, especially from their maxima week until their demise. It seems that rings in the starting week might not have enough intensity to trap water masses, reaching this stage of closed waters in vortex center during the following weeks. From the week of maxima SSHa, water masses are trapped until ring demise.

Furthermore, we performed the temperature and salinity 3-month profiles anomalies for each ring center identified, removing the climatology (based on the 24-years data from ARMOR 3D) from ring vertical profiles for each position. Three-month anomaly profiles were calculated in the central points of initial, maximum and final rings positions. The greatest anomalies observed in depth were located at ring SSHa maxima for both temperature and salinity (Figure 8). For initial and final positions, both the temperature and salinity anomalies profiles are not well defined, although rings initial position seems to relate to a stronger downward flux than final vortex locations (Figures S3a and S3b, respectively), since the latter is closer to Antilles bathymetry, what causes mixing. This behavior is an indication of an increased water downwelling in the eddy max position, while in initial and final positions the downward water flux at the ring center is weakened. Overall, regarding temperature profiles, maximum positive anomalies of 5°C are observed from 150 to 200 m deep, with no clear seasonality (Figure 8a). The downwelling associated with anticyclonic eddies increased the thermocline depth until 200 m in this region. Polo et al. (2015) indicated maxima MLD of 80 m for the WTNA region, showing that NBC rings can generate deeper thermocline and consequently greater mixed layer depths. For salinities, in general, negative anomalies (~-0.5) are observed at 100 m, settling above positive anomalies of 1.0 at 200 m (Figure 8b). These vertical salinity anomalies are also an indication of water sinking at NBC rings centers, that transport surface tropical saltier and coastal fresher waters to deeper layers. From this, the denser and saltier TWs settle under the less dense and fresher CW related to Amazon and Orinoco river plumes. Since Amazon discharge is more present in rings waters generated in JJA (Figure 7c), the most well-defined salinity anomalies profiles are referred to rings generated in this season, reaching SSHa max position at SON months, generating a more well-defined stratification in

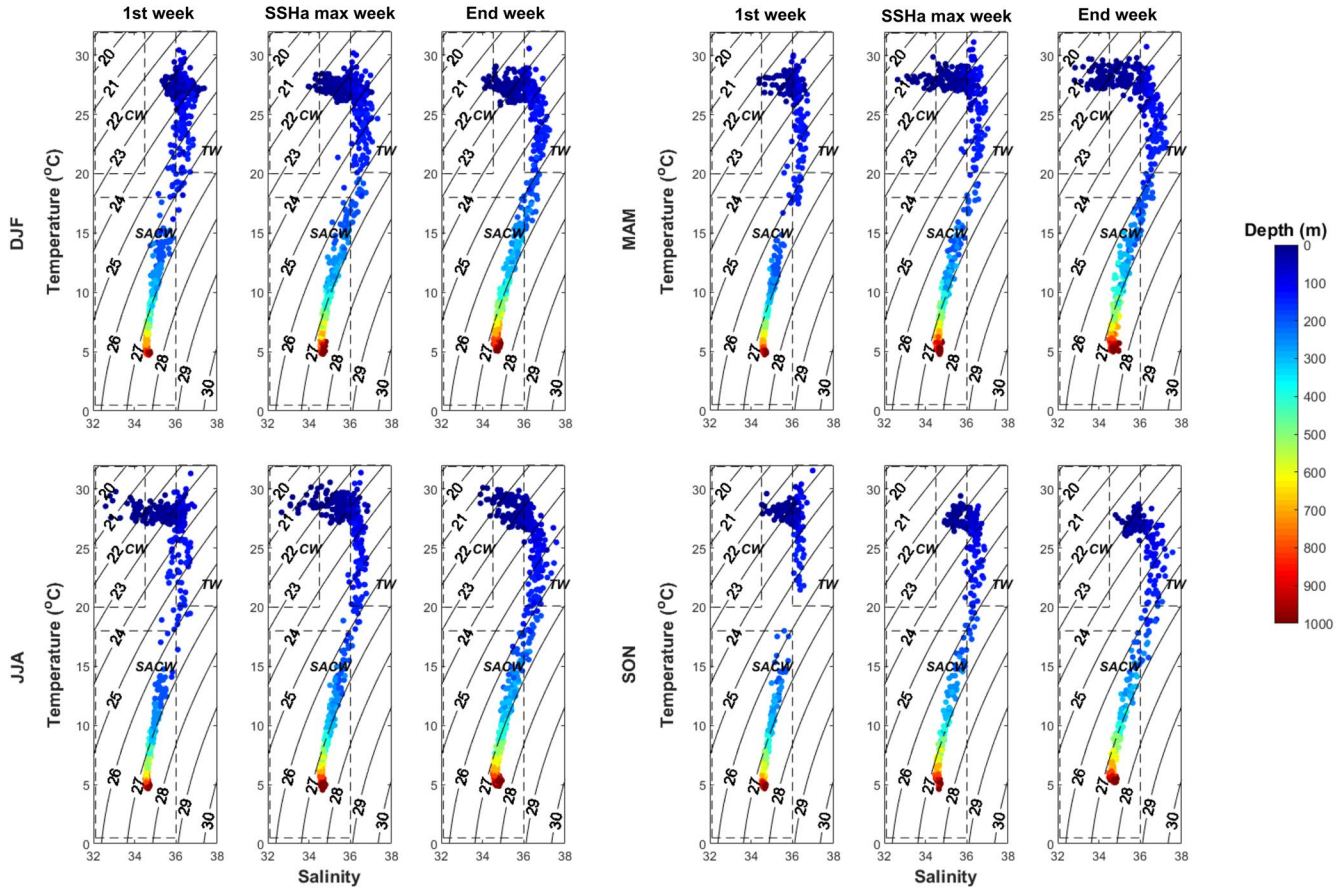


**Figure 7.** T-S diagram for each ring generated in the four different seasons from ARMOR 3D data set: DJF (a), MAM (b), JJA (c), SON (d). DJF, December-January-February trimester; JJA, June-July-August trimester; MAM, March-April-May trimester; SON, September-October-November trimester.

salinity anomalies profiles (Figure 8b). The increase in thermocline depth associated with sinking of riverine and TWs within NBC rings might spawn shifts on physical and biogeochemical features at WTNA, such as surface heat content, and $CO_2$ saturation. Further studies on this could indicate those answers.

A striking innovation of AMEDA algorithm is the capacity to detect merging between two eddies, and this capacity was explored in the present study. We detected only four merging rings events in the 24-year study period for NBC eddies, indicating that NBC rings did not interact much within each other. However, Castelão and Johns (2011) pointed that the presence of an inner core surrounded by an outer core of opposite vorticity is able to "isolate" the NBC rings, allowing them to be very close to each other without merging (Castelão & Johns, 2011). This structural configuration might explain why only 1 merging event was identified for each 6 years on average in the present study. In addition, few moments of NBC ring interaction with westward propagating anticyclonic eddies could be observed during the analyses. Plus, cyclonic eddies were also identified in certain weeks (Figure 9). Previous studies pointed for the formation of two different types of anticyclones in the region, the intermediate ones, and the NBC rings, that could coalesce within each other and generate deep-reaching rings (Garraffo et al., 2003; Jochum & Malanotte-Rizzoli, 2003). Cui et al. (2019) found that eddy merging is not likely to happen between eddies with similar intensities. Instead, the most common to happen is a strong eddy merging with a weaker one. Therefore, it is possible that NBC rings interact more often with weaker eddies (e.g., intermediate eddies, cleavaged eddies, eddies associated with NECC-NBC flow) present in the region than with other true NBC rings. Preceding works also identified cyclonic eddies in the region (Didden & Schott, 1993; Fratantoni & Richardson, 2006), which are associated with the NBC/NECC system variability, as well as with the dynamics of the anticyclonic NBC rings.

In order to highlight the typical evolution of the dynamical parameters of NBC rings during their northwestward propagation along the coast, and to analyze if there are significant changes in rings parameters

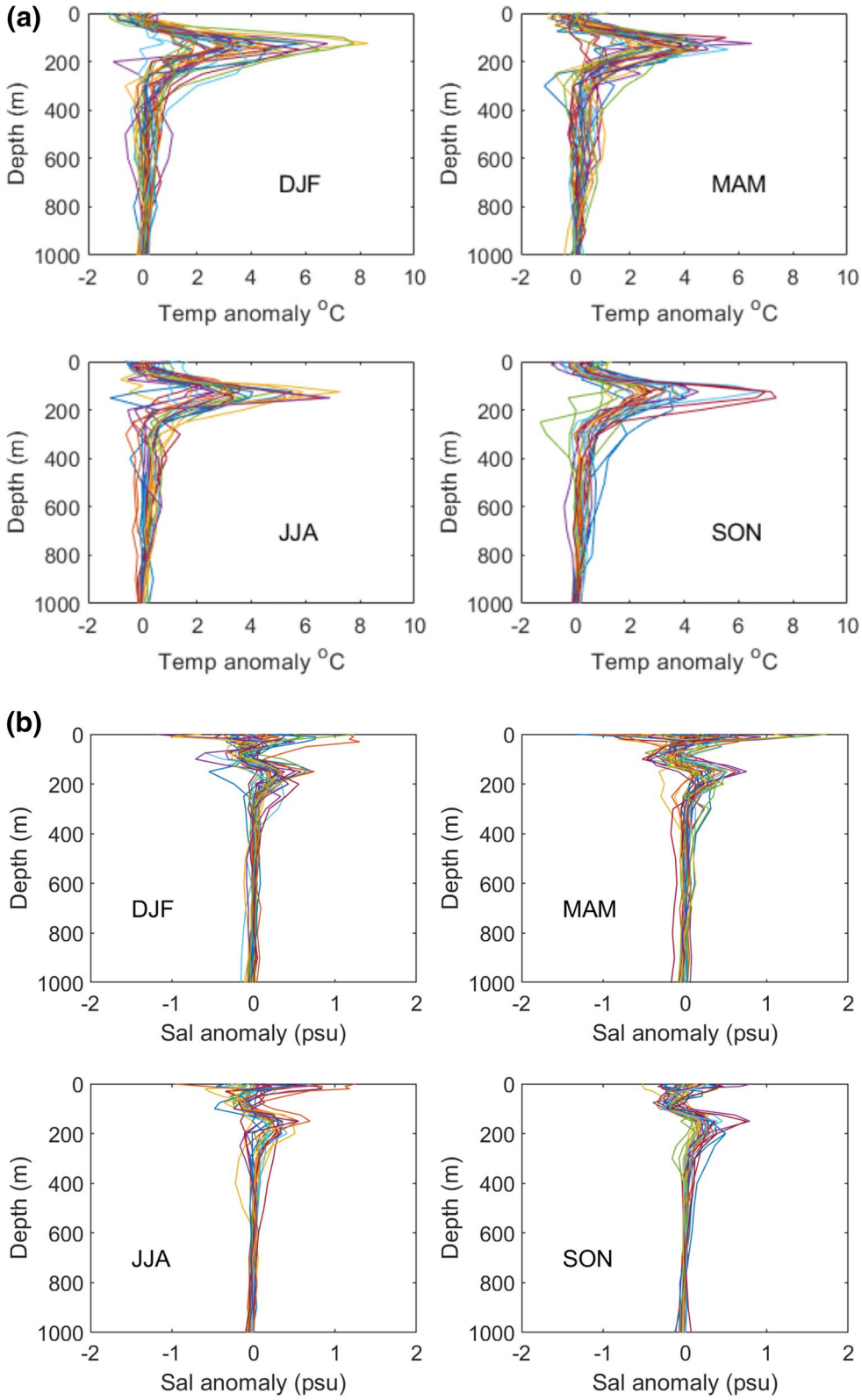


**Figure 8.** Temperature (a) and salinity (b) profiles anomalies for each ring center identified for Max sea surface height anomaly position, removing the climatology from ring vertical profiles for each position.

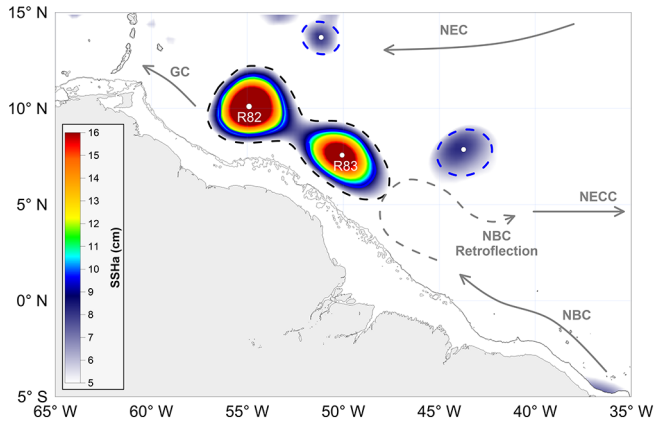


**Figure 9.** Large scale circulation features in Western Tropical North Atlantic over a sea surface height anomaly (SSHa) background from ARMOR 3D data set at week of 24th March 2009. R82 and R83 are two North Brazil Current (NBC) rings and two anticyclonic eddies identified by angular momentum eddy detection and tracking algorithm. Dashed (filled) lines represents outermost ($R_{max}$) closed contour $R_{max}$. Blue contours indicate anticyclonic eddies. Gray lines denotes large scale currents. SSHa smaller than 5 cm were removed for better visualization of rings. NECC, North Equatorial Countercurrent.

after merging, we computed the parameters for every week of occurrence of the 8 isolated rings which turned to four merged rings events. Rings parameters evolution is depicted in Figure S4 and Table S4. Weeks with NaN values represent weeks that AMEDA could not identify eddy. Figure 10 shows the trajectories of rings in the four analyzed events. From the four events, three rings remained merged until their demise (Figures 10a, 10c, 10d), while one of them merged and then splitted into two rings after 2 weeks (Figure 10b). All observed merging rings were generated from 52°W to east, above 5°N, and traveled northwestward along the northern coast of Brazil (Figure 10). Plus, the four merging events took place from mid-February to start of April, where six isolated rings were generated in DJF, one in September and one in March. Dated only in the first half of the year, the time of merging events corresponds with the time of increased ring formation (Figure 1). Other works also observed merging events only in this period (Barnier et al., 2001; Fratantoni & Richardson, 2006). It is believed that in the second half of the year the ring generation rate is not sufficient to promote a ring encounter when translating, before one of them demise in the Antilles. Still, regarding the location of merging events, all 4 events settled in the area indicated by the red rectangle in Figure 10. This area is located in a topographic depression between the start of Caribbean topography and the extended continental shelf from 53°W to 55°W (Figure 10). It is hypothesized that in this highlighted region NBC rings decelerate as reaching Antilles topography, allowing upcoming NBC rings to reach the previous eddy and merge. In fact, Barnier et al. (2001) indicated that a NBC eddy was slowed down as it encountered the Trinidad–Tobago topographic rise, which contributed for ring merging. The authors still indicated that such ring merging was also reported by Didden and Schott (1993). Further studies on the influence of this topography for the fusion of NBC rings are required. Lastly, Figure 10 also displays that rings trajectory right after merging are slightly deviated to west-southwest. De Marez et al. (2020) indicated that anticyclonic eddies are more likely to be orientated southwest-northeast due to the β-effect. It seems that NBC rings are also influenced by this effect.

In addition, the change on NBC ring vertical and translation structure is related not only to ring and current field dynamics but also to the influence of topography in the region, especially regarding ring demise (Fratantoni & Richardson, 2006; Jochumsen et al., 2010). Hence, since ring parameters evolve in time and could be strongly affected by bottom bathymetry, especially when the vortexes reach Caribbean coastal shelves, we attempted to evaluate the influence of topography in NBCRs parameters. To do that, we used the merged events M1 and M4 (Table S4) as case studies for comparison of their parameters before and after reaching 58°W (i.e., where influence of bottom topography seems to increase), computing their characteristics only 1 week after they merged to remove merging effects, and performing t student tests. M3 merged after 58°W, where merging effects could superimpose topographic effects, so we did not consider this event as a case study. On the other hand, M2 splits when reaches 58°W, what could indicate bathymetry influence. For M1, we observed significant decrease in $R_{max}$ ($p = 0.002$), while total ratio and $V_{max}$ did not change ($p = 0.9432$ and $p = 0.7154$, respectively). In the case of M4, no shifts were observed at all ($R_{max}$, $p = 0.1740$; total ratio, $p = 0.7800$; $V_{max}$, $p = 0.1383$). By potential vorticity conservation, it was expected that when reaching shallow waters eddies would flatten and increase their size, while diminish their velocities. However, only a significant reduction in $R_{max}$ was observed. This uncertainty might be due to effects of the bathymetry in the algorithm identification using this data set spatial resolution (1/4°), where further studies using an increased data resolution could better indicate current vectors around the island chain, improving ring identification, and allowing a finer evaluation of the effects of Lesser Antilles bathymetry in NBC ring parameters

Moreover, significant changes were observed for three parameters of NBC rings after rings merging. To address that, we performed *t*-student tests for the parameters computed for each of the eight isolated and the four merged NBC rings, which results are indicated in Table 1. We removed the weeks immediately before

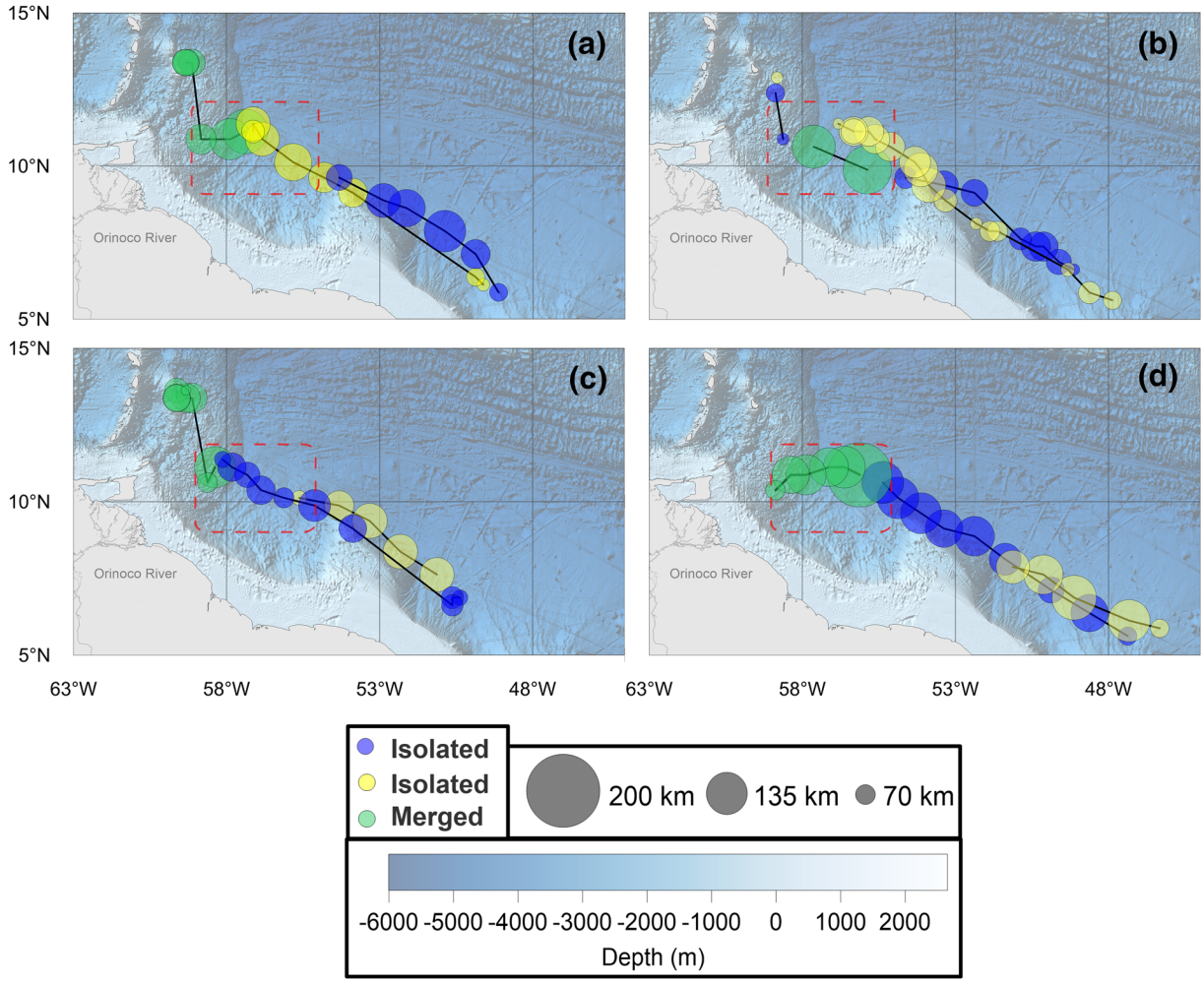


**Figure 10.** Merging rings trajectory. M1 from R20 (yellow) and R21 (blue) (a); M2 from R39 (yellow) and R40 (blue) (b); M3 from R78 (yellow) and R77 (blue) (c); M4 from R83 (yellow) and R82 (blue) (d). Red rectangle indicates area where all rings merged. Black lines represent rings trajectory. Circle size depicts $R_{max}$. Circle height is four times lower that the real circle height based on $R_{max}$. Circle shapes do not depict real ring shapes, are displayed only as ring representations.

**Table 1**
*Test t-Student Between Isolated and Merged Rings*

| | *t*-student | Mean solo | Mean merged | Significant difference (%) |
|---|---|---|---|---|
| $R_{max}$ | 0.4091 | 113.6 km | 121.2 km | NA |
| $V_{max}$ | **0.0291** | 0.23 m/s | 0.28 m/s | **+22.0** |
| Ro | **0.0194** | 0.11 | 0.08 | **−27.3** |
| KE | **0.0141** | 187.6 $cm^2/s^2$ | 285.1 $cm^2/s^2$ | **+52.0** |
| SSHa | 0.9775 | 6.4 cm | 6.4 cm | NA |

*Note*. Significant differences were considered in a 95% confidence interval ($p < 0.05$) and are indicated in bold. Significant difference (%) indicates the percentage of change between mean solo and mean merged rings parameters.

Abbreviations: KE, kinetic energy; Ro, Rossby number; SSHa, sea surface height anomaly.

and right after ring merging from the test t, in order to remove effects of definition of the eddy radius during the merging event, since for a perfect merging between two symmetric eddies their radii should tend to zero just before a single eddy contours emerge (Le Vu et al., 2018). Significant changes were verified for $V_{max}$, Ro and KE, while $R_{max}$ and SSHa did not present considerable difference between isolated and merged vortex (Table 1). Shift in Ro occurred due to increased $V_{max}$ and the maintenance of $R_{max}$ from isolated to merged eddies. A $V_{max}$ positive change of 22.0% resulted in merged rings with 52% more KE that the isolated, in average. This increase in ring KE might disrupt local circulation around Caribbean islands in a greater scale, impacting also fish larvae recruitment, and ocean-atmosphere energy exchanges. In addition, eddy merging events could function as a "large-scale energy pump" in the inverse energy cascades in two ways: from changes from small- to large-scale eddies and increasing residence time (Klein et al., 2019; Wang et al. 2019). After merging, there is a significantly increase the total KE and strengthen of the large geostrophic eddies by making them more coherent with a longer life time (Klein et al., 2019). In this study, however, we did not identified

shifts in $R_{max}$ after merging (rings maintained their length scale), and due to interaction with Antilles right after merging did not allowed a longer residence time (i.e., they are not isolated eddies). Then, we cannot affirm that NBC rings play this role. Further studies on this might spark answers for this question. The increase ring KE was also observed by Cui et al. (2019). The authors reported that splitting or merging events can change eddy properties by a factor of 2 or more (Cui et al., 2019). The observed changes in this study did not represent such a variation in eddy properties after merging. However, it showed that NBC ring merging has a considerable impact in its rotational speed, KE and intensity variation, and that those events should be taken into account when evaluating physical and biogeochemical impacts of NBC rings in the WTNA. On the other hand, Wang et al. (2019) stated that, overall, eddies KE decreased while total mechanical energy increased after merging, and that merging events require external energy input into rings. Therefore, we theorized that only in specific years this necessary energy input coincided with times of NBC rings close enough to merge with each other, making a NBC ring merging event such a rare event. More studies on the relation of ring merging years and climate indexes that could provide the required amount of energy for rings merging might elucidate this hypothesis. To evaluate how ring parameters are related with each other, we performed a correlation analysis between the computed parameters for the eight isolated the four merged rings, where Pearson correlation index are indicated in Table S5. We observed that $V_{max}$ and KE are well correlated with all analyzed parameters, in exception of Ro, while SSHa did not present high correlation with $R_{max}$ . Therefore, the use of maximum KE as a proxy for rings maxima is more indicated than the SSHa used in this study, since it includes a correlation not only with ring speed and energy, but also with ring size.

## 4. Conclusions

We applied the AMEDA for the identification of NBC rings occurrence, trajectories, and physical parameters. This work uses a 24-year (1993–2016) reanalysis database of geopotential height and geostrophic velocity fields, standing as the first study to apply an eddy detection algorithm for NBC ring identification in a decadal period. The choice of AMEDA is based on its robustness and ease of use for eddy properties time series analysis, since it considers not only dynamical but also geometrical properties of the velocity field. Here, we identified an average rate of five NBC rings shed by year, which presented an average lifetime of 15.3 (±5.4) weeks, $R_{max}$ from 87.3 to 204.8 km, with an average radius of 139.5 (±23.6) km, and were associated with mean SSHa within their centers of 9.4 (±4.0) cm. The mean observed $V_{max}$ was 0.27 (±0.08) m/s, while the averaged Ro value was 0.08 (±0.04) and averaged KE was 255.3 (±154.8) $cm^2/s^2$. It is pointed that the azimuthal velocity and Ro values might be underestimated due to the use of purely geostrophic velocity fields.

NBC rings occur more frequently in the first half of the year. In fact, a decrease in ring generation rate of 47.37% was detected between maxima (boreal winter) and minima (boreal fall) trimesters. Moreover, NBC rings have larger dimensions, rotate faster, and present shorter lifetimes in boreal winter months, also carrying more KE within them. On the other hand, NBC rings shed last longer, have smaller diameters, and carry less energy during summer and early boreal fall. 2009 was a year of anomalous conditions, since it presented maximum values of KE, $V_{max}$, and SSHa associated with NBC rings. Another pattern identified in this work was the positive trend in SSHa anomalies from 2009 to 2016. This shows that SSHa within NBC rings is increasing in the last years, which could be further investigated.

Furthermore, we identified that downwelling within NBC rings center cause a thermocline deepening and anomalies in the salinity profile, indicating downward transport of tropical and CWs. Also, the analysis of T-S diagram allowed us to identify seasonality in relation to water masses in the interior of NBC rings. River water was observed within eddies center only in the ones formed from May to August, implying that NBC rings generated at those months might play different biogeochemical impacts in the WTNA region, such as shifts $CO_2$ fugacity in the ocean and $CO_2$ flux between ocean–atmosphere. The vertical change in temperature and salinity profiles can as well influence these physical and biogeochemical effects. More studies on this could provide this response. In addition, we observed in the year of 2009 a possible influence of Amazon river discharge on NBC ring dynamical parameters, such as $V_{max}$ and KE, through effects in water density, flow vorticity and velocity, what might also have contributed for a ring merging event in that

year. Still, NBC rings merging events, although not very frequent, can significantly increase ring velocity and energy. However, the mechanism and energy supply that allow then to occur with NBC rings remains unclear. Moreover, these increase in ring KE can have an impact in the current dynamics around Caribbean, influencing, for example, phytoplankton distribution. Further works on this would provide this answer.

In this study, the use of reanalysis data associated with this AMEDA tool allowed the investigation of the intra- to inter-annual variability of NBC rings occurrence and dynamics. Further, the algorithm demonstrated to be straightforward in the identification of interaction among rings, which facilitate the analysis of these events. Overall, quantifying ring parameters seasonal and inter-annual variability, and identifying interaction between eddies, is crucial for understanding ring dynamics and consequently its impacts on the physics and biogeochemistry of the ocean.

## Data Availability Statement

ARMOR 3D data supplied by Copernicus Marine Environment Monitoring Service (CMEMS) at http://marine.copernicus.eu/. The 24 years of monthly Amazon discharge values recorded at the Óbidos Gauging Station, are available from the Environmental Research Observatory– Geodynamical, hydrological, and biogeochemical control of erosion/alteration and material transport in the Amazon basin (ORE–HYBAM: http://www.ore-hybam.org).

**Acknowledgments**
This project was supported by the TRIATLAS project, which has received funding from the European Union's Horizon 2020 research and innovation program under grant agreement No 817578. The authors also acknowledge the support of the Brazilian Research Network on Global Climate Changes – Rede CLIMA (FINEP Grants 01.13.0353-00). The received funding did not lead to any conflict of interests regarding the publication of this manuscript. L. C. Aroucha thanks to Thomaz Arsouze, Briac Le Vu, and Alexandre Stegner for making AMEDA available and for the orientation of its use.

## References

Arnault, S., & Cheney, R. E. (1994). Tropical Atlantic sea level variability from Geosat (1985–1989). *Journal of Geophysical Research*, *99*, 18207–18223. https://doi.org/10.1029/94JC01301

Barnier, B., Reynaud, T., Beckmann, A., Boning, C., Molines, J.-M., Barnard, S., & Jia, Y. (2001). On the seasonal variability and eddies in the North Brazil Current: insight from model intercomparison experiments. *Progress in Oceanography*, *44*, 195–230. https://doi.org/10.1016/S0079-6611(01)00005-2

Buongiorno Nardelli, B., Droghei, R., & Santoleri, R. (2016). Multi-dimensional interpolation of SMOS sea surface salinity with surface temperature and *in situ* salinity data. *Remote Sensing of Environment*, *180*, 392–402. https://doi.org/10.1016/j.rse.2015.12.052

Castelão, G. P., & Johns, W. E. (2011). Sea surface structure of North Brazil Current rings derived from shipboard and moored acoustic Doppler current profiler observations. *Journal of Geophysical Research*, *116*(C1). https://doi.org/10.1029/2010JC006575

Chaigneau, A., Gizolme, A., & Grados, C. (2008). Mesoscale eddies off Peru in altimeter records: Identification algorithms and eddy spatio-temporal patterns. *Progress in Oceanography*, *79*, 106–119. https://doi.org/10.1016/j.pocean.2008.10.013

Chelton, D. B., de Szoeke, R. A., Schlax, M. G., El Naggar, K., & Siwertz, N. (1998). Geographical variability of the first baroclinic Rossby radius of deformation. *Journal of Physical Oceanography*, *28*, 433–459. https://doi.org/10.1175/1520-0485(1998)028%3C0433:GVOTFB%3E2.0.CO;2

Cowen, R. K., Sponaugle, S., Paris, C. B., Lwiza, K., Fortuna, J., & Dorsey, S. (2003). Impact of North Brazil Current rings on local circulation and coral reef fish recruitment to Barbados, West Indies. In G. J. Goni & P. Malanotte-Rizzoli (Eds.), *Interhemispheric water exchange in the Atlantic Ocean, Elsevier Oceanographic Series* (Vol. 68, pp. 443–455), Amsterdam, Netherlands: Elsevier. https://doi.org/10.1016/S0422-9894(03)80157-5

Cruz-Gómez, R., & Salcedo-Castro, J. (2013). Analysis of horizontal and vertical ring structure based on analytical model and satellite data: Application to the North Brazil Current Rings. *Ocean Science Journal*, *48*(2), 161–172. https://doi.org/10.1007/s12601-013-0013-2

Cui, W., Wang, W., Zhang, J., & Yang, J. (2019). Multi core structures and the splitting and merging of eddies in global oceans from satellite altimeter data. *Ocean Science*, *15*, 413–430. https://doi.org/10.5194/os-15-413-2019

de Marez, C., Carton, X., L'Hégaret, P., Meunier, T., Stegner, A., Le Vu, B., & Morvan, M. (2020). Oceanic vortex mergers are not isolated but influenced by the $\beta$-effect and surrounding eddies. *Scientific Reports*, *10*(2897), https://doi.org/10.1038/s41598-020-59800-y

Didden, N., & Schott, F. (1993). Eddies in the North Brazil Current retroflection region observed by Geosat altimetry. *Journal of Geophysical Research*, *98*, 121–131. https://doi.org/10.1029/93JC01184

Doglioli, A. M., Blanke, B., Speich, S., & Lapeyre, G. (2007). Tracking coherent structures in a regional ocean model with wavelet analysis: Application to Cape Basin eddies. *Journal of Geophysical Research*, *112*(C5). https://doi.org/10.1029/2006JC003952

Douglass, E. M., & Richman, J. G. (2015). Analysis of ageostrophy in strong surface eddies in the Atlantic Ocean. *Journal of Geophysical Research: Oceans*, *120*, 1490–1507. https://doi.org/10.1002/2014JC010350

Ffield, A. (2005). North Brazil Current rings viewed by TRMM Microwave Imager SST and the influence on Amazon River Plume. *Deep Sea Research Part I Oceanographic Research Papers*, *52*, 137–160. https://doi.org/10.1016/j.dsr.2004.05.013

Foltz, G. R., McPhaden, M. J., & Lumpkin, R. (2012). A strong Atlantic Meridional Mode Event in 2009: The role of mixed layer dynamics. *Journal of Climate*, *25*, 363–380. https://doi.org/10.1175/JCLI-D-11-00150.1

Fonseca, C. A., Goni, G. J., Johns, W. E., & Campos, E. J. D. (2004). Investigation of the North Brazil Current retroflection and north equatorial countercurrent variability. *Geophysical Research Letters*, *31*. https://doi.org/10.1029/2004GL020054

Fratantoni, D. M., & Glickson, D. A. (2002). North Brazil Current ring generation and evolution observed with SeaWiFS. *Journal of Physical Oceanography*, *32*, 1058–1074. https://doi.org/10.1175/1520-0485(2002)032%3C1058:NBCRGA%3E2.0.CO;2

Fratantoni, D. M., Johns, W. E., & Townsend, T. L. (1995). Rings of the North Brazil Current: Their structure and behavior inferred from observations and a numerical simulation. *Journal of Geophysical Research*, *100*, 10633–10654. https://doi.org/10.1029/95JC00925

Fratantoni, D. M., Johns, W. E., Townsend, T. L., & Hurlburt, H. E. (2000). Low-latitude circulation and mass transport pathways in a model of the tropical Atlantic Ocean. *Journal of Physical Oceanography*, *30*, 1944–1966. https://doi.org/10.1175/1520-0485(2000)030%3C1944:LLCAMT%3E2.0.CO;2

Fratantoni, D. M., & Richardson, P. L. (2006). The evolution and demise of North Brazil Current Rings. *Journal of Physical Oceanography*, *36*, 1241–1264. https://doi.org/10.1016/S0422-9894(03)80154-X

Garraffo, Z., Johns, W. E., Chassignet, E., & Goni, G. (2003). North Brazil Current rings and transport of southern waters in a high resolution numerical simulation of the North Atlantic. In *Interhemispheric water exchange in the Atlantic Ocean, Elsevier Oceanography Series* (Vol. 68, pp. 375–410), Amsterdam: Elsevier. https://doi.org/10.1016/S0422-9894(03)80155-1

Garreau, P., Dumas, F., Louazel, S., Stegner, A., & Le Vu, B. (2018). High-resolution observations and tracking of a dual-core anticyclonic eddy in the Algerian Basin. *Journal of Geophysical Research: Oceans*, *123*(12), 9320–9339. https://doi.org/10.1029/2017JC013667

Garzoli, S. L., Ffield, A., & Yao, Q. (2003). North Brazil Current rings and the variability in the latitude of retroflection. In *Interhemispheric water exchange in the Atlantic Ocean, Elsevier Oceanography Series* (Vol. 68, pp. 357–373), Amsterdam: Elsevier. https://doi.org/10.1016/S0422-9894(03)80154-X

Goni, G. J., & Johns, W. E. (2001). A census of North Brazil Current rings observed from TOPEX/POSEIDON altimetry: 1992–1998. *Journal of Geophysical Research*, *28*, 1–4. https://doi.org/10.1029/2000GL011717

Goni, G. J., & Johns, W. E. (2003). Synoptic study of warm rings in the North Brazil Current retroflection region using satellite altimetry. In *Interhemispheric water exchange in the Atlantic Ocean, Elsevier Oceanography Series* (Vol. 68, pp. 335–356), Amsterdam: Elsevier. https://doi.org/10.1016/S0422-9894(03)80153-8

Guinehut, S., Dhomps, A.-L., Larnicol, G., & Le Traon, P.-Y. (2012). High resolution 3D temperature and salinity fields derived from in situ and satellite observations. *Ocean Science*, *8*, 845–857. https://doi.org/10.5194/os-8-845-2012

Halo, I., Backeberg, B., Penven, P., Ansorge, I., Reason, C., & Ullgren, J. (2014). Eddy properties in the Mozambique Channel: A comparison between observations and two numerical ocean circulation models. *Deep Sea Research Part II: Topical Studies in Oceanography*, *100*, 38–53. https://doi.org/10.1016/j.dsr2.2013.10.015

Hellweger, F. L., & Gordon, A. L. (2002). Tracing Amazon river water into the Caribbean sea. *Journal of Marine Research*, *60*, 537–549.

Ioannou, A., Stegner, A., Le Vu, B., Taupier-Letage, I., & Speich, S. (2017). Dynamical evolution of intense Ierapetra Eddies on a 22 year long period. *Journal of Geophysical Research: Oceans*, *122*(11), 9276–9298. https://doi.org/10.1002/2017JC013158

Ioannou, A., Stegner, A., Tuel, A., LeVu, B., Dumas, F., & Speich, S. (2019). Cyclostrophic corrections of AVISO/DUACS surface velocities and its application to mesoscale eddies in the Mediterranean Sea. *Journal of Geophysical Research: Oceans*, *124*(12), 8913–8932. https://doi.org/10.1029/2019JC015031

Jochum, M., & Malanotte-Rizzoli, P. (2003). On the generation and importance of North Brazil Current rings. *Journal of Marine Research*, *61*, 147–162. https://doi.org/10.1357/002224003322005050

Jochumsen, K., Rhein, M., Hüttl-Kabus, S., & Böning, C. W. (2010). On the propagation and decay of North Brazil Current rings. *Journal of Geophysical Research*, *115*(C10). https://doi.org/10.1029/2009JC006042

Johns, W. E., Lee, T. N., Beardsley, R. C., Candela, J., Limeburner, R., & Castro, B. (1998). Annual cycle and variability of the North Brazil Current. *Journal of Physical Oceanography*, *28*, 103–128. https://doi.org/10.1175/1520-0485(1998)028%3C0103:ACAVOT%3E2.0.CO;2

Johns, W. E., Lee, T. N., Schott, F. A., Zantopp, R. J., & Evans, R. H. (1990). The North Brazil Current retroflection: Seasonal structure and eddy variability. *Journal of Geophysical Research*, *95*, 22103–22120. https://doi.org/10.1029/JC095iC12p22103

Johns, W. E., Zantopp, R. J., & Goni, G. J. (2003). Cross-gyre transport by North Brazil Current rings. In G. J. Goni & P. Malanotte-Rizzoli (Eds.), *Interhemispheric water exchange in the Atlantic Ocean, Elsevier Oceanographic Series* (Vol. 68, pp. 411–441), Amsterdam: Elsevier. https://doi.org/10.1016/S0422-9894(03)80156-3

Klein, P., Lapeyre, G., Siegelman, L., Qiu, B., Fu, L., Torres, H., et al. (2019). Ocean-scale interactions from space. *Earth and Space Science*, *6*, 795–817. https://doi.org/10.1029/2018ea000492

Le Vu, B., Stegner, A., & Arsouze, T. (2018). Angular Momentum Eddy Detection and Tracking Algorithm (AMEDA) and its application to coastal eddy formation. *Journal of Atmospheric and Oceanic Technology*, *35*, 739–762. https://doi.org/10.1175/JTECH-D-17-0010.1

Legeckis, R., & Gordon, A. L. (1982). Satellite observations of the Brazil and Falkland currents – 1975 to 1976 and 1978. *Deep Sea Research Part A Oceanographic Research Papers*, *29*, 375–401. https://doi.org/10.1016/0198-0149(82)90101-7

Li, Q.-Y., Sun, L., Liu, S.-S., Xian, T., & Yan, Y.-F. (2014). A new mononuclear eddy identification method with simple splitting strategies. *Remote Sensing Letters*, *5*, 65–72. https://doi.org/10.1080/2150704X.2013.872814

Lumpkin, R., & Garzoli, S. L. (2005). Near-surface circulation in the tropical Atlantic Ocean. *Deep Sea Research Part I: Oceanographic Research Papers*, *52*, 495–518. https://doi.org/10.1016/j.dsr.2004.09.001

Ma, H. (1996). The dynamics of the North Brazil Current retroflection eddies. *Journal of Marine Research*, *54*, 35–53. https://doi.org/10.1357/0022240963213493

McWilliams, J. C. (1990). The vortices of two-dimensional turbulence. *Journal of Fluid Mechanics*, *219*, 361–385. https://doi.org/10.1017/S0022112090002981

Mélice, J.-L., & Arnault, S. (2017). Investigation of the intra-annual variability of the North Equatorial Countercurrent/North Brazil Current eddies and of the instability waves of the North tropical Atlantic Ocean using satellite altimetry and Empirical Mode Decomposition. *Journal of Atmospheric and Oceanic Technology*, *34*, 2295–2310. https://doi.org/10.1175/JTECH-D-17-0032.1

Mkhinini, N., Coimbra, A. L. S., Stegner, A., Arsouze, T., Taupier-Letage, I., & Beranger, K. (2014). Long-lived mesoscale eddies in the eastern Mediterranean sea: Analysis of 20 years of AVISO geostrophic velocities. *Journal of Geophysical Research: Oceans*, *119*, 8603–8626. https://doi.org/10.1002/2014JC010176

Mulet, S., RioMignot, M. -H. A., Guinehut, S., & Morrow, R. (2012). A new estimate of the global 3D geostrophic ocean circulation based on satellite data and in-situ measurements. *Deep Sea Research Part II: Tropical Studies in Oceanography*, *77–80*, 70–81. https://doi.org/10.1016/j.dsr2.2012.04.012

Nencioli, F., Dong, C., Dickey, T., Washburn, L., & McWilliams, J. (2010). A vector geometry-based eddy detection algorithm and its application to a high-resolution numerical model product and high-frequency radar surface velocities in the Southern California Bight. *Journal of Atmospheric and Oceanic Technology*, *27*(3), 564–579. https://doi.org/10.1175/2009JTECHO725.1

Neumann-Leitão, S., Melo, P. A. M. C., Schwamborn, R., Diaz, X., Figueiredo, L., Silva, A., et al. (2018). Zooplankton from a reef system under the influence of the Amazon River Plume. *Frontiers in Microbiology*, *9*, 355. https://doi.org/10.3389/fmicb.2018.00355

Nurser, A. J. G., & Bacon, S. (2014). The Rossby radius in the Arctic ocean. *Ocean Science*, *10*, 967–975. https://doi.org/10.5194/os-10-967-2014

Pauluhn, A., & Chao, Y. (1999). Tracking eddies in the subtropical North-Western Atlantic Ocean. *Physics and Chemistry of the Earth*, *24A*, 415–421. https://doi.org/10.1016/S1464-1895(99)00052-6

Polo, I., Lazar, A., Rodriguez-Fonseca, B., Mignot, J. (2015). Growth and decay of the equatorial Atlantic SST mode by means of closed heat budget in a coupled general circulation model. *Frontiers of Earth Science*, *3*, 37. https://doi.org/10.3389/feart.2015.00037

Richardson, P. L., Hufford, G. E., Limeburner, R., & Brown, W. S. (1994). North Brazil Current retroflection eddies. *Journal of Geophysical Research*, *99*, 5081–5093. https://doi.org/10.1029/93JC03486

Richardson, P., & Walsh, D. (1986). Mapping climatological seasonal variations of surface currents in the tropical Atlantic using ship drifts. *Journal of Geophysical Research*, *91*, 10537–10550. https://doi.org/10.1029/jc091ic09p10537

Rudzin, J. E., Shay, L. K., Jaimes, B., & Brewster, J. K. (2017). Upper ocean observations in eastern Caribbean Sea reveal barrier layer within a warm core eddy. *Journal of Geophysical Research: Oceans*, *122*, 1057–1071. https://doi.org/10.1002/2016JC012339

Sadarjoen, I. A., & Post, F. H. (2000). Detection, quantification, and tracking of vortices using streamline geometry. *Computers & Graphics*, *24*, 333–341. https://doi.org/10.1016/S0097-8493(00)00029-7

Sharma, N., Anderson, S. P., Brickley, P., Nobre, C., & Cadwallader, M. L. (2009). Quantifying the seasonal and inter-annual variability of the formation and migration pattern of *N*orth Brazil *C*urrent rings. Conference paper presented at OCEANS 2009, MTS/IEEE Biloxi – Marine Technology for Our Future: Global and Local Challenge, IEEE, pp. 1–7. https://doi.org/10.23919/OCEANS.2009.5422142

Tanabe, A., & Cenedese, C. (2008). Laboratory experiments on mesoscale vortices colliding with an island chain. *Journal of Geophysical Research*, *113*, C04022. https://doi.org/10.1029/2007JC004322

Tyaquiçã, P., Veleda, D., Lefèvre, N., Araujo, M., Noriega, C., Caniaux, G., et al. (2017). Amazon plume salinity response to ocean teleconnections. *Frontiers in Marine Science*, *4*, 250. https://doi.org/10.3389/fmars.2017.00250

Verbrugge, N., Mulet, S., Guinehut, S., & Buongiorno-Nardelli, B. (2017). ARMOR 3D: A 3D multi-observations T, S, U, V product of the ocean. *Geophysical Research Abstracts*, 19th EGU General Assembly, EGU2017, p. 17579.

Wang, Z.-F., Sun, L., Qiu-Yang, L., & Chemg, H. (2019). Two typical merging events of oceanic mesoscale anticyclonic eddies. *Ocean Science*, *15*, 1545–1559. https://doi.org/10.5194/os-15-1545-2019

Yi, J., Du, Y., He, Z., & Zhou, C. (2014). Enhancing the accuracy of automatic eddy detection and the capability of recognizing the multi-core structures from maps of sea level anomaly. *Ocean Science*, *10*, 39–47. https://doi.org/10.5194/os-10-39-2014

Zharkov, V., & Nof, D. (2010). Why does the North Brazil Current regularly shed rings but the Brazil Current does not? *Journal of Physical Oceanography*, *40*, 354–367. https://doi.org/10.1175/2009JPO4246.1